

Development of Magneto-Responsive Pickering Emulsion based on Cellulose Nanocrystal as Novel Controlled Drug Delivery Carrier

Low Liang Ee
M. Eng. (Hons.) (Chem.)

A Thesis Submitted to the Monash Institute of Graduate Research for the Requirements of the Degree of Doctor of Philosophy in Chemical Engineering



MONASH UNIVERSITY
2018

STATEMENT OF AUTHORSHIP

The thesis contains no material which has been accepted for the award of any other degree or diploma in any university or other institution. I affirm that, to the best of my knowledge, the thesis contains no material previously published or written by another person, except where due reference is made in the text of the thesis.



Signed:

ACKNOWLEDGEMENT

Foremost, I would like to express a deep sense of gratitude to my supervisor Dr. Patrick Tang Siah Ying for his patience, expertise and invaluable guidance. He has taught me a great deal about both scientific research and life in general. It was a great privilege and honor to carry out my doctoral research under his professional guidance. Without his continual support, this thesis work would not have been possible.

Besides my supervisor, I would like to extend my heartfelt thanks to my associate supervisory committee, Prof. Tey Beng Ti and Prof. Chan Eng Seng as well as Assoc. Prof. Ong Boon Hoong from University of Malaya for providing their insightful comments and encouragements in all the time of research and thesis writing. My sincere thanks should also be dedicated to Dr. Goh Bey Hing and his Phd student, Mr. Tan Loh Teng Hern from School of Pharmacy for their kind assistance and guidance in in vitro cytotoxicity assays. It is important to show my warmest thanks to my fellow lab mates for their senior advices and guidance. To them goes my deep appreciation and sincere gratitude.

Special thanks should be deserved to Monash Graduate Research Merit Scholarship and Ministry of Higher Education Malaysia for their financial grant support which enables me to pursuing this doctorate program.

I am extremely grateful to my parents for supporting me spiritually throughout writing this thesis and my life. Also, I very much thankful to all support staffs from Chemical Engineering Discipline especially Nurul, Isha, Azreen, and Azarudin for their professionalism and invaluable contribution in various technical matters. Last but not least, I would like thank Dr Edward Ooi Chien Wei, Dr. Lee Chern Leing and Assoc. Prof. Wu Ta Yeong for their encouragement, constructive feedback and useful criticism throughout all phases of my PhD research study.

LOW LIANG EE

JULY 2018

ABSTRACT

Possessing excellent biodegradability and biocompatibility properties, cellulose nanocrystal (CNC)-based nanocomposites has recently gained immense research interest and holds great potential as novel drug carrier. The use of CNC-based nanomaterials to deliver drugs is an attractive idea, however many of these class of CNC-based nanocarriers generally lack active targeting or triggered drug release components, making them difficult to obtain effective drug delivery, thus limiting the dose achievable within the tumour. The incorporation of magnetite nanoparticles (Fe_3O_4 NPs) into CNC matrix is a feasible solution to improve the drug delivery and targeting properties. The utilization of magnetic cellulosic nanocomposite has in fact recently attracted more and more attention, in which they have been suggested to be applicable as magnetic aerogel, magnetically retrievable oil absorbent, and recyclable catalyst. In present study, author proposed to develop a magnetically responsive cellulose nanocrystals as Pickering stabilizer for emulsion with the goal of utilizing them as controlled drug delivery carrier. To achieve this, Fe_3O_4 @CNC (MCNC) nanocomposites were first synthesized via a facile one-step ultrasound-assisted in situ co-precipitation technique. Results of physicochemical analysis demonstrated the feasibility of utilising the as-synthesised MCNCs as stabilizer for the formation of highly stable palm olein-in-water Pickering emulsions. The developed MCNC-stabilized Pickering emulsions (MCNC-PE) exhibits responsiveness to both pH and external magnetic field (EMF). It has been found that the magnetization of the MCNC-PE destabilized when the pH falls around 8 to 11. Using curcumin as model drug, the loading efficiency and in-vitro release behaviour of MCNC-PE were investigated. The loading efficiency of curcumin in emulsion template was found to be 99.35%. Effect of pH and EMF affected the curcumin release rate of MCNC-PE matrices. Exposure to EMF (0.7 T) under simulated buffer solution (pH 7.5) significantly enhanced the bioactive release, achieving a total of 53.30 ± 5.08 % of the initial loading over a period of 96 hr. The release mechanism from MCNC-PE based matrices was the non-Fickian transport in which the sustainable curcumin release rate from Pickering emulsions could be improved by external magnetic stimulus. The MTT assay demonstrated that the curcumin-loaded MCNC-PE is effective in reducing human colon

cancer cells growth down to 60% in the absence of EMF. A noticeable further reduction of $\sim 42\%$ in the cell viability was observed when oscillating EMFs were applied. The findings of our study suggest that the developed magnetic palm-based Pickering emulsions could be promising stimuli-responsive micro-carriers which offer preservation and controlled delivery of bioactive and therapeutic.

COMMUNICATION OF RESULTS

Publications

1. **Low, L. E.**, Tey, B. T., Ong, B. H., Chan, E. S., and Tang, S. Y. (2016). Dispersion Stability, Magnetivity, and Wettability of CNC-dispersed Superparamagnetic Fe₃O₄ Nanoparticles. *RSC Advances*, 6(114), pp.113132-113138. (Q2, IF: 2.936).
2. **Low, L. E.**, Tey, B. T., Ong, B. H., Chan, E. S., and Tang, S. Y. (2017). Palm olein-in-water Pickering emulsion stabilized by Fe₃O₄-cellulose nanocrystal nanocomposites and their responses to pH. *Carbohydrate Polymers*, 155, pp.391–399. (Q1, IF: 5.158).
3. **Low, L. E.**, Tey, B. T., Ong, B. H., and Tang, S. Y. (2018). Unravelling pH-responsive Behaviour of Fe₃O₄@CNCs-stabilized Pickering Emulsions under the Influence of Magnetic Field. *Polymer*, 141, pp.93-101. (Q1, IF: 3.483)
4. **Low, L. E.**, Tey, B. T., Ong, B. H., and Tang, S. Y. (2018). A Facile and Rapid Sonochemical Synthesis of Monodispersed Fe₃O₄@CNC Nanocomposites without Inert Gas Protection. *Asia-Pacific Journal of Chemical Engineering*, e2209, pp.1-13. (Q3, IF: 1.238).
5. **Low, L. E.**, Tan, L. T. -H., Goh, B. -H., Tey, B. T., Ong, B. H., and Tang, S. Y. (2018). Magnetic Cellulose Nanocrystal stabilized Pickering Emulsions for Enhanced Bioactive Release and Human Colon Cancer Therapy. *International Journal of Biological Macromolecules*. (Under Review) (Q1, IF: 3.909).

Conference Papers

1. **Low, L. E.**, Tey, B. T., Ong, B. H., and Tang, S. Y. Magnetite-cellulose Nanocrystal Composite Stabilized Magnetic Pickering Emulsion: Effects of CNC-Fe₃O₄ Ratio. *The 7th Asian Conference on Colloid and Interface Science*, 8-11th August, 2017, Kuala Lumpur, Malaysia.
2. **Low, L. E.**, Tey, B. T., Ong, B. H., and Tang, S. Y. An Ultrafast and Facile Sonochemical Synthesis of Fe₃O₄-CNC Nanocomposites without Inert Gas Protection. *The 17th Asia Pacific Confederation of Chemical Engineers Congress*, 23-27th August, 2017, WanChai, Hong Kong.
3. **Low, L. E.**, Tey, B. T., Abd-Rahim, A. -H., and Tang, S. Y. A novel Ultrasonic Pipe Technology for the Production of Carotene-rich Palm Olein Nanoemulsions. *30th Symposium of Malaysian Chemical Engineers*, 6 & 7th December, 2017, Bandar Sunway, Selangor, Malaysia.
4. Tang, S. Y., **Low, L. E.**, and Abd-Rahim, A. -H. A Novel Emulsification Approach based on Ultrasonic Intensifying Tube Reactor. *The 7th Asian Conference on Colloid and Interface Science*, 8-11th August, 2017, Kuala Lumpur, Malaysia.
5. Chew, C. L., **Low, L. E.**, Hilmi, S. M. H. S., Chan, E. S., and Tang, S. Y. Separation of Water-in-crude Palm Oil Emulsions by Indirect Ultrasound Irradiation, *8th International Colloids Conference*, 10-13th June, 2018, Shanghai, China.
6. **Low, L. E.**, Tey, B. T., Ong, B. H., and Tang, S. Y. Tunable Droplet Stability of Palm Olein-based Pickering Emulsions stabilized by Fe₃O₄@CNC Nanocomposites, *5th International Conference on Oils and Fats 2018*, 14 & 15th August 2018, Universiti Kebangsaan Malaysia (UKM), Bangi, Selangor, Malaysia.

Table of Contents

STATEMENT OF AUTHORSHIP	ii
ACKNOWLEDGEMENT	iii
ABSTRACT	iv
COMMUNICATION OF RESULTS	vi
<i>Publications</i>	vi
<i>Conference Papers</i>	vii
LIST OF ABBREVIATIONS	xi
LIST OF TABLES	xiv
LIST OF FIGURES	xv
CHAPTER ONE INTRODUCTION	1
1.1 Research Background	1
1.2 Problem Statements	3
1.3 Aims and Objectives	5
1.4 Contribution of Studies	5
CHAPTER TWO LITERATURE REVIEW	6
2.1 Pickering Emulsion Formation	6
2.1.1 <i>Nanoparticles as Stabilizer for Pickering Emulsion</i>	6
2.1.2 <i>Destabilization Mechanisms</i>	7
2.1.3 <i>Methods of Pickering Formation</i>	10
2.1.4 <i>Factors affecting Pickering Emulsion Properties and Stability</i>	10
2.1.5 <i>Types of Particulate Emulsifier</i>	13
2.2 Green Pickering Emulsion Stabilizer: Nanocellulose	14
2.2.1 <i>Microfibrillated Cellulose (MFC)</i>	15
2.2.2 <i>Bacterial Nanocellulose (BNC)</i>	16
2.2.3 <i>Cellulose Nanocrystal (CNC)</i>	16
2.3 Surface Functionalization of Cellulose Nanocrystal (CNC)	17
2.3.1 <i>Thermal Properties</i>	17
2.3.2 <i>Photoluminescent Properties</i>	18
2.3.3 <i>Conductive Properties</i>	18
2.3.4 <i>Magnetic Properties</i>	19
2.4 Magnetic Nanoparticles	20
2.4.1 <i>Concept of Magnetism</i>	20
2.4.2 <i>Magnetism in Magnetite Nanoparticle (MNP)</i>	22
2.4.3 <i>General Techniques in the Synthesis of MNP</i>	23
2.4.4 <i>Surface Functionalization and Stabilization of MNP for Drug Delivery System</i>	30
2.4.5 <i>Pickering Emulsion Formation using MNP</i>	32
2.5 Applications of Magneto-Responsive Cellulosic Materials	33
2.6 Pickering Emulsion: Application as Drug Delivery System	35
2.6.1 <i>Stimuli-Responsiveness for Magnetic-cellulosic-based Pickering Emulsion</i>	37

CHAPTER THREE MNPS@CNC NANOCOMPOSITE: RAPID PREPARATION AND REACTION MECHANISM	39
Overview	39
3.1 Introduction	40
3.2 Materials and Methodology	42
3.2.1 <i>Materials</i>	42
3.2.2 <i>Synthesis of MCNC Nanocomposite</i>	42
3.2.3 <i>Characterisation of MCNCs</i>	43
3.2.4 <i>Statistical Analysis</i>	44
3.3 Results and Discussion	44
3.3.1 <i>Facile Preparation of MCNCs under Open Atmosphere</i>	44
3.3.2 <i>The Mechanism of MCNCs</i>	55
3.4 Conclusions	60
CHAPTER FOUR PHYSICOCHEMICAL AND WETTING CHARACTERISTICS OF MCNC NANOCOMPOSITES	61
Overview	61
4.1 Introduction	62
4.2 Materials and Methodology	63
4.2.1 <i>Materials</i>	63
4.2.2 <i>Synthesis and Characterisation of MCNC Nanocomposite</i>	63
4.2.3 <i>Characterisation of MCNCs</i>	65
4.2.4 <i>Conductometric Titration</i>	65
4.2.5 <i>Statistical Analysis</i>	66
4.3 Results and Discussion	66
4.3.1 <i>MCNCs Preparation: Impact of Reaction Conditions</i>	66
4.3.2 <i>Surface Wettability of MCNCs</i>	85
4.4 Conclusions	93
CHAPTER FIVE PHYSICAL PROPERTIES AND COLLOIDAL STABILITY OF MCNC-STABILIZED PICKERING EMULSION (MCNC-PE)	94
Overview	94
5.1 Introduction	95
5.2 Materials and Methodology	97
5.2.1 <i>Materials</i>	97
5.2.2 <i>Synthesis and Characterisation of MCNC Nanocomposite</i>	97
5.2.3 <i>Preparation of MCNC-PE</i>	98
5.2.4 <i>Characterisation of MCNC-PE</i>	100
5.2.5 <i>Statistical Analysis</i>	100
5.3 Results and Discussion	101
5.3.1 <i>Physical Properties of MCNC-PE</i>	101
5.3.2 <i>Factors Affecting the Colloidal Characteristics of MCNC-PE</i>	105
5.4 Conclusions	129

CHAPTER SIX STIMULI-RESPONSIVENESS OF MCNC-PE	130
Overview	130
6.1 Introduction	131
6.2 Materials and Methodology	133
6.2.1 <i>Materials</i>	133
6.2.2 <i>Synthesis and Characterisation of MCNC Nanocomposites</i>	133
6.2.3 <i>Formation and Characterisation of MCNC-PE</i>	134
6.2.4 <i>Effects of External Magnetic Field (EMF), pH and MCNC Particles Concentration on MCNC-PE Stability</i>	134
6.2.5 <i>Temperature Variation Test</i>	134
6.2.6 <i>Reversibility Potential of MCNC-PE Upon pH Changes</i>	135
6.2.7 <i>Statistical Analysis</i>	135
6.3 Results and Discussion	135
6.3.1 <i>Physical Stability of MCNC-PE</i>	135
6.3.2 <i>pH and Magneto-responsiveness of MCNC-PE</i>	139
6.4 Conclusions	147
CHAPTER SEVEN BIOACTIVE MICROENCAPSULATION AND TRIGGERED RELEASE BEHAVIOUR OF MCNC-PE	148
Overview	148
7.1 Introduction	149
7.2 Materials and Methodology	151
7.2.1 <i>Materials</i>	151
7.2.2 <i>Synthesis and Characterisation of MCNC Nanocomposites</i>	151
7.2.3 <i>Preparation and Characterisation of MCNC-PE</i>	152
7.2.4 <i>Curcumin Loading Efficiency in MCNC-PE</i>	152
7.2.5 <i>Retention of Curcumin in MCNC-PE</i>	153
7.2.6 <i>Stability of MCNC-PE with/without Exposure to EMFs</i>	153
7.2.7 <i>In-vitro Curcumin Release Studies</i>	153
7.2.8 <i>Determination of Anticancer Activity Using MTT Assay</i>	154
7.2.9 <i>Apoptotic Hallmark Detection by Hoechst 33342 Nuclear Staining</i>	155
7.2.10 <i>Cellular Uptake of MCNC-PE</i>	155
7.2.11 <i>Statistical Analysis</i>	155
7.3 Results and Discussion	155
7.3.1 <i>Preparation and Characterisation of Curcumin-loaded MCNC-PE</i>	155
7.3.2 <i>In-vitro Release Profile of Curcumin from MCNC-PE</i>	157
7.3.3 <i>Anticancer Efficacy of Curcumin-loaded MCNC-PE</i>	159
7.4 Conclusions	164
FUTURE WORKS	165
REFERENCES	167

LIST OF ABBREVIATIONS

γ	Interfacial tension
θ	Contact angle
g	Gravitational acceleration
ρ	Density
v	Gravitational settling velocity
μ	Viscosity
φ	Volume fraction
ΔE	Energy of detachment
ΔG	Free energy
∇H	Magnetic field
A	Interfacial area
ANOVA	Analysis of variance
AR	Analytical reagent
BNC	Bacteria nanocellulose
C	Constant
CNC	Cellulose nanocrystal
CNF	Cellulose nanofibril
Co	Cobalt
CRC	Colorectal cancer cell
CTAB	Cetyltrimethylammonium bromide
DMSO	Dimethyl sulfoxide
E_c	Centrifugal work
E_M	Magnetic energy
EDC	1- ethyl-3-(3-dimethylaminopropyl)carbodiimide
EE	Encapsulation efficiency
EMF	External magnetic field
FDA	Food and drug administration

Fe	Iron
Fe ⁱ⁺	Iron ions
Fe(acac) _i	Tris(acetylacetonato) iron
FE-SEM	Field emission scanning electron microscopy
FTIR	Fourier transform infrared spectroscopy
H ₂	Hydrogen gas
MCNC	Fe ₃ O ₄ @cellulose nanocrystal
MCNC-PE	Fe ₃ O ₄ @cellulose nanocrystal-stabilized Pickering emulsion
MD	Multidomain
MFC	Microfibrillated cellulose
MNPs	Magnetite Nanoparticles
M _p	Magnetization of particles
mAb	Monoclonal antibodies
MRI	Magnetic resonance imaging
MTT	3-(4,5-dimethylthiazol-2-yl)-2,5-diphenyltetrazolium bromide
N ₂	Nitrogen gas
NCC	Nanocrystalline cellulose
NFC	Nanofibrillated cellulose
NHS	N- hydroxysulfosuccinimide
NPs	Nanoparticles
o/w	Oil-in-water
PE	Pickering emulsion
PEG	Poly(ethylene glycol)
PEI	Poly(ethylenimine)
PNIPAAm	Poly(N-isopropylacrylamide)
QDs	Quantum dots
SAED	Selective area electron diffraction
SD	Single domain
SEM	Scanning electron microscopy

SL	Sonoluminescence
STEM	Scanning transmission electron microscopy
TEM	Transmission electron microscopy
TGA	Thermogravimetric analysis
Thc	Thioctic acid
TiO ₂	Titanium dioxide
US	Ultrasound
V _{vdw}	Van der waal interaction potential
V _e	Electrostatic interaction potential
V _{sr}	Short-range interaction potential
V _{Tint}	Total interaction potential
V _i	Volume of i
VSM	Vibrating sample magnetometry
w/o	Water-in-oil emulsion
XRD	X-ray diffractometry

LIST OF TABLES

- I. Table 2.1. Differences between nanocellulose types (adapted from (Zhen, 2015)).
- II. Table 2.2. Advantages and disadvantages of reviewed magnetite nanoparticles synthesis techniques.
- III. Table 3.1. Total amount of sulphate group ($-\text{SO}_3$) and surface hydroxyl group ($-\text{OH}$), and percentage of sulphate groups coverage on CNC surface.
- IV. Table 4.1. Concentration of Fe^{3+} representing samples at different temperature. UV absorbance was recorded at UV-vis wavelength of 300 nm. Different alphabetic letters indicated significant differences at $P \leq 0.05$ by Bonferroni's Multiple Comparison Test.
- V. Table 4.2. Water-air and interfacial contact angle of CNC, MNP, and MCNCs samples different alphabetic letters was significantly different at $P \leq 0.05$ by Bonferroni's Multiple Comparison Test.
- VI. Table 4.3. Water-air and interfacial contact angle of MCNCs samples varying pH. Different alphabetic letters was significantly different at $P \leq 0.05$ by Bonferroni's Multiple Comparison Test.
- VII. Table 5.1. Surface coverage of MCNC-PE prepared under different MCNC concentration, C_{mcnc} .
- VIII. Table 5.2. Surface coverage of MCNC-PE prepared under different oil volume fraction φ_{oil} .
- IX. Table 5.3. $\frac{D}{V_{oil}}$ of MCNC-PE prepared under different oil volume fraction φ_{oil} .
- X. Table 6.1. Droplet surface coverage by MCNCs at different particle concentrations.
- XI. Table 7.1. Release parameters of curcumin from different emulsion samples based on Korsmeyer – Peppas model. Different alphabetic letters was significantly different at $P \leq 0.05$ by Bonferroni's Multiple Comparison Test.

LIST OF FIGURES

- I. *Figure 1.1. An illustration showing the four phases in this project.*
- II. *Figure 2.1. Graphical illustration of solid particles with different wettability (contact angle) at the interface of two immiscible liquids. (a) $\theta < 90^\circ$, and (b) $\theta > 90^\circ$.*
- III. *Figure 2.2. Graphical illustration of different destabilization mechanisms on emulsion.*
- IV. *Figure 2.3. Schematic view of Pickering emulsion droplet stabilized by (a) larger size particles and (b) smaller size particles.*
- V. *Figure 2.4. Schematic view of (a) high particles concentration versus (b) low particles concentration in stabilizing Pickering emulsion droplet.*
- VI. *Figure 2.5. Vector model showing the spin-orbital interaction for a bound electron (adapted from (Brailsford, 1966)).*
- VII. *Figure 2.6. Magnetic behaviour of magnetite NPs at different size range (adapted from (Hitchhiker's Guide, 2015)).*
- VIII. *Figure 2.7. Schematic illustration of structures of (a) single domain and (b) multidomain (adapted from (Hitchhiker's Guide, 2015)).*
- IX. *Figure 2.8. An exaggerated illustration of the growth of a cavitation bubble when it is subjected to sound field and leads to eventual collapse (adapted from (Mason and Peters, 2003)).*
- X. *Scheme 3.1. (a) Conventional and (b) proposed sonochemical co-precipitation method for MCNC preparation.*
- XI. *Figure 3.1. FTIR spectra of (a) pure MNP, (b) pure CNC, as well as MCNC prepared under (c) atmosphere condition, and (d) N_2 condition.*
- XII. *Figure 3.2. Raman spectroscopy spectra of (a) pure MNP, (b) pure CNC, as well as MCNC prepared under (c) atmosphere condition, and (d) N_2 condition.*
- XIII. *Figure 3.3. XRD pattern for (a) pure MNP, (b) pure CNC, as well as MCNC prepared under (c) atmosphere condition, (d) N_2 condition, and the standard XRD peaks for (e) Fe_3O_4 , and (f) Fe_2O_3 .*
- XIV. *Figure 3.4. Image of MCNC (a) without EMF, and (b) being attracted under EMF.*

- XV. *Figure 3.5. FE-SEM images of (a) Pure MNP, (b) Pure CNC, as well as MCNC prepared under (c) atmosphere condition, and (d) N₂ condition. MNPs feret diameter distribution histogram for STEM images. (e) Atmosphere condition, and (f) N₂ condition.*
- XVI. *Figure 3.6. EDX data representing (a) MNP, (b) CNC, as well as MCNC prepared under (c) air-flow condition, and (d) N₂ condition.*
- XVII. *Figure 3.7. TGA data representing weight loss % at different temperature for (a) MNP, (b) CNC, as well as MCNC prepared under (c) atmosphere condition, and (d) N₂ condition.*
- XVIII. *Figure 3.8. SAED image of sonochemically prepared MCNC under atmosphere condition.*
- XIX. *Figure 3.9. Magnetization curve for (a) MNP, MCNC prepared under (b) atmosphere condition, and (c) N₂ condition. The inset shows the negligible coercivity in all samples.*
- XX. *Figure 3.10. FTIR spectra of (a) Sample E1, in-situ with US, (b) Sample E2, in-situ with mechanical stirring, (c) Sample E3, without in-situ with US, and (d) Sample E4, without in-situ with mechanical stirring.*
- XXI. *Figure 3.11. STEM images of (a) E1, US assisted In-situ prepared MCNC, (b) E2, Mechanical stirred In-situ prepared MCNC, (c) E3, US assisted non-In-situ prepared MCNC, and (d) E4, mechanical stirred non-In-situ prepared MCNC. All scale bar are representing 300 nm.*
- XXII. *Figure 3.12 Histogram of MNPs diameter on the STEM images for (a) E1, US assisted in-situ prepared MCNC, and (b) E2, mechanical stirred in-situ prepared MCNC, and (c) E3, US assisted non-in-situ prepared MCNC.*
- XXIII. *Figure 3.13. TGA data representing weight loss % at different temperature for (a) E1, US assisted in-situ prepared MCNC, (b) E2, mechanically stirred in-situ prepared MCNC, (c) E3, US assisted non-in-situ prepared MCNC, and (d) E4, mechanically stirred non-in-situ prepared MCNC.*
- XXIV. *Figure 3.14 Magnetization plot of MCNC samples of (a) E1, US assisted in-situ prepared MCNC, (b) E2, mechanical stirred in-situ prepared MCNC, (c) E3, US assisted*

non-in-situ prepared MCNC, and (d) E4, mechanical stirred non-in-situ prepared MCNC. The inset shows the negligible coercivity in all samples.

- XXV. *Scheme 4.1. Schematic illustration of the hydrophilic groups on the surface of CNC and MCNC.*
- XXVI. *Figure 4.1. FTIR spectra of MCNC samples prepared with different CNC/MNP ratio, (a) 0.2, (b) 1, (c) 2, (d) 10, and (e) 20.*
- XXVII. *Figure 4.2. STEM images of (a) MCNC0.2, (b) MCNC1, (c) MCNC2, (d) MCNC10, and (e) MCNC20. The inset shows the images at higher magnification. All scale bar are representing 100 nm.*
- XXVIII. *Figure 4.3. (a) MNPs feret diameter in different MCNC samples, Standard error of mean of triplicate readings were represented by the error bars in each graph, different alphabetic letters was significantly different at $P \leq 0.05$ by Bonferroni's Multiple Comparison Test. (b) Histogram generated from the STEM images for the feret diameter of MNPs deposited on CNC. Samples (i) MCNC0.2, (ii) MCNC1, (iii) MCNC2, (iv) MCNC10, (v) MCNC20.*
- XXIX. *Figure 4.4. (a) Surface charge, and (b) photograph of water dispersion of (i) pure MNPs, (ii) MCNC0.2, (iii) MCNC1, (iv) MCNC2, (v) MCNC10, (vi) MCNC20, and (vii) pure CNC. Images captured 10 min after preparation.*
- XXX. *Figure 4.5. TGA data representing weight loss % at different temperature for (a) MCNC0.2, (b) MCNC1, (c) MCNC2, (d) MCNC10, and (e) MCNC20.*
- XXXI. *Figure 4.6. Magnetization plot of MCNC samples with CNC/MNP ratio of (a) 0.2, (b) 1, (c) 2, (d) 10, and (e) 20. The inset shows the negligible coercivity in all samples.*
- XXXII. *Figure 4.7. FTIR spectra of MCNC samples prepared at different pre-heated temperature, with (a) 25, (b) 45, (c) 65 and (d) 85 °C.*
- XXXIII. *Figure 4.8. STEM images with the respective histogram for MNPs deposited on MCNC samples prepared at different pre-heated temperature. (a) 25, (b) 45, (c) 65 and (d) 85 °C. All scale bar are representing 100 nm.*
- XXXIV. *Figure 4.9. TGA data representing weight loss % for MCNC samples prepared at different pre-heated temperature. (a) 25, (b) 45, (c) 65 and (d) 85 °C.*

- XXXV. *Figure 4.10. Magnetization plot of MCNC samples prepared under different pre-heated temperature. (a) 25, (b) 45, (c) 65 and (d) 85 °C. The inset shows the negligible coercivity in all samples.*
- XXXVI. *Figure 4.11. FTIR spectra of MCNC samples prepared at different US power, with (a) 40 w, (b) 60 w, and (c) 80 w.*
- XXXVII. *Figure 4.12. STEM images with the respective histogram for MNPs deposited on MCNC samples prepared at (a) 40, (b) 60 and (c) 80 w US power. All scale bar are representing 100 nm.*
- XXXVIII. *Figure 4.13. TGA data representing weight loss % at different temperature with US power of (a) 40, (b) 60 and (c) 80 w.*
- XXXIX. *Figure 4.14. Magnetization plot of MCNC samples prepared under different US power. (a) 40, (b) 60 and (c) 80 w. The inset shows the negligible coercivity in all samples.*
- XL. *Figure 4.15. FTIR spectra of MCNC samples prepared at different sonication time, with (a) 1 min, (b) 3 min, (c) 5 min, (d) 7 min, and (e) 10 min.*
- XLI. *Figure 4.16. STEM images with the respective histogram for MNPs deposited on MCNC samples prepared under (a) 1, (b) 3 (c) 5, (d) 7 and (e) 10 min ultrasonication. All scale bar are representing 100 nm.*
- XLII. *Figure 4.17. TGA data representing weight loss % at different temperature with sonication time of (a) 1, (b) 3, (c) 5, (d) 7 and (e) 10 min.*
- XLIII. *Figure 4.18. Magnetization plot of MCNC samples prepared under different sonication time. (a) 1, (b) 3, (c) 5, (d) 7 and (e) 10 min. The inset shows the negligible coercivity in all samples.*
- XLIV. *Figure 4.19. XPS spectra for (a) wide scan, (b) narrow scan Fe 2p and (c) narrow scan O 2p & valence band of MCNC nanocomposites prepared at (i) 1, (ii) 5 and (iii) 10 min ultrasonication time.*
- XLV. *Figure 4.20. Sulphate group content in medium containing various CNC/MNP ratio estimated by conductometric titration. Standard error of mean of triplicate readings were represented by the error bars in each graph, different alphabetic letters was significantly different at $P \leq 0.05$ by Bonferroni's Multiple Comparison Test.*

- XLVI. *Figure 4.21. EDX mapping for (a) sulphur content and (b) iron content in (i) pure CNC, (ii) MCNC20, (iii) MCNC10, (iv) MCNC2, (v) MCNC1, (vi) MCNC0.2, and (vii) pure MNP. MCNC samples were obtained under different CNC/MNP ratio.*
- XLVII. *Figure 4.22. Photographs of (a) CNC suspensions and (b) MCNC suspensions prepared under pH ranging from 1.5 to 13.0.*
- XLVIII. *Figure 5.1. Schematic representation for preparation of MCNC-PE.*
- XLIX. *Figure 5.2. Fresh Pickering emulsion produced with (a) 0.1 wt% pure MNP, (b) 0.1 wt% pure CNC, and (c) 0.1 wt% MCNC nanocomposite.*
- L. *Figure 5.3. Surface charge of Pickering emulsion stabilized by (black) pure MNP, (green) pure CNC, and (purple) MCNC nanocomposite. Standard error of mean of triplicate readings were represented by the error bars in each graph, different alphabetic letters was significantly different at $P \leq 0.05$ by Bonferroni's Multiple Comparison Test.*
- LI. *Figure 5.4. Fluorescent micrographs of MCNC-PE at pH 6 with double staining. Images (a) showing MCNC nanocomposites, (b) showing red palm oil phase, and (c) Combined image. (Red palm oil phase stained with Nile red, MCNC stained with calcofluor).*
- LII. *Figure 5.5. Magnetic attractability of the as-formulated MCNC-PE at pH 6 (left, small) and pH 3 (right, big) from point (A) to (B), (i) without EMF, (ii – vii) with EMF.*
- LIII. *Figure 5.6. Photograph of O/W Pickering emulsion stabilized by MCNC at (a) pH 1.5, (b) pH 2, (c) pH 3, (d) pH 4, (e) pH 5, (f) pH 6, (g) pH 7, (h) pH 8, (i) pH 9, (j) pH 10, (k) pH 11, (l) pH 12, and (m) pH 13. Image captured 10 minutes after preparation.*
- LIV. *Figure 5.7. (a) Raw size distribution data and (b) mean droplet diameters of MCNC-PE ranging from pH 1.5 to pH 13. Standard error of mean of triplicate readings were represented by the error bars in each graph, different alphabetic letters was significantly different at $P \leq 0.05$ by Bonferroni's Multiple Comparison Test.*
- LV. *Figure 5.8. Microscopic images of O/W MCNC-PE at (a) pH 1.5, (b) pH 2, (c) pH 3, (d) pH 4, (e) pH 5, (f) pH 6, (g) pH 7, (h) pH 8, (i) pH 9, (j) pH 10, (k) pH 11, (l) pH 12, and (m) pH 13.*
- LVI. *Figure 5.9. Zeta potential of MCNC particles as function of pH.*

- LVII. *Figure 5.10. Storage stability for MCNC-PE with 0.05 wt% MCNC, produced under (a) pH 6, and (b) pH 8. Image captured in (i) day 0, (ii) day 7, and (iii) day 14 of formulation. Line (x) indicating the point where emulsion samples were extracted for mastersizer analysis.*
- LVIII. *Figure 5.11. (a) Change in the volume fraction of the stable emulsion vs storage time for MCNC-PE at pH 6 and 8. (b) Change in emulsion droplets diameter of MCNC-PE at pH 6 and 8 up to 14 days of storage. (c) Microscopic images of MCNC-PE at pH 6 (Left), and pH 8 (Right), for (i) day 0, (ii) day 7, and (iii) day 14.*
- LIX. *Figure 5.12. (a) Raw droplet size distribution data and (b) Mean droplet diameters of MCNC-PE as a function of MCNC concentration (wt%). All formulations contain fixed φ_{oil} of 0.3. Standard error of mean of triplicate readings were represented by the error bars in each graph, different alphabetic letters was significantly different at $P \leq 0.05$ by Bonferroni's Multiple Comparison Test. (c) Microscopic images of Pickering emulsion prepared at the MCNC particle concentration, C_{mcnc} of (i) 0.025, (ii) 0.050, (iii) 0.100, (iv) 0.200, and (v) 0.300 wt%.*
- LX. *Figure 5.13. Changes in emulsion droplets diameter for MCNC-PE stabilized by MCNC nanocomposites at 0.025 to 0.300 wt% up to 14 days of storage.*
- LXI. *Figure 5.14. (a) Day 0 and (b) day 14 of photograph of O/W Pickering emulsion stabilized by MCNC at (i) 0.025, (ii) 0.050, (iii) 0.100, (iv) 0.200, and (v) 0.300 wt%. (c) creaming index, and (d) creaming rate of the respective Pickering emulsion.*
- LXII. *Figure 5.15. (a) Raw droplet size distribution data and (b) Mean droplet diameters of MCNC-PE prepared at different φ_{oil} of 0.1 to 0.5. All formulations contain fixed $C_{mcnc} = 0.100$ wt%. Standard error of mean of triplicate readings were represented by the error bars in each graph, different alphabetic letters was significantly different at $P \leq 0.05$ by Bonferroni's Multiple Comparison Test. (c) Microscopic images of MCNC-PE prepared at oil volume fraction, φ_{oil} of (i) 0.1, (ii) 0.2, (iii) 0.3, (iv) 0.4, and (v) 0.5.*
- LXIII. *Figure 5.16. (a) Changes of MCNC-PE droplet diameter as a function of φ_{oil} throughout 14 days of storage. (b) Fluorescent microscopic image of MCNC-PE prepared at $\varphi_{oil} = 0.1$ (40x magnification). All formulations contain fixed $C_{mcnc} = 0.100$ wt%.*

- LXIV. *Figure 5.17. Photographs of MCNC-PE at (a) day 0, and (b) day 14, (c) creaming profile and, (d) creaming rate of the MCNC-PE prepared using different ϕ_{oil} . All formulations contain fixed $C_{mcnc} = 0.100$ wt%.*
- LXV. *Figure 5.18. (a) Mean droplet diameters of MCNC-PE as a function of US power and time. Error bars represented the standard error in measurement. Raw droplet size distribution data of MCNC-PE under different US power at (b) 0.5, (c) 3 and (d) 7 min sonication time.*
- LXVI. *Figure 5.19. Optical microscopic images of MCNC-PE prepared using different US power at (a) 0.5, (b) 3 and (c) 7 min.*
- LXVII. *Figure 5.20. The creaming index and creaming rate of MCNC-PE prepared under different US power and sonication time. The inset shows a clearer view of the creaming rate of samples with sonication time of 2 min or longer.*
- LXVIII. *Figure 5.21. Changes in emulsion droplets diameter of MCNC-PE prepared under (a) 40, (b) 60 and (c) 80 W throughout a storage period of 30 days.*
- LXIX. *Figure 5.22. (a) Mean droplet diameter and creaming profiles of MCNC-PE as a function of ionic strength (mM NaCl). (b) Raw droplet size distribution data of Pickering emulsions using different NaCl concentrations. All formulations contain fixed oil, ϕ_{oil} of 0.3 and MCNC particle concentration, $C_{mcnc} = 0.100$ wt%, and was stored at room temperature for 14 days prior to measurement. (c) Microscopic images of MCNC-PE prepared NaCl concentration of (i) 0, (ii) 100, (iii) 200, (iv) 300, (v) 400, and (vi) 500 mM.*
- LXX. *Figure 5.23. MCNC dispersions (a) without NaCl, and (b) with 500 mM NaCl.*
- LXXI. *Scheme 6.1. Schematic illustration of the MCNC-PE stabilization-destabilization mechanism.*
- LXXII. *Figure 6.1. (a) Raw droplet size distribution data, (b) Mean droplet diameter, and (c) Optical micrograph of the MCNC-PE prepared at (i) 0.1, (ii) 0.2, (iii) 0.3, (iv) 0.4 and (v) 0.5 wt%. Error bar represents standard error in measurement. Different alphabetic letters were significantly different at $P \leq 0.05$ by Bonferroni's Multiple Comparison Test.*

- LXXIII. *Figure 6.2. Changes in the mean droplet diameter of MCNC-PE upon storage up to 14 days. Error bar represents standard error in measurement.*
- LXXIV. *Figure 6.3. Fluorescent microscopic images of Pickering emulsion stabilized with 0.5 wt% MCNC nanocomposite, showing the location of (a) MCNC nanocomposite, (b) oil globule and (c) MCNC-PE droplets.*
- LXXV. *Figure 6.4. (a) Mean droplet diameter of MCNC-PE prepared under different MCNC particle concentration as a function of pH without EMFs, and the respective droplet size distribution data at (b) 0.3, (c) 0.4 and (d) 0.5 wt% MCNC content. Error bar represents standard error in measurement.*
- LXXVI. *Figure 6.5. Optical microscopy and photograph of MCNC-PE stabilized using particles concentration of (a) 0.3 wt%, (b) 0.4 wt% and (c) 0.5 wt% at (i) pH 1.5, (ii) pH 3.0, (iii) pH 5.0, (iv) pH 7.5 and (v) pH 8.5 without EMF. The photograph of each emulsion is shown beside the optical microscope image.*
- LXXVII. *Figure 6.6. (a) Mean droplet diameter of MCNC-PE prepared under different MCNC particle concentration as a function of pH with EMFs, and the respective droplet size distribution data at (b) 0.3, (c) 0.4 and (d) 0.5 wt% MCNC content. Error bar represents standard error in measurement.*
- LXXVIII. *Figure 6.7. Optical microscopy and photograph of MCNC-PE stabilized using particles concentration of (a) 0.3 wt%, (b) 0.4 wt% and (c) 0.5 wt% at (i) pH 1.5, (ii) pH 3.0, (iii) pH 5.0, (iv) pH 7.5 and (v) pH 8.5 with EMF. The photograph of each emulsion is shown beside the optical microscope image.*
- LXXIX. *Figure 6.8. Temperature variation of MCNC-PE with and without its exposure to EMF.*
- LXXX. *Figure 6.9. Mean droplet diameter of MCNC-PE after various destabilization and stabilization cycles with/without the presence of an EMF. The error bar represents the standard error in measurement. Different alphabetic letters were significantly different at $P \leq 0.05$ by Bonferroni's Multiple Comparison Test.*
- LXXXI. *Figure 7.1. Mean droplet diameter of the curcumin-loaded MCNC-PE. Error bar represents standard error in measurement. Inset shows the raw droplet size distribution data.*

- LXXXII. *Figure 7.2. Percent retention of curcumin in Pickering emulsions stabilized with 0.1 wt% MCNC particles. Black arrow indicates the loading efficiency of curcumin in the respective sample. Error bar represents standard error in measurement.*
- LXXXIII. *Figure 7.3. Optical microscopic image and photograph of curcumin-loaded MCNC-PE at pH 7.5 (a) without and (b) with exposure to oscillating EMFs.*
- LXXXIV. *Figure 7.4. (a) Percent curcumin released from different emulsion samples under pH 7.5. (b) Plots of the release of curcumin from the both MCNC-PEs samples based on Korsmeyer–Peppas model.*
- LXXXV. *Figure 7.5. Cell viability test of curcumin-loaded MCNC-PE on HCT116 colon cancer cell line. The cell line analysis was performed using MCNC-PE stabilized by 0.1 wt% of MCNC nanocomposite, with curcumin content of 30 µg/ml of incubation serum (equivalent to 1 mg/ml oil basis). Error bar represents standard error in measurement. Different alphabetic letters was significantly different at $P \leq 0.05$ by Bonferroni's Multiple Comparison Test.*
- LXXXVI. *Figure 7.6. Cell viability test of MCNC suspensions with or without EMF on HCT116 colon cancer cell line. The cell line analysis was performed using 0.1 wt% of MCNC nanocomposite. Error bar represents standard error in measurement. Different alphabetic letters was significantly different at $P \leq 0.05$ by Bonferroni's Multiple Comparison Test.*
- LXXXVII. *Figure 7.7. Morphological changes of HCT116 cells at different time point for (a) control, (b) pure curcumin, (c) blank MCNC-PE, (d) curcumin-loaded MCNC-PE and (e) curcumin-loaded MCNC-PE + EMF treated samples.*
- LXXXVIII. *Figure 7.8. Nuclear morphology changes of HCT116 cells at 24 hour incubation for (a) control and (b) curcumin-loaded MCNC-PE treated samples.*
- LXXXIX. *Figure 7.9. Fluorescence and bright field-fluorescence overlay images of HCT116 cells after 2 hours incubation (a) without and (b) with Nile red stained MCNC-PE.*

CHAPTER ONE

INTRODUCTION

1.1 Research Background

By definition, Pickering emulsions are new class of emulsion stabilized by fine solid particles of intermediate wettability at the interface between two immiscible liquids (e.g. oil/water interface). Recently, there have been a renewed interest in these colloidal particle-stabilized systems in the past decade due to the new emerging applications of Pickering emulsion in oil recovery (Sharma, Kumar, and Sangwai, 2015), composites (Kim *et al.*, 2013) and drug delivery (Frelichowska *et al.*, 2009). Pickering stabilization was first reported by Walter Ramsden (Ramsden, 1903) and Spencer Umfreville Pickering in 1907 (Pickering, 1907), and these particle-laden interfaces possess remarkable resistance against coalescence compared to conventional emulsions stabilized by classic surfactant. In Pickering emulsions, the adsorption of solid particles onto the deformable interface is virtually irreversible thus high energy is required for detaching the adsorbed particles from the interface. The ability of solid particles to adhere to fluid-fluid interfaces has resulted in the widespread use of Pickering emulsion in food, cosmetics, and personal care products in which valuable ingredients and nutrients are encapsulated in the dispersed phase as the active cargo to be delivered (Dickinson, 2012; Marefati *et al.*, 2015; Wahlgren *et al.*, 2013). Besides, Pickering emulsions offer many advantages over traditional surfactant-stabilized emulsions, including lower cost and lower toxicity (Dyab *et al.*, 2014), self-assembly capability (Fujii, Okada, and Furuzono, 2007), enhanced long-term stability (Melle, Lask, and Fuller, 2005) and reduced foaming during preparation (Binks, 2002) because of their “surfactant free” character.

In the past decade, a variety of particulate emulsifier have been explored to prepare Pickering emulsion throughout the literatures. Some of the examples include latex-, laponite-, carbon black-, silica-, gold-, and calcium carbonate-based inorganic solids (Chevalier and Bolzinger, 2013). It is generally recognized that these particles are able to effectively adsorb at the oil–water interface, forming a dense film (monolayer or multilayer)

around the dispersed drops impeding coalescence, however, such inorganic particles are limited in their relevance in applications requiring biocompatibility and biodegradability. Furthermore, some of the particles require complex and laborious synthesis procedures and these particles tend, more often than not, to aggregate or fuse completely forming larger non-spherical structures. Thus, there has been a shift toward studying biologically derived materials for the stabilization of emulsion systems. Many biomacromolecules like chitin nanocrystal particles (Liu *et al.*, 2012; Nan *et al.*, 2014; Wei *et al.*, 2012), modified starch nanocrystals (Li, Sun, and Yang, 2012; Tan *et al.*, 2012), soy protein nanoparticles (Liu and Tang, 2013), and flavonoids (Luo *et al.*, 2011) have emerged as potential and versatile Pickering emulsifiers due to their biodegradability, ease of modifications, cost effectiveness, and wide availability. These excellent properties render these bio-based Pickering stabilizers appealing in both fundamental research fields and in industries.

On recent strong trend, the design of CNC-based nanocomposite has become an intense field of research due to their eco-friendliness and attractive combination of properties such as biodegradability, biocompatibility, high aspect ratios (length-to-width), high surface-to-volume ratios, optical transparency and flexible surface chemistry (Capron and Cathala, 2013; Cunha *et al.*, 2014; Kalashnikova *et al.*, 2011; Zoppe, Venditti and Rojas, 2012). In the present study, author, for the first time, proposed the preparation of magnetic cellulose nanocrystals hybrid nanocomposite as novel Pickering emulsifiers. When incorporated in pharmaceutical emulsion systems, they can be used to magnetically guide drug-containing droplets at the targeted tumor site, and subsequently release the encapsulated drug in a controlled manner upon application of a local high frequency alternating magnetic field. Or due to the magnetic hyperthermia effect (Reddy *et al.*, 2012). To achieve this, we will first strongly combine the CNC with Fe_3O_4 to form a hybrid Fe_3O_4 @CNC (MCNC) nanocomposite via a facile one-step ultrasound (US)-assisted *in-situ* co-precipitation technique. The surface and interfacial properties as well as the physicochemical properties of the as-synthesized MCNC nanocomposite will be characterized. Then, the obtained MCNCs will be applied to form Pickering emulsion and their impact on the colloidal stability will be investigated systematically. As part of this

work, the effects of drug loading and *in-vitro* release behaviour of MCNCs-stabilized Pickering emulsions (MCNC-PE) will also be studied by using curcumin as a model drug. These research phases are shown schematically in Figure 1.1. It is deduced that these magnetically driven Pickering emulsion may enhance the stability and shelf life of a drug formulation, while permitting the controlled delivery of active pharmaceutical ingredients when desired in response to magnetic field.

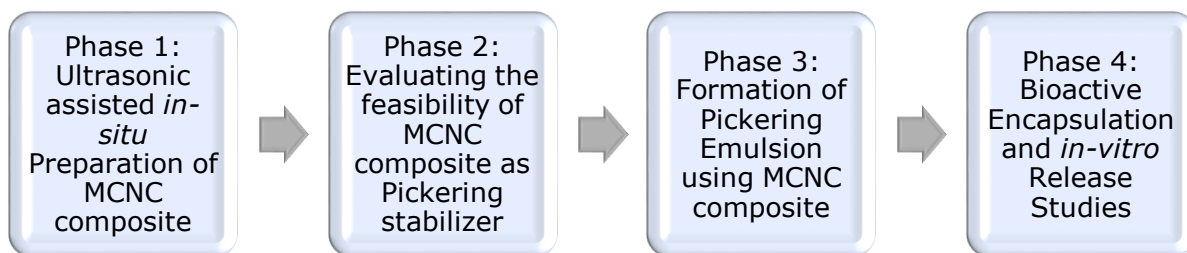


Figure 1.1. An illustration showing the four phases in this project.

1.2 Problem Statements

Cellulose is the most abundant and versatile biopolymer in nature. Cellulose nanocrystals (CNCs) are extracted from several kinds of cellulose, such as tunicate, cotton, straw as well as bacterial cellulose. In the past decade, CNCs have gained more and more attention in the nanotechnology field because of their stimuli and combination properties, including such as biocompatibility, a high elastic modulus, low density and thermal expansion coefficient, optical transparency and anisotropy, chemical tunability and environmentally sustainability making it of interest in applications such as green nanocomposites (Dufresne, 2006), security film (Zhang *et al.*, 2012), wound dressings and medical implants (Webster, 2007). In the recent literature, an extensive list of cellulose and CNC-based materials has been presented and they show great potential for biomedical applications.

Possessing excellent biodegradability and biocompatibility properties, CNCs has recently attracted a great deal of research interest in the pharmaceutical industry, in particular as novel drug carriers for various routes of administration. For instance, Lin *et al.* (2011) developed a pH-sensitive CNC/sodium alginate microsphere as controlled drug delivery systems. The incorporation of CNC in alginate-based microspheres gave rise to

higher encapsulation efficiency and prolong drug release in addition to a more consistent swelling patterns. Similarly, Akhlaghi, *et al.* (2013) demonstrated that using polymer grafting technique, novel (CNC)/chitosan oligosaccharide hybrid bio-nanocomposites were synthesized and the study showed that they could be used as potential drug carriers for transdermal delivery applications. More recently, Rescignano *et al.* (2014) had successfully combined CNC and poly (D,L-lactide-co-glycolide) (PLGA) nanoparticles (NPs) loaded with bovine serum albumin fluorescein isothiocyanate conjugate (FITC-BSA) and the formed PVA/CNC/NPs-based composites appeared to be promising potential vehicle for both localized and fast controlled drug delivery. Nevertheless, these novel CNC-based nanomaterials lack of active targeting properties, making them difficult to obtain satisfactory therapeutic efficacy, thus limiting their applications in the clinical settings.

Hence, creating CNC-based drug vehicle containing stimuli-sensitive components, able to respond to externally applied triggers will be essential and beneficial to pave the way for greater acceptance of nanocellulose as an ideal sustainable biomaterial in pharmaceutical applications. In the present study, author, for the first time, proposed to develop a magnetically responsive Pickering emulsion based on magneto-sensitive CNCs to be used as a novel controlled drug delivery carrier. The applications of magnetic cellulose nanomaterials with tailored surface functionalities have, in fact, been reported and suggested as magnetic aerogel (Olsson *et al.*, 2010), magnetically retrievable oil absorbent (Chin *et al.*, 2014), recyclable catalyst (Xiong *et al.*, 2013). However, the application of proposed Fe₃O₄@CNC (MCNC) nanocomposite has yet to be explored in literature for the preparation of Pickering emulsions and this is an interesting aspect as there are so far no data available on the mechanisms of stabilization and drug controlled release of this magnetically controllable colloidal delivery systems. Furthermore, the therapeutic efficacy of this novel MCNC-based Pickering stabilizer encapsulating anti-tumor drug is also worthy of study. This remains a major research gap that is addressed in this proposed work.

1.3 Aims and Objectives

The aim of current proposed work is to produce a new MCNC-stabilized Pickering emulsion (MCNC-PE) with the goal of utilizing them as cargo for controlled drug delivery application.

The following objectives listed are to be met in order to achieve the main goal of the study.

1. To synthesize MCNC nanocomposites via ultrasound-assisted *in-situ* synthesis under atmospheric conditions.
2. To characterise MCNC nanocomposites in term of magnetivity, wettability, size, morphology, and compositions.
3. To produce stable Pickering emulsion droplets using fabricated MCNC nanocomposites and determine its magnetic- and pH-responsivity.
4. To investigate the drug loading and *in-vitro* release behaviour of the MCNC-PE.

1.4 Contribution of Studies

The controlled delivery of pharmaceutically active ingredients is of considerable interest in drug delivery application. Stimuli-responsive Pickering emulsions are regarded as useful tool with great potentials in the pharmaceutical sectors to incorporate and deliver drug or active cargos to provide the desired outcome. Several triggering approaches include chemical, biological, light and thermal stimuli have been developed to release the encapsulated emulsion contents. Magnetically-induced release is an especially enticing drug delivery method because rapid and controlled release of the payload is possible at the site of interest upon the application of magnetic field. In the present work, the proposed study contributes to the design and manufacture of smart magneto-responsive Pickering emulsion systems as new controlled drug delivery systems. This research enables to prove that MCNC nanocomposite could be a green and effective Pickering stabilizer for the generation of pharmaceutical grade emulsions. This study will provide an important additional perspective that is complementary to the current state of understanding of environmentally-responsive Pickering emulsions, and we hypothesize that the success of this new generation of therapeutic formulation will benefit and revolutionize the current and emerging research on the design and development of smart CNC-based drug delivery systems.

CHAPTER TWO

LITERATURE REVIEW

2.1 Pickering Emulsion Formation

2.1.1 Nanoparticles as Stabilizer for Pickering Emulsion

Pickering emulsion is an emulsion of oil-in-water (o/w) or water-in-oil (w/o) stabilized by solid particles in place of surfactants. The 'surfactant-free' characteristic makes Pickering emulsions as an attractive formulation in numerous applications including food, cosmeceutical and pharmaceutical where surfactants often caused adverse effects, i.e. cytotoxicity, irritancy, and gastric discomfort. Solid stabilization leads to high energy particles' attachment at liquid-liquid interfaces, thus resulting in excellent emulsion stability against coalescence. Based on earlier studies, successful evidence of Pickering emulsion stabilized by surface-modified magnetite nanoparticles had been reported by Qiao *et al.* (2012) and Zhou *et al.* (2012). The nano-size magnetite was reported to remarkably stabilize emulsion droplets as small as few micrometres.

For Pickering emulsion, the stabilization of emulsion droplets occurred when the solid nanoparticles are attached to the interface between emulsion droplets and the continuous phase. The particles attachment are almost irreversible because the energy required for detachment is extremely high. The energy can be calculated from Equation (2.1) (Katepalli, 2014):

$$\Delta E = \pi r^2 \gamma_{ow} (1 - |\cos \theta_{ow}|)^2 \quad [\text{Equation 2.1}]$$

Where r is the particle radius (m), γ_{ow} is the oil-water interfacial tension (N/m). The types of Pickering emulsions (either o/w or w/o) formed are strongly dependents on the particles partial wettability (or contact angle θ_{ow} with water and oil) (Binks and Lumsdon, 2000c). Hydrophilic particles with $\theta_{ow} < 90^\circ$ have the ability to stabilize o/w emulsions, while hydrophobic particles with $\theta_{ow} > 90^\circ$ are able to stabilize w/o emulsions (as shown in Figure 2.1).

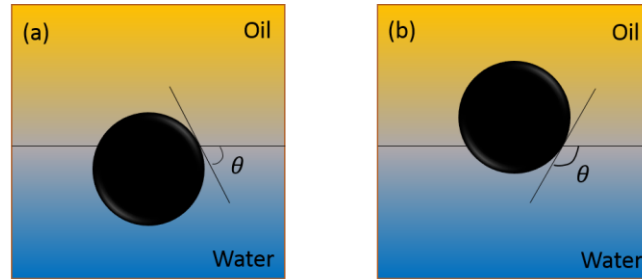


Figure 2.1. Graphical illustration of solid particles with different wettability (contact angle) at the interface of two immiscible liquids. (a) $\theta < 90^\circ$, and (b) $\theta > 90^\circ$.

2.1.2 Destabilization Mechanisms

The most stable condition between two immiscible liquid is when the system attains minimum free energy (minimal contact area between the two phases) (Pichot, 2010). Therefore, emulsions are considered thermodynamically unstable since emulsification involved homogeneous mixing of two immiscible phases (i.e. oil and water) that will eventually lead to an increase in oil-water contact area (higher free energy). In Pickering emulsions formation, the high energy particles' attachment at liquid-liquid interfaces forms a barrier that promotes great defences for the emulsions against coalescence, which in turn delayed the phase separations process. However, an enhanced defence against destabilization does not always mean a total prevention. Pickering emulsions are still subjected to destabilisation in terms of various mechanisms similar to that of surfactant stabilized emulsions such as Ostwald ripening, coalescence, flocculation, sedimentation, and creaming. These mechanisms are highly interrelated to each other in term of definitions. Concisely, Ostwald ripening occurs as an outcome of the steady growth of larger droplets by expensing the smaller droplets, where those tiny droplets formed initially would disappear in time (Tcholakova *et al.*, 2008). This phenomenon. In brief, indicated the diffusion of small droplets into larger one. This is highly similar to the coalescence incident where smaller droplets collided with each other to form a larger ones (Marruchi, 1969), and the flocculation where fine droplets clump together into a floc (Guzey and McClements, 2006). When coalescence occurred, the flocs/larger droplets may either settled down (sedimentation) or floated (creaming) due to gravitational separation (Choi *et al.*, 2014)

and finally leads to phase separation. Figure 2.2 shows the schematic explanation of the de-stabilizing phenomena mentioned.

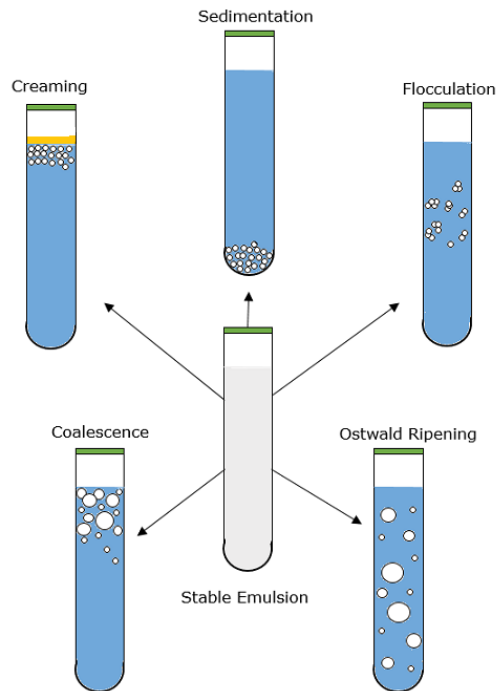


Figure 2.2. Graphical illustration of different destabilization mechanisms on emulsion.

2.1.2.1 Interfacial Free Energy

As described earlier, a system with minimum contact area between two immiscible liquid specifies the minimum free energy condition. To achieve that small droplets tend to collide with each other to form larger emulsion droplets with lower free energy. As expressed in Equation (2.2) (Jatin, Somnath, and Dash, 2010), an increase in contact area between the two immiscible liquid pointers to free energy (ΔG) increment in the system (and vice versa). Therefore, emulsion droplets size provide a good indication of the interfacial free energy and so it is an important parameter to monitor in order to determine the stability of an emulsion.

$$\Delta G = \gamma_{ow}A \quad \text{[Equation 2.2]}$$

Where γ_{ow} is the oil-water interfacial tension (N/m), and A is the total interfacial area (m²).

2.1.2.2 Interaction Potential

The interaction potential between emulsion droplets shows whether repulsive or attractive force dominates. It is expressed as the sum of van der Waals, electrostatic, and short-range interactions (Equation 2.3) (Demetriades, Coupland, and McClements, 1997).

$$V_{Tint} = V_{vdw} + V_e + V_{sr} \quad \text{[Equation 2.3]}$$

Where V_{Tint} , V_{vdw} , V_e , and V_{sr} are total, van der Waals, electrostatic, and short-range interaction respectively.

In particular, *van der Waals* interactions are normally attractive. Electrostatic interactions, on the other hand, are usually repulsive since the particulate emulsifier used in Pickering emulsion generation are usually having similar charges. Lastly, short-range interaction occurs when droplets emulsifier layers started to overlap. In this situations, both repulsive (steric and thermal fluctuation) and attractive interactions (hydrophobic and depletion) may take place depending on the nature of the emulsions and particulate emulsifier (Dickinson, 1992; Israelachvili, 1992; Walstra, 1996). The three types of interactions mentioned could be effectively examined through optical visualization under a microscope.

2.1.2.3 Gravitational Separation

Gravitational separation or phase separation are interrelated to sedimentation and creaming. It happened mainly regarded to the density differences between the continuous phase and disperse phase that causes the lighter phase to move up while the heavier phase settles down. This separation can be explained by Stoke's equation (Equation 2.4).

$$v = \frac{2gr^2(\rho_{cont} - \rho_{disp})}{9\mu_{cont}} \quad \text{[Equation 2.4]}$$

Where v is the settling velocity by gravity (m/s), r is the droplet radius, g is the gravitational force (m/s^2), μ is the viscosity of continuous phase (kg/ms), ρ_{cont} and ρ_{disp} are the density of continuous and disperse phase respectively (kg/m^3).

Gravitational effects can be examined by simply measuring the volume fraction of cream/sediment in emulsions in accordance with time.

2.1.3 Methods of Pickering Formation

Much equipment have been invented recently for the production of emulsions/Pickering emulsions. In this section, the rotor-stator and ultrasound (US) system on two Pickering emulsion production methods (rotor-stator and ultrasonic system) will be focused.

Rotor-stator system utilizes mechanical energy that drives the droplet disruptions. It is one the most commonly used homogeniser (Schubert and Engel, 2004). Its operation involved high-speed agitation that emulsified every ingredient present in a vessel. Thus, the size of emulsion droplets produced under this method is directly affected by the rotating speed and homogenizing time. Next, US system is a famous and green system for emulsification of oil globules (Chen *et al.*, 2011). It employed ultrasonic acoustic wave to create instability to the bulk system and caused droplets formation (Pichot, 2010). These coarse droplets are then disrupted further by the high energy acoustic cavitation to reduce the oil globule size. In the US system, parameters that have the most effect on Pickering emulsion sizes would be ultrasonic power and sonication time.

2.1.4 Factors affecting Pickering Emulsion Properties and Stability

Emulsion stability often refers to the ability of an emulsion to stay away from properties variation over a period of time. Factors affecting the stability and characteristics of Pickering emulsion includes Particles partial wettability (or hydrophobicity), particulate emulsifier size, concentration, oil type, oil/water ratio, and electrolyte concentration. As mentioned in section 2.1.1, types of Pickering emulsion and strength of particles adsorption at the oil-water interface depends on its partial wettability. In short, particles must be partially wettable by both liquids in order to get adsorbed at the interface. Therefore, excessive in hydrophobicity or hydrophilicity would retard the particle adsorption at the interface, and consequently failing the generation of stable Pickering emulsion. From literature, Kaptay (2006) claimed that optimum θ_{ow} for o/w emulsions falls between 70 – 86°, and 94 – 110° for w/o type emulsions.

Since Pickering emulsion is stabilized by adsorbing particles at the oil/water interface of emulsion droplets, smaller particle size would results in smaller emulsion droplets

because smaller particles favoured lesser voids available on the Pickering emulsion droplets (as expressed in Figure 2.3). However, these Pickering emulsion droplets generated by smaller particles may not be as stable as those prepared by larger particles. This can be explained via equation 1. With fixed interfacial tension and interfacial contact angle (same oil/water content, same particulate emulsifier), detachment energy, E is a function of particle size ($E = f(r^2)$). Therefore, smaller particles lead to lower detachment energy, and thus the Pickering emulsion formed will ease the destabilization. Henceforth, there will always be an optimum ratio between particulate emulsifier and Pickering emulsion sizes for the generation of small yet stable Pickering emulsions. This theory was further supported by Pichot's research where phase separation was observed on emulsions prepared with silica particles of size 50 nm, but not on the emulsions stabilized by larger particles (85 nm and 120 nm) (Pichot, 2010).

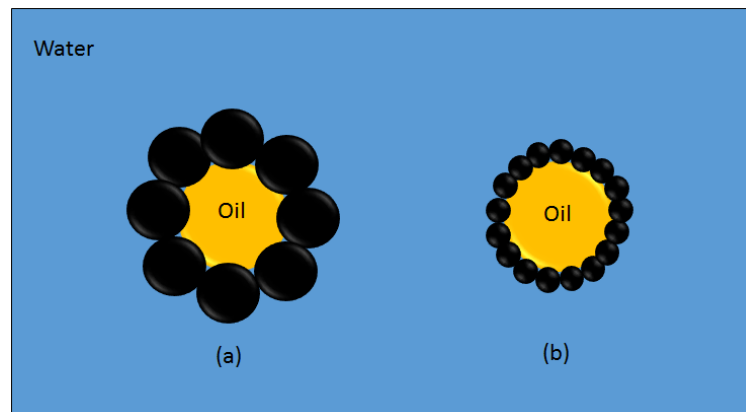


Figure 2.3. Schematic view of Pickering emulsion droplet stabilized by (a) larger size particles and (b) smaller size particles.

The concentration of solid particles also affects the stability of Pickering emulsion. The reason behind is mainly attributed to the low coverage of emulsion droplets by particles that resulted in the insufficient repulsive barrier against coalescence (Tambe and Sharma, 1993). At higher particles concentration, more colloids are available in the system particles adsorption. This contributed to limited coalescence where the emulsion droplets only coalesced up to a point where the Pickering barrier is sufficient for shielding the coalescence (see Figure 2.4). This principle was braced by several other researchers in literature. For

example, Kalashnikova *et al.*, (2011), and Zoppe and others (2012) work shows that emulsion stability was enhanced with increased nanocellulose concentration in the system. Furthermore, they also showed that emulsions droplet size could be controlled by controlling the nanocellulose concentration.

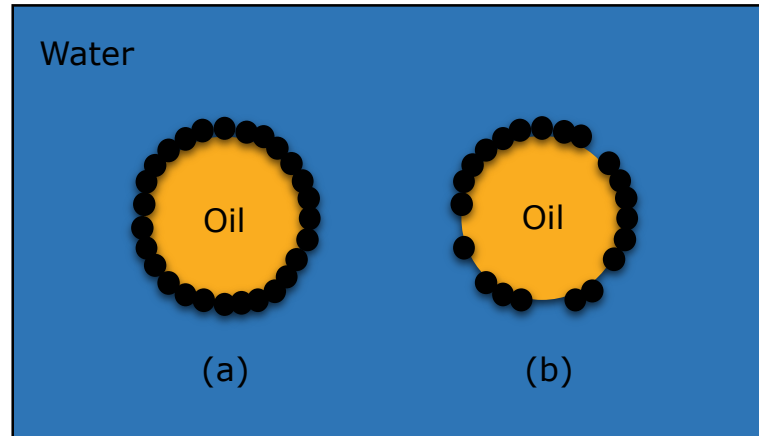


Figure 2.4. Schematic view of (a) high particles concentration versus (b) low particles concentration in stabilizing Pickering emulsion droplet.

Moving on to oil type and oil/water ratio, Binks and Lumsdon (2000b) reported that with particles of intermediate hydrophobicity (approximately 90°), o/w emulsion type is more preferred when non-polar oils such as that formed by hydrocarbons is used, whereas w/o is preferable when polar oils such as esters and alcohols are used. The reason behind is again related to equation 1, the oil-water interfacial tension γ_{ow} and particles contact angle at interface θ_{ow} that has direct effects on detachment energy. Non-polar hydrocarbons oil with high γ_{ow} exhibit low values of θ_{ow} and thus favour o/w emulsions, and polar alcohols or esters with low γ_{ow} would increase the θ_{ow} values and gives w/o emulsions (Binks and Lumsdon, 2000b). Besides oil type, the same research group also investigated on effects of oil/water ratio on emulsion types and stability. Their research showed that at w/o types were formed with increased oil/water ratio (high oil fraction) and o/w emulsion were acquired at a reduced ratio (Binks and Lumsdon, 2000b).

Lastly, emulsion stability can also be altered by changing the electrolyte/salt concentration. In particular, the addition of salts contribute to the reduction of particles

surface charge and thus causing flocculation of particles. From literature, Binks and Lumsdon (2000a) reported that stability of emulsion with the addition of salt is strongly dependent on the types of particulate emulsifier employed in the system. For instance, with the addition of salt, no emulsion was formed when hydrous maghemite (Fe_2O_3) is used as the particulate emulsifier (Binks and Lumsdon, 2000a). However, for aerosil silica particles and nanocellulose, stable emulsions will only be produced if particles were flocculated by salt (Binks and Lumsdon, 2000a; Zoppe, Venditti and Rojas, 2012). This phenomenon is related to the particles surface charge. If the particles originally possessed high charges, its repulsion force will hold as a barrier to retard the stability of the emulsions. Thus a certain amount of salt is required to be added into the particles suspension to screen its surface charge to favour stable emulsions. On the other hand, if the particle's surface charge is low, further addition of salt will merely cause the reduction of the charges and trigger coalescence between particles, resulting in destabilization of the emulsions.

2.1.5 Types of Particulate Emulsifier

Types of particulate emulsifier can be categorized into inorganic and organic molecules, with inorganic particles dominating in the literature (Binks and Lumsdon, 2001) due to their availability in different size and shape as well as the existence of their surface functional groups, which makes them possible for modification (Lam *et al.*, 2014). In spite of these benefits, most of these inorganics are not biocompatible nor biodegradable. Hence, in recent years significant attentions have been paid to Pickering emulsion stabilization using organic-based materials as the particle-based stabilizer that is biocompatible, biodegradable, non-toxic, and widely available. Previous studies had reported that there are many organic or hybrid (mixture of organic and inorganic) nanoparticles that are biocompatible while able to be used as Pickering stabilizer for emulsion. Some common examples are clays (Ashby and Binks, 2000), magnetic particles (Melle, Lask and Fuller, 2005; Qiao *et al.*, 2012; Zhou *et al.*, 2012), natural latex (Binks and Lumsdon, 2001; Gautier *et al.*, 2007), Nanocellulose (Capron and Cathala, 2013; Cunha *et al.*, 2014;

Kalashnikova *et al.*, 2011; Zoppe, Venditti and Rojas, 2012), chitosan (Liu *et al.*, 2012; Nan *et al.*, 2014; Wei *et al.*, 2012), and so on (Chevalier and Bolzinger, 2013).

These nanoparticles were chemically grafted or surface adsorbed with other chemicals to achieve the circumstance of partial wetting by water and oil. Between the two techniques mentioned, chemical grafting is able to produce solid nanoparticles with grafts attached tightly on its surface, whereas adsorbed molecules in equilibrium with free molecules and bulk phase may undergo desorption when the equilibrium condition altered (Chevalier and Bolzinger, 2013). Although the procedure of chemical grafting method is much complex as compared to the surface adsorption method (Chevalier and Bolzinger, 2013; Lee *et al.*, 2006; Skaff *et al.*, 2002). It allowed the formation of a solid composite with better physicochemical stability as compared to the adsorbed ones. Thus, chemical grafting approach is focused in this project to synthesize magneto-responsive nanocellulose that will be further utilized for the formation of Pickering emulsion.

2.2 Green Pickering Emulsion Stabilizer: Nanocellulose

To date, this world is more and more concerned about the development of environmentally friendly and renewable resources. Same goes for the research community where the development of renewable biomaterials for advanced applications has been recently gained momentum (Hamad, 2006; Kamel, 2007). In particular, cellulose is an attractive material source that has been the main focused of researchers nowadays due to its availability, biodegradability, renewability, and amenability for surface modification (Kalashnikova *et al.*, 2011; Zoppe, Venditti and Rojas, 2012). The cellulose that contained crystalline and amorphous regions, could be subjected to various preparation methods to yield rod-like nanocrystals with even more unique surface, optical, and mechanical properties (Dufresne, 2008; Habibi *et al.*, 2010). In overall, classes of nanocellulose can be categorized into three groups depending on their sources, dimensions, and preparation methods. They are termed as microfibrillated cellulose (MFC), bacterial nanocellulose (BNC), and cellulose nanocrystal (CNC). Table 2.1 showed a brief summary of the differences between the three mentioned groups of nanocellulose. From literature, many examples have shown that stable Pickering

emulsion formation is feasible with the use of surface modified/unmodified nanocellulose. These examples will be mentioned in the subdivision in this section.

Table 2.1. Differences between nanocellulose types (adapted from (Zhen, 2015)).

Nanocellulose type	Synonyms	Synthesis method	Dimensions
Microfibrillated cellulose (MFC)	<ul style="list-style-type: none"> Cellulose nanofibril (CNF) Nanofibrillated cellulose (NFC) 	<ul style="list-style-type: none"> Mechanically de-structuring 	<ul style="list-style-type: none"> Diameter: 5 – 60 nm Length: up to several micrometres
Bacteria nanocellulose (BNC)	<ul style="list-style-type: none"> Bacterial cellulose Biocellulose Microbial cellulose 	<ul style="list-style-type: none"> Bacterial biosynthesis 	<ul style="list-style-type: none"> Diameter: 20 – 100 nm Length: up to several micrometres
Cellulose nanocrystal (CNC)	<ul style="list-style-type: none"> Nanocrystalline cellulose (NCC) Nanowhisker 	<ul style="list-style-type: none"> Acid hydrolysis 	<ul style="list-style-type: none"> Diameter: 5 – 70 nm Length: up to few hundred nanometres

2.2.1 Microfibrillated Cellulose (MFC)

MFC is also named as cellulose nanofibril (CNF) or nanofibrillated cellulose (NFC). Its typical dimensions are ranging from 5 to 60 nm for diameter and up to several micrometres in length. They are normally produced through mechanically induced de-structuring approach (Zhen, 2015). However, the process for its production often required high-energy consumption due to the employment of high-power homogenizers (Zimmermann, Bordeanu and Strub, 2010). From recent collected works, MFC is found to have good ability to form a rigid network due to its high length to diameter aspect ratio and low percolation level. Furthermore, it has adjustable hydrophobicity and is non-toxic. Thus, it has been the choice

for researchers to be utilized in stabilizing Pickering emulsion droplets for oil recovery and drug delivery applications (Zhen, 2015).

2.2.2 Bacterial Nanocellulose (BNC)

Moving onto BNC, it was biosynthesized from bacteria strains as resulted from explicit environments (Zhen, 2015). Unlike the MFC and CNC that are obtained from fibre cellulose, BNC is the product of the excretion of bacteria as exopolysaccharide through bioassembly processes from nutrient media (Cherian *et al.*, 2013; Zhen, 2015). The dimensions of BNC are controllable over the length scale of nano to micron scale, and its properties could be engineered by regulating the substrates, cultivation conditions, additives, and bacteria strain. Because BNC is morphologically similar to collagen and proved to have no foreign-body reaction, it has been widely exploited for many medical applications namely biological implant, cell immobilization, cell support and others (Gatenholm and Klemm, 2010). As for its application in stabilizing Pickering emulsion, Kalashnikove *et al.* (2011) performed an examination of forming Pickering emulsion using bacterial nanocellulose and received a positive outcome with stable Pickering micro-emulsion.

2.2.3 Cellulose Nanocrystal (CNC)

CNC has synonyms of cellulose nanowhiskers and nanocrystalline cellulose (NCC). It is favoured from acid hydrolysis. Its surface functionality depends highly on the acid used for hydrolysis (Zhen, 2015). CNC produced is neutral charged under hydrochloric acid (HCl) hydrolysis, and is highly negatively charged if sulphuric acid hydrolysis is taken place to form the CNC since sulphuric acid hydrolysis provides uniform aqueous dispersions and the ability to self-assemble into chiral-nematic liquid crystals due to the presence of sulphate ester groups installed on the surface (Dong *et al.*, 1998; Elazzouzi, 2006). It has a similar diameter range to MFC but the length is much shorter than that of both MFC and BNC (only up to few hundred nanometers). Many examples have shown that stable Pickering emulsion formation is feasible with cellulose nanocrystal, for example, Kalashnikove *et al.* (2012)

formed stable Pickering emulsion using unmodified cellulose nanocrystal, Hu *et al.* (2015) and Zoppe and others, (2012) produced stable Pickering emulsion with surface modified cellulose nanocrystal.

In overall, the use of nanocellulose as the stabilizer for Pickering emulsions is more advantageous over some inorganic nanoparticles when considering biocompatibility, biodegradability, density, and cost issues. Thus in this project, Fe₃O₄@CNC (MCNC) nanocomposite will be focused, aimed not only to produce green Pickering emulsion droplets but also with magnetic properties, for targeted controlled drugs delivery processes.

2.3 Surface Functionalization of Cellulose Nanocrystal (CNC)

The surface functionality of CNC depends highly on the acid used for the hydrolysis process. In brief, CNC will be neutrally charged under hydrochloric acid (HCl) hydrolysis while highly negatively charged under sulphuric acid (H₂SO₄) hydrolysis due to the introduction of sulphate ester groups onto its surface (Zhen, 2015). To utilize CNC in drug delivery technology, researchers often incorporate CNC with certain fillers to introduce one or multiple stimuli-responses and to control its stability. Extra properties including thermal, photoluminescent, conduction, magnetic properties and others have been investigated to date. In this section, a few examples of modified CNC will be concisely reviewed for thus far works and for future potential applications.

2.3.1 Thermal Properties

Thermos-responsive CNC has been well reported to control the colloidal stability of CNC. It was found that thermo-reversible aggregation could be introduced to CNC activate the self-assembling and disassembling functionalities (Wu *et al.*, 2015; Zoppe, Venditti and Rojas, 2012). Such response to temperature is advantageous especially when the particles are utilized in Pickering emulsion stabilization. As previously noted, Pickering emulsion stabilizer often required very high mechanical energy for desorption to happen as compared to the surfactant-stabilized emulsion. The introduction of temperature-sensitive properties allowed one to effectively control the stability of the Pickering carrier via altering the

surrounding temperature. This can be useful in various biomedical applications especially when triggered release of bioactive ingredient is required. An example of such achievement is done by Zoppe and others (2012) who have successfully produced thermo-responsive CNC by grafting poly(NIPAM) brushes onto CNC and formed Pickering emulsion utilizing the mentioned composite.

2.3.2 Photoluminescent Properties

Photoluminescent responsive nanocellulose are attractive materials in sensing technology. To induce photoluminescent or fluorescent properties to nanocellulose, an interesting approach nowadays is the incorporation of quantum dots (QDs) to nanocellulose. Recently Wang *et al.*, (2013) showed successful covalent attachment of quantum dots onto the active functional groups on cellulose surface. Besides QDs, fluorescent materials have also been widely used as filler to synthesize photoluminescent nanocellulose. For instance, Helbert *et al.* (2003) successfully produced fluorescent micro/nano- fibril via grafting of 5-(4,6-dichlorotriazinyl)aminofluorescein (DTAF) onto bacteria nanocellulose for detection of cellulase activity. Furthermore, Wu *et al.*, (2015) performed the grafting of fluorescent and thermos-responsive poly(N-isopropylacrylamide) (PNIPAAm) brushes onto CNC, resulting in dual stimuli-responsive CNC. Last but not least, Navarro *et al.* (2015) produced multicolour CNF by first modifying CNF with furan and maleimide groups, followed by the coating of CNF with several fluorescent probes. Their results showed that two luminescent dyes could be selectively labelled onto CNF, yielding CNF with multicolour (Navarro *et al.*, 2015). These achievements could definitely aid in boosting the advancing photoluminescent nanocellulose in various sensing applications.

2.3.3 Conductive Properties

Conductive cellulosic materials have generated great interest due to their potential in developing flexible electronics with benefits of lightweight, good thermal and chemical stability (Johnston, Moraes and Borrmann, 2005). Out of those electronics, supercapacitor served as one of the most commonly produced devices from the conductive nanocellulose.

For example, CNC based composite electronics have been reported as flexible organic field effect transistor by incorporating CNC with tin oxide (Valentini *et al.*, 2014). These coatings are said to be done through the reaction of surface coating agents with surface hydroxyl groups of nanocellulose (Johnston *et al.*, 2006). In fact, paper sheet based on polypyrrole and polyaniline coated cellulose fibres were produced using ferric chloride as an oxidant in the study and they claimed the interaction to be chemical bonding between the H and N in pyrrole ring with the hydroxyl groups of cellulose (Johnston *et al.*, 2005, 2006). The incorporation of conductive filler to cellulosic materials not only advanced the properties of various commercial electronics but also enhancing the development of green electronics as future devices.

2.3.4 Magnetic Properties

Introduction of magnetic properties onto cellulosic materials is in fact, a newly extended area for nanocellulose surface functionalization. Literatures reported on incorporation of magnetic NPs and cellulosic materials claimed the working principle behind this remarkable combination to be mostly in hydrogen bonding between carboxyl/hydroxyl group of cellulose and hydroxyl group on magnetic NPs surface, or anchoring of magnetic NPs in pores of cellulosic materials (Li *et al.*, 2013; Xiong *et al.*, 2013). Besides that, another available interaction was reported by Liu *et al.*, (2013) in the case of *in-situ* synthesis, there would be electrostatic interactions between carboxyl/hydroxyl groups of cellulosic materials and metal ions (e.g. Fe^{2+} & Fe^{3+}). These ferrous & ferric ions are then transformed to Fe_3O_4 NPs by adjusting the pH of the medium to 11 by a base solution, resulting in Fe_3O_4 NPs/cellulosic composites (Liu *et al.*, 2013). Thus by far, it is safe to say that there are three testified interactions available for interacting magnetic NPs with cellulosic materials. To the best knowledge of the author, in most of the works done by researchers, magnetic NPs incorporated nanocellulose are directly employed for applications such as oil recovery, hyperthermia, enzyme immobilization, drug delivery, antibacterial activity and catalytic activity (Chin *et al.*, 2014; Mahmoud *et al.*, 2013; Nypelö *et al.*, 2014; Xiong *et al.*, 2013). There is, however, no reported investigation on the formation of Pickering emulsion using

such nanocomposite. With inspiration from the mentioned accomplishment, the author proposed to investigate and develop a facile *in-situ* synthesis of MCNC nanocomposite, aiming ultimately to serve as Pickering emulsion stabilizer.

2.4 Magnetic Nanoparticles

Magnetic NPs allow the targeted transportation of drug carrier to cellular tissues through a direct manipulation by an external magnetic field (EMF) (Plank *et al.*, 2003). To date, the most commonly used magnetic NPs is claimed to be the ferrites (Fe) nanoparticles (Lu *et al.*, 2007). In this project, magnetite (Fe_3O_4) is proposed to serve as the targeted magnetic NPs as it is one of the most commonly used magnetic NPs that provides superparamagnetic properties in room temperature (Lu *et al.*, 2007), furthermore it has been approved by the Food and Drug Administration (FDA), implying that magnetite is quite benign toward humans (Lattuada and Hatton, 2007). General applications of magnetite include magnetic resonance imaging (Kim *et al.*, 2001), drug targeting (Zhang and Misra, 2007), hyperthermia (Silva *et al.*, 2011; Fortin *et al.*, 2007), magnetic recording tape (Lu *et al.*, 2007), ferrofluid (Zubarev and Iskakova, 2004) etc.

2.4.1 Concept of Magnetism

Magnetism is claimed to be magnetic phenomena in materials, resulted from moving charges of atoms, sourced from two electronic motions namely, orbital and spin motion of electron, where orbital motion is an electron with a rest mass and a charge moving in a circular orbit of a radius at a velocity (Figure 2.5), and spin motion is magnetic moment based on the spin of the electrons (Chen, 1977a; Sorensen, 2002). The two magnetic moment are combined into a resultant magnetic moment of an electron. However, the combination of both magnetic moment is affected by the spin-orbital interaction, in short, an electrostatic interaction is taken place between the orbital and spin motion because each motion produces a magnetic field that would affect the other (Chen, 1977a). Thus, the magnetic effects of a material are literally dependent on the arrangement of the atoms in crystalline lattices and the alignment of the spins. For magnetic materials, the magnetic

properties are branded into 5 main categories: diamagnetic, paramagnetic, ferromagnetic, ferrimagnetic, and antiferromagnetic (Chen, 1977b). A solid is said as diamagnetic if it repelled from a permanent magnet and as paramagnetic, ferromagnetic, and ferrimagnetic if it attracted by a permanent magnet, with ferromagnetic having the strongest attraction, followed by ferrimagnetic with slightly weaker interaction due to the presence of different lattice sites in the crystalline network (Zhang, 2007), and paramagnetic that is weakly attractive towards a magnetic pole (Chen, 1977b; Sorensen, 2002). Antiferromagnetic materials, on the other hand, indicating that it does not sustain a magnetic field due to the opposite alignment from both moments in the crystalline lattice. Besides these five main categories, it is worth to mention that there are still other kinds of magnetism that are not included because they could be viewed as variations of the ones listed (Chen, 1977b). Out of the unlisted magnetism, the superparamagnetism that lines up their moments with an external applied magnetic field and loses the alignment once the field is detached is the main magnetic working principles for magnetite nanoparticles employed in this project.

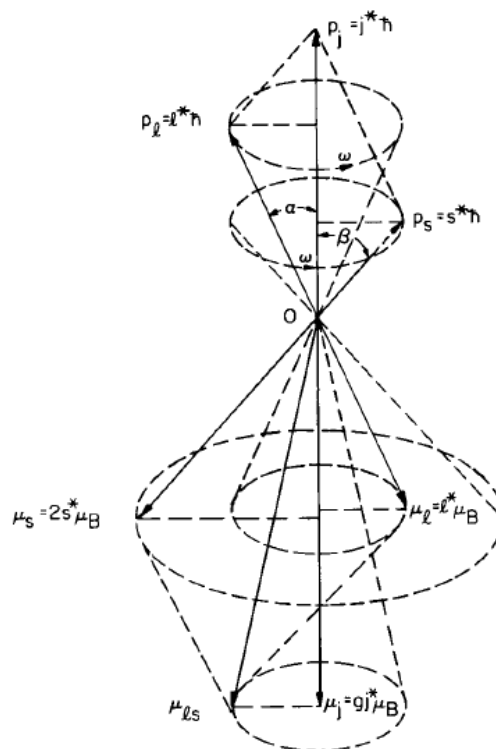


Figure 2.5. Vector model showing the spin-orbit interaction for a bound electron (adapted from (Brailsford, 1966)).

2.4.2 Magnetism in Magnetite Nanoparticle (MNP)

Magnetite (Fe_3O_4) is a type of ferrimagnetic material that is most commonly used due to its low toxicity and good biocompatibility, in addition with approval by the Food and Drug Administration (FDA), that it is safe to human body (Lattuada and Hatton 2007). The magnetic properties of this nanoparticles differ from its bulk form because its dimensions are much smaller than the typical domain size (typical domain size mentioned here are approximately > 100 nm (Hitchhiker's Guide, 2015)), when the magnetic moments of the atoms aligned under an EMF, at multidomain (MD) structure to reduce the magnetostatic energy associated with a large stray field (Bogart *et al.*, 2014). If the nanoparticles sizes are smaller than the typical domain size in bulk form, the nanoparticles will be in single domain (SD), where further reduction would lead to the superparamagnetic state (Figure 2.6), which the magnetic moment is now sensitive to thermal effect that could cause random flipping of magnetic moment (Apsel *et al.*, 1996; Bean and Livingston, 1959; Bogart *et al.*, 2014). An example of single- and multi-domain structures are as illustrated in Figure 2.7. Thus, the size of magnetite nanoparticles (MNPs) is utmost important because it has a strong relationship with its magnetic properties. To date, there are several common synthesis techniques reported in the literature, namely co-precipitation, thermal decomposition, hydrothermal synthesis, microemulsion, and sonochemical synthesis. These techniques have their own advantages and limitations when they are utilised in preparing MNPs. Thus the properties of products synthesized under each approach must be taken into account so that appropriate techniques could be selected for synthesizing magnetite nanoparticles to be used in different applications.

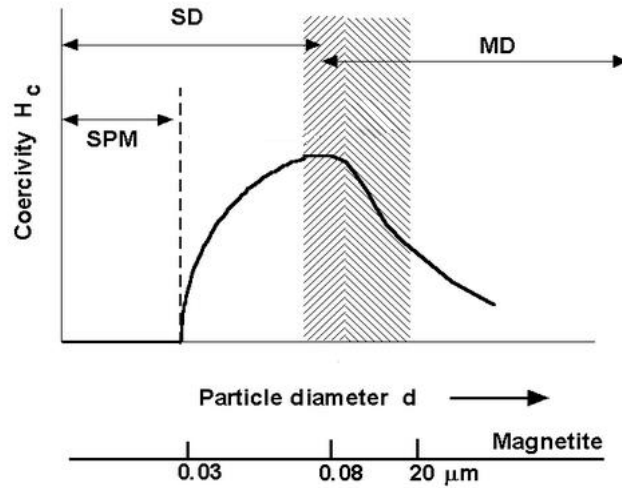


Figure 2.6. Magnetic behaviour of MNPs at different size range (adapted from (Hitchhiker's Guide, 2015)).

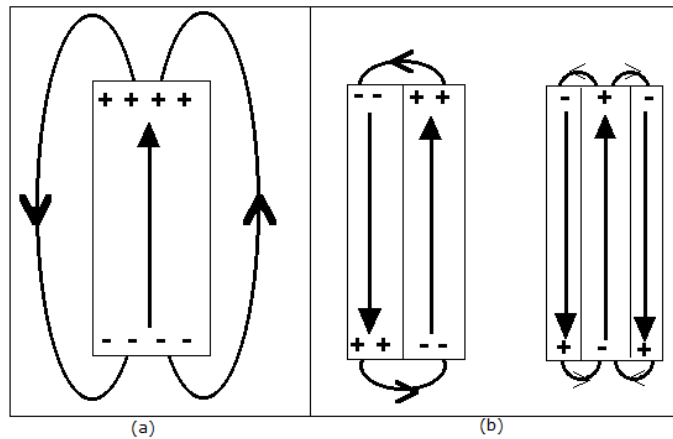


Figure 2.7. Schematic illustration of structures of (a) single domain and (b) multidomain (adapted from (Hitchhiker's Guide, 2015)).

2.4.3 General Techniques in the Synthesis of MNP

MNPs with controlled sizes and shapes are important criteria for its synthesis as regarded by the strong correlation between these parameters and magnetic properties. Among the different techniques used in synthesizing MNPs, other requirements such as cost, simplicity, nanoparticles quality, and time consumption should also be considered. At present, there are several common synthesis techniques reported in the literature as mentioned in the previous section, they are co-precipitation, thermal decomposition, hydrothermal synthesis, microemulsion, and sonochemical synthesis. These techniques have their own

advantages and limitations when they are utilised in preparing MNPs. Therefore, synthesis technique must be wisely chosen so that the desired magnetite products can be obtained.

2.4.3.1 Co-precipitation

Co-precipitation method is the simplest method for obtaining MNPs. This method involved the mixing of ferric and ferrous ions in a 2:1 molar ratio in high basic solutions at either room or at elevated temperature. Wu *et al.*, (2009) reported that the size and shape of the MNPs are dependent on the type of salt used, the ferric and ferrous ions ratio, the reaction temperature, pH, ionic strength of the media, stirring rate, and many other aspects. However, it was also reported that MNPs are very unstable under ambient condition and are easily oxidised or dissolved in an acidic medium, and thus the synthesis process must be performed in the anaerobic condition. Additionally, this fabrication technique generally resulted in magnetite nanoparticles with a wide particle size distribution. The waste from this process is also very alkaline and will require additional treatments before discharging to cope with environmental legislation. Despite the mentioned disadvantages, many researchers still focused on co-precipitation method due to its process simplicity. Recently, many researchers have successfully synthesized monodispersed MNPs using co-precipitation method by adding surfactant that would prevent the magnetite agglomeration. For example, Lopez *et al.*, (2010), and Mahdavi *et al.*, (2013) synthesized monodispersed MNPs with sizes range of 7 to 18 nm using oleic acid as surfactant. Furthermore, Agotegaray *et al.* (2014), also successfully synthesized such monodispersed MNPs by coating chitosan to prevent aggregation. On the other hand, the formation of MNPs *in-situ* in biotemplate that contain antioxidant or reducing agent such as plant materials showed not only the successful prevention for agglomeration but also inhibition of the oxidation of MNPs under ambient conditions. I.e. Cai *et al.* (2010) successfully synthesized MNPs with an average diameter of 8 nm, *in-situ* under the presence of soya bean sprouts without the needs of anaerobic conditions. Therefore, the polydispersity issue and requirement of anaerobic conditions for MNPs synthesized utilizing this method are considered solved and the only problem that still exists is the treatment of waste generated from this system.

2.4.3.2 Thermal Decomposition

Thermal decomposition route has been widely utilised in the magnetite synthesis. The process covered a decomposition step, followed by oxidation to give high-quality monodispersed MNPs. From literature, Sun and Zeng (2002) reported the synthesis of monodispersed MNPs without size-selection process via thermal decomposition of $\text{Fe}(\text{acac})_3$ in phenyl ether in the presence of alcohol, oleic acid, and oleylamine, at 265 °C, and yield MNPs with size ranging from 4 nm to 16 nm dependent on controlling the quantity of nanoparticle seeds. In another study, Lee *et al.*, (2010) also reported a large-scale synthesis of monodispersed MNPs (with a size of 2.2 ± 0.2 nm) by decomposing $\text{Fe}(\text{acac})_3$, $\text{Fe}(\text{acac})_2$, and 1,2-hexadecanediol in the presence of octyl alcohol at 210 °C. Although this method allowed the generation of MNPs with good monodispersity and in large scale, however, it is very complicated and required a very high temperature (e.g. up to 200+ °C), and the resulting NPs from this methods are generally only dissolved in nonpolar solvents.

2.4.3.3 Hydrothermal

Hydrothermal synthesis method has been used to produce dislocation-free crystal particles. The grains formed through this process can give a better crystallinity than those from other processes and hence, the hydrothermal process was claimed to be able to obtain the high crystalline iron oxide NPs (Wu *et al.*, 2009). Wang *et al.*, (2003) reported a one-step hydrothermal process in preparing highly crystalline monodispersed MNPs without surfactants. Next, Zheng *et al.*, (2006) also reported the production of MNPs of 27 nm in the presence of sodium bis(2-ethylhexyl)sulfosuccinate (AOT) via hydrothermal process, and both have reported that a superparamagnetic behaviour is available for the MNPs at room temperature. Despite there are many benefits utilising this technique, the fabrication necessitates the process to be performed at a relatively high temperature (140 °C) for quite a long time. Furthermore, the sizes of MNPs synthesized under this methods is also very much depends on the operating temperature. For instance, MNPs produced by Wang *et al.*,

(2003) shows different sizes under different temperature (25 nm at 100 °C, 40 nm at 140 °C and 45 nm at 180 °C).

2.4.3.4 Microemulsion

Microemulsion and inverse micelles route are claimed to be a possible way to generate shape- and size-controlled MNPs. First of all, stable microemulsion can be produced by emulsifying two immiscible phases (water and oil) under the presence of surfactant, where the surfactant will form a layer around the water-oil interface. Similarly to normal emulsion system, different types of self-assembled structures of emulsion could be formed, ranging from (inverted) spherical and cylindrical micelles to lamellar phases and bicontinuous microemulsions and thus aiding in generating shape- and size-controlled MNPs (Wu *et al.*, 2008). In particular, water-in-oil (w/o) microemulsions are formed by dispersing the nanodroplets of aqueous phase by the assembly of surfactant in a continuous oil phase (Wu *et al.*, 2008). From literature review, monodisperse maghemite NPs were synthesized by one-pot microemulsion method (Vidal-Vidal *et al.*, 2006). The reported synthesis involved the capping of spherical particles with monolayer coating of oleylamine, and was able to produce a narrow size distribution (3.5 ± 0.6 nm), in spherical shaped, having high saturation magnetization (M_s), and are strongly protected by a monolayer coating (Vidal-Vidal *et al.*, 2006). Moreover, the results have shown that oleylamine is acting as precipitating and capping agent. However, it does not prevent particle aggregation. In overall, although this fabrication method has many advantages, it requires further stabilizing treatments to reduce the high surface energy of the produced particles to avoid aggregation.

2.4.3.5 Sonochemistry

The sonochemical method has been famous for the synthesis of various nanocomposites. The working principle behind this synthesis method is due to the ultrasonic induced acoustic cavitation, which involved the formation, growth, and collapse of bubbles in liquid, that could generate an intense local heating, and high pressure (as shown in Figure 2.8) and

producing a short burst of light (known as sonoluminescence, SL) and microjets in a very short lifetime (Suslick and Price, 1999). These extreme conditions are beneficial and are prone to the preparation of highly monodisperse nanoparticles. Out of all the nanocomposites produced, its versatility has been successfully demonstrated in iron oxide nanoparticles preparation (Bang and Suslick, 2007). In particular, MNPs can be synthesised by sonication of iron(II) acetate in water with inert (argon) surrounding. From literature, a sonochemical synthetic route for preparing the nanosized magnetite powders with superparamagnetic properties at room temperature was reported (Vijayakumar *et al.*, 2000). In addition to that, another facile route combining co-precipitation and sonochemistry was also reported by Dorniani *et al.* (2012), where solution consists of ferrous chloride tetrahydrate ($\text{FeCl}_2 \cdot 4\text{H}_2\text{O}$) and ferric chloride hexahydrate ($\text{FeCl}_3 \cdot 6\text{H}_2\text{O}$), in deionized water were sonicated in the presence of ammonia hydroxide to yield monodispersed MNPs of approximately 10 nm.

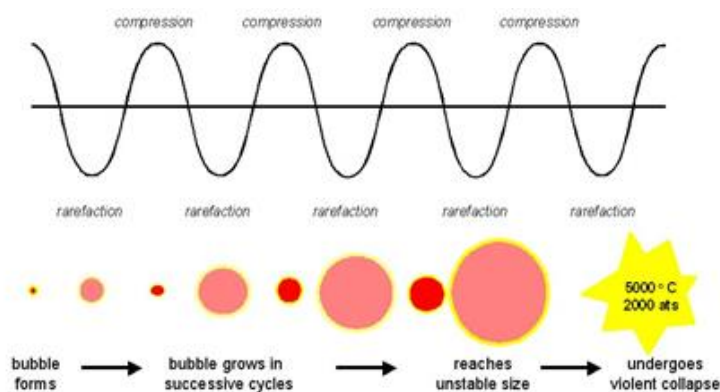


Figure 2.8. An exaggerated illustration of the growth of a cavitation bubble when it is subjected to sound field and leads to eventual collapse (adapted from (Mason and Peters, 2003)).

2.4.3.6 Overall Comparison of Synthesis Techniques

In overall, there were many synthesis methods reported to date with their respective advantages and limitations when they are used to prepare MNPs. Thus when deciding the synthesis methods, such advantages and limitations must be taken into account to ensure the right method is chosen for the respective right application. Properties of each synthesis

techniques as reviewed in Table 2.2 were considered for the selection of appropriate techniques used in this study for magnetite nanoparticles synthesis. In this project, sonochemical co-precipitation method is focused due to its advantageous properties such as process simplicity, time saving, and its possibility in producing highly monodispersed magnetite nanoparticles.

Table 2.2. Advantages and disadvantages of reviewed magnetite nanoparticles synthesis techniques.

Synthesis Techniques	Advantages	Disadvantages
<p>Co-precipitation (Cai <i>et al.</i>, 2010; Nazrul Islam <i>et al.</i>, 2011; Jadhav <i>et al.</i>, 2013; Wu <i>et al.</i>, 2009) (Mixing ferric and ferrous ions in a 2:1 molar ratio in high basic solutions)</p>	<ul style="list-style-type: none"> • Widely documented • Simple • Do not requires high temperature 	<ul style="list-style-type: none"> • Unstable under ambient condition without antioxidant/surfactant • Polydispersity without surfactant • Additional treatments for waste
<p>Thermal decomposition (Lee <i>et al.</i>, 2010; Sun and Zeng, 2002; Wu <i>et al.</i>, 2009) (Decomposition steps, followed by oxidation at very high temperature)</p>	<ul style="list-style-type: none"> • High-quality monodispersity 	<ul style="list-style-type: none"> • High temperature process • Complicated process • Resulted nanoparticles generally only dissolved in nonpolar solvents

Table 2.2. (Continued)

Synthesis Techniques	Advantages	Disadvantages
<p>Hydrothermal (Wang <i>et al.</i>, 2003; Wu <i>et al.</i>, 2009; Zheng <i>et al.</i>, 2006) (Crystallization process in autoclaves chamber)</p>	<ul style="list-style-type: none"> • Production of dislocation-free crystal particles • Monodispersity • Stable with superparamagnetic properties in room condition 	<ul style="list-style-type: none"> • Process involving two temperature zones in a chamber • Time consuming • Required surfactant
<p>Microemulsion (Vidal-Vidal <i>et al.</i>, 2006; Wu <i>et al.</i>, 2009) (Dispersing nano-droplets of aqueous phase by the assembly of surfactant in a continuous oil phase)</p>	<ul style="list-style-type: none"> • Shape- and size-controlled • Could be performed in room condition 	<ul style="list-style-type: none"> • requires further stabilizing treatments
<p>Sonochemical (Dang <i>et al.</i>, 2009; Dolores <i>et al.</i>, 2015; Dorniani <i>et al.</i>, 2012; Suslick and Price, 1999; Teo <i>et al.</i>, 2010; Vijayakumar <i>et al.</i>, 2000; Wu <i>et al.</i>, 2009) (Intense local heating, high pressure with short burst of light and microjets due to ultrasonic induced acoustic cavitation)</p>	<ul style="list-style-type: none"> • Simple • Monodispersity • Does not required high temperature • Stable with superparamagnetic properties at room condition 	<ul style="list-style-type: none"> • Acoustic wave of US cannot be controlled with normal ultrasonic equipment

2.4.4 Surface Functionalization and Stabilization of MNP for Drug Delivery System

In the preparation of MNPs, its stability against agglomeration is of utmost importance. Binding agents such as organic molecules, biological molecules, and various inorganic molecules are often employed to reduce the surface energy of MNPs to avoid agglomeration. Besides being utilised as surface passivate agent, the choice of molecules to be bonded to the surface of MNPs often takes into account of the possibility of the expansion of its application scope (e.g. for medical applications, choosing molecules with surface functional groups to coat with MNPs so that other drugs can be loaded on the MNPs carrier). To date, researchers often coat MNPs with either organic or inorganic molecules with good biocompatibility to ensure magnetic properties remain in the nanostructure material (Sun *et al.*, 2005). Organic molecules such as polymer (chitosan, gelatin, dextran, poly(ethylenimine) (PEI), poly(ethylene glycol) (PEG)), copolymers, (PEI-PEG-chitosan) or biomolecules (oleic acid), have been widely used for producing MNPs that is feasible for biomedical applications. For example, a successful coating of chitosan on MNPs was reported by Dorniani *et al.*, (2012), where magnetite was coated with chitosan, utilizing the negatively charged surface of MNPs. Because of this factor, magnetite had an affinity towards amine groups of chitosan and hence the protonated chitosan could be coated on the surface of magnetite by electrostatic interaction and chemical reaction through epichlorohydrin crosslinking (Saifuddin and Dinara, 2012). Besides that, Agotegaray *et al.*, (2013), and Zhang *et al.*, (2006) successfully coated MNPs with oleic acid and chitosan to form magnetite nanocomposite for targeted Diclofenac delivery based on covalent bonding between oleic acid and magnetite, and electrostatic interaction between oleic acid and chitosan (Bonferoni *et al.*, 2014), and Mahdavi *et al.*, (2013), synthesized biocompatible MNPs coated with oleic acid alone for biomedical applications.

On the other hand, inorganic molecules were also used as an alternative to coat MNPs. The reason for inorganic molecules to be hired for surface functionalization are often because the simultaneous control of the shape, stability, biocompatibility, surface structure, and retaining the magnetic properties of MNPs is much easier as compared to organic molecules functionalized MNPs (Wu *et al.*, 2009). Besides that, such approach could also

extend the application scope of MNPs, i.e. for bioseparation or biosensing that requires appropriate dimensions that are comparable to that of virus (20-500 nm), protein (5-50 nm), or DNA (10-100 nm) (Wu *et al.*, 2009). In particular, quantum dots incorporated MNPs for biosensing applications have been inspiring because the synergistic effect of both MNPs and quantum dots allowed targeted cellular imaging. Ahmed *et al.*, (2013) reported an example of quantum dots incorporated MNPs for imaging colon carcinoma cells. Another inorganic molecule that is most often used for surface functionalization of MNPs is silica because it provides good stability and biocompatibility to the MNPs. Consequently, the size of silica coated MNPs can also be tuned specifically because of its maturity in preparation technology (Wu *et al.*, 2009). Furthermore, silica coating has been reported for biosensing application. For example, Quy *et al.*, (2013) synthesized silica coated MNPs for the detection of pathogenic viruses such as hepatitis virus type B (HBV) and Epstein-Barr virus (EBV). Their findings showed that the efficiency of magnetite-silica nanoparticles on purifying DNA of both HBV and EBV to be superior to the commercialized magnetite-silica microparticles (Quy *et al.*, 2013).

Beside the mentioned stabilizers, cellulose-based materials have gained momentum recently as alternatives for integrating MNPs since cellulose is a renewable and widely available natural resource on Earth (Wu *et al.*, 2011; Xiong *et al.*, 2013). Additionally, cellulose can undertake variety of properties including magnetic (Anirudhan and Rejeena, 2014; Li *et al.*, 2013; Mahmoud *et al.*, 2013; Nypelo *et al.*, 2014; Wu *et al.*, 2011), conductive (Johnston *et al.*, 2006), photoluminescent (Khan and Sundararajan, 2011), and other specific properties (Wu *et al.*, 2011) if they are incorporated with the appropriate fillers. Though many researchers have investigated the feasibility of incorporating MNPs with cellulosic materials, the focuses are not on Pickering emulsion formation. Hence, a study on the synthesis of MNPs coated on cellulose nanocrystal (CNC) can literally open up the doors for *in-situ* synthesis of monodispersed green Pickering emulsion emulsifier with synergistic effect from both magnetite and CNC.

Being inspired by several recent achievements, author have planned to achieve the *in-situ* synthesis of monodispersed MNPs stabilized with CNC, and further utilizing it for Pickering emulsion formation with the goal of using it as a potential drug carrier.

2.4.5 Pickering Emulsion Formation using MNP

Utilization of superparamagnetic MNPs in stabilizing Pickering emulsion have been extensively investigated by many researchers in recent years. Surface modification of MNPs with surfactants are normally required in order to alter the surface wettability of MNPs to result in stable and small Pickering emulsion. From literature, many surface modified MNPs such as cyclohexane and cetyltrimethylammonium bromide (CTAB) modified, and oleic acid modified MNPs were used to produce Pickering emulsion droplets (Ingram *et al.*, 2010; Shen *et al.*, 2007). However, works reporting the production of magnetic Pickering emulsion stabilized by unmodified MNPs remained limited. Work done by Zhou *et al.*, (2011) found that unmodified MNPs can only stabilize Pickering emulsion if non-polar oil with high oil/water interfacial tension is used. In addition, the size of the emulsion droplets is large (20-100 micron) and polydispersed. Thus, surface modification of MNPs is preferred to favour small and stable Pickering emulsion droplets. As previously mentioned, nanocellulose are able to form stable Pickering emulsion of very small size. Additionally, the used of nanocellulose as the stabilizer can lead to the preparation of “green and surfactant-free” Pickering emulsions since nanocellulose is a renewable, and environmentally friendly material. Furthermore, nanocellulose can undertake a variety of properties dependent on incorporated filler. This suggested a great potential in generating the Pickering emulsion droplets with magnetic stimuli responses. Hence, in this project nanocellulose will be the main focus for the synthesis of monodispersed MNPs, aiming to produce magnetically controllable and surfactant free Pickering emulsions to be employed as a new generation of smart drugs carrier.

2.5 Applications of Magneto-Responsive Cellulosic Materials

Magneto-responsive cellulosic materials have been recently utilized in myriad of applications due to its ability to imply magnetic properties into products that made up of cellulosic materials. In literature, magneto-responsive cellulose nanocomposite materials have been proposed to be applicable as magnetic paper (Li *et al.*, 2013), conductive paper (Liu *et al.*, 2015), magnetically retrievable oil absorbent (Chin *et al.*, 2013), recyclable catalyst (Xiong *et al.*, 2013), anti-bacterial activity (Xiong *et al.*, 2013), drug delivery (Anirudhan and Rejeena, 2014), and enzyme immobilization (Mahmoud *et al.*, 2013). In overall, MNPs do not usually provide uniform dispersion in nanocellulose due to their agglomeration. To overcome this issue, one can either stabilize MNPs with inorganic or other stabilizers as mentioned in section 2.4.4. In this project, the MNPs will be synthesized *in-situ* with nanocellulose to deposits the MNPs onto the cellulose dispersion matrix. In most cases, the magnetic properties of magneto-responsive nanocellulose depend on MNPs size and concentration in the matrix (Li *et al.*, 2013; Liu *et al.*, 2013). Here some conveyed examples on the applications of the mentioned magnetic nanocomposite will be summarized and linked to the initiation of this study.

First of all, one of the most practised application with this magnetic nanocomposites is the formation of magnetic paper for magneto-optical applications. Li *et al.*, (2013) produced highly transparent magnetic nanopaper prepared by the immobilization of MNPs on Nanofibrillated cellulose (NFC). In Li's paper, the mechanism for the reaction between MNPs and NFC were claimed to be hydrogen bonding between carboxyl/hydroxyl groups of NFC and surface hydroxyl groups of MNPs (Li *et al.*, 2013). In addition, the produced cellulose paper also showed strong magnetivity and mechanical strength, and lastly, cellulose paper was also found feasible to function as conductive paper and proved the effect of MNPs loading concentration on the paper transparency (Li *et al.*, 2013, Liu *et al.*, 2015).

Besides being applied as magnetic paper, the magnetic nanocomposites has also found its application as magnetically retrievable oil recovery absorbent. For instance, Chin *et al.*, (2013) synthesized magnetic cellulose aerogels and claimed them to be efficient and

economical absorbent for cleaning oil spillage from the water surface. In this paper, MNPs was incorporated in-situ into cellulose gel during the solvent exchange process before the supercritical point drying to obtain magnetic aerogel. Then, titanium dioxide (TiO₂) was coated onto the magnetic aerogel for surface functionalization purposes for oil removal (Chin *et al.*, 2013). The outcomes revealed a reusable magnetic aerogel with excellent oil absorption capacity. The aerogels were easily removed from water by a magnet, and the absorbed oil could be removed by simply soaking the aerogels in ethanol (Chin *et al.*, 2013). To sum up, the produced magnetic cellulose aerogels have envisaged great potential in oil recovery fields as it was easily retrievable, and can selectively absorbs oil up to 28 times of its original weight, as compared to normal cellulose aerogels that could only achieve oil absorption up to 5 times its original weight (Chin *et al.*, 2013).

The magneto-sensitive cellulosic materials were also employed for drug/gene delivery applications. One obvious benefits of utilizing the magnetic nanocellulose for drug delivery is regarded to the feasibility of the nanocomposites for external magnetic-controllable transportation of the drug-loaded magneto cargo. For example, Anirudhan and Rejeena (2014) prepared aminated β -cyclodextrin-modified-carboxylated magnetic cobalt/nanocellulose composite (ACDC-Co/NCC) for efficient transfection of genes into tumour cells. They claimed that higher DNA transfection efficiency can be achieved by using the produced magnetic-targeted composite as compared to the transfection using model transfecting agent poly(ethyleneimine) (PEI) (Anirudhan and Rejeena, 2014). Another study performed by Supramaniam *et al.* (2018) also demonstrated the potential of the magnetic cellulose alginate hydrogel beads for drug delivery. The outcome of the study revealed the magnetic swelling controllable release of ibuprofen from the magnetic vehicles. However, drawbacks such as low loading of ibuprofen (only up to 38% maximum) and obvious initial burst release are recorded in all formulation examined in the study (Supramaniam *et al.*, 2018). Thus further research is still required to superiorised the physicochemical properties as well as improvising the encapsulation efficiency of drug in the magnetic-cellulose hydrogel prior to next-stage *in-vitro* cell line cytotoxicity evaluation.

In addition to drug delivery applications, magnetic nanocomposites were also utilised for catalytic enzyme immobilisation and antibacterial activity. In these studies, magnetic nanocellulose are usually further incorporated with certain particles that drive the required processes. As an example, in a study done by Xiong *et al.* (2013), MNPs/NFC nanocomposites was further coated with silver (Ag) NPs that is well known for its catalytic properties and antibacterial activity (Axe, 2015; Borase *et al.*, 2014). Another reason for the use of Ag NPs for incorporation was mentioned to be the prevention of its aggregation during catalytic/antibacterial activity as well as its disposal to the environment because the magnetic attractability of MNPs allowed the Ag NPs to be easily recovered/separated from the treated medium (Xiong *et al.*, 2013). Besides that, an investigation related to enzyme immobilization for enhancing the enzyme's lifetime, enzymatic activity, and stability, Mahmoud *et al.* (2013) coated MNP/CNC nanocomposite with gold NPs, and surface activated with thioctic acid (Thc), 1-ethyl-3-(3-dimethylaminopropyl)carbodiimide (EDC), and N-hydroxysulfosuccinimide (NHS) to provide functional groups for immobilization of papain. Despite that the interactions between most of the involved chemicals were discussed, the interaction between MNP and CNC remained unclear. This served as a research gap in the actual interactions between the two solids and thus leading to the first stage of this work where facile and rapid synthesis and characterisation of MNP@CNC (MCNC) nanocomposite will be performed. In addition, to the current knowledge of the author, there are yet to be any reported studies on the preparation of Pickering-emulsion using MCNC nanocomposites. Furthermore, the potential of MCNC-stabilized Pickering emulsion (MCNC-PE) as drug carrier has yet to be explored too. Hence this work is proposed, aiming to develop a new magnetic Pickering emulsion stabilized by MCNC for drug delivery purposes.

2.6 Pickering Emulsion: Application as Drug Delivery System

Before increasing attentions were given to the Pickering emulsion-based drug delivery carrier, various drug delivery system such as surfactant-stabilized emulsion and nanosuspension have been the commonly employed system for drug delivery applications

due to their ability to improve the efficiency of drug delivery. For example, Anuchapreeda *et al.* (2012) developed the lipid nanoemulsions loaded with curcumin and showed its effective cytotoxicity on leukemic cell lines. In another study, Wang *et al.* (2007) also showed the enhanced anti-inflammation activity of curcumin when it was encapsulated in surfactant stabilized nanoemulsions. As for the nanosuspension approach, Yallapu and his co-workers (2012) demonstrated the increased cellular uptake and cell cytotoxicity of curcumin in prostate cancer cell line PC-3 by loading the curcumin onto cellulose nanosuspensions. Besides the nanoemulsion and nanosuspension methods, Pickering emulsions constitute a promising strategy for encapsulation and transport of drugs in the pharmaceutical formulation. The utilization of solid particles as stabilizer promoted enhanced stability due to the irreversible attachment of solid particles onto the interface of oil and water (Frelichowska *et al.*, 2009a). In addition, encapsulation of drugs within the emulsion aid in preserving and protecting drugs from enzymatic degradation and gastrointestinal hydrolysis (Marti-Mestres and Nielloud, 2002). Besides that, its surfactant free nature also made possible for the Pickering emulsions to avoid irritations that are sometimes caused by surfactant (Tang *et al.*, 2015; Welss *et al.*, 2004). It has been proven that Pickering emulsion can alter (by either increase or decrease) the levels of transdermal transport across skin compared to traditional emulsions (Frelichowska *et al.*, 2009b). Other than that, due to the enhanced resistivity to de-stabilization, Pickering emulsion have been extensively used for drug delivery. For example, studies on oral delivery of curcumin showed that the encapsulation of curcumin in the emulsion for drugs delivery enhanced its poor oral bioavailability. Such findings were provided in Huang and colleagues' study that discovered the capability of curcumin emulsions for inhibiting inflammation when compared to curcumin solution (Huang, Yu and Ru, 2010).

Besides the enhanced stability, application of emulsion on drug delivery nowadays often require them to be stimuli-responsive so that the encapsulated drugs can be released when it is triggered. Such triggering release effect can simply be introduced via incorporation of stimuli-responsive substances into the Pickering emulsion formulation. In current study where nanocellulose-based Pickering emulsion is to be employed, there exist

several examined responses by researchers recently including pH, magnetism, US, temperature, and so on. In this project, the focus will be targeted on pH and magnetism. These responses will be described in the next section.

2.6.1 Stimuli-Responsiveness for Magnetic-cellulosic-based Pickering Emulsion

Stimuli-responsive drug release system refers to an attractive approach for targeted drug delivery, which uses certain devices to release drugs in response to external stimulus. The stimulus includes pH (Lan *et al.*, 2007), magnetism (Sander *et al.*, 2012), US (Fabiilli *et al.*, 2010), temperature (Lee, Blumenthal and Ivkov, 2014), and others (Fabiilli, 2010). The purpose of introducing such delivery system is the attempt to enable the manipulation of drug release instead of being dependent on drugs or active agents coated (Fabiilli, 2010). Specifically for this study, only pH, and magnetism triggered effect will be investigated because pH is claimed to be able to precisely control the phase inversion of magnetic emulsions while the magnetic properties can be utilized for magneto-guidable transport of the Pickering emulsion-based drug carrier (Lan *et al.*, 2007). In fact, Lan *et al.* (2007) worked on pH-responsive magnetic Pickering emulsion and found that pH changes could dramatically inverse the emulsion types. They demonstrated that w/o emulsions were preferred from acidic to neutral pH, and from pH 12 onwards, while o/w emulsions were formed around pH 8 to 11. This demonstrated the occurrence of phase inversion that could result in drugs release (Lan *et al.*, 2007).

Utilization of magnetism for triggering the discharge of drug polymer capsules are often introduced by magnetic fields induced hyperthermia effect that causes the temperature to rise and resulted in carrier decomposition (Lee, Blumenthal and Ivkov, 2014; Oliveira *et al.*, 2013). In emulsion system, the disruption mechanisms are much simpler by magnetically induced coalescence under strong magnetic field since MNPs are only adsorbed on the interface between oil and water. This phenomenon was examined by Sander and colleagues, where emulsion de-stabilization happened when the attractive magnetic dipole forces were strong enough to reduce the droplet equilibrium separation distance to a critical value (Sander *et al.*, 2012). In summary, the effect of utilizing these

external stimuli for drug releasing will be examined and compared to that released from normal shaking to evaluate improvement made under external stimuli responses.

CHAPTER THREE

MNPS@CNC NANOCOMPOSITE: RAPID PREPARATION AND

REACTION MECHANISM

Overview

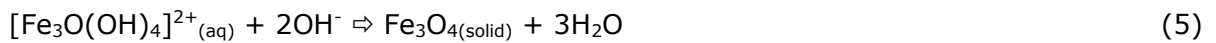
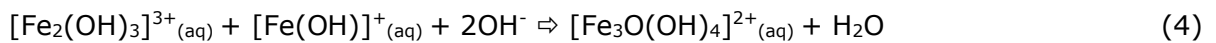
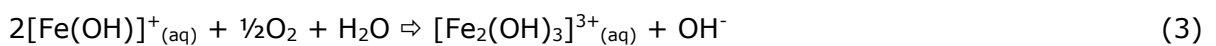
In this chapter we proposed a rapid sonochemical *in-situ* co-precipitation approach to prepare Fe₃O₄@cellulose nanocrystal (MCNC) nanocomposites. Differed from conventionaly method, the proposed *in-situ* co-precipitation reaction was performed under atmospheric condition without N₂ purging to yield the MCNC. The chemical interaction between the Fe₃O₄ nanoparticles (MNP) and the CNC has been characterized by FTIR, Raman and XRD analysis. The obtained results from Raman and XRD suggested no occurrence of oxidation of MNP to undesired maghemite due to the presence of CNC as the antioxidant. The proposed method showed higher magnetivity (due to higher MNP loading on the MCNC nanocomposites) as compared to those produced under typical N₂ protection. Our study revealed that the use of ultrasound (US) horn in place of conventional mechanical stirrer accelerated the nucleation, growth and dispersibility of MNPs on CNC fibres, which thus shortened the reaction times. The findings suggest that the proposed sonochemical synthesis without inert N₂ purging could be an alternative facile and efficient approach to fabricate well-dispersed MCNC nanocomposites that hold great potential for biomedical applications.

3.1 Introduction

Iron oxide, or Fe_3O_4 nanoparticle (MNP) is an excellent superparamagnetic material that have recently attracted increasing attentions in various biomedical applications such as magnetic resonance imaging (Kim *et al.*, 2001), drug targeting (Zhang and Misra, 2007), hyperthermia (Silva *et al.*, 2011), and ferrofluid (Zubarev and Iskakova, 2004) due to its low cost, negligible toxicity, and good biocompatibility properties (Lattuada and Hatton, 2007; Szpak *et al.*, 2013). More importantly, magnetite-based adsorbent were generally known to be reusable and easily separable as a result of its magnetic responsive properties. The *in-situ* co-precipitation appears to be the most popular fabrication approach in the preparation of MNP due to its simplicity and mild reaction condition (Wu He, and Jiang, 2008). The conventional chemical co-precipitation process typically involves two stages: (i) nucleation and growth as primary processes for formation of magnetite (Fe_3O_4), and (ii) secondary processes such as agglomeration, and subsequent oxidation to produce Fe_2O_3 nanoparticles. However, the current synthesis method often associated with the problems of particle aggregation and undesired oxidation of MNPs to maghemite (Fe_2O_3), resulting in the reduced saturation magnetization (M_s) of MNPs due to the fact that Fe_2O_3 have a very low magnetic susceptibility at room temperature (Mascolo, Pei and Ring, 2013; Wu, He, and Jiang, 2008).

To prevent magnetite from further oxidation and to avoid particle aggregation, coating the surface of MNP with organic polymers such as starch, dextran, chitosan, and nanocellulose have been proposed (Carmen Bautista *et al.*, 2005; Kim *et al.*, 2003; Peng *et al.*, 2002; Wu He, and Jiang, 2008; Zhu, Yuan, and Liao, 2008). This led not only to the effective preparation of non-agglomerated MNPs in nanoscale, but also successfully extended the uses of the resultant polymer coated MNPs nanocomposites in various applications such as magnetic paper, hyperthermia, oil recovery, recoverable catalyst, drugs delivery, and antibacterial activity (Anirudhan and Rejeena, 2014; Chin, Binti Romainor and Pang, 2014; Li *et al.*, 2013; Nypelö *et al.*, 2014; Xiong *et al.*, 2013). Because of high potential of the resultant magnetic nanocomposites in many applications, a facile and efficient coating method will be beneficial for its future development. Due to the

simplicity nature and non-extreme reaction requirement, the *in-situ* co-precipitation method was still the most favourite approach for most researchers. Based on the practices by most researchers, the chemical co-precipitation of MNPs generally took place under oxygen-free/inert N₂ gas condition to prevent the undesired oxidation of the MNPs. Under N₂ gas environment, the co-precipitation reaction in highly alkaline media is represented by the following equations (Dang *et al.*, 2007; Roonasi and Holmgren, 2009):



In the presence of ammonia hydroxide as alkali media, iron (II) chloride rapidly precipitates into Fe(OH)₂. As depicted in Equation (1-3), Fe(OH)₂ then dissociates and undergoes oxidation by the dissolved O₂ in water to form intermediates [Fe₂(OH)₃]³⁺. The intermediates then combine with the dissolved [Fe(OH)]⁺ to form Fe₃O₄ via dehydroxylation reaction. During the intermediate reaction steps, the presence of O₂ was utmost important to increase the yield of magnetite nucleation (primary process) despite the fact that O₂ could lead to the oxidation (secondary process) of Fe₃O₄ to Fe₂O₃ at later MNP formation stage. In this regard, Dang *et al.* (2007) reported that the absence of O₂ decreased the nucleation rate of iron oxide during the co-precipitation reaction, leading to a lower yield of MNPs.

In this work, we investigated a new one-pot sonochemical co-precipitation approach for preparation of Fe₃O₄@CNC (MCNC) nanocomposite under atmospheric gas environment. The as-synthesized MCNC nanocomposites were characterized using FTIR, Raman, electron microscopy, TGA and VSM for its reaction mechanism, surface morphology, chemical composition, and magnetic strength. Several studies demonstrated that CNCs have a strong anti-oxidant effect and synthesis of MNPs within CNC matrix has led to preparation of well-dispersed magnetic nanocellulose structures (Liu *et al.*, 2015; Nypelö *et al.*, 2014; Olsson

et al., 2010; Tam, 2012). However, to the best of our knowledge, there is no report concerning the non-inert protected *in-situ* synthesis and the resultant properties of magnetic cellulosic nanocomposites. This study was, therefore, undertaken to investigate the effect of atmospheric gas (natural air) and US on the preparation of MCNC nanocomposites, aiming ultimately to provide an alternative facile approach with shorter reaction time and increased MNP yield for magnetic-cellulose nanocomposites preparation.

3.2 Materials and Methodology

3.2.1 Materials

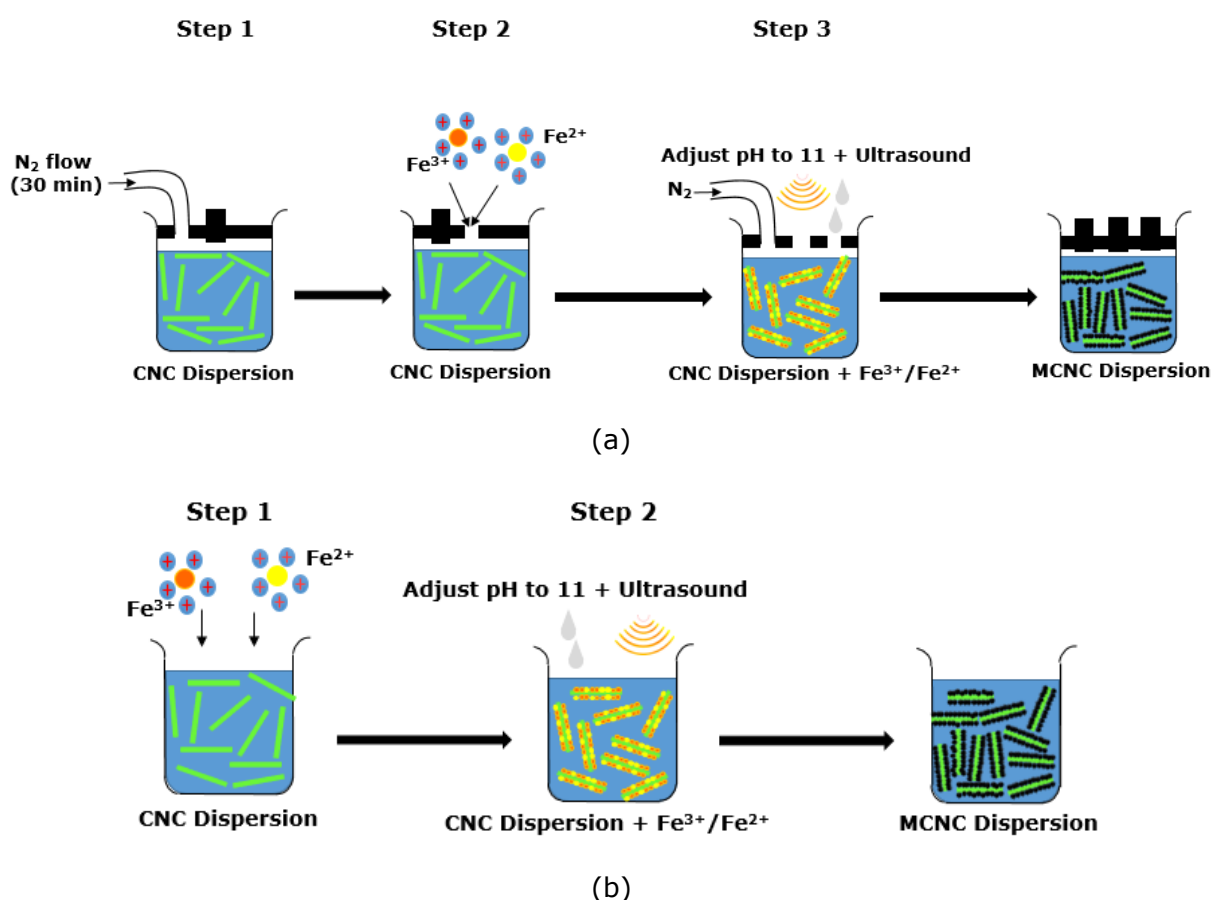
Iron (II) chloride tetrahydrate ($\text{FeCl}_2 \cdot 4\text{H}_2\text{O}$, $\geq 99\%$), iron (III) chloride hexahydrate ($\text{FeCl}_3 \cdot 6\text{H}_2\text{O}$, 99%), and ammonium hydroxide (28% NH_3 in H_2O), were purchased from Sigma-Aldrich. CNC (Freeze dried, 0.96 wt% sulphur content) was procured from University of Maine. All water used in this experiment are ultrapure water ($18.2 \text{ M}\Omega \text{ cm}^{-1}$) obtained from Milli-Q® Plus apparatus (Millipore, Billerica, USA). Ethanol (AR standard) acquired from R & M Chemical (Syarikat Saintifik Jaya, Malaysia). All experiments involving US were conducted using an ultrasound probe sonicator (20 kHz, Lab750, Sinaptec) under pulse mode (15 s pulse on, 10 s pulse off). All chemicals in this study were of analytical grade and employed without further purification.

3.2.2 Synthesis of MCNC Nanocomposite

MCNC nanocomposites were prepared by US assisted *in-situ* co-precipitation method. In particular, CNC was first dispersed (0.05 wt%) in water under US cavitation for 2 minutes. Next, fixed amount of iron (III) and iron (II) chloride (1.5/1 $\text{Fe}^{3+}/\text{Fe}^{2+}$ mol ratio) were added into the CNC dispersion. Consequently, the mixtures were stirred and heated to 45 °C. Then, the mixtures were sonicated in the presence of ammonium hydroxide (2.2 ml) for 5 minutes. For control sample prepared under anaerobic condition, the CNC dispersion was first bubbled with nitrogen gas for 30 minutes prior to addition of iron precursors. Then,

the later syntheses steps were all carried out under N_2 stream. Scheme 3.1 illustrated the conventional and proposed sonochemical co-precipitation methodology.

After that, the MCNC nanocomposite were precipitated and the residual obtained were magnetically separated and washes 3 times with ethanol to remove ammonium hydroxide. Lastly, the remained MCNCs were centrifuged at 4500 rpm for 20 minutes, and dried in an oven overnight. The dried samples were stored for characterisation.



Scheme 3.1. (a) Conventional and (b) proposed sonochemical co-precipitation method for MCNC preparation.

3.2.3 Characterisation of MCNCs

Particle size and surface morphology of the sonochemically prepared MCNCs were analysed using field emission scanning electron microscope (FE-SEM) (SU8010, Hitachi, Japan) at 15 kV. Elemental analysis were performed through Energy-dispersive X-ray spectroscopy

(EDX) using the same FE-SEM. Functional groups available were examined through Fourier transform infrared spectroscopy (FTIR) over a range of 550 – 4000 cm^{-1} on a FTIR spectrophotometer (Nicolet iS10, Thermo Scientific, USA) equipped with diamond probe. Raman spectroscopy was recorded under an excitation wavelength of 514 nm employing a raman spectrophotometer (LabRAM-HR-PL, Horiba Scientific, UK). X-Ray diffraction (XRD) was carried out in the range of 20 to 80 degrees on X-Ray diffractometer (Bruker Discover D8, Bruker, USA) using $\text{CuK}\alpha$ radiation ($\lambda = 1.5406 \text{ \AA}$) at 40 kV and 40 mA. Magnetization of MCNCs was measured via vibrating sample magnetometry (VSM) (Lakeshore 7400 Series, Lakeshore Cryotronics, USA). Chemical composition and thermal stability was evaluated by thermogravimetric analysis (TGA) in the temperature range of 25 to 900 $^{\circ}\text{C}$ at 10 $^{\circ}\text{C}/\text{min}$ using a thermogravimetric analyser (Q50 TGA, TA instrument, USA).

3.2.4 Statistical Analysis

Analysis of variance (ANOVA) were performed using Prism software and $p < 0.05$ was considered as statistically significant. FE-SEM images were analysed with ImageJ to determine the size of MNPs on CNC.

3.3 Results and Discussion

3.3.1 Facile Preparation of MCNCs under Open Atmosphere

In the present study, we prepared the MCNC nanocomposites by employing one-step US-aided *in-situ* co-precipitation method. To determine the components of MCNC nanocomposite. FTIR, Raman, and XRD analysis were carried out. From FTIR analysis, the spectra of MCNC samples prepared under both air-flow and N_2 conditions showed no distinct differences (Figure 3.1a). The Fe–O bonding peak at 561 cm^{-1} shows the presence of MNPs (Mahmoud *et al.*, 2013). CNC characteristics functional groups were presences at 610 (C–O bonding), 664 (C–OH bonding), 1011 (C–O bonding), 2896 (CH_2 bonding), and 3334 cm^{-1} (–OH hydrogen bonding) (Mahmoud *et al.*, 2013). The reaction between Fe ions of

MNPs and surface hydroxyl groups of CNC was evidenced by the absence of the characteristic peak of C—OH group at around 664 cm^{-1} (Figure 3.1a).

Typical Raman spectra had been obtained for pure magnetite nanoparticles (MNPs), CNC and MCNC nanocomposites and the results were presented in Figure 3.2a to d. Pure crystalline CNC contained four characteristic peaks at 380 cm^{-1} (C—C—O or C—O) (Agarwal *et al.*, 2012), 898 cm^{-1} (C—OH bonding), and 1098 and 1120 cm^{-1} (C—O—C stretching and bending)) (Agarwal *et al.*, 2012; Dhar, Kumar and Katiyar, 2016; Schenzel and Fischer, 2001; Zhang, Feldner and Fischer, 2011) whereas MNPs displayed the characteristic peak of magnetite (Fe_3O_4) at around 670 cm^{-1} (Adar, 2014). The Raman spectral patterns of MCNC nanocomposites synthesized under atmospheric and N_2 conditions were found to be highly similar. As can be seen from Figure 3.2c and d, the signal at 898 cm^{-1} assigned to the C—OH of CNC was absent in Raman spectra of the MCNC, indicating the complete reaction between the Fe ions and the hydroxyl groups of CNCs. The observed Raman peak at 670 cm^{-1} in both MCNC samples confirmed the formation of magnetite on CNC matrix, implying that no Fe_2O_3 was generated during the reaction. This was also confirmed from the absent of the characteristic dual peak of maghemite at around 665 and 730 cm^{-1} (Hanesch, 2009). It is noted that the peak at around 380 cm^{-1} was also observed in the nanocomposite spectrum. This indicated that the Fe_3O_4 were mainly deposited on the surfaces of CNCs (Agarwal *et al.*, 2012; Dhar, Kumar and Katiyar, 2016; Zhang, Feldner and Fischer, 2011). To support that, literature investigation by Zhang, Feldner and Fischer, (2011) on the changes in Raman spectroscopy of CNC upon various acetylation degree, have proven that the peak at 380 cm^{-1} declined significantly when the degree of acetylation was no longer limited to the surface. The enhanced effect of oxidative resistance of Fe_3O_4 was mainly attributed to the potential antioxidant utilization activity of CNC fibre (Tam, 2012). Based on analytical studies by FTIR and Raman, one could perceive that the use of CNC as template for iron oxide synthesis not only led to the efficient immobilization of magnetite nanoparticles on the surface of CNC, but also give rise to an enhanced shielding to oxidation of MNPs after the magnetite was formed.

As shown in Figure 3.3c and d, the XRD spectrum of MCNC produced at ambient condition are similar to those prepared under N₂ gas protection. The XRD patterns of both samples showed the peaks that can be indexed to (220), (311), (400), (422), (511), (440), (533) planes of a cubic cell of Fe₃O₄ according to ICDD database (ICDD 00-019-0629), indicating the high degree of crystallinity and structural homogeneity of MNPs. The characteristics peaks of (110), (200), and (004) represents the typical signatures of cellulose crystalline structure (JCPDS 00-050-2241). The disappearance of cellulose peak at (200) was possibly due to the occurrence of co-precipitation reaction in the presence of ammonia, which in turn reduce the crystallinity of CNCs, resulting in a lower diffraction intensities in the obtained cellulosic nanocomposites (Dhar, Kumar and Katiyar, 2016). The crystallite size of MNPs deposited on the CNC surfaces was estimated to be approximately 9.8 and 10.4 nm in diameter, respectively for MCNC prepared under atmospheric and N₂ environment.

In summary, based on FTIR, Raman, and XRD, the reaction mechanism works as follow: As the iron precursors were added into CNC dispersion, positively charged ferrous and ferric ion were attracted to negatively charged hydroxyl groups on CNC, forming Fe–O[–]CNC. At basic pH environment, a competition between of Fe³⁺–O[–], Fe²⁺–O[–] bonds with the formation of OH–Fe³⁺ and OH–Fe²⁺ bonds resulted in formation of intermediates such as Fe₂(OH)₃ or Fe(OH)₂, and finally MNPs formed spontaneously after the dehydroxylation reaction between the intermediates. To support this, similar reaction pathway were reported by Cai *et al.* (2010) on preparation of soya bean sprouts (containing celluloses) mediated superparamagnetic MNPs, and Awwad and Salem, (2012) on role of hydroxyl groups during MNPs formation. On the same hand, the distribution of these reactions onto CNC were speeded up by mean of effects of microjets and shockwaves resulted from ultrasonic cavitation from simultaneous US treatment. Lastly, the magnetic attract ability of the resultant MCNC nanocomposite has been evidenced in Figure 3.4. The MCNC (black powder) was found to stay at rest without external magnetic field (EMF), and get drawn towards the origin of magnetic field as a magnet was brought near to them.

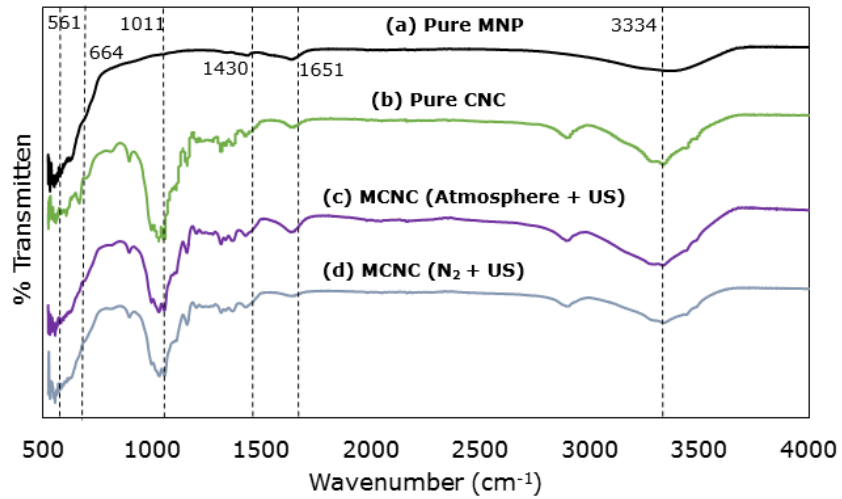


Figure 3.1. FTIR spectra of (a) pure MNP, (b) pure CNC, as well as MCNC prepared under (c) atmosphere condition, and (d) N₂ condition.

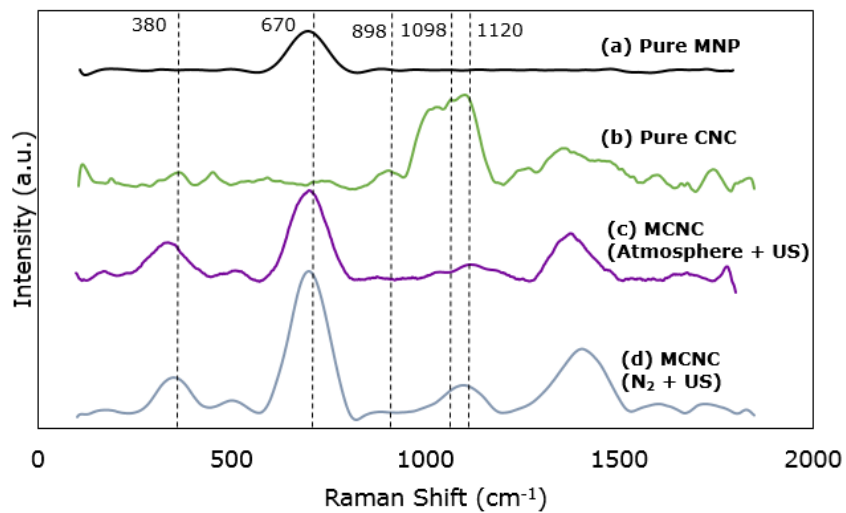


Figure 3.2. Raman spectroscopy spectra of (a) pure MNP, (b) pure CNC, as well as MCNC prepared under (c) atmosphere condition, and (d) N₂ condition.

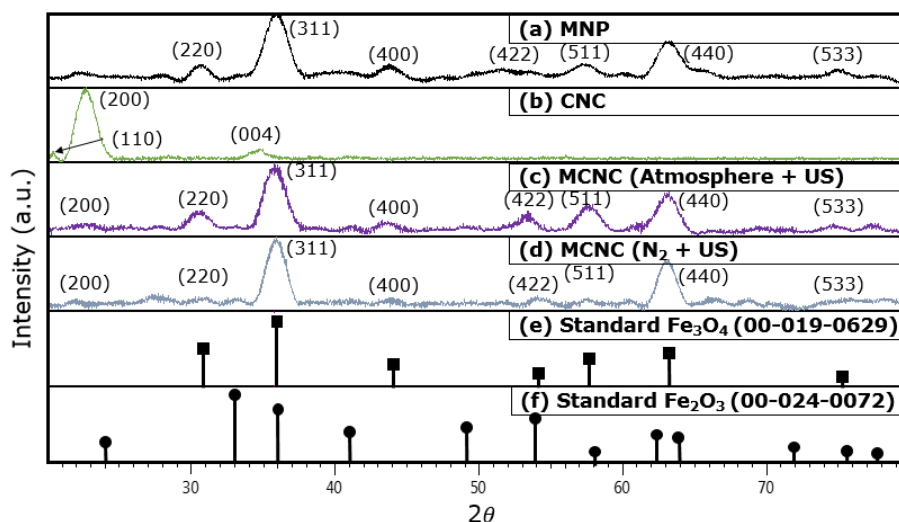


Figure 3.3. XRD pattern for (a) pure MNP, (b) pure CNC, as well as MCNC prepared under (c) atmosphere condition, (d) N₂ condition, and the standard XRD peaks for (e) Fe₃O₄, and (f) Fe₂O₃.

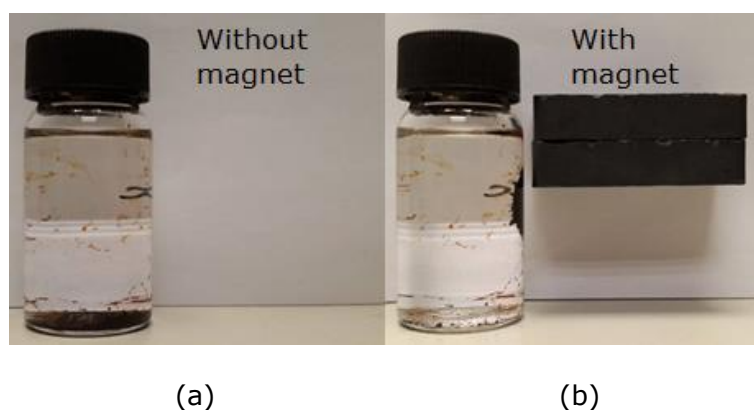


Figure 3.4. Image of MCNC (a) without EMF, and (b) being attracted under EMF.

From STEM images (Figure 3.5a and b), the freshly prepared pure MNP exhibited severe particle agglomeration while pristine CNC, on the other hand, showed a web-like linked network from its rod-like structure. As illustrated in Figure 3.5c and d, the use of CNC as dispersant caused the MNPs to be distributed uniformly on the surface of the CNC fibre. Based on the histogram data (Figure 3.5e and f), no significant differences were detected for both nanocomposite samples prepared under aerobic (11.92 ± 5.32 nm) and N₂ atmosphere (11.43 ± 5.81 nm). The elemental analysis by EDX demonstrated the

existence of ferrous, carbon, oxygen, and sulphur in our samples prepared under both aerobic and inert conditions (Figure 3.6).

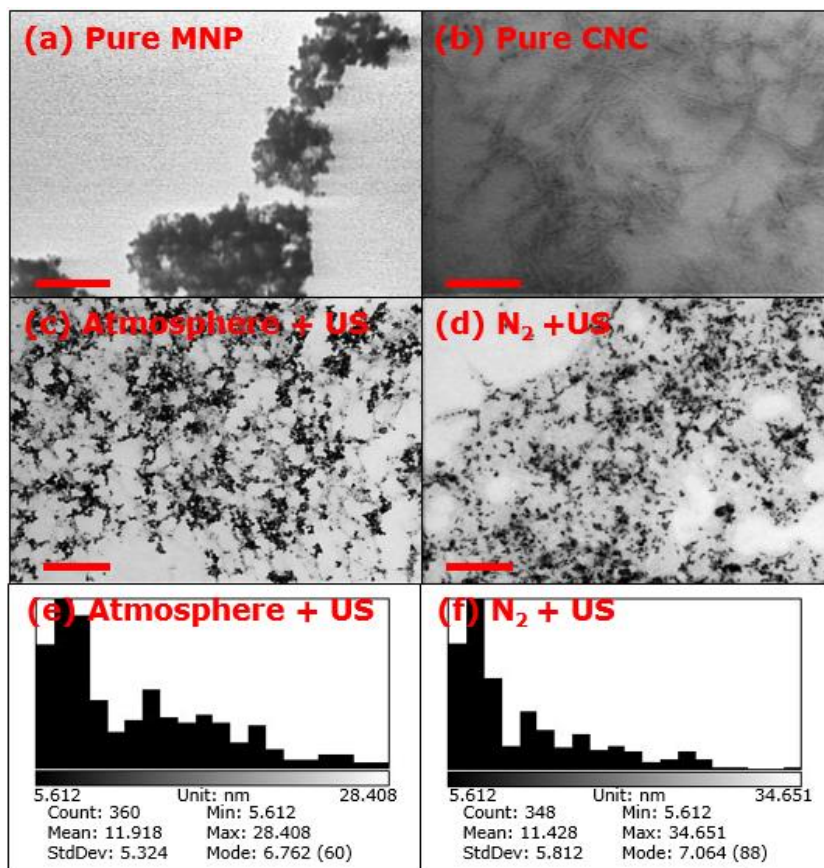


Figure 3.5. FE-SEM images of (a) Pure MNP, (b) Pure CNC, as well as MCNC prepared under (c) atmosphere condition, and (d) N₂ condition. MNPs feret diameter distribution histogram for STEM images. (e) Atmosphere condition, and (f) N₂ condition.

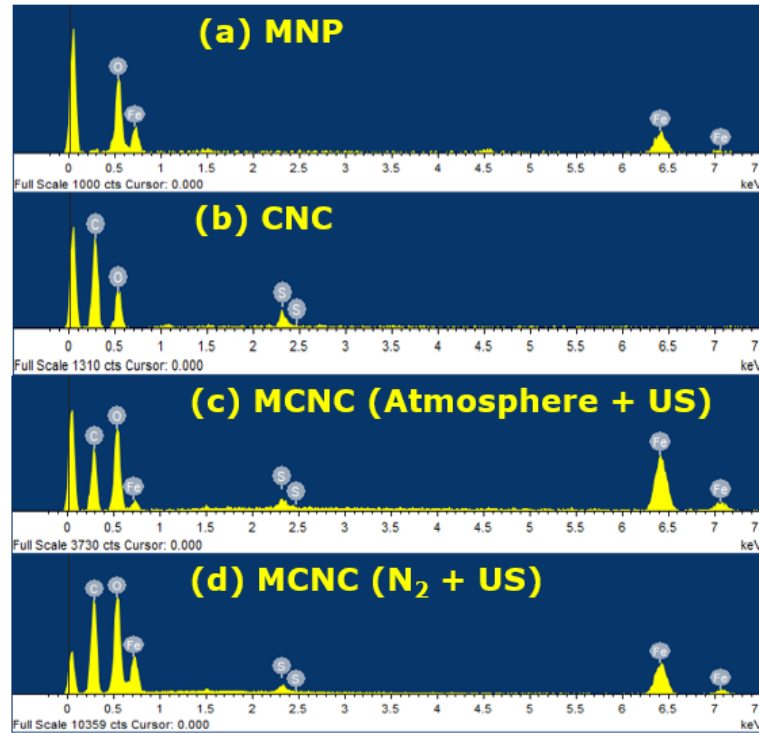


Figure 3.6. EDX data representing (a) MNP, (b) CNC, as well as MCNC prepared under (c) atmosphere condition, and (d) N₂ condition.

To estimate the surface coverage of hydroxyl and sulphate groups on CNC surfaces, an estimation calculation was performed as prescribed by Lin and Dufresne, (2014), Gu *et al.* (2013), and Lin, Huang, and Dufresne, (2012). First the sulphate groups content were obtained from supplier to be 1.5×10^{-4} mol/g (equivalent to 0.96 wt% of sulphur content). The total hydroxyl groups content, on the other hand, was estimated using Equation (3.1)

$$N_{OHA} = \frac{120}{N_A(2(A_{110} + A_{1\bar{1}0}))} \quad [\text{Equation 3.1}]$$

$$A_{110} = c(B110) \quad [\text{Equation 3.1-1}]$$

$$A_{1\bar{1}0} = c(B1\bar{1}0) \quad [\text{Equation 3.1-2}]$$

From Equation (3.1), it was mentioned by Gu *et al.* (2013) that 36 glucan chains are present along the surface of a crystal. This resulted in total 120 hydroxyl groups available on 36 cellobiose units (Lin and Dufresne, 2014; Gu *et al.*, 2013; Lin, Huang, and Dufresne, 2012). The value of d_{110} and $d_{1\bar{1}0}$ was extracted from information reported by Ju *et al.* (2015) based on CNC from wood pulp. In addition, it was shown in literature that the elementary

crystallite region for CNC demonstrated a square section of 10×10 glucose units based on the d-spacing of (110), (1 $\bar{1}$ 0), and (200) planes (Lin and Dufresne, 2014; Gu *et al.*, 2013; Lin, Huang, and Dufresne, 2012). This thus gives B_{110} and $B_{1\bar{1}0}$ values of 5.31 and 5.93 nm respectively. Next, studies done by Habibi, Lucia, and Rojas, (2010) showed that the crystal and molecular structure of cellulose I β exists in monoclinic P2₁ crystal had dimensions of ($a = 7.784 \text{ \AA}$, $b = 8.201 \text{ \AA}$, $c = 10.38 \text{ \AA}$, and $\gamma = 96.5^\circ$). Therefore, this gives, $A_{110} = 5.31 \times 1.038 \text{ nm}^2$, $A_{1\bar{1}0} = 5.93 \times 1.038 \text{ nm}^2$, and N_a (Avogadro's number) = 6.02×10^{23} . Substituting these information into Equation (3.1) subsequently gives the total number of hydroxyl groups per unit surface area (N_{OHA}) of $8.5426 \times 10^{-6} \text{ mol m}^{-2}$. Consequently, the total number of hydroxyl groups per unit mass CNC (N_{OHM}) can be calculated using Equation (3.2). Here the total specific surface area ($A_{totalCNC}$) can be calculated from Equation (3.2-1) (Ju *et al.*, 2015).

$$N_{OHM} = N_{OHA} \frac{A_{totalCNC}}{m_{cnc}} \quad [\text{Equation 3.2}]$$

$$\frac{A_{totalCNC}}{m_{cnc}} = \frac{1}{\rho_{cnc}} \frac{4}{W} \quad [\text{Equation 3.2-1}]$$

Where W , m_{cnc} and ρ_{cnc} are width (5 nm), mass (1 g), and density of CNC (1.5 g cm^{-3}), respectively. The data calculated were tabulated in Table 3.1

Based on the calculations, N_{OHM} was found to be $1.7523 \times 10^{-3} \text{ mol/g}$. The surface coverage of sulphate groups on CNC surfaces under every sample is around 8.5 %. This suggested that the sulphate groups existed as minor functional groups on CNC surfaces.

Table 3.1. Total amount of sulphate group ($-\text{SO}_3$) and surface hydroxyl group ($-\text{OH}$), and percentage of sulphate groups coverage on CNC surface.

Functional Group	Surface Content (mol/g)	Surface Coverage (%)
Sulphate ($-\text{O}_3\text{S}$)	1.5000×10^{-4}	8.56
Hydroxyl ($-\text{OH}$)	1.7523×10^{-3}	91.44

TGA experimental results of MNP samples show no significant loss of weight over a temperature range of 0 to 900 °C (Figure 3.7a). On the other hand, CNC experienced a drastic weight reduction at temperature of about 280 °C, with a pronounced plateau corresponding to 2 % ash residues remained at 600 °C (Figure 3.7b). The abrupt reduction in the weight loss of CNC was primarily caused by the typical thermal degradation of cellulose fibre following by the breakdown of CNC core region (Criado *et al.*, 2016; Moon *et al.*, 2011; Petersson, Kvien, and Oksman, 2007; Tang *et al.*, 2014; Zoppe *et al.*, 2010). The TGA curves of both as-prepared MCNC displayed similar trend and shows two steps of thermal weight loss. During the first step cellulose fibre was pyrolyzed at around 200 °C as the result of thermal decomposition of CNC. The second weight reduction at around 780 °C can be considered as removal of the oxygen atoms which symmetrically bonded to Fe₃O₄ NPs. From Figure 3.7c, it was found that there was nearly 55 % residue left in MCNC sample before the second weight losses. This shows that MCNC contained 55 % of Fe₃O₄. After the second step drop, the weight drops to 39 %. This information correlate well with the theoretical relative molecular weights calculations of Fe₃O₄. Fe₃O₄ with 3 Fe and 4 O have relative molecular weights of 232 g/mol. Relative atomic mass of Fe and O are 56 and 16 g/mol respectively. Hence, the total Fe and O content are 72.4 and 27.6 % respectively. One could envision that there were 71 % of Fe and 29 % of O in the sample by comparing the TGA information. Thus we could confirmed that the degradation at 780 °C were representing the removal of O content from Fe₃O₄.

The as-prepared MCNC, however, possessed lower thermal stability as the second weight loss at around 780 °C was not observed in pristine MNPs. When Fe₃O₄ obtained the oxygen content from the surface functional groups of CNC, its structure was more dependent on the availability of surface functional groups. Hence, a more polycrystalline structure Fe₃O₄ will be produced. The less dense structure thus caused the deposited MNPs to have slightly lower thermal stability as compared to the pure MNPs. To support that, Kalska-Szostko *et al.*, (2015) have reported the supreme thermal stability of monocrystalline magnetite nanoparticles over the polycrystalline one. In fact, our selective area electron diffraction data also verified the hypothesis mentioned above (see Figure 3.8).

It is noted that the weight loss of atmospheric pressure-induced MCNC was relatively lower (≈ 6 wt% lesser) than its counterpart prepared under N_2 stream, suggesting the presence of higher content of magnetite NPs. One possible explanation was that the abundance of O_2 -rich air as oxidant increase the rate of Fe^{2+} oxidation, and subsequently enhance the nucleation and growth rate of Fe_3O_4 particle, thereby giving rise to a higher magnetite content. The same phenomena was also observed and recorded by other author (Dang *et al.*, 2007).

To investigate the magnetic properties of the MCNC nanocomposites, magnetization measurements have been performed using VSM and the magnetization hysteresis loops of MNP and MCNC samples were presented in Figure 3.9. The magnetization plot revealed that the saturation magnetization (M_s) of the pure MNPs was found to be 38.967 emu/g, while MCNCs prepared under atmospheric and N_2 conditions exerted lower value of 27.974 and 22.909 emu/g respectively. The decrease in M_s was mainly due to the existence of non-magnetic responsive CNCs in the MCNC samples. Besides that, Figure 3.8 also showed that the M_s of MCNC nanocomposites prepared under N_2 gas bubbling was relatively lower (≈ 23 emu/g) in comparison to those prepared in aerobic mode (≈ 27 emu/g). The observed lower magnetivity was mainly attribute to the lower content of MNPs present in MCNC sample obtained under N_2 environment, as mentioned previously in TGA analysis. The VSM results demonstrated that the magnetivity of all samples diminished upon removal of the EMF (superparamagnetic behaviour). This was also highly similar to the phenomena in Figure 3.4, where the MCNC remain at rest without an EMF, and get attracted in the presence of a magnet.

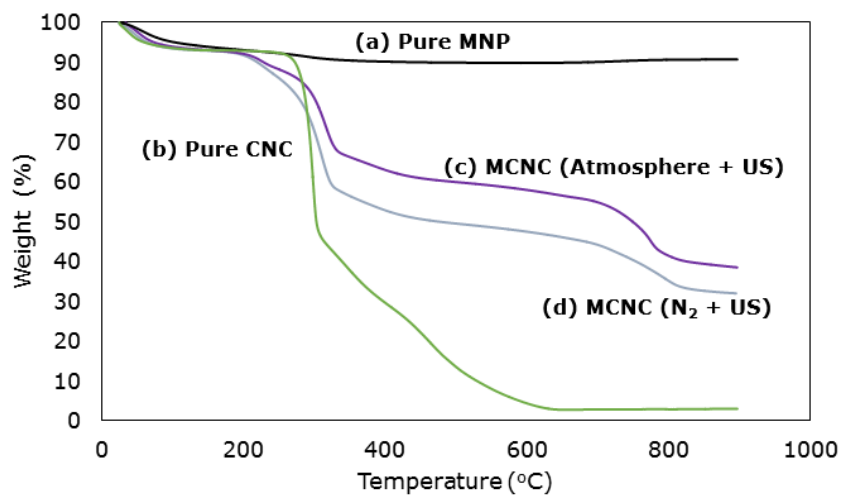


Figure 3.7. TGA data representing weight loss % at different temperature for (a) MNP, (b) CNC, as well as MCNC prepared under (c) atmosphere condition, and (d) N₂ condition.

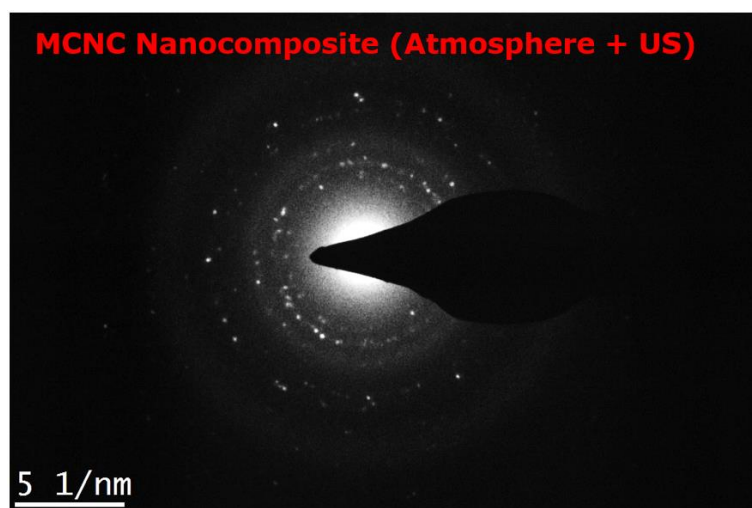


Figure 3.8. SAED image of sonochemically prepared MCNC under atmosphere condition.

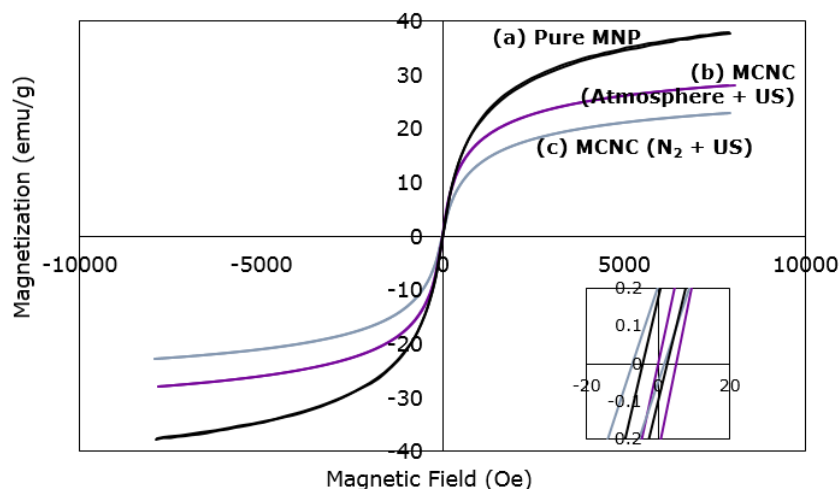


Figure 3.9. Magnetization curve for (a) MNP, MCNC prepared under (b) atmosphere condition, and (c) N_2 condition.

3.3.2 The Mechanism of MCNCs

For control purposes, MCNC nanocomposite under different controlled conditions was prepared for comparison. The samples E1, E2, E3, and E4 represented samples prepared *in-situ* with US, *in-situ* without US, without *in-situ* with US, and without *in-situ* without US respectively (Figure 3.10). From FTIR analysis, it was obvious that sample E4 presented spectra similar to pure MNP, indicating that there was no interaction between MNP and CNC. The FTIR spectra of E3, on the other hand, was similar to pristine CNC. This was most likely due to low MNPs content in the sample. The MNPs that were deposited onto CNC was only due to the US-induced physical deposition, where the MNPs were forcefully anchored in CNC matrix due to the US. In contrast to E3 and E4, the FTIR spectra of E1 and E2 were highly identical. This correlated well with our FTIR analysis in section 3.3.1, where the Fe (II) and (III) ions electrostatically interacted with surface hydroxyl and sulphate ester groups of CNC, and this ultimately led to the growth of MNPs on the anchored surface functional group's sites.

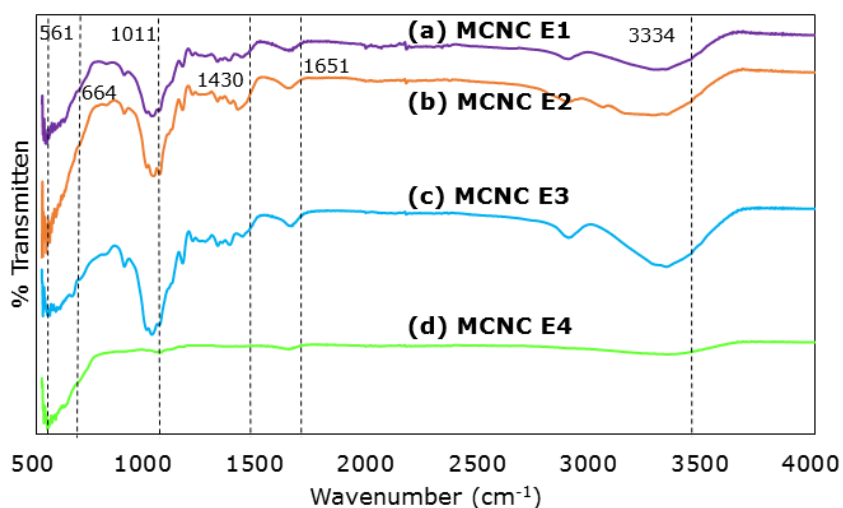


Figure 3.10. FTIR spectra of (a) Sample E1, *in-situ* with US, (b) Sample E2, *in-situ* with mechanical stirring, (c) Sample E3, without *in-situ* with US, and (d) Sample E4, without *in-situ* with mechanical stirring.

STEM analysis was next performed. From STEM analysis, sample E4 (Figure 3.11d) showed that the MNPs were still highly aggregated, and the deposition of MNPs on CNC was negligible. This suggested that there were no interactions between MNPs and CNC in sample E4. Sample E3, on the other hand, provided a less aggregated MNPs with slightly higher deposition (Figure 3.11c). This was due to ultrasonic cavitation effects that help in dispersing the MNPs during the coating process. However, the MNPs loading remained low. In addition, because MNPs have been formed prior to its deposition on CNC surfaces, the resultant MNPs showed an average MNPs diameter of 66.86 ± 32.17 nm (Figure 3.12c). The presence of CNC as the dispersant (*in-situ* preparation conditions) led to uniform MNPs dispersion (Samples E1 and E2) (Figure 3.11a and b). By comparing the MNPs diameter for both E1 and E2, one can easily observe that E1 gives a much smaller MNPs diameter of 12.31 ± 3.07 nm as compared to E2 with MNPs diameter of 29.03 ± 14.55 nm (Figure 3.12a and b). It is likely that the US aided in dispersing the MNPs during its preparation. This ultimately led to a shorter time requirement for better dispersibility and lower diameter of MNP on CNC surface. In overall, the findings supported our previous claims on all

samples. In addition, this also proved the feasibility and efficiency of ultrasonic cavitation in the preparation of MCNC hybrid nanocomposite.

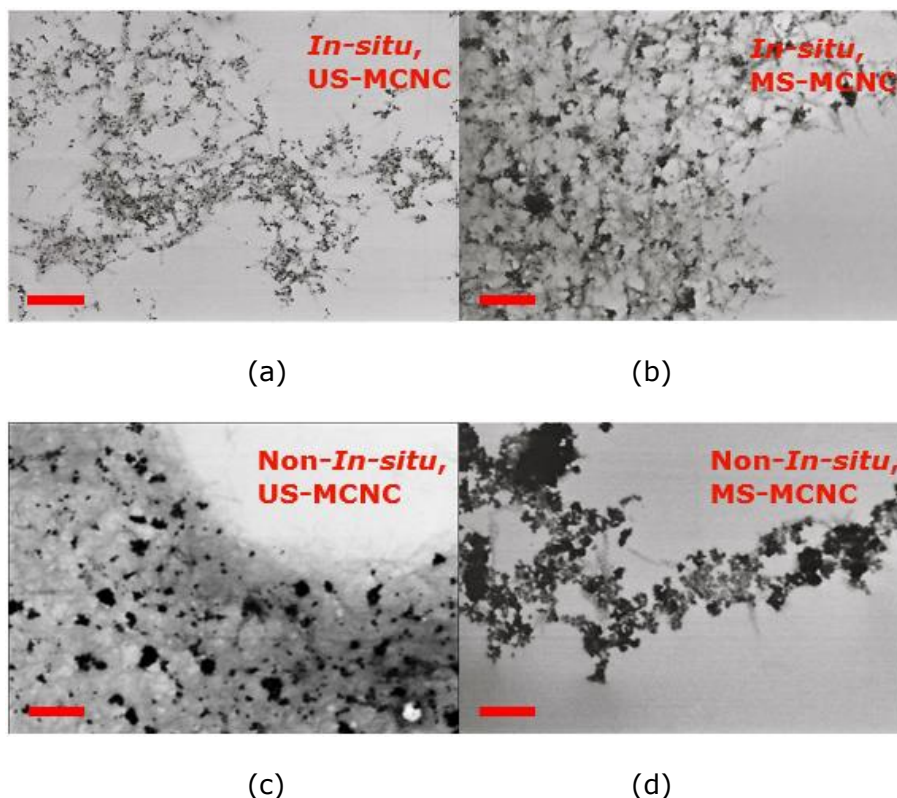


Figure 3.11. STEM images of (a) Sample E1, in-situ with US, (b) Sample E2, in-situ with mechanical stirring, (c) Sample E3, without in-situ with US, and (d) Sample E4, without in-situ with mechanical stirring. All scale bar are representing 300 nm.

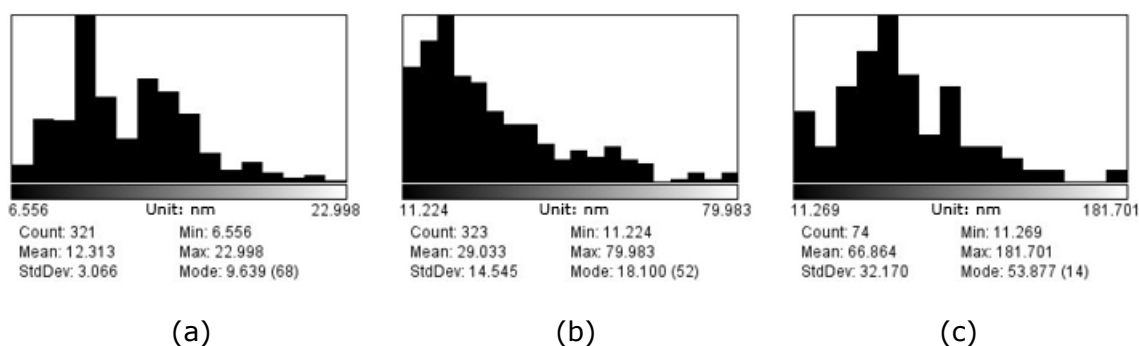


Figure 3.12 Histogram of MNPs diameter on the STEM images for (a) E1: US assisted in-situ prepared MCNC, (b) E2: mechanically stirred in-situ prepared MCNC, and (c) E3: US assisted non-in-situ prepared MCNC.

TGA analysis was again carried out to check the composition of MNP and CNC in all samples (Figure 3.13). Interestingly, there were distinct differences in the elemental composition of all samples. While MCNC E1, E2, and E3 are similar to the previous MCNC samples, there was only one small step loss for MCNC E4. This showed that there was no direct interaction between MNP and CNC. It is likely that the presence of small amount of CNC (resulted from the small weight loss at typical degradation temperature for CNC) was due to the inefficiency in separating the MNPs from CNC dispersion after the reaction. A tiny amount of CNC may have stuck around with MNPs and get drawn together from magnetic separation. On the other hand, sample E3 was found to have the least amount of MNPs. This is in agreement with the STEM images in Figure 3.11 since it was obvious that the deposition of MNPs in E3 was much lesser as compared to both E1 and E2. Moving on to E1 and E2 samples, The E1 sample showed higher MNPs content as compared to E2. This is attributed to the acceleration of MNPs formation due to ultrasonic irradiation; under mechanical stirring (E2 sample), the Fe^{2+} was oxidized mainly by the dissolved oxygen in the aqueous medium (Dang *et al.*, 2007). Otherwise during US treatment, the Fe^{2+} undergoes oxidation by the sonication-induced radical ($\bullet\text{OH}$ and $\bullet\text{H}$) and H_2O_2 (Dang *et al.*, 2007; Vijayakumar *et al.*, 2000). This thus led to the acceleration on oxidation of Fe^{2+} , thereby speeding up the nucleation and growth rate of MNPs on cellulose fibre. In literature, the similar trend has been observed by Dang *et al.* (2007) in the preparation of MNPs via both mechanical stirring and US routes.

Magnetization plot for all samples was shown in Figure 3.14. It was noticed that the M_s was highest for E4 (≈ 29 emu/g), followed by E1 (≈ 27 emu/g), then E2 (≈ 26 emu/g), while E3 has the lowest magnetic strength (≈ 8 emu/g). This demonstrated a relation between the magnetivity and the MNPs content of the corresponding sample. Since VSM method allowed one to measure the magnetivity of solid samples per unit mass of magnetic particles, by hypothesizing that all magnetic particles presence were Fe_3O_4 , the M_s of the resultant sample will drop if lower MNPs content was detected. The investigation suggested that US assisted in-situ co-precipitation method give rise to MCNC nanocomposite with

highest magnetic strength and finest MNPs dispersion as compared to other methods investigated in this section.

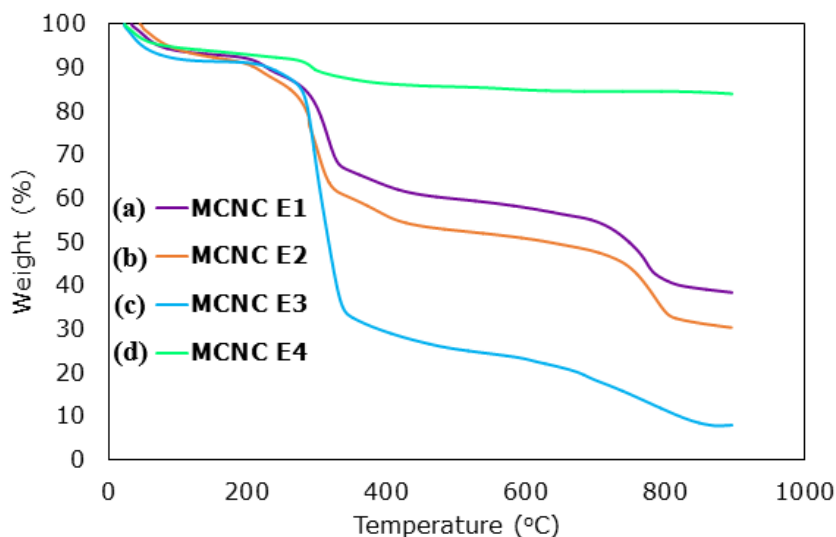


Figure 3.13. TGA data representing weight loss % at different temperature for (a) E1, US assisted in-situ prepared MCNC, (b) E2, mechanically stirred in-situ prepared MCNC, (c) E3, US assisted non-in-situ prepared MCNC, and (d) E4, mechanically stirred non-in-situ prepared MCNC.

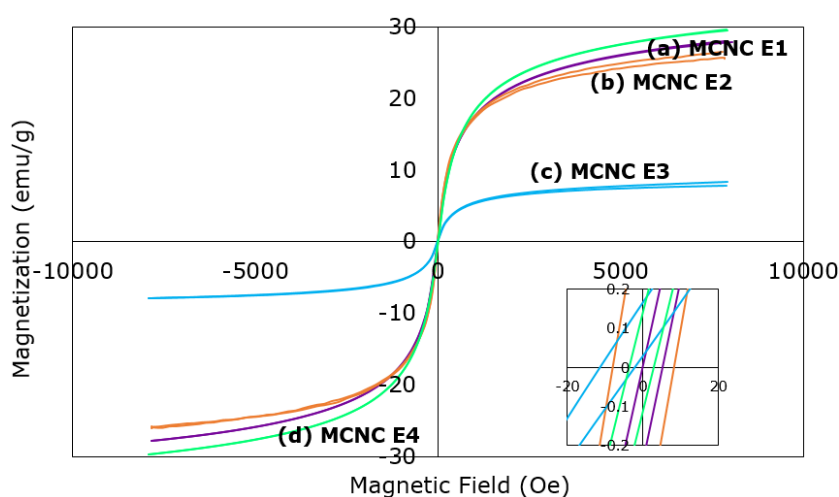


Figure 3.14 Magnetization plot of MCNC samples of (a) E1, US assisted in-situ prepared MCNC, (b) E2, mechanically stirred in-situ prepared MCNC, (c) E3, US assisted non-in-situ prepared MCNC, and (d) E4, mechanically stirred non-in-situ prepared MCNC. The inset shows the negligible coercivity in all samples.

3.4 Conclusions

CNC coated with superparamagnetic MNPs were successfully synthesized *in-situ* via ultrasonic-assisted co-precipitation method. The reaction between iron precursors and surface hydroxyl groups of CNC was confirmed through FTIR analysis. The absence of dual peaks at around 665 and 730 cm^{-1} in Raman spectrum confirmed no occurrence of oxidation of Fe_3O_4 to Fe_2O_3 . The CNC's surface functional groups directly interact with the Fe ions, suggesting that surface functional groups act as anchoring sites for Fe ions via electrostatic attraction during *in-situ* formation of MCNC to prevent MNPs from agglomerating. The presence of CNC as antioxidant minimized unwanted oxidation of MNPs. EDX studies confirmed the presence of all necessary elements in the MCNC samples. The XRD and FE-SEM results confirmed that MNPs diameter falls around 11 ± 5 nm. VSM results proved the superparamagnetic properties of all MCNC samples. The TGA data of both sonochemically prepared MCNCs revealed that there was higher MNPs content in MCNC nanocomposite prepared under atmospheric condition (55 wt% in nanocomposite) as compared to those prepared under N_2 protection (49 wt% in nanocomposite). The higher MNPs content then leads to higher magnetic strength in atmospheric-induced MCNC nanocomposite. The current study also showed that there were no chemical interactions between the MNP and CNC if the preparation were carried out without *in-situ* situation. The MCNC nanocomposite prepared via *in-situ* US assisted method shows supreme dispersibility of MNPs and desired magnetivity as compared to others controlled samples that either without US or without *in-situ* conditions. The *in-situ* sonochemical co-precipitation method under atmospheric conditions will be employed for all MCNC preparation in this project.

CHAPTER FOUR

PHYSICOCHEMICAL AND WETTING CHARACTERISTICS OF MCNC

NANOCOMPOSITES

Overview

In this chapter we performed a detailed parametric study on the preparation of MCNC nanocomposites. Parameters including the ratio of MNP and CNC, pre-heated temperature, ultrasound (US) power and sonication time were investigated based on the morphology, magnetivity and colloidal stability of the resultant MCNC have been carried out. Results showed that increasing CNC/MNP ratio from 0.2 to 1 improved the dispersion of MNPs on CNC fibres. This, however, led to the decrement in the amount of deposited MNPs on CNC, which thus resulted in the reduction of the magnetic strength of the resultant MCNC nanocomposites. The pre-heated temperature was found to affect the saturation magnetization strength of the nanocomposites but not the MNPs dispersion on the CNC rod. The best pre-heated temperature for the $\text{Fe}^{2+}/\text{Fe}^{3+}$ @CNC mixture prior to Fe_3O_4 preparation was 45 °C. Increasing US irradiation time allowed a noticeable reduction of mean MNP size from 46 to 12 nm with reduced particle aggregation. However, increasing the sonication time above 5 min leads to the oxidation of Fe_3O_4 to Fe_2O_3 . Based on our findings, only the CNC/MNP ratio influenced the colloidal stability of the nanocomposites. The MCNC obtained were colloidally stable at CNC/MNP ratio ≥ 1 as regarded by the considerably high surface zeta potential values. Further, we evaluated the Pickering stabilizing performance of the MCNC nanocomposites by determining the effects of CNC/MNP ratio and pH on the surface wettability of the nanocomposites. The results suggested that the MCNC suspensions (CNC/MNP ratio = 1) at pH 3 to 7 are more likely to provide a stable Pickering emulsions system due to the obtained surface wetting contact angle that is close to 90 °. This estimation will be verified in the next chapter during the preparation of MCNC-stabilized Pickering emulsions.

4.1 Introduction

Iron oxide or Fe_3O_4 nanoparticles (MNPs) are excellent superparamagnetic material that has been drawing increasing attention in various biomedical applications since decades ago due to its low cost, negligible toxicity, good biocompatibility properties as well as its reusable tendencies (Lattuada and Hatton, 2007; Szpak *et al.*, 2013). In the previous stage, cellulose nanocrystals (CNCs) have been proven to be able to bind firmly with the MNPs via covalent bonding in the sonochemical *in-situ* co-precipitation process. The deposition of MNP on the CNC not only improve the dispersion of MNPs in aqueous suspensions but also successfully extended its usage as a cellulose-based magnetic nanocomposites in various applications including magnetic hyperthermia, drugs delivery, and antibacterial activity (Anirudhan and Rejeena, 2014; Nypelö *et al.*, 2014; Xiong *et al.*, 2013).

Although extensive researches have been performed on determining the performance of the MNP@CNC (MCNC) nanocomposites in many applications, the fundamental knowledge relating the factors affecting the properties of the resultant MCNC nanocomposites as well as its feasibility to work as an effective Pickering stabilizer for emulsions remained undetermined. To tackle this problem, we performed detailed parametric studies to determine a desirable reaction condition for the preparation of MCNC nanocomposites basing on its morphology, dispersibility, and magnetivity. Further, since the surface wettability of a particle stabilizer is the most vital factors that affect the Pickering emulsion formation performance (Binks and Lumsdon, 2000c, 2001), the wetting behaviour of MCNC was measured and evaluated thoroughly in this work to examine the practicality of the as-prepared MCNC nanocomposites as the particle stabilizer for Pickering emulsions production. In brief, parameters including CNC/MNP ratio, pre-heated temperature as well as US power and sonication time were investigated to determine their influences on the MCNC preparation. On the other hand, since MNP is a pH-responsive material (Tremaine and Leblanc, 1980; Vepsäläinen and Saario, 2010), The effects of pH on the surface wettability of the resultant MCNC is also studied to verify the feasibility of the MCNC nanocomposites as a particle stabilizer for the emulsion.

4.2 Materials and Methodology

4.2.1 Materials

Iron (II) chloride tetrahydrate ($\text{FeCl}_2 \cdot 4\text{H}_2\text{O}$, $\geq 99\%$), iron (III) chloride hexahydrate ($\text{FeCl}_3 \cdot 6\text{H}_2\text{O}$, 99%) and ammonium hydroxide (28% NH_3 in H_2O) were purchased from Sigma-Aldrich. CNC (Freeze dried, 0.96 wt%) purchased from University of Maine. All water used in this experiment are ultrapure water ($18.2 \text{ M}\Omega \text{ cm}^{-1}$) obtained from Milli-Q® Plus apparatus (Millipore, Billerica, USA), ethanol (AR standard), 1M hydrochloric acid (HCl), and sodium hydroxide (NaOH) purchased from R & M Chemical (Syarikat Saintifik Jaya, Malaysia). All experiments involving US were conducted on an ultrasound probe sonicator (20 kHz, Lab750, Sinaptec) under pulse mode (15 s pulse on, 10 s pulse off). All chemicals in this study were of analytical grade and employed without further purification.

4.2.2 Synthesis and Characterisation of MCNC Nanocomposite

4.2.2.1 MCNCs Prepared with Different CNC/MNP ratio

CNC was first dispersed in water at various concentrations (0.01, 0.05, 0.1, 0.5, and 1 wt%). Next, fixed amount of iron (III) and iron (II) chloride (1.5/1 $\text{Fe}^{3+}/\text{Fe}^{2+}$ mol ratio) were added into the CNC dispersion. The mixtures were stirred and the temperature were fixed at 45 °C. Subsequently, the CNC + $\text{Fe}^{2+/3+}$ mixtures were and sonicated at 60 w US power using ultrasonic horn in the presence of ammonium hydroxide (2.2 ml) for 5 minutes. The resulted MCNC were magnetically separated and washes 3 times with water to remove all ammonium hydroxide. Lastly, the leftover were centrifuged at 4500 rpm for 20 minutes, and dried in an oven overnight. The dried sample were stocked and utilized for characterisation. The CNC/MNP ratio represented by each CNC concentrations will be 0.2, 1, 2, 10 and 20 respectively.

4.2.2.2 MCNCs Prepared with Different Pre-heating temperature

CNC was first dispersed in water at 0.05 wt%. Next, fixed amount of iron (III) and iron (II) chloride (1.5/1 $\text{Fe}^{3+}/\text{Fe}^{2+}$ mol ratio) were added into the CNC dispersion. The mixtures were

stirred and the temperature were adjusted to (25, 45, 65, and 85 °C). Subsequently, the CNC + Fe^{2+/3+} mixtures were and sonicated at 60 w US power using ultrasonic horn in the presence of ammonium hydroxide (2.2 ml) for 5 minutes. The resulted MCNC were magnetically separated and washes 3 times with water to remove all ammonium hydroxide. Lastly, the leftover were centrifuged at 4500 rpm for 20 minutes, and dried in an oven overnight. The dried sample were stocked and utilized for characterisation.

4.2.2.3 MCNCs Prepared with Different Ultrasound Power

CNC was first dispersed in water at 0.05 wt%. Next, fixed amount of iron (III) and iron (II) chloride (1.5/1 Fe³⁺/Fe²⁺ mol ratio) were added into the CNC dispersion. The mixtures were stirred and the temperature were fixed at 45 °C. Subsequently, the CNC + Fe^{2+/3+} mixtures were and sonicated under different US power (40, 60, and 80 w) using ultrasonic horn in the presence of ammonium hydroxide (2.2 ml) for 5 minutes. The resulted MCNC were magnetically separated and washes 3 times with water to remove all ammonium hydroxide. Lastly, the leftover were centrifuged at 4500 rpm for 20 minutes, and dried in an oven overnight. The dried sample were stocked and utilized for characterisation.

4.2.2.4 MCNCs Prepared with Different Sonication Time

CNC was first dispersed in water at 0.05 wt%. Next, fixed amount of iron (III) and iron (II) chloride (1.5/1 Fe³⁺/Fe²⁺ mol ratio) were added into the CNC dispersion. The mixtures were stirred and the temperature were fixed at 45 °C. Subsequently, the CNC + Fe^{2+/3+} mixtures were and sonicated under 60 w US power using ultrasonic horn in the presence of ammonium hydroxide (2.2 ml) for 1, 3, 5, 7, and 10 minutes. The resulted MCNC were magnetically separated and washes 3 times with water to remove all ammonium hydroxide. Lastly, the leftover were centrifuged at 4500 rpm for 20 minutes, and dried in an oven overnight. The dried sample were stocked and utilized for characterisation.

4.2.3 Characterisation of MCNCs

The size and surface morphology of the sonochemically prepared MCNCs were analysed using field emission scanning electron microscope (FE-SEM) (SU8010, Hitachi, Japan) at 15 kV. Elemental mapping were performed through Energy-dispersive X-ray spectroscopy (EDX) using the same FE-SEM. Functional groups available were examined through Fourier transform infrared spectroscopy (FTIR) over a range of 550 – 4000 cm^{-1} on a FTIR spectrophotometer (Nicolet iS10, Thermo Scientific, USA) equipped with diamond probe. Magnetic strength of MCNCs was measured via vibrating sample magnetometry (VSM) (Lakeshore 7400 Series, Lakeshore Cryotronics, USA). Surface wettability of MCNCs was analysed using a contact-angle goniometer (Ramé-hart, USA). Chemical composition and thermal stability was evaluated by thermogravimetric analysis (TGA) in the temperature range of 25 to 900 °C at 10 °C/min using a thermogravimetric analyzer (Q50 TGA, TA instrument, USA). X-ray photoelectron spectroscopy (XPS) spectra were obtained using a scanning X-ray microprobe PHI Quantera II (Ulvac-PHI, USA) with a monochromatic Al $K\alpha$ X-ray source ($h\nu = 1486.6 \text{ eV}$).

4.2.4 Conductometric Titration.

The sulphate groups content of CNC were determined with a method done by Jiang, Esker and Roman (Jiang, Esker and Roman, 2010) with slight modification. Briefly, 50g of CNC suspensions at different concentration, with the presence of 1mM sodium chloride, was placed in a 50 mL beaker, and a conductivity electrode was inserted to the dispersion. The dispersion was titrated against 0.02 M NaOH solution and all conductivity values were measured using a Eutech Instrument PC700 conductometer (Eutech Instruments, USA), at the temperature of $24.5 \pm 0.1 \text{ }^\circ\text{C}$. The amount of sulphate group was then calculated as described in the standard procedure (SCAN-CM 65:02).

4.2.5 Statistical Analysis

Experiment is repeated for obtaining triplicate measurements. Analysis of variance (ANOVA) would be conducted utilizing Prism software and $p < 0.05$ is considered as statistically significant. Images obtained from microscopic analysis would be evaluated using ImageJ software.

4.3 Results and Discussion

4.3.1 MCNCs Preparation: Impact of Reaction Conditions

4.3.1.1 CNC/MNP ratio

The CNC/MNP ratio was one of the most important factor to be evaluated for MCNC preparation. The FTIR analysis revealed that the surface hydroxyl groups became in excess with increasing CNC content. As observed in Figure 4.1, the characteristic C—OH peak at 664 cm^{-1} make it's pronounce existence in MCNC10 and MCNC20 samples. This showed that the MNPs formed were too little as compared to the dispersant concentration.

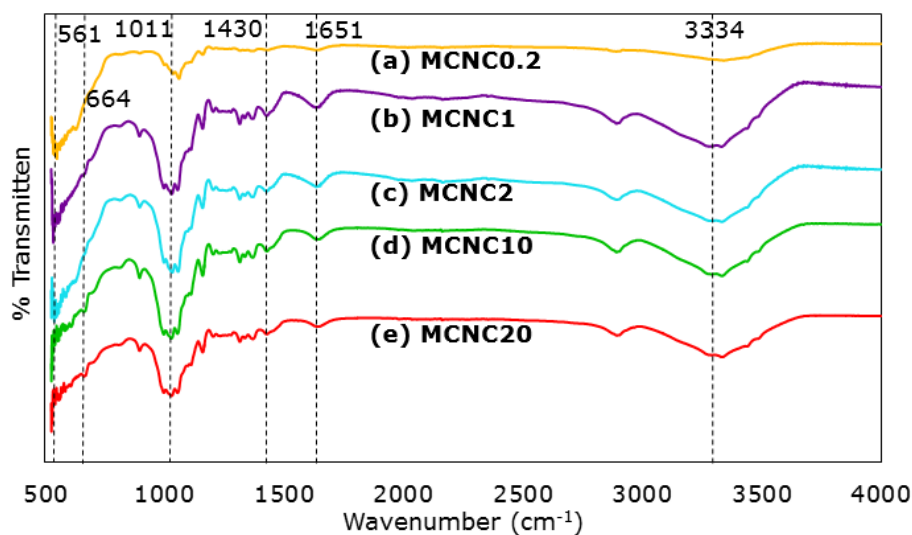


Figure 4.1. FTIR spectra of MCNC samples prepared with different CNC/MNP ratio, (a) 0.2, (b) 1, (c) 2, (d) 10, and (e) 20.

STEM analysis was performed to evaluate the dispersion of MNPs on CNC template with varying the ratio. From Figure 4.2, the highest MNPs coverage were spotted on MCNC0.2 sample (Figure 4.2b). However, the inset of MCNC0.2 showed that there was severe aggregation of MNPs (Figure 4.2b inset) as compared to the other sample (Figure 4.2c – f insets). Despite of slightly lowered surface coverage, a much improved dispersion of MNPs was observed at MCNC1 (Figure 4.2c inset). Besides that, Figure 4.2c – f showed that the dispersivity of MNPs gradually improved when CNC/MNP ratio increased from 1 to 20. This STEM analysis confirmed the role of CNC as an effective dispersant for MNPs.

The microscopic images (Figure 4.2) illustrated that MNPs diameter decreased with increasing CNC/MNP ratio. Based on ImageJ analysis, the average particle size of MNPs reduced significantly ($P < 0.05$) from 16 nm to 12 nm when CNC/MNP ratio increased from 0.2 to 1 (Figure 4.3a). Interestingly, negligible changes was observed in MNPs diameter when the ratio was more than 1 (Figure 4.3a). The main reason for this size reduction was due to the insufficient amount of CNC for stabilizing all MNPs at CNC/MNP ratio of 1. In this study, CNC1 led to a good dispersion for MNPs with smallest MNPs diameter around 12 nm. It was noticeable that the counts of MNPs on MCNC samples reduces when CNC concentration increases. Thus the sample MCNC0.2 results in slight aggregation of MNPs, while MCNC20 shows most scattered MNPs loading. The microscopic images implies that lower CNC concentration will resulted in higher MNPs loading and vice versa.

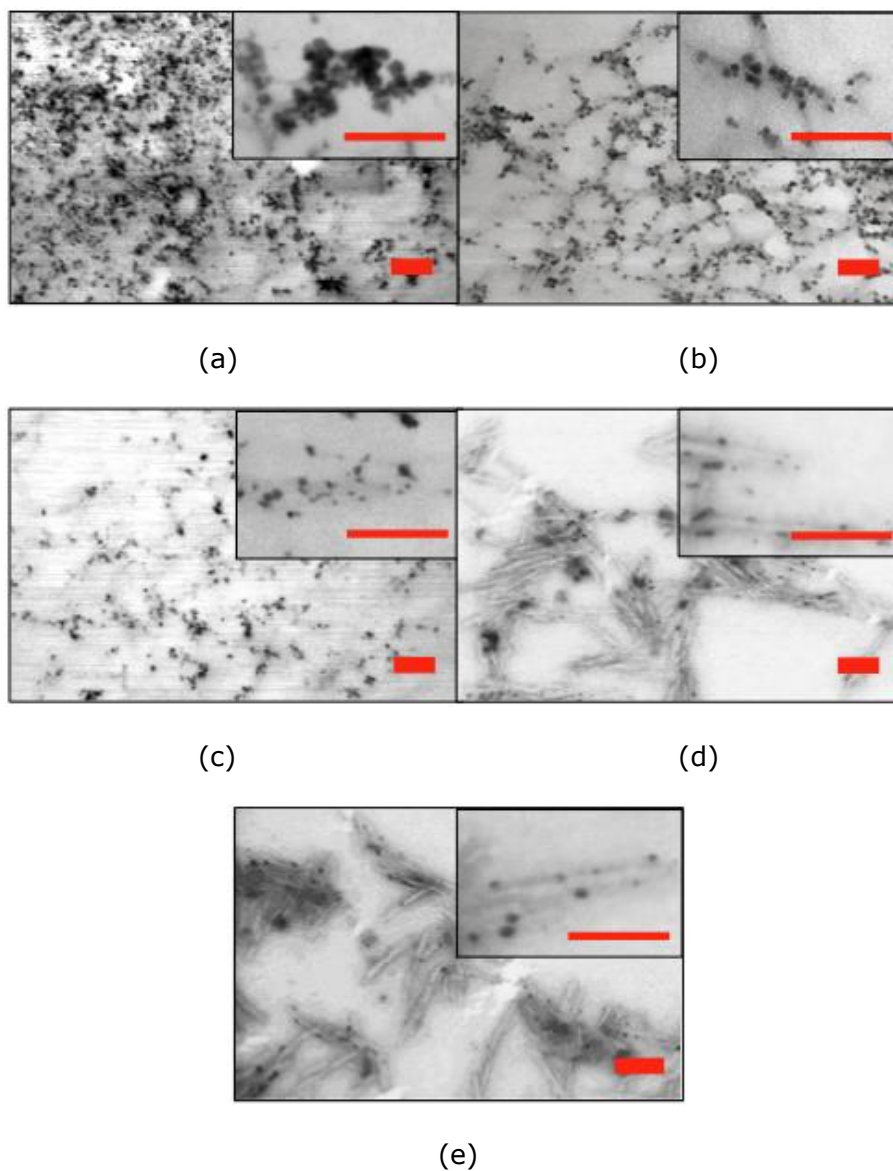


Figure 4.2. STEM images of (a) MCNC0.2, (b) MCNC1, (c) MCNC2, (d) MCNC10, and (e) MCNC20. The inset shows the images at higher magnification. All scale bar are representing 100 nm.

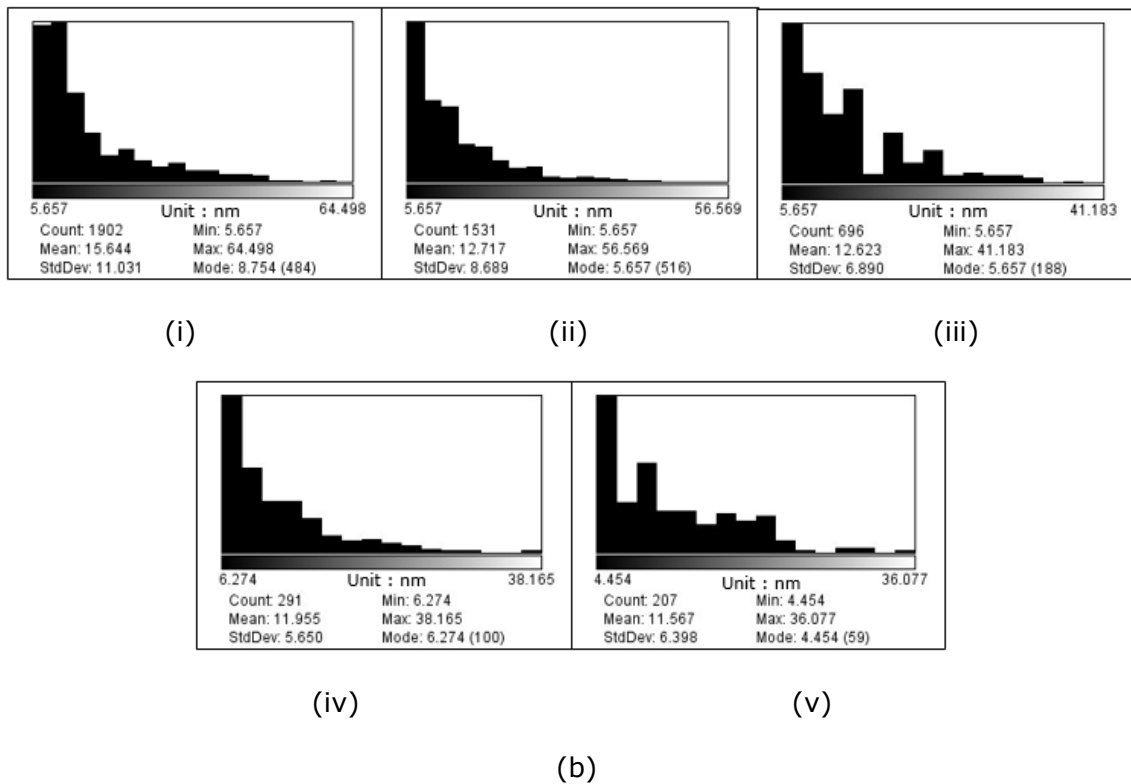
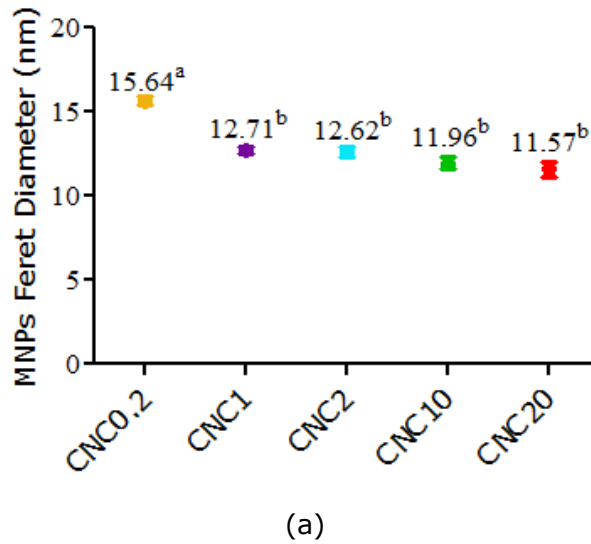
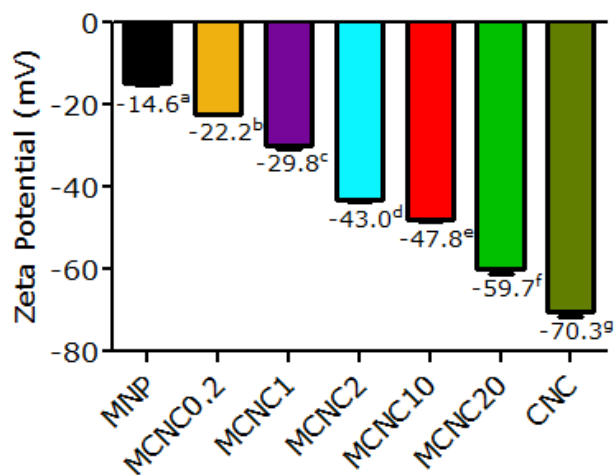
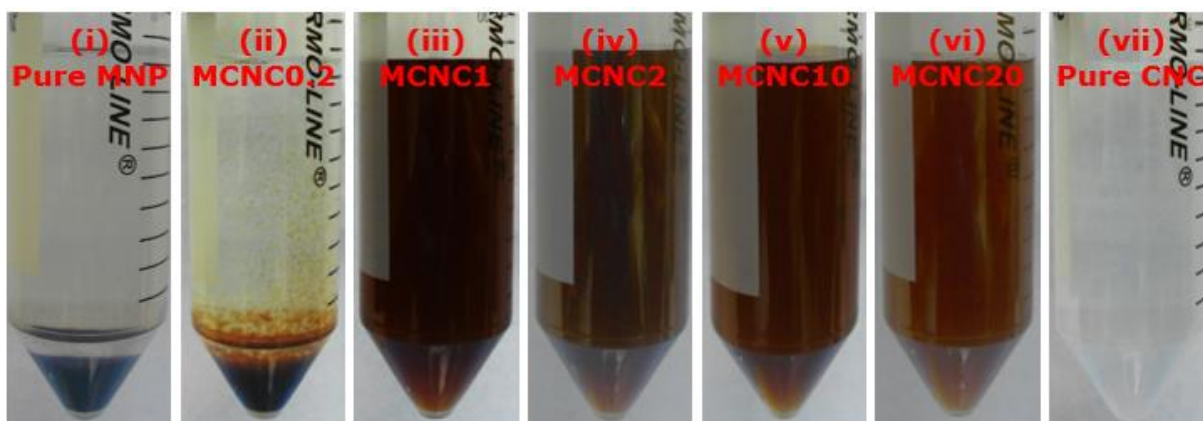


Figure 4.3. (a) MNPs feret diameter in different MCNC samples, Standard error of mean of triplicate readings were represented by the error bars in each graph, different alphabetic letters was significantly different at $P \leq 0.05$ by Bonferroni's Multiple Comparison Test. (b) Histogram generated from the STEM images for the feret diameter of MNPs deposited on CNC. Samples (i) MCNC0.2, (ii) MCNC1, (iii) MCNC2, (iv) MCNC10, (v) MCNC20.

The sign and magnitude of the surface charge is an important parameter in determining the stability of a dispersion and zeta potential is commonly used to predict and control dispersion stability. Figure 4.4a shows the zeta potential values of MCNC samples. The result shows that CNC possess very high surface charge (-70.3 ± 2.0 mV) as a result of ester sulphate groups introduced during acid-hydrolysis process in native CNC production. MNPs, on the other hand, have much lower surface charge (-14.6 ± 0.7 mV) and thus it has great tendency to particle agglomeration. At fixed concentration of MNP, one can observe that the surface charges of MCNC reduce significantly from -22.2 ± 0.2 to -59.7 ± 2.5 mV with increasing CNC/MNP ratio. It was found that the MCNC samples exhibited stable surface charged starting from CNC1 (see Figure 4.4a) (Nanocomposix, 2016). This trend is mainly due to the presence of more and more anionic surface functional groups when more and more CNC is used. These results were in good agreement with our STEM results. At increasing CNC/MNP ratio, the ratio of Fe ions to CNC functional groups reduced greatly, rendering more and more un-reacted surface functional groups remained after the synthesis. This study implies that higher ratio of CNC to MNP enhances the electrostatic stability of MCNC, thereby improves its dispersion stability. To visualize the data, photograph of suspension of pure MNPs, pure CNCs, and all MCNC samples were presented in Figure 4.4b. It was obvious that the pure MNPs settled down quickly (Figure 4.4b (i)), while the pure CNC remain dispersed in water medium (Figure 4.4b (vii)). For the MCNC samples, the nanocomposites settled down when the CNC concentration was at the ratio of 0.2 (Figure 4.4b (ii)). The suspensions with CNC/MNP ratio of 1 or above, on the other hand, were stable towards sedimentation (Figure 4.4b (iii) to (vi)). This correlate well with our zeta potential results where stable zeta potential were observed starting from CNC/MNP ratio of 1.



(a)



(b)

Figure 4.4. (a) Surface charge, and (b) photograph of water dispersion of (i) pure MNP, (ii) MCNC0.2, (iii) MCNC1, (iv) MCNC2, (v) MCNC10, (vi) MCNC20, and (vii) pure CNC. Images captured 10 min after preparation.

TGA demonstrated that the final weight of MCNC samples reduced with increasing CNC concentration. This was mainly because the MNP/CNC ratio decreased as the CNC content increased. Apart from that, the TGA curves revealed that MCNC10 and MCNC20 (Figure 4.5d and e) involved only 1 step losses that was attributed to the chemical degradation of CNC at approximately 280 °C. The absent of the second step losses, which occurred in MCNC0.2 to MCNC2 (Figure 4.5a to c) was most likely because of the presence of polycrystalline MNPs. As per described in Chapter 3, the anchoring of MNPs onto CNC was highly dependent on the availability of surface functional groups of CNC around it. In

MCNC10 and MCNC20 (with both samples having very high CNC/MNP ratio), the amounts of surface functional groups on CNC have outnumbered the iron precursors. Thus the iron ions have plenty of oxygen containing hydroxyl groups for nucleation and growth. So, single crystal MNPs were favoured. This was also observed in STEM images for MCNC10 and MCNC20 (Figure 4.2d and e), where almost all MNPs deposited were single particles. On the other hand, when the iron precursor's concentration increased, the availability of hydroxyl groups reduced. This thus results in limited nucleation sites for MNPs. Therefore, less compact structures MNPs were obtained. Interestingly, TGA curve suggested that small amounts of polycrystalline MNPs were found in MCNC2 sample even though most of the MNPs were scattered apart (Figure 4.2c). This was most likely attributed to the aggregating nature of pristine MNPs, where they tend to get attracted to each other and nucleated nearby.

Besides that, it was noted that both MCNC2 and MCNC0.2 encountered much smaller weight losses as compared to MCNC1 (Figure 4.5a to c). The incident in MCNC2 was most likely because the total MNPs content was much lower as compared to MCNC1. In MCNC0.2, however, was most probably because there exists a large amount of MNPs that was not having any reaction with CNC. When the surface hydroxyl groups on CNC was insufficient for all MNPs to nucleate, some of the MNPs undergo nucleation in CNC-free environment. These free MNPs then agglomerated onto the MNPs that were already anchored with the CNC, and thus leading to high degree of aggregation as observed in STEM image (Figure 4.2a). The thermal stability of those MNPs will be similar to those pristine MNPs where no significant step losses was observed (see Figure 3.8). Therefore, the small step losses observed was most likely attributed to the limited MNPs that have anchored with the CNC. The high weight losses in MCNC1 sample, on the other hand revealed that most of the MNPs were reacted with the surface functional groups of CNC (as previously described in Chapter 3).

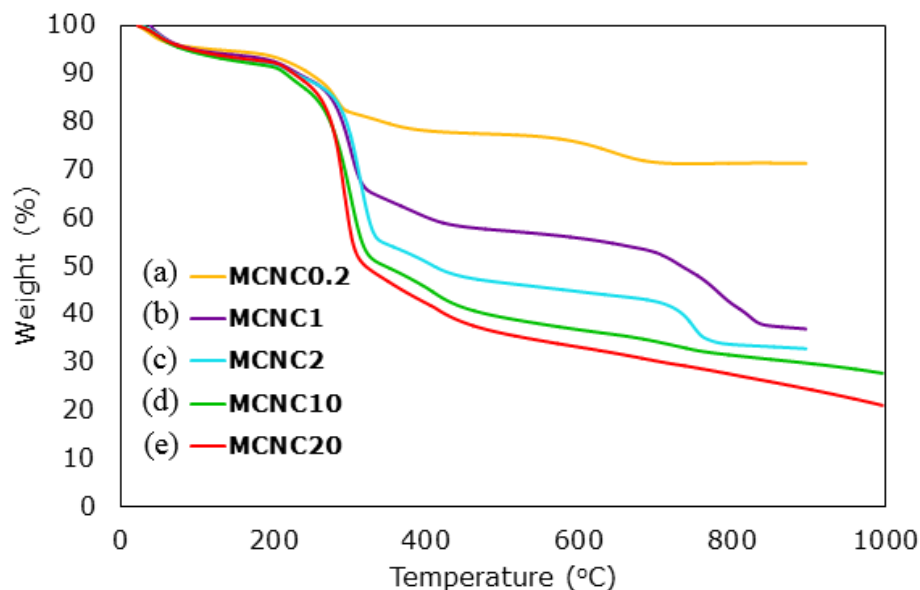


Figure 4.5. TGA data representing weight loss % at different temperature for (a) MCNC0.2, (b) MCNC1, (c) MCNC2, (d) MCNC10, and (e) MCNC20.

Figure 4.6 presented the magnetization curve of MCNC with varying CNC/MNP ratio. It had been observed that all MCNC samples showed superparamagnetic properties, with negligible coercivity, as manifested by the inset. An evident decrease in the saturation magnetization (M_s) of the MCNC nanocomposite was observed as CNC/MNP ratio increases (Figure 4.6). This might be due to the fact that at fixed concentration of MNPs, the elevated amount of CNC in the dispersion gradually reduces the magnitude of M_s of the MCNC. In literature, studies showed that the M_s of MNPs at single domain (<30 nm) reduced gradually as its particle size decreased due to spin canting effect at the surface (Linderoth *et al.*, 1994; Roca *et al.*, 2006). In present study, one can, however, notice that the measured MNPs size remained unchanged despite a marked reduction in M_s from CNC/MNP ratio of 2 to 20. One possible explanation for this observation was likely because MNPs were immobilized firmly in the CNC network, thus reducing the surface energy of the MNPs and preventing them from particle aggregation. The firm bonding between MNPs and CNC has been observed in the FTIR analysis. The reduction in M_s of MCNCs was mainly due to excess quantity of CNC in aqueous solution.

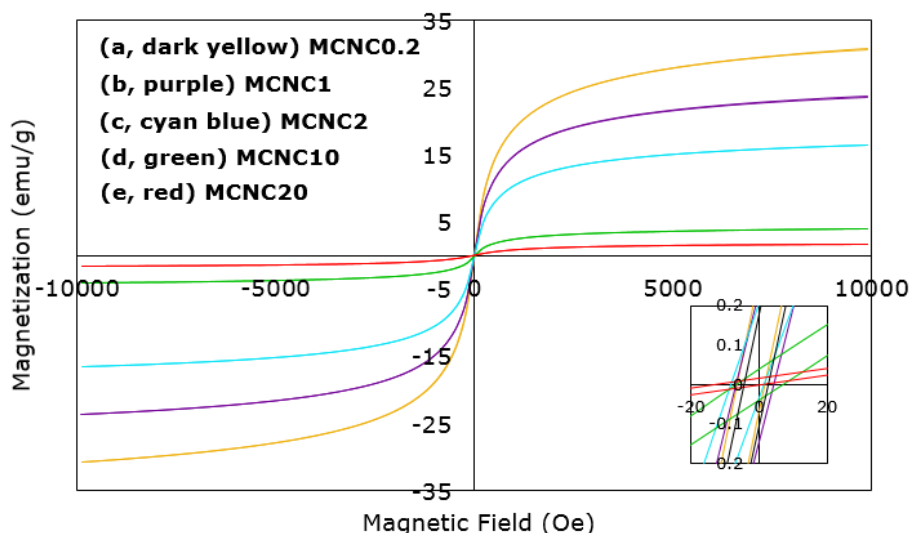


Figure 4.6. Magnetization plot of MCNC samples with CNC/MNP ratio of (a) 0.2, (b) 1, (c) 2, (d) 10, and (e) 20. The inset shows the negligible coercivity in all samples.

4.3.1.2 Pre-heated Temperature

The FTIR analysis revealed that no distinct differences were observed in the samples prepared with the four studied pre-heated temperature. This was likely to indicate that the pre-heated temperature have minimal effects on the preparation of MCNC nanocomposites. Further characterisation was carried out to ensure the claim.

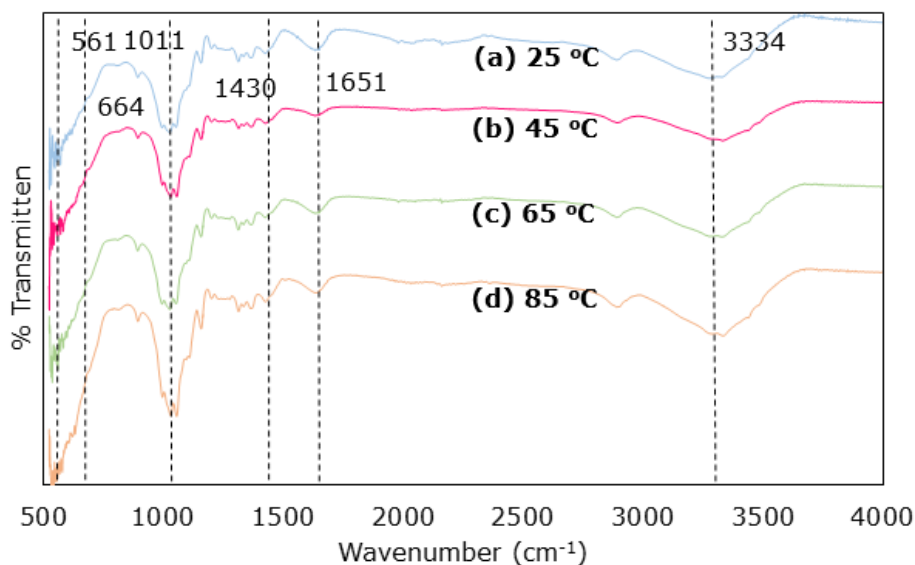


Figure 4.7. FTIR spectra of MCNC samples prepared at different pre-heated temperature, with (a) 25, (b) 45, (c) 65 and (d) 85 °C.

Results from STEM analysis showed that the MNP's diameter and loading amount remains unaffected under different temperature, suggesting that temperature does not affect the overall surface morphology and the particles diameter of the deposited MNPs (see Figure 4.8). These diverse results to the pure MNPs preparation as reported by Mahdavi *et al.* (2013), was likely to due to the presence of CNC in the preparation formulation. From literature, the particles diameter of the MNPs was claimed that will increased as reaction temperature increased (Mahdavi *et al.*, 2013). This was owing to the increase in energy within the solution that led to higher mobility of the particles, which then results in greater number of collisions between the particles. In the present study, pertaining to the ability of CNC to firmly immobilise the MNPs on its surface during its nucleation and growth, the MNPs aggregation due to the collisions effect has been minimized. Thus the temperature showed no effects on the dispersibility of MNPs on CNC.

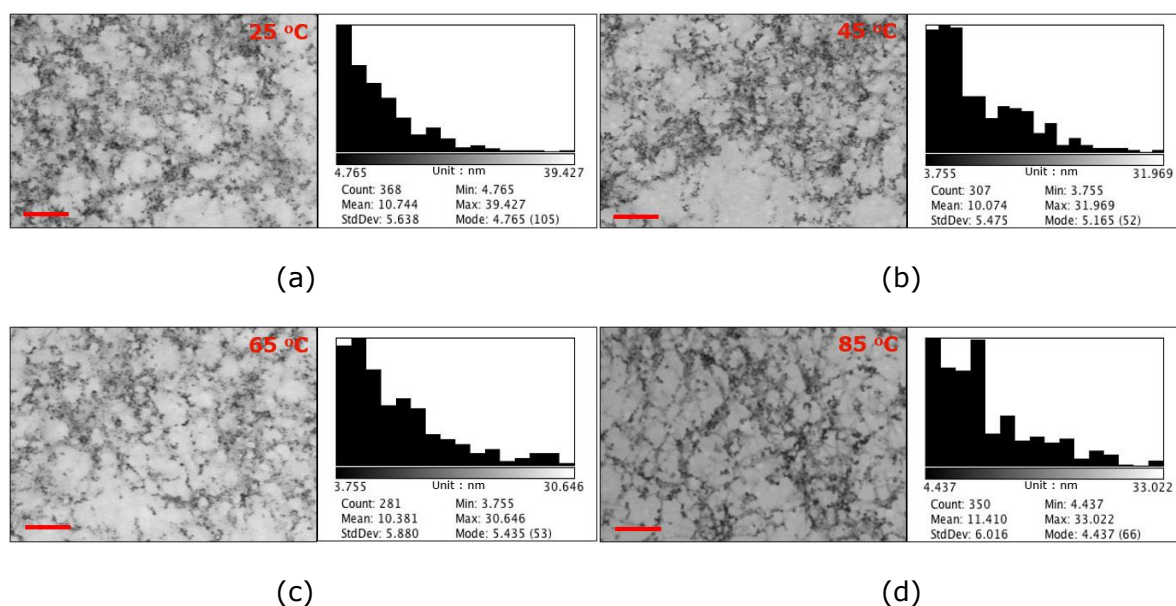


Figure 4.8. STEM images with the respective histogram for MNPs deposited on MCNC samples prepared at different pre-heated temperature. (a) 25, (b) 45, (c) 65 and (d) 85 °C. All scale bar are representing 100 nm.

TGA was performed to evaluate the composition of MNPs as a result of varying initial reaction temperature. From Figure 4.9, it was observed that the final ash content of the MCNC samples increased slightly from 40 to 41 wt% when temperature increased from 25 to 45 (Figure 4.9 insets). However, the insets clearly showed that further increasing the initial reaction temperature only resulted in reducing MNPs weight content. This was most likely pertaining to the oxidation of Fe^{2+} to Fe^{3+} in the initial CNC- $\text{Fe}^{2+,3+}$ mixture before co-precipitation. Generally, the oxidation of Fe^{2+} was due to the dissolved oxygen in the aqueous medium. When temperature increased, the water molecule in the medium gained energy and starts moving vigorously. This thus increased the collision between the water molecules, which eventually undergo partial separation, and led to the oxidation of the Fe^{2+} ions. In current situation, higher temperature simply caused more Fe^{2+} to get oxidized. As Fe_3O_4 requires 2 Fe^{3+} and 1 Fe^{2+} to be formed, if too much Fe^{2+} was oxidized from the mixture, the final content of Fe_3O_4 will definitely drop. To verify that, the concentration of Fe^{3+} , estimated using UV-vis spectrometry in all investigated temperatures was depicted in Table 4.1. It was observed that the concentration of Fe^{3+} increased linearly from 4.4212 ± 0.2578 to 5.8748 ± 0.2077 as temperature increased from 25 to 85 °C. This verified the above hypothesis on the effect of preheated temperature on MNPs formation.

VSM analysis revealed a similar trend as that in TGA analysis. The saturation magnetization, M_s of MCNC samples rose slightly from 26 to 27 emu/g when pre-heated temperature increases from 25 to 45 °C. It was then followed by slow reduction as temperature was further increased (Figure 4.10). This is similar to the phenomena discussed in Chapter three, as a result of the reduction in Fe_3O_4 in the resultant MCNC sample.

Table 4.1. Concentration of Fe^{3+} representing samples at different temperature. UV absorbance was recorded at UV-vis wavelength of 300 nm. Different alphabetic letters indicated significant differences at $P \leq 0.05$ by Bonferroni's Multiple Comparison Test.

Temperature ($^{\circ}\text{C}$)	Concentration ($\mu\text{mol}/\text{dm}^3$)
Room $\approx 22 \pm 1$	$4.1395 \pm 0.2578^{\text{a}}$
25	$4.1797 \pm 0.2505^{\text{b}}$
45	$4.4518 \pm 0.2693^{\text{c}}$
65	$4.9927 \pm 0.2106^{\text{d}}$
85	$5.6334 \pm 0.2077^{\text{e}}$

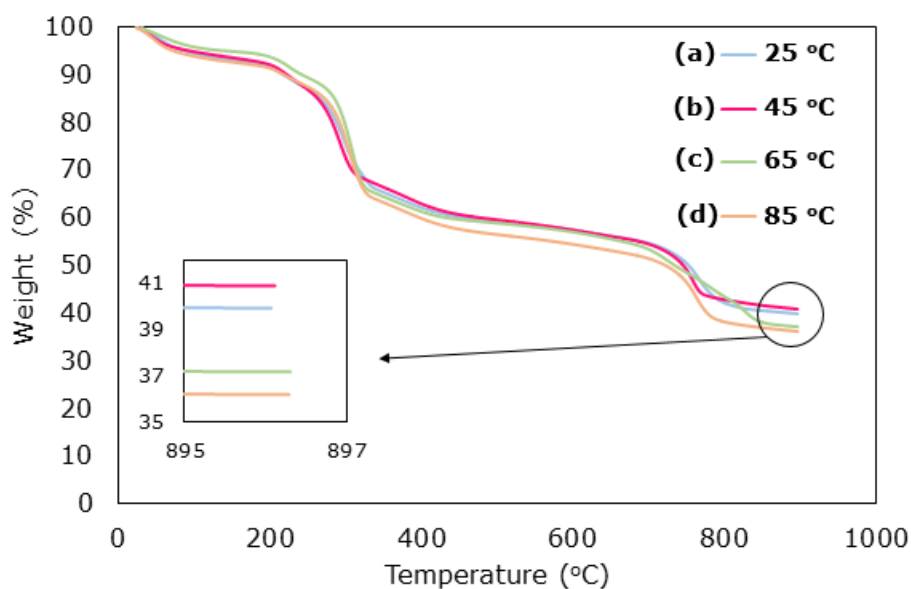


Figure 4.9. TGA data representing weight loss % for MCNC samples prepared at different pre-heated temperature. (a) 25, (b) 45, (c) 65 and (d) 85 $^{\circ}\text{C}$.

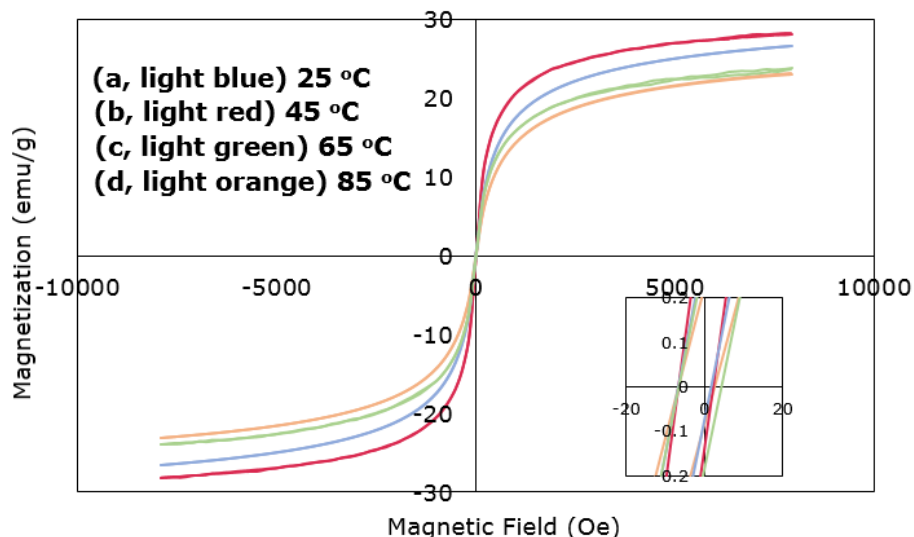


Figure 4.10. Magnetization plot of MCNC samples prepared under different pre-heated temperature. (a) 25, (b) 45, (c) 65 and (d) 85 °C. The inset shows the negligible coercivity in all samples.

4.3.1.3 Ultrasound Power

No distinct differences were spotted in the FTIR spectral of MCNC nanocomposites prepared under all investigated US power. Further characterisation was performed to evaluate the effects of US power on the nanocomposites preparation.

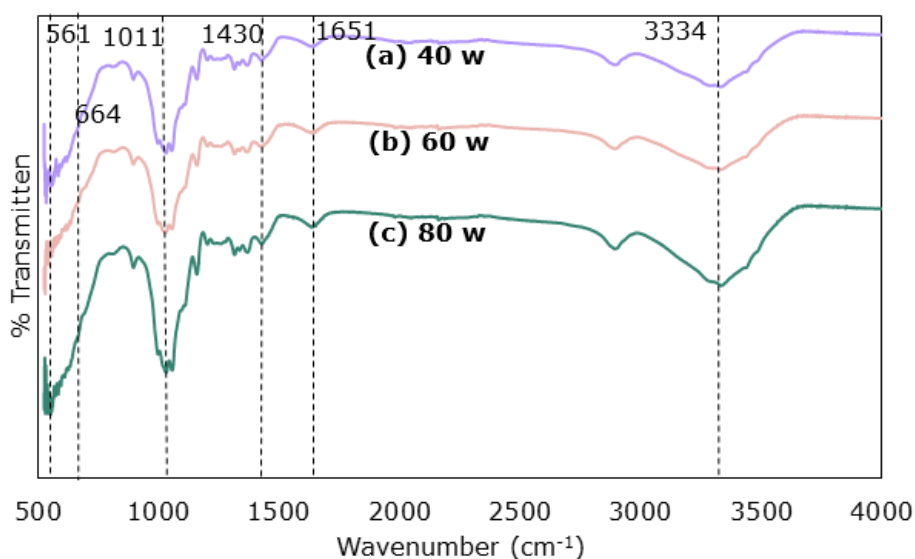


Figure 4.11. FTIR spectra of MCNC samples prepared at different US power, with (a) 40, (b) 60 and (c) 80 w.

STEM analysis showed that the MNP's diameter were highly similar under all US power. Suggesting that differs in US power does not affect the overall surface morphology and the particles diameter of the deposited MNPs (see Figure 4.12a to c). This outcome was most likely due to the extreme conditions induced by typical US cavitation. The existence of US alone was most likely sufficient enough to ensure a uniform distribution MNPs on CNC. To support this, investigation done by Dang *et al.*, (2007) on sonochemical preparation of Fe₃O₄ has reported a similar finding.

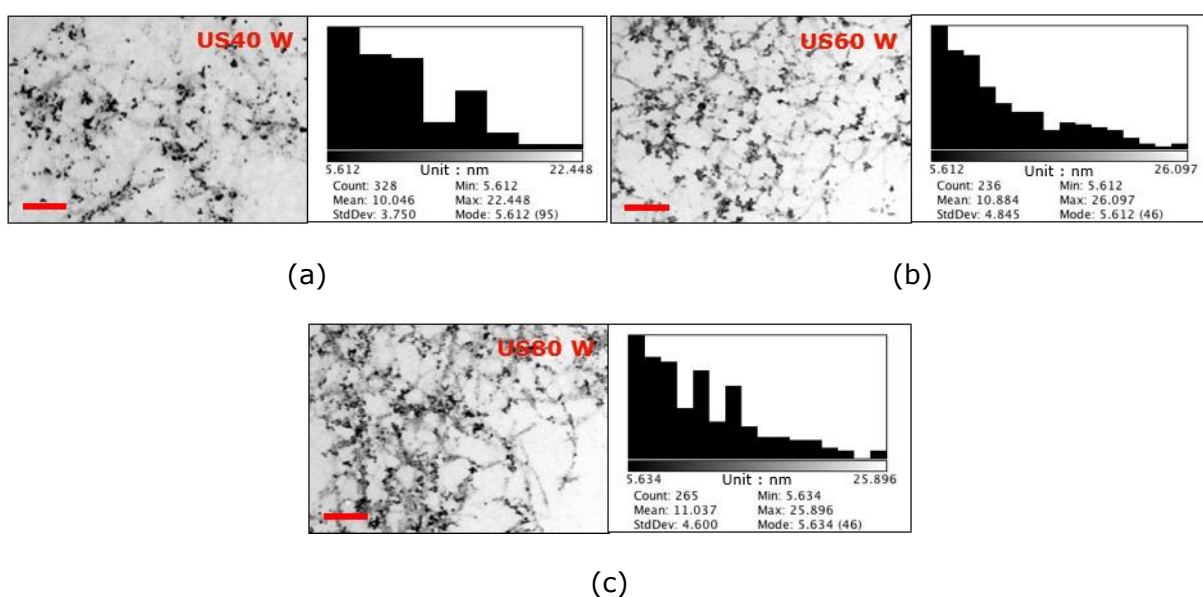


Figure 4.12. STEM images with the respective histogram for MNPs deposited on MCNC samples prepared at (a) 40, (b) 60 and (c) 80 w US power. All scale bar are representing 100 nm.

TGA has been carried out to determine the elemental composition of MNPs as a result of varying US power. From Figure 4.13, no distinct difference in chemical composition was observed among all US power-induced samples. As observed from the insets, the final ash content for all samples was at around 34 wt%. However, VSM plot revealed that the respective magnetic strength of MCNC increased from 25.256 to 27.116 emu/g with increasing US power from 40 to 60 w (Figure 4.14). The magnetivity then increased in minor magnitude from 27.116 to 27.691 under stronger US power at 80 w. This phenomena

was most likely because the desired nucleation and growth rate acceleration was achieved at US power of 60 w. A similar trend was reported in literature study on pristine MNPs by Dang *et al.*, (2007).

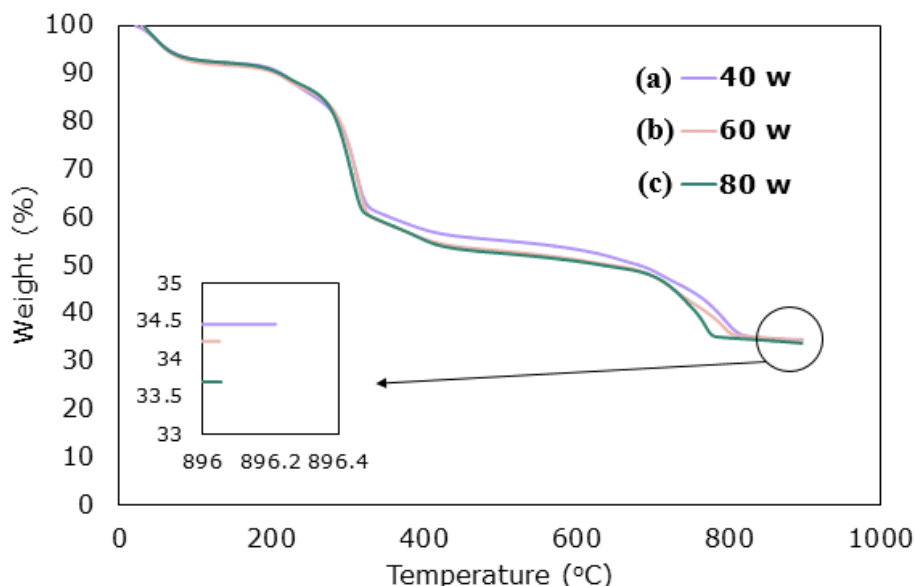


Figure 4.13. TGA data representing weight loss % at different temperature with US power of (a) 40, (b) 60 and (c) 80 w.

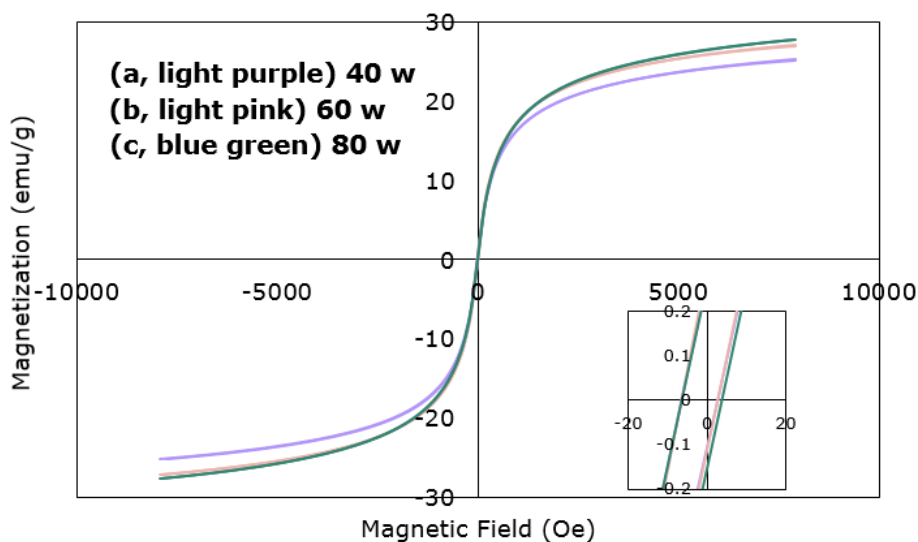


Figure 4.14. Magnetization plot of MCNC samples prepared under different US power. (a) 40, (b) 60 and (c) 80 w. The inset shows the negligible coercivity in all samples.

4.3.1.4 Sonication Time

The FTIR analysis revealed that sonication time have no effects towards the preparation of MCNC nanocomposites. To confirm this, various characterisation was later done to evaluate the effects of US cavitation time on the MNPs diameter.

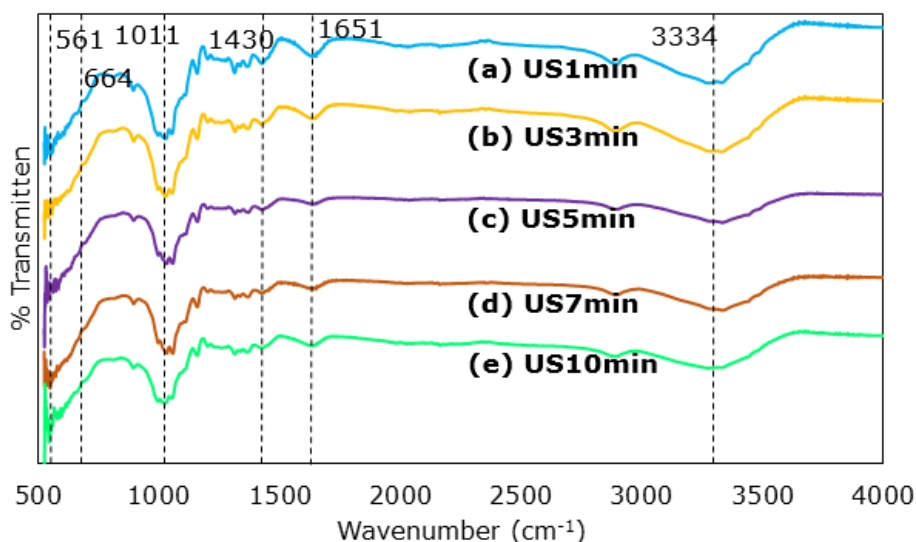


Figure 4.15. FTIR spectra of MCNC samples prepared at different sonication time, with (a) 1, (b) 3, (c) 5, (d) 7 and (e) 10 min.

Based on STEM analysis. Figure 4.16a illustrated that US1min nanocomposite sample exhibited a pronounce MNPs agglomeration with average cluster diameter of 45.92 ± 53.60 nm. Increasing the sonication time, on the other hand, improves the homogeneous dispersion of the MNPs, as evidenced by Figure 4.16. The measured average MNP diameter reduced to around 12 nm when US irradiation time was 5 min or above. The severe particle agglomeration obtained at 1 and 3 min of sonication time was believed to be caused by the insufficient cavitation energy applied to the system due to short US irradiation time.

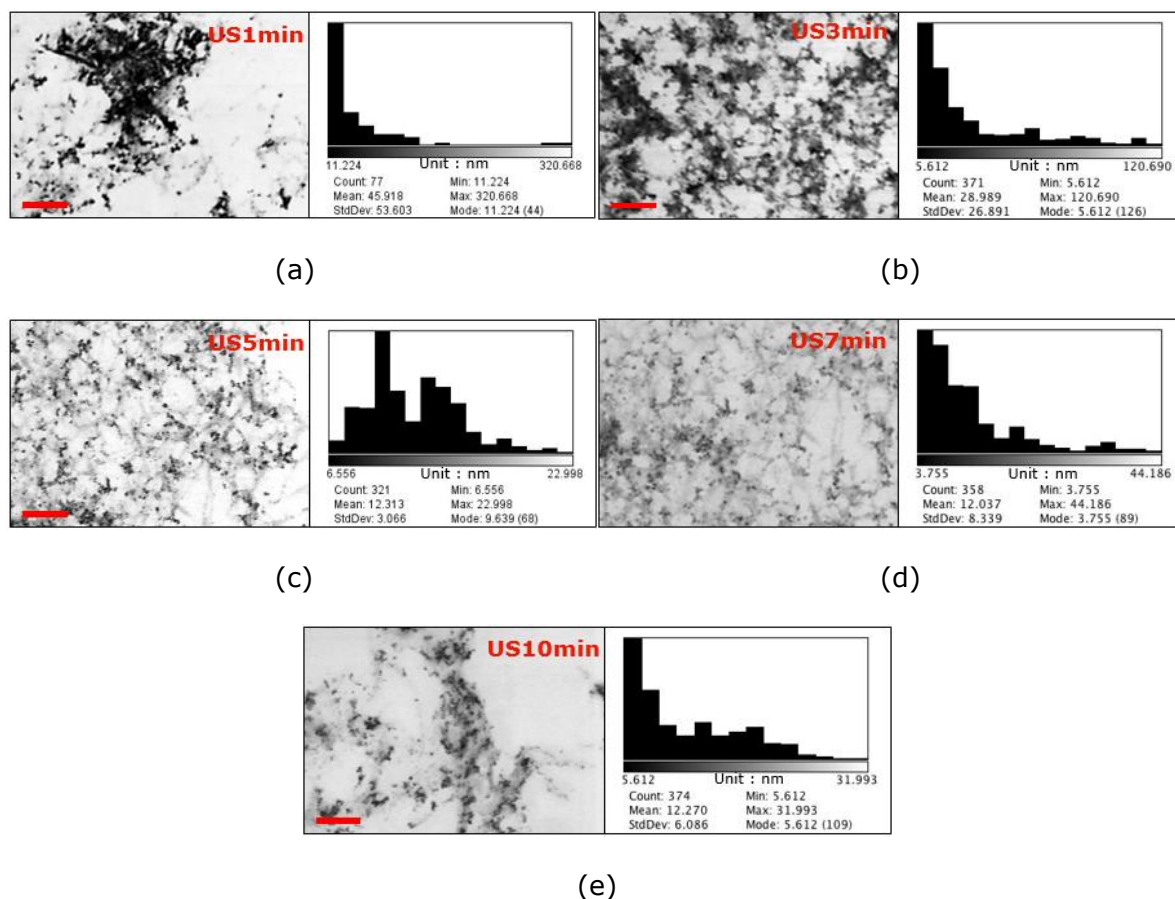


Figure 4.16. STEM images with the respective histogram for MNPs deposited on MCNC samples prepared under (a) 1, (b) 3 (c) 5, (d) 7 and (e) 10 min ultrasonication. All scale bar are representing 100 nm.

TGA has been carried out to determine the elemental composition of US-induced MCNC samples (Figure 4.17). The ashes content increased as US irradiation increased, recorded maximum values of around 41 wt% at 5 min sonication time. The trend then reversed with further sonication at 7 and 10 min. As expected, a similar trend was noticed from the VSM result. The M_s of US-induced MCNC samples increased accordingly from 17.510 to 27.856 emu/g when US irradiation time increased from 1 to 5 min (Figure 4.18). However, the M_s value then dropped substantially to 23,760 and 18.824 emu/g at extended sonication time at 7 and 10 min respectively. The observed lower ash content and M_s for US1min was simply attributed to the uncompleted co-precipitation reaction as result of shorter sonication time that is not sufficient for all MNPs in the medium to reach its growth

saturation (Gnanaprakash *et al.*, 2007). This was supported by the presence of rod-like structures of unreacted $\text{Fe}(\text{OH})_2$ as shown in Figure 4.16a. The M_s reduction in US7min and US10min was mainly due to the secondary oxidation process from the crystal structure of MNPs (Dang *et al.*, 2007). Since the magnetic strength of MNPs were mainly pertained from the Fe^{2+} ion, the oxidation of Fe^{2+} on the MNPs structure as resulted from long US irradiation will lead to reduced M_s (Dang *et al.*, 2007). XPS study was also carried out to further elucidate the composition of MCNC samples. From the wide scan image of XPS (Figure 4.19a), the presence of CNC and magnetic nanoparticles was confirmed through the typical band spectra for carbon (≈ 287 eV), oxygen (≈ 25 & 533 eV) and ferrum (≈ 711 eV) respectively (Xiong *et al.*, 2014; Zhang *et al.*, 2013). To examine the presence of magnetite rather than maghemite, narrow XPS scanning was performed. The characteristic binding energy of Fe $2p_{3/2}$ of Fe_3O_4 falls around 709 and 711 eV for Fe^{2+} and Fe^{3+} respectively (Li, Jiang and Bai, 2011). Our narrow scanning across the Fe 2p region in Figure 4.19b demonstrated that the formation of Fe_3O_4 existed in all the measured samples. Another extra peak situated at about 719 eV was observed in the MCNC samples prepared upon sonication for 1 and 10 min. This characteristics peak of Fe^{3+} in Fe_2O_3 (Wu *et al.*, 2012), suggested that the MNPs on 1 and 10 min samples were partly oxidized, which thus validated the claims on the VSM analysis. The valence band spectra showed slight differences between the 5 min samples and the others, with 5 min MCNC sample having the typical fingerprint of magnetite (Figure 4.19c) (Moulder *et al.*, 1995). This also suggested the oxidation inhibition of MNPs in the MCNC sample prepared at 5 min US irradiation.

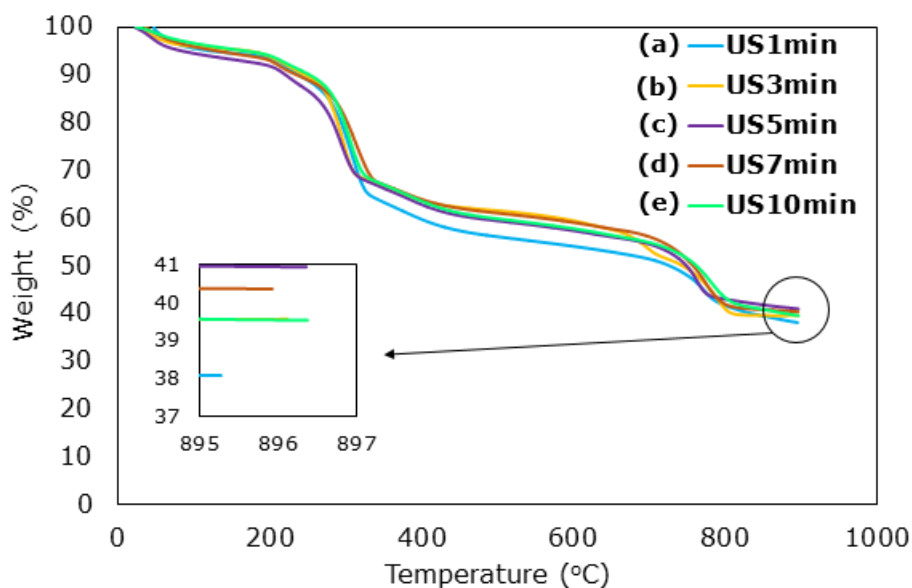


Figure 4.17. TGA data representing weight loss % at different temperature with sonication time of (a) 1, (b) 3, (c) 5, (d) 7 and (e) 10 min.

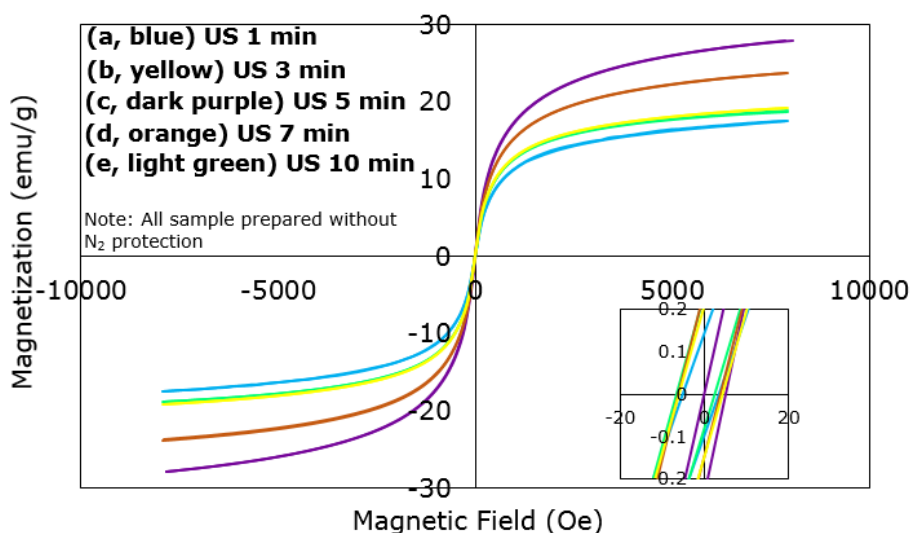


Figure 4.18. Magnetization plot of MCNC samples prepared under different sonication time. (a) 1, (b) 3, (c) 5, (d) 7 and (e) 10 min. The inset shows the negligible coercivity in all samples.

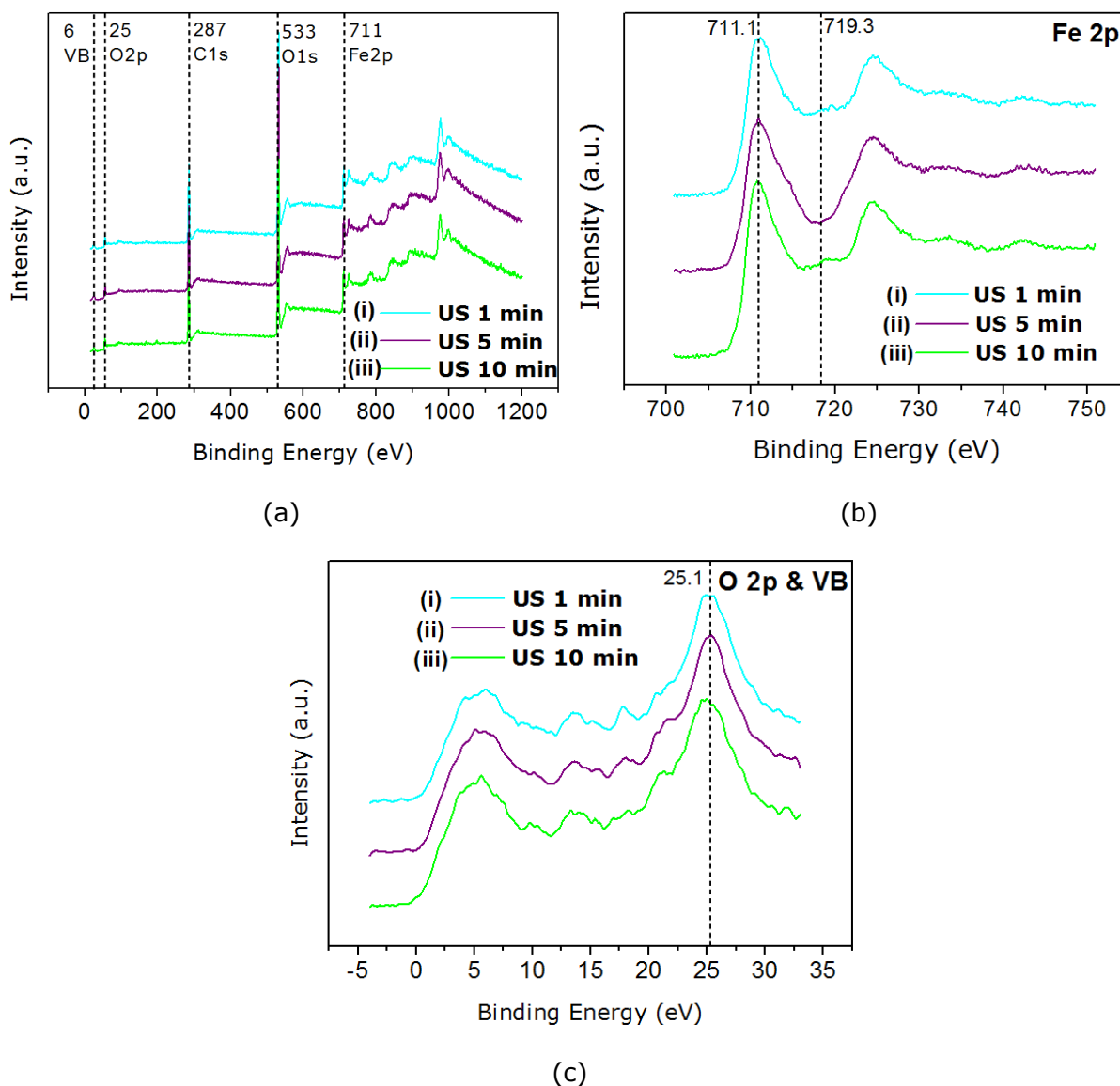


Figure 4.19. XPS spectra for (a) wide scan, (b) narrow scan Fe 2p and (c) narrow scan O 2p & valence band of MCNC nanocomposites prepared at (i) 1, (ii) 5 and (iii) 10 min ultrasonication time.

4.3.2 Surface Wettability of MCNCs

4.3.2.1 Surface Hydrophilic Group Content of CNC

As mentioned in Chapter 3, the surface of CNC consists of minor but significant amount of sulphate groups (8.5 %). Here the sulphate group content was employed to symbolize all surface functional groups on CNC to estimate the total functional groups changes as CNC concentration increased. Conductometry was performed on pure CNC at different

concentration to determine the total sulphate group content. The conductometry results were shown in Figure 4.20. As expected, the results demonstrated that CNC20 possessed highest sulphate group content compared to the samples containing lower CNC/MNP ratio. The functional groups content showed considerable decrease ($P < 0.05$) as CNC/MNP ratio gradually reduced to 0.2. The results are reasonable since at higher CNC concentration, there should be higher sulphate groups in the medium. This also proved that the total functional groups in the medium, readily available for dispersing MNPs increased as CNC concentration increased.

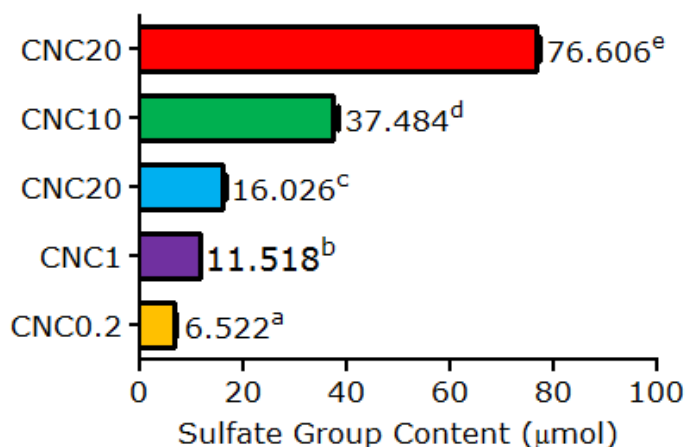


Figure 4.20. Sulphate group content in medium containing various CNC/MNP ratio estimated by conductometric titration. Standard error of mean of triplicate readings were represented by the error bars in each graph, different alphabetic letters was significantly different at $P \leq 0.05$ by Bonferroni's Multiple Comparison Test.

The conductometry results were well supported by EDX study on MCNC samples (Figure 4.21a and b). In the current study, because hydrogen and oxygen does not only appeared in the surface functional groups but also the entire core of CNC, thus sulphur content was utilized as representative to illustrate all the available surface functional groups on the samples. Meanwhile, pure MNPs (Figure 4.21a (i) and b (i)) and CNCs (Figure 4.21a (vii) and b (vii)) were produced for comparison of the sulphur content (cyan dots), and iron content (orange red dots) with MCNC samples. Results presented in Figure 4.21a (ii) to (vi)

showed that the amount of cyan dots dramatically increased when CNC/MNP ratio inclined. This suggested that the free surface functional groups become excess in amount with an increase in CNC/MNP ratio. Besides that, an inverse behaviour was noticed on the iron content (Figure 4.21b (ii) – (vi)). It can be clearly seen that the orange red dots population decreased as CNC/MNP ratio increased from 1 to 20 (Figure 4.21b (ii) – (v)), with maximum coverage achieved on CNC/MNP ratio of 1 and 0.2. This indicates that iron oxides content on MCNC samples increases as CNC amount decreases. This phenomenon continued until the maximum surface coverage was achieved at MCNC1. In overall, the conductometry and EDX studies showed that there was a direct relationship between the MNPs loading and CNC concentration.

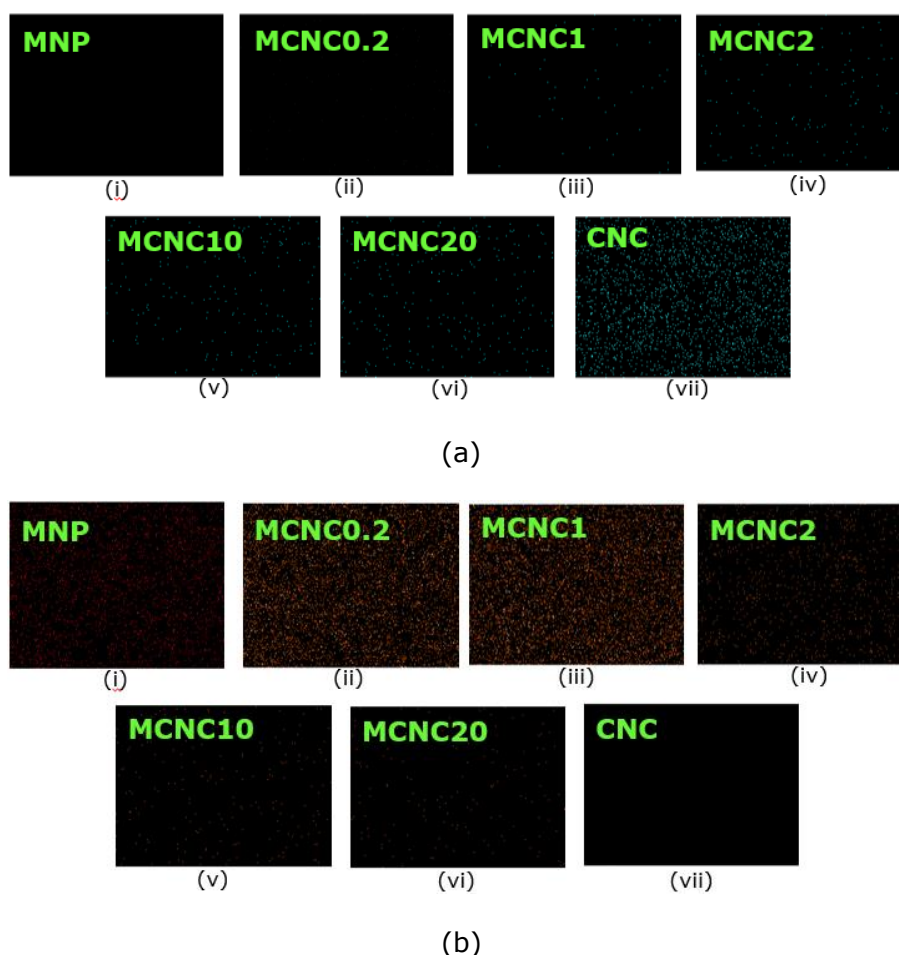


Figure 4.21. EDX mapping for (a) sulphur content and (b) iron content in (i) pure CNC, (ii) MCNC20, (iii) MCNC10, (iv) MCNC2, (v) MCNC1, (vi) MCNC0.2, and (vii) pure MNP. MCNC samples were obtained under different CNC/MNP ratio.

The surface wettability of the as-prepared MCNC samples were presented in Table 4.2. It was generally reported that pristine CNCs are amphiphilic cellulose fibres that easily disperse in water medium (Kalashnikova, Bizot and Cathala, 2012), while pure MNPs are typically hydrophilic particles (Zhou *et al.*, 2011). From Table 4.2, it has been observed that all MCNC samples were more hydrophobic as compared to the two control samples (pristine CNC and MNPs), as evidenced with their higher contact angle. The results revealed that the contact angle of the samples increased while decreasing CNC/MNP ratio from 20 to 1. However, the contact angle decline considerably from 51.87 ± 0.17 to $44.98 \pm 0.23^\circ$ as the ratio was further reduced from 1 to 0.2. This noticeable trend was most likely due to the decrease in amount of hydrophilic groups introduced as a result of reduction in CNC/MNP ratio. When decreasing the CNC/MNP ratio progressively from 20 to 1, the water-wettability of MCNC is directed by the limited amount of amphiphilic CNC particles. During the *in-situ* sonochemical reaction, the CNC surface hydrophilic hydroxyl groups ($-OH^-$) react with Fe ions to form MCNC nanocomposites. As illustrated in Scheme 4.1, it is proposed that three Fe ion would require four oxygen ions in order to form a single MNP coated on CNCs. One $-OH^-$ group of CNC possesses, however, only one oxygen ions. Thus, four $-OH^-$ groups are necessary to allow the deposition of a single MNP on CNC surface. A stepwise formation of MNP was also reported by Awwad and Salem (2012) on the preparation of MNPs stabilized by carob leaf extract. In the present study, the trend reverses at CNC/MNP ratio ≤ 1 . Further decrease in CNC/MNP ratio to 0.2 results in excess amount MNPs deposited on the CNC surface. With more deposited MNPs, a more hydrophilic behaviour of MCNC nanocomposite was observed, as witnessed by lower contact angle. To support this, our STEM images showed a considerable increase in MNP content from samples CNC20 to CNC1 (Figure 4.2a to e), with the largest amount of aggregated MNPs observed in MCNC0.2 (Figure 4.2a). Furthermore, EDX presented progressive decline in sulphur population and gradual increment in amount of MNPs content with increasing MNP/CNC ratio (Figure 4.21a and b).

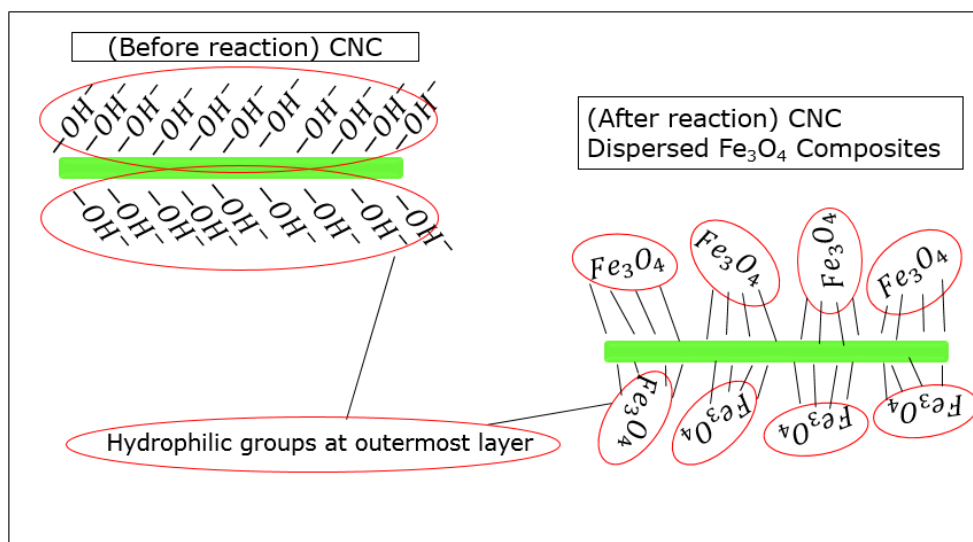
Using the information from the wettability, the interfacial contact angle of all examined samples were estimated using an Equation derived by Zhou *et al.* (2011) using Washburn method.

$$\cos\theta_{ow} = \frac{\gamma_{aw}}{\gamma_{ow}} \cos\theta_{aw} - \frac{\gamma_{ao}}{\gamma_{ow}} \cos\theta_{ao} \quad [\text{Equation 4.1}]$$

where θ_{ow} , θ_{aw} , and θ_{ao} are the interfacial, air-water, and air-oil contact angle respectively, while γ_{ow} is the interfacial tension between oil and water phase, and γ_{aw} & γ_{ao} are surface tension of oil and water respectively. The estimated θ_{ow} for all samples were then depicted in Table 4.2. As observed, a similar trend was observed as compared to the surface wettability data. However, all the recorded contact angle values were relatively low, with the highest only at around 47 °. This requires improvement since the most of the stable Pickering emulsion were produced using solid particles with an interfacial contact angle near 90 °. In the next sub-section, the effects of pH on the MCNC nanocomposites will be evaluated.

Table 4.2. Water-air and interfacial contact angle of CNC, MNP, and MCNCs samples. Different alphabetic letters was significantly different at $P \leq 0.05$ by Bonferroni's Multiple Comparison Test.

Sample	Water-air contact angle (°)	Interfacial contact angle (°)
CNC	36.723 ± 0.25 ^a	15.708
MCNC20	43.421 ± 0.36 ^b	15.690
MCNC10	44.836 ± 0.17 ^c	17.343
MCNC2	49.102 ± 0.15 ^d	37.644
MCNC1	51.869 ± 0.17 ^e	47.015
MCNC0.2	44.983 ± 0.23 ^c	26.421
MNP	21.170 ± 0.35 ^f	0.000



Scheme 4.1. Schematic illustration of the hydrophilic groups on the surface of CNC and MCNC.

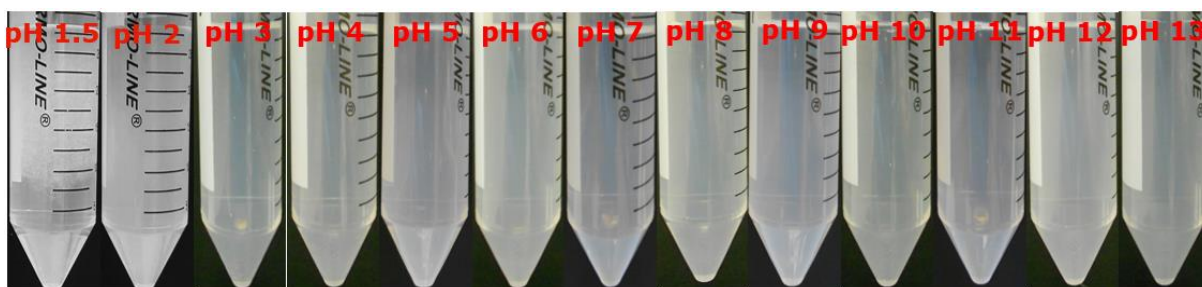
4.3.2.2 pH Conditions

pH is another important factor to be examined since the pure MNPs are pH-responsive (Tremaine and Leblanc, 1980). The surface wettability of the MCNC nanocomposites across pH 1.5 to 13.0 has been examined. Results from Table 4.3 demonstrated that the surface wettability of MCNC reduced linearly from 87.993 ± 3.030 to 18.739 ± 3.059 ° as pH increased from 1.5 to 11. The surface wettability of MCNC nanocomposites at pH 12 and 13, however was unable to be measured accurately due to the presence of extremely high salt content as a result of pH tuning. Nevertheless, the results showed that MCNC possessed hydrophobic surface properties under low pH, but turned hydrophilic as pH increased. Since native CNC was not pH responsive under the examined pH ranges (Figure 4.22a), MNP is the material that contributes to the changes. The changes of water wetting ability, or solubility of MNP upon pH variation was previously observed in literature reports by Tremaine and Leblanc (1980). They have demonstrated that MNP was poorly soluble in water (hydrophobic) at acidic pH. The solubility slowly increased and reached maximum at around pH 11 (hydrophilic), and drastically reduced as pH was further increased (Tremaine and Leblanc, 1980; Vepsäläinen and Saario, 2010). In fact, the solubility of MCNC nanocomposites in water has shown a similar trend as that of pure MNPs, even at pH 12

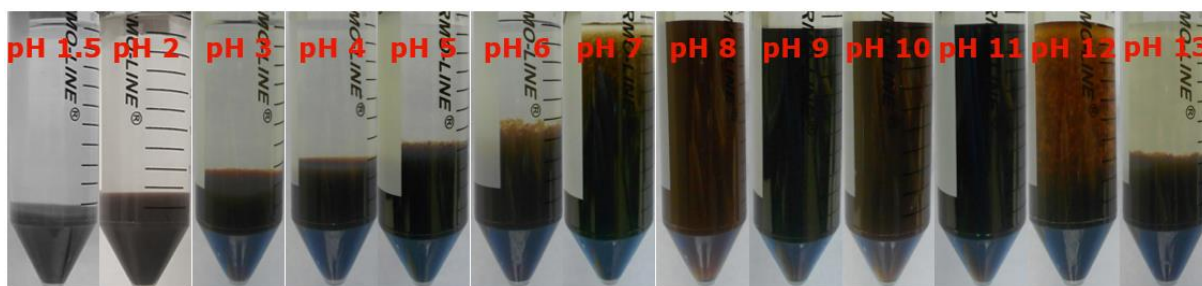
and 13 (Fig. 4.22b). Using Equation (4.1), the interfacial contact angle for MCNC nanocomposites varying pH was estimated and tabulated in Table 4.3. The outcomes revealed that the interfacial contact angles reduced from 159.522 to eventually 0.000 ° when pH increased from 1.5 to 11. Based on the previous claims by Kaptay *et al.* (2006) where the optimum interfacial contact angles for Pickering stabilization falls around 70 to 110 °, we suspect that the suitable pH ranges for Pickering emulsion preparation were most likely falls in between 4 to 7. To verify that, the pH effects on Pickering emulsion formation will be evaluated in the next Chapter.

Table 4.3. Water-air and interfacial contact angle of MCNCs samples varying pH. Different alphabetic letters was significantly different at $P \leq 0.05$ by Bonferroni's Multiple Comparison Test.

Sample pH	Water-air contact angle (°)	Interfacial contact angle (°)
1.5	87.993 ± 3.030 ^a	159.522
2.0	79.577 ± 4.222 ^b	143.497
3.0	73.761 ± 4.906 ^c	117.660
4.0	71.359 ± 2.239 ^d	110.020
5.0	67.797 ± 0.867 ^e	97.208
6.0	63.419 ± 1.169 ^f	84.295
7.0	58.265 ± 3.189 ^g	70.366
8.0	53.468 ± 0.853 ^h	53.551
9.0	48.918 ± 1.762 ⁱ	37.736
10.0	30.810 ± 1.709 ^j	0.000
11.0	18.739 ± 3.059 ^k	0.000
12.0	N/A	N/A
13.0	N/A	N/A



(a)



(b)

Figure 4.22. Photographs of (a) CNC suspensions and (b) MCNC suspensions prepared under pH ranging from 1.5 to 13.0.

4.4 Conclusions

Effects of CNC/MNP ratio, temperature, and US power and US irradiation time on physicochemical properties of the sonochemically prepared MCNC nanocomposites were examined. Excess surface hydroxyl groups were spotted from FTIR results when high dispersant content was employed as compared to the iron oxides amount. The increase in dispersant concentration gives rise to direct improvement on the MNPs dispersibility on CNC fibre while having an inverse relationship with the magnetic strength of the resultant MCNC nanocomposites (30.798 to 1.625 emu/g with increasing ratio from 0.2 to 20). The pre-heated temperature of the CNC + Fe²⁺/Fe³⁺ dispersion showed no significant effects on the dispersion of MNPs on CNC. However, it leads to reduced M_s as an outcome of excessive oxidation of Fe²⁺ to Fe³⁺ prior to co-precipitation reaction, which thus resulted in reduced MNPs content. Besides that, the current investigation also revealed that the corresponding dispersivity of MNPs improved as sonication time increased from 1 to 5 min, and then remained similar upon further sonication to 10 min. Despite the fact that utilization of US accelerated the overall nucleation and growth of MNPs, an overduely long US irradiation time caused unwanted oxidation of Fe²⁺ on the surface structures of the already-formed MNPs to Fe³⁺. This was confirmed from our XPS analysis. The effects of CNC concentration and pH of the MCNC dispersion towards the surface wettability of the respective MCNC nanocomposites were then evaluated by estimating the interfacial contact angles of the MCNC. The CNC concentration analysis revealed that the interfacial contact angle increases from 15.690 to 47.015° as CNC/MNP ratio reduced from 20 to 1 as regarded by the reducing amount of hydrophilic groups on the composites surfaces. In the present study, the trend reverses after the ratio of 1. Further decreasing the ratio to 0.2 resulted in excess amount MNPs deposited on the CNC surface. With more deposited MNPs, a more hydrophilic behaviour of MCNC nanocomposite was observed. pH examination, on the other hand, showed that interfacial contact angles reduced from 159.522 to eventually 0.000° when pH increased from 1.5 to 11, suggesting that the suitable pH ranges for Pickering emulsion preparation were most likely falls in between 4 to 7. The pH effects on Pickering emulsion formation will be addressed in the next Chapter.

CHAPTER FIVE

PHYSICAL PROPERTIES AND COLLOIDAL STABILITY OF MCNC-STABILIZED PICKERING EMULSION (MCNC-PE)

Overview

The formation of palm olein-in-water (O/W) Pickering emulsion stabilized by Fe_3O_4 @Cellulose nanocrystals (MCNC) nanocomposites is investigated in this chapter. The synthesized MCNC nanocomposites successfully stabilized Pickering emulsion with dual responses. The magnetic tests revealed a direct-relation between attractability of MCNC-stabilized Pickering emulsions (MCNC-PE) and the emulsion droplet diameter. The MCNC-PE showed stable monodisperse emulsion droplets under acidic pH. The physical stability substantially reduced as the MCNC-PE falls around mild alkali pH, and regained slowly when approaching pH 13. In the parametric studies, it has been noticed the changes in MCNC particles concentration, C_{mcnc} and oil volume ratio, φ_{oil} lead to the changes in the mean emulsion sizes and the surface coverage (S_{mcnc}) of emulsions by MCNC particles. Increasing ultrasound (US) power and time are found to favour MCNC-PE with smaller sizes and higher monodispersity. The desired ultrasonic conditions in this work that provides MCNC-PE with smallest possible sizes were 60 W US power and 3 min sonication time. Lastly, the results demonstrated that the ionic strength does not affect the mean droplet size, creaming stability and magnetic strength of the MCNC-PE.

5.1 Introduction

Emulsion is a system of two immiscible liquids in which one of the liquid is dispersed in the other. Generally, conventional emulsions were stabilized by surfactants. However, the cost of surfactant is normally high, and their recovery is not practical (Binks, 2002; Tang *et al.*, 2015). Furthermore, some surfactants may also induce tissue irritation and cell damage (Tang *et al.*, 2015). Therefore, the use of solid particles as emulsifier is getting more attentions recently due to their low cost, low toxicity, and their remarkable resistance against coalescence compared to the conventional emulsions stabilized by surfactant (Frelichowska *et al.*, 2009; Pickering, 1907; Ramsden, 1903). The solid-stabilized emulsions system, termed as Pickering emulsion were pioneered by Ramsden, (1903) and Pickering, (1907) back in the 19th century. Their findings allowed the generation of surfactant-free emulsions. This is vitally useful especially in various health and cosmetics applications where the use of lethal surfactants are undesirable. By definition, the advanced resistances to de-stabilization of Pickering emulsions were due to the irreversible adsorption of colloidal solid particles onto the interfaces of two immiscible liquids (Binks and Lumsdon, 2001; Cunha *et al.*, 2014; Tambe and Sharma, 1993). The strong shielding effects imparted by the solid particles, however, have restricted the employment of the Pickering emulsion in various applications that requires temporal stabilization and subsequent demulsification. This includes oil recovery (Sharma *et al.*, 2015; Tang *et al.*, 2015), drug delivery (Frelichowska *et al.*, 2009; Marku *et al.*, 2012; Tang *et al.*, 2015), and emulsion polymerization (Chen *et al.*, 2008; Tang *et al.*, 2015; Zhang *et al.*, 2009).

The stabilization of Pickering emulsion is normally affected by the surface wettability of particles (Binks and Lumsdon, 2000). Hence, nanoparticles with switchable partial surface wetting properties are desirable. This can be done by designing Pickering stabilizer that responds to external stimuli. Generally, this requires particle that undergo some physical or chemical transformation under responses to external triggers that, in turn, changing its wetting ability. This can ultimately result in generating remote controllable Pickering emulsion. To date, various responses such as thermosensitive (Tang *et al.*, 2014; Zoppe *et al.*, 2012), pH responsive (Lan *et al.*, 2007; Tang *et al.*, 2014), and magnetic

responses (Lan *et al.*, 2007; Zhou *et al.*, 2011), have been attempted for Pickering emulsions preparation. In fact, Pickering emulsions with multiple stimuli responses were also demonstrated (Tang *et al.*, 2014). One of the popular material that has gained attentions for its stimuli responsive properties is the Fe₃O₄ nanoparticles (MNPs). Besides being known for its superparamagnetic properties, recent study by Lan *et al.* (2007) demonstrated that oleic acid stabilized MNPs experienced several phase transition when the pH was adjusted from acidic to alkali condition. However, study by Zhou *et al.* (2011) showed that pure MNPs were only able to stabilize certain non-polar oil based Pickering emulsion. This highly constrained the uses of MNPs for the as-mentioned applications.

In search for approaches to improve the feasibility of MNPs to stabilize more types of oil-based Pickering emulsion, cellulose nanocrystal (CNC), was one of the most widely investigated Pickering stabilizer due to its biocompatibility, biodegradability, non-toxicity, and sustainability (Capron and Cathala, 2013; Kalashnikova *et al.*, 2011; Zoppe *et al.*, 2012). In literature, CNC had been reported to exhibit remarkable performance as Pickering stabilizer for emulsion. Furthermore, it was reported that CNC can undertake variety of responses when incorporated with fillers with respective responses (Wu *et al.*, 2011). In fact, literature evidence have proven that the incorporation of MNPs into CNC matrix give rise to magnetic cellulosic materials with great dispersion stability (Liu *et al.*, 2015). Despite the wide documentation of CNC-based stimuli responsive Pickering emulsions, magneto-responsive Pickering emulsions based on Fe₃O₄@CNC (MCNC) nanocomposites has, however, not been adequately explored.

This leads to the objective of this paper where preparation of magneto-responsive Pickering emulsions stabilized by MCNC nanocomposite is studied. In addition, several important parameters, including the pH, CNC/MNP ratio, MCNC particle concentrations, oil volume fraction φ_{oil} , US power, sonication time and ionic strength on the preparation of MCNC-stabilized Pickering emulsion were also studied in the current work to prepare the magnetic- and pH-responsive Pickering emulsions using MCNC nanocomposites as Pickering stabilizer. Additionally, since the MCNC-PE aimed ultimately to be a drug delivery carrier, the oil phase in our formulation was chosen as the red palm olein. Red palm olein is an

edible oil that is rich in natural phytonutrients such as tocotrienols and carotenoids that exhibit nutritional properties and oxidative stability (Bonnie and Choo, 2000). Besides, it is also proven to have potent cardioprotective, antioxidant, anti-inflammatory and anti-diabetic activities (Loganathan *et al.*, 2017).

5.2 Materials and Methodology

5.2.1 Materials

All chemicals in this study were employed without further purification. Iron (II) chloride tetrahydrate ($\text{FeCl}_2 \cdot 4\text{H}_2\text{O}$, $\geq 99\%$), iron (III) chloride hexahydrate ($\text{FeCl}_3 \cdot 6\text{H}_2\text{O}$, 99%), ammonium hydroxide (28% NH_3 in H_2O) and sodium chloride (NaCl) were purchased from Sigma-Aldrich. CNC (Freeze dried) purchased from University of Maine. Red palm superolein (melting point 19 °C) was purchased from Sime Darby Jomalina Sdn Bhd (Malaysia). All water used in this experiment are ultrapure water ($18.2 \text{ M}\Omega \text{ cm}^{-1}$) obtained from Milli-Q® Plus apparatus (Millipore, Billerica, USA), ethanol (AR standard), 1M hydrochloric acid (HCl), and sodium hydroxide (NaOH) purchased from R & M Chemical (Syarikat Saintifik Jaya, Malaysia). All experiments involving US were conducted on an ultrasound probe sonicator (20 kHz, Lab750, Sinaptec) under pulse mode (15 s pulse on, 10 s pulse off).

5.2.2 Synthesis and Characterisation of MCNC Nanocomposite

MCNC nanocomposites were prepared by sonochemical co-precipitation methods as mentioned in previous section. Briefly, CNC was first dispersed in water and later mixed with iron (III) and iron (II) chloride (1.5/1 $\text{Fe}^{3+}/\text{Fe}^{2+}$ mol ratio). Subsequently, the mixtures were stirred and heated to 45 °C., and sonicated using ultrasonic horn at 60 w in the presence of ammonium hydroxide for 5 minutes.

After that, the MCNCs were precipitated, and magnetically separated and washes 3 times with ethanol to remove all ammonium hydroxide. Lastly, the leftover were centrifuged at 4500 rpm for 20 minutes, and dried in an oven overnight. The dried sample were stocked and utilized for characterisation as discussed in Chapter 3.

5.2.3 Preparation of MCNC-PE

Pickering emulsions were prepared by using the as-synthesized MCNC nanocomposites as solid particle stabilizers and β -carotene rich red palm olein as oil phase. A brief preparation procedure of MCNC-stabilized Pickering emulsions was as shown in Figure 5.1, and discussed in details as follow:

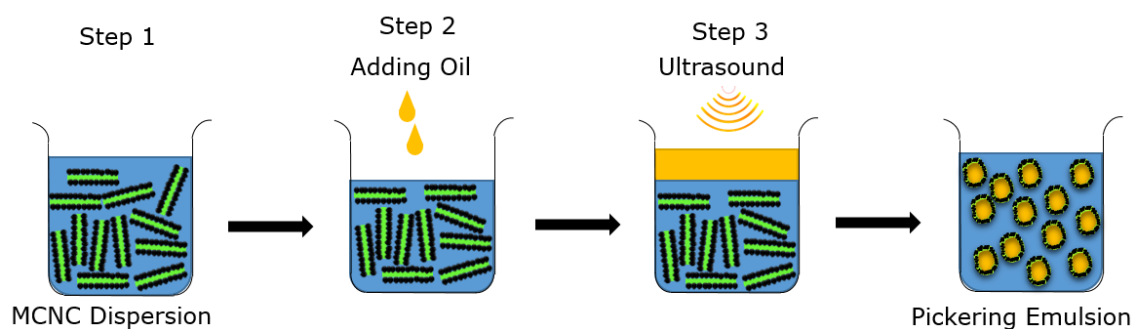


Figure 5.1. Schematic representation for preparation of MCNC-PE.

5.2.3.1 Pickering Emulsions at Different pH

Emulsions with fixed oil content were prepared by mixing 30 vol% palm olein ($\varphi_{oil} = 0.3$) with aqueous suspension of fixed MCNC particle concentrations (0.050 wt%) at various pH (1.5 to 13.0), adjusted using HCl and NaOH of analytical grade. Subsequently, the mixture was emulsified for 3 minutes using an ultrasonic horn at 60 w. The resultant emulsion was transferred to glass vials and stored at room temperature for further characterisation.

5.2.3.2 Pickering Emulsions with Different MCNC Particle Concentrations

Emulsions with fixed oil content were prepared by mixing 30 vol% palm olein ($\varphi_{oil} = 0.3$) with aqueous suspension of different MCNC particle concentrations (0.025, 0.050, 0.100, 0.200, and 0.300 wt%) at pH 6.5. Subsequently, the mixture was emulsified for 3 minutes using an ultrasonic horn at 60 w. The resultant emulsion was transferred to glass vials and stored at room temperature for further characterisation.

5.2.3.3 Pickering Emulsions with Different Oil Volume Fraction

Emulsions with different oil contents were prepared by taking 0.1 wt% MCNC particles dispersion at pH 6.5, with different MCNC oil volume fractions ($\varphi_{oil} = 0.1, 0.2, 0.3, 0.4,$ and 0.5). The mixture was then emulsified for 3 minutes using an ultrasonic horn at 60 w. The resultant emulsion was transferred to glass vials and stored at room temperature for further studies.

5.2.3.4 Pickering Emulsions with Different Ultrasound Power

Emulsions with fixed oil content were prepared by mixing 30 vol% palm olein ($\varphi_{oil} = 0.3$) with aqueous suspension of fixed MCNC particle concentrations (0.050 wt%) at pH 6.5, adjusted using HCl and NaOH of analytical grade. Subsequently, the mixture was emulsified for 3 minutes using an ultrasonic horn operated at various US power (40, 60, 80 w). The resultant emulsion was transferred to glass vials and stored at room temperature for further characterisation.

5.2.3.5 Pickering Emulsions with Different Sonication Time

Emulsions with fixed oil content were prepared by mixing 30 vol% palm olein ($\varphi_{oil} = 0.3$) with aqueous suspension of fixed MCNC particle concentrations (0.050 wt%) at pH 6.5, adjusted using HCl and NaOH of analytical grade. Subsequently, the mixture was emulsified for 1, 3, 5, 7, and 10 minutes using an ultrasonic horn operated at 60 w US power. The resultant emulsion was transferred to glass vials and stored at room temperature for further characterisation.

5.2.3.6 Pickering Emulsions with Different NaCl Concentrations

To examine the effects of salt on the MCNC-stabilized Pickering emulsion properties, emulsions with different ionic strengths were prepared by adding different amount of NaCl (0, 100, 200, 300, 400, and 500 mM) into the freshly made Pickering emulsions containing a fixed oil volume fractions ($\varphi_{oil} = 0.3$) stabilized by 0.1 wt% MCNC particles. The emulsion

samples were then gently stirred for 5 min and transferred to glass vials and stored at room temperature for 14 days for analysis.

5.2.4 Characterisation of MCNC-PE

MCNC stabilized Pickering emulsion droplets diameter was measured using a Mastersizer (Mastersizer 3000, Malvern Instruments, UK) equipped with a Hydro EV wet dispersion unit. The emulsions were analysed periodically up to 14th days of preparation to determine the storage stability of the emulsions. Stability of Pickering emulsions were checked via traces of phase separation or coalescence of the emulsions. Visualization of Pickering emulsion droplets were performed using an inverted optical microscope (Nikon Eclipse TS100, Nikon Instruments Inc., USA) at 10x magnification. Localization of MCNC at the oil/water interface were checked using inverted fluorescent microscope (Nikon Eclipse Ti-E, Nikon Instruments Inc., USA) at 10x magnification. The emulsions sample for fluorescent microscopy were prepared at pH 6 with double staining. Red palm oil were stained with Nile red prior to emulsions preparation. After preparation, the Pickering emulsions were diluted 30 times with water. The MCNC were then stained with calcofluor white. The motion of MCNC-PE under an external magnetic field (EMF) was evaluated based on a method similar to that by Lin, Yang, Petit, and Lee, (2015) on examination of motion of MRGO-Pickering emulsion under an EMF. For instance, 50 μ l of the MCNC-PE was dropped in petri dishes. Then, a magnet was located near to it to attract them.

5.2.5 Statistical Analysis

Experiment was repeated for obtaining triplicate measurements. Analysis of variance (ANOVA) was conducted utilizing Prism software and $p < 0.05$ was considered as statistically significant.

5.3 Results and Discussion

5.3.1 Physical Properties of MCNC-PE

To compare the effectiveness of MCNC in stabilizing Pickering emulsions, pristine MNPs and CNC stabilized emulsions were prepared as control samples to be compared to the emulsions emulsified by the MCNC. The result showed that pure MNPs could not produce stable palm oil-based Pickering emulsion (Figure 5.2a). The reason for poor stability in MNPs may be simply because MNPs possessed low surface charges after they aggregated. This thus caused the MNPs to settle down easily and led to destabilization of the freshly formed emulsions. The Pickering emulsion produced by pristine CNC was not stable as well, as shown in Figure 5.2b. This could be explained where CNC have an extremely high surface charges up to a point where the repulsion forces hold as barrier to retard the emulsion stability. In fact, certain amount of electrolyte were often added to CNC dispersion for charge screening before utilizing it as Pickering emulsifier to favour stable Pickering emulsions (Kalashnikova *et al.*, 2012). Thus it is reasonable that stable Pickering emulsions could not formed in the current situation since no electrolyte were added prior to Pickering emulsions preparation. In contrast, stable Pickering emulsions were obtained when MCNC was used as stabilizer (Figure 5.2c). This is mainly because the deposition of MNPs onto CNC matrix providentially acted as charge screening function as that of electrolyte. Thus, we could confirm that MCNC contributes well in stabilizing Pickering emulsion.

To prove the above explanation, surface charges of the materials are examined by measuring the zeta potential of pristine MNPs, CNC, and MCNC nanocomposite. As shown in Figure 5.3, MNPs exert low zeta potential of -18.8 ± 1.4 mV that falls within a range that favours de-stabilization (Nanocomposix, 2016). CNC, on the other hand, have high zeta potential of -69.6 ± 2.6 mV. As compared to both pure solids, the surface charges of MCNC were lower than that of CNC. The reduction ($P < 0.05$) in zeta potential for MCNC stabilized Pickering emulsions was due to the incorporation of weakly charged MNPs onto CNC matrix. Furthermore, even with such reduction, the zeta potential of MCNC nanocomposites still falls within the safe range (ranges < -25 mV or > 25 mV) against coalescence

(Nanocomposix, 2016), with recorded value of -35.6 ± 4.0 mV. This thus led to stable Pickering emulsion formation.

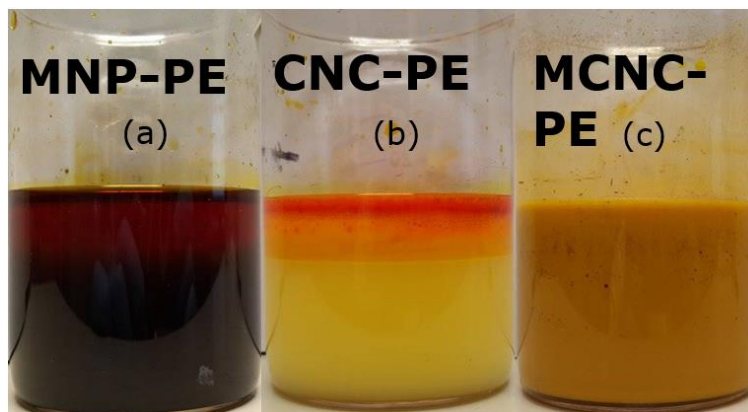


Figure 5.2. Fresh Pickering emulsion produced with (a) 0.1 wt% pure MNP, (b) 0.1 wt% pure CNC, and (c) 0.1 wt% MCNC nanocomposite.

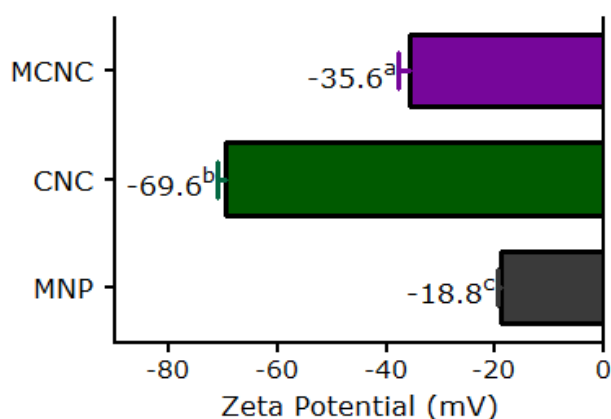


Figure 5.3. Surface charge of Pickering emulsion stabilized by (black) pure MNP, (green) pure CNC, and (purple) MCNC nanocomposite. Standard error of mean of triplicate readings were represented by the error bars in each graph, different alphabetic letters was significantly different at $P \leq 0.05$ by Bonferroni's Multiple Comparison Test.

The localization of MCNC at O/W interface was checked by fluorescent microscopy. Calcofluor was used to stain the cellulosic material, while Nile red was contributed to oil phase staining. This double staining allows one to clearly distinguish the inner oil phase and the surface covered by MCNC nanocomposites. Figure 5.4a and b showed the presence and location of MCNC and red palm oil respectively. On the same hand, Figure 5.4c revealed

that the micrograph produced by combining both image in Figure 5.4a and b. It was obvious that the red palm oil was surrounded by the MCNC. This thus confirmed the existence of both MCNC and red palm oil in the O/W Pickering emulsion prepared.

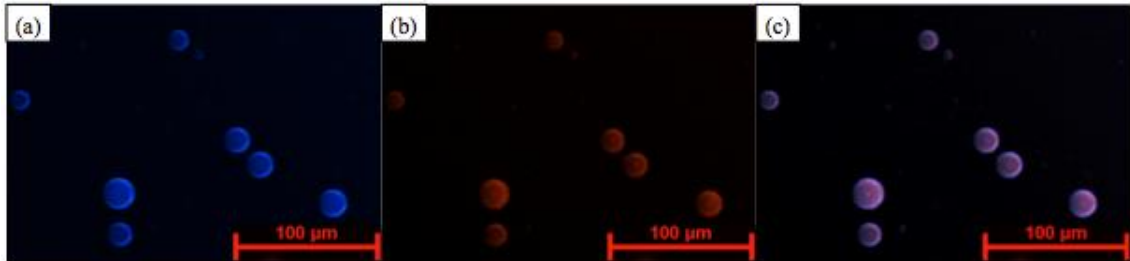


Figure 5.4. Fluorescent micrographs of MCNC-PE at pH 6 with double staining. Images (a) showing MCNC nanocomposites, (b) showing red palm oil phase, and (c) Combined image. (Red palm oil phase stained with Nile red, MCNC stained with calcofluor).

Magnetic properties of MCNC-PE were evidenced from the motion of droplets under an EMF (see Figure 5.5). For comparing the magnetic attract ability, stable Pickering emulsion droplets at two different diameter was evaluated. Emulsion at pH 3 with diameter of 109.00 µm was representing big emulsion, while emulsion at pH 6 (diameter of 25.64 µm) was chosen to represent small emulsion (note*, the effect of pH on MCNC stabilized Pickering emulsion will be discussed in the next section). It was obvious that both emulsions responded to EMF. However, the motion of emulsions with smaller droplet diameter towards the household magnet was much faster as compared to the bigger emulsions. This is due to the drag force acted on the droplets. From the famous drag equation (Equation 5.1) (Yamaguchi, 2008).

$$F_D = C_D \rho A u^2 / 2 \quad [\text{Equation 5.1}]$$

Where F_D is the drag force, C_D is the drag coefficient, ρ is the density of fluid, A is the cross sectional area of droplet, and u is the velocity of the object. The drag coefficient for very small droplet with small Reynolds number ($Re < 1$) is considered to be as Equation (5.2):

$$C_D = 24/Re \quad [\text{Equation 5.2}]$$

$$Re = \rho u d / \mu \quad [\text{Equation 5.3}]$$

Where Re is Reynolds number, d is droplet diameter, μ is viscosity of fluid. Using these equations, one can notice that the corresponding drag force for small and big droplets are 2.053 nN and 25.309 nN respectively. The drag force experienced by the big droplet are approximately 12 times larger than that by small droplet. Hence, smaller emulsion will get much easily drawn as compared to the big emulsion. In overall, the findings showed the feasibility of producing magnetically controlled Pickering emulsion employing the as-synthesized MCNC nanocomposite.

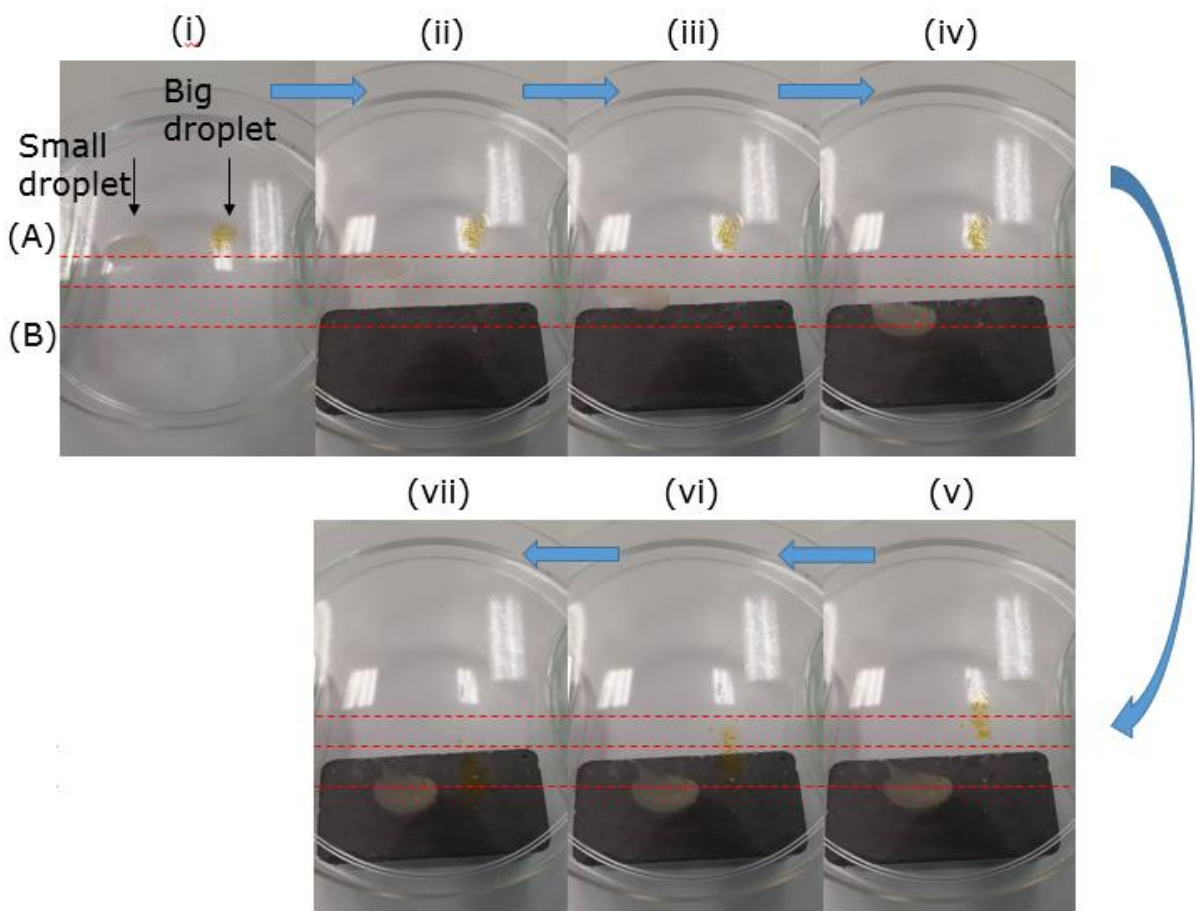


Figure 5.5. Magnetic attractability of the as-formulated MCNC-PE at pH 6 (left, small) and pH 3 (right, big) from point (A) to (B), (i) without EMF, (ii – vii) with EMF.

5.3.2 Factors Affecting the Colloidal Characteristics of MCNC-PE

5.3.2.1 Effect of pH

MCNC stabilized Pickering emulsion at different pH conditions can be seen in Figure 5.6. The Pickering emulsions were found to be stable from pH 1.5 to 7. The stability decreased progressively at alkali condition (pH 8 to 11), and then recovered at pH 12 and 13 (see Figure 5.6). It is well known that CNCs are normally amphiphilic yet dispersed easily in water (Kalashnikova *et al.*, 2012), so the reduction in hydrophilicity of MNPs alter the MCNC nanocomposites overall surface wettability to a level that favour the formation of stable emulsions. This was further confirmed when pH of the environment were tuned to moderate alkali condition (pH 8 to 11) where non-stable emulsions were produced. The observed phenomenon is mainly because MNP were hydrophilic dominance (highly soluble in water) under these pH. Thus, the hydrophobic properties of the hybrid nanocomposites were essentially imparted only by CNC. This, in turn, causing the wettability of MCNC nanocomposite to be hydrophilic dominance, thereby resulting in decreased Pickering emulsion stability. From Figure 5.6i, one can clearly see that emulsions at pH 11 experienced phase separation.

On the other hand, emulsion droplets at pH 12 showed a better stability as compared to the emulsions at pH 11 (Figure 5.6i and j). In addition, further adjustment of pH to 13 also provided Pickering emulsions with much improved stability (Figure 5.6k). This was resulted from the reduced MNP solubility in water after pH 11. This phenomenon was supported by research report done by Vepsäläinen and Saario, (2010) where the solubility of MNP in water will experience a drastic fall after pH 11.

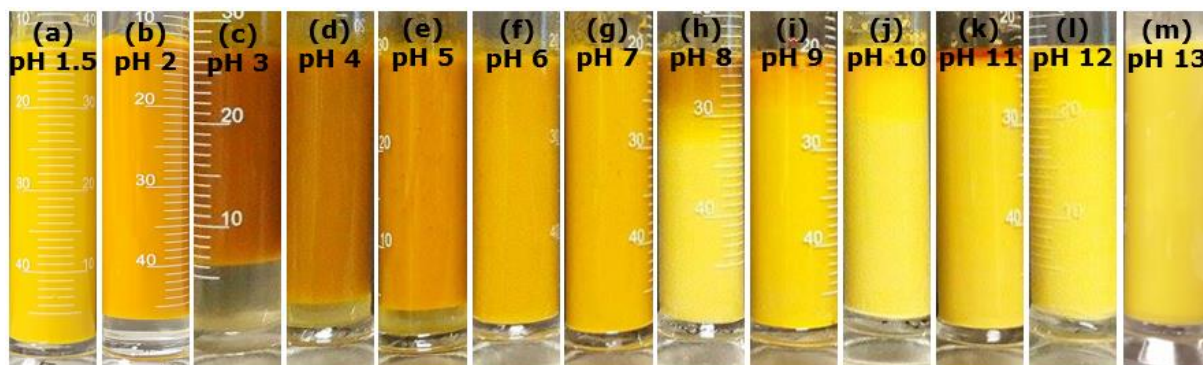


Figure 5.6. Photograph of O/W Pickering emulsion stabilized by MCNC at (a) pH 1.5, (b) pH 2, (c) pH 3, (d) pH 4, (e) pH 5, (f) pH 6, (g) pH 7, (h) pH 8, (i) pH 9, (j) pH 10, (k) pH 11, (l) pH 12, and (m) pH 13. Image captured 10 minutes after preparation.

The mastersizer and optical microscope analysis were shown in Figure 5.7 and Figure 5.8. The size distribution curve (Figure 5.7a) of Pickering emulsion under different pH conditions revealed that monomodal distributions were obtained at pH 1.5, 2, 3, 4, 5, 6, 7 and 13, showing that emulsions prepared were monodispersed. In contrast, bimodal distributions were observed in MCNC-stabilized Pickering emulsion formed under pH 8, 9, 10, 11, and 12, indicating that the prepared emulsions were polydispersed. Using the data from Figure 5.8a, the average emulsion droplet diameter at different pH was plotted in Figure 5.7b. Figure 5.7b clearly shows that the Pickering emulsions size first increased when pH increased from 1.5 to 3, and then reduced substantially ($p < 0.05$) as pH is further increased. The droplets diameter increased from 22.2 to 109 from pH 1.5 to 3, and reduced from 109.00 μm to 11.90 μm as pH increased from 3 to 7. However, it then sharply increased with further pH increment to 11 (66.30 μm), and dropped significantly as pH approaches 13 (1.40 μm). As per discussed in previous chapter, the contact angle of MCNC at pH 1.5 to 3 falls outside the safe ranges for effective Pickering stabilization. Under such circumstance, the adsorption of MCNC particles onto the liquid-liquid interface will be harder as compared to those that fall within the safe ranges. In this study, the increment of mean oil globule sizes across pH 1.5 to 3 is most likely regarded to the electronegative behaviour of the MCNC. As pH increased from 1.5 to 3, the positive surface charge of MCNC not only reversed but also showed a higher magnitude (see Figure 5.9). This is most likely due to

the dissociation of functional groups on the surfaces of MCNC particles. As a result, strong repulsion force arose between MCNC particles adsorbing at the liquid-liquid interface. This, in conjunction with the high hydrophobicity (high contact angle) eventually leads to the retardation of the effective stabilization of Pickering emulsion. On the other hand, the reduction of average emulsions size from pH 3 to pH 7 could be explained not only on the reduction in 3-phase contact angle of the MCNC particles into the preferable ranges for Pickering stabilization, but also due to the zeta potential increment. This allowed emulsion droplets to ward off with each other to remain in smaller size.

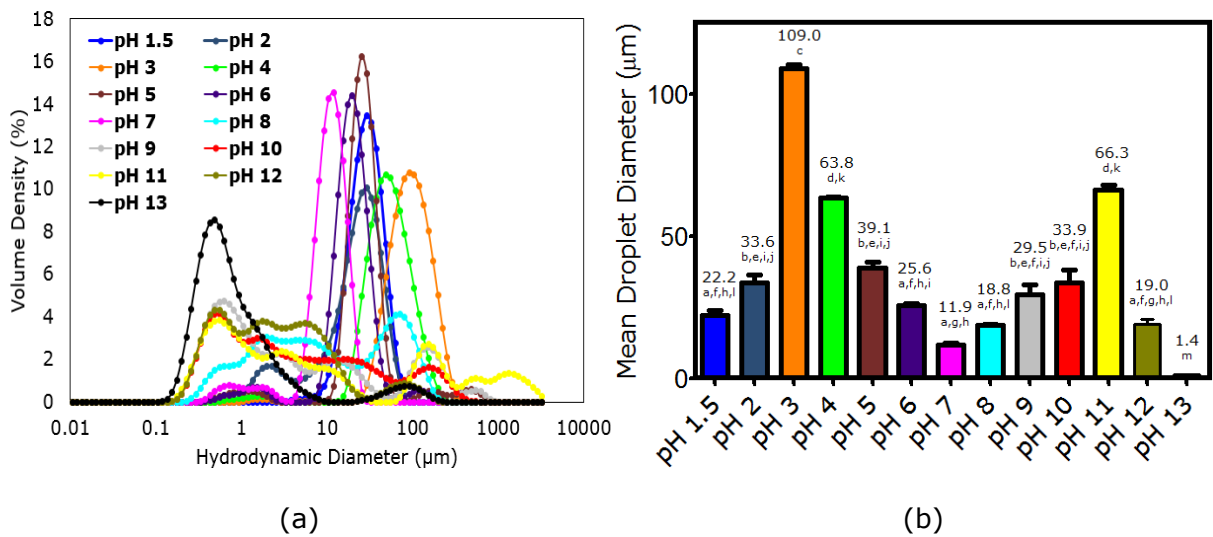


Figure 5.7. (a) Raw size distribution data and (b) mean droplet diameters of MCNC-PE ranging from pH 1.5 to pH 13. Standard error of mean of triplicate readings were represented by the error bars in each graph, different alphabetic letters was significantly different at $P \leq 0.05$ by Bonferroni's Multiple Comparison Test.

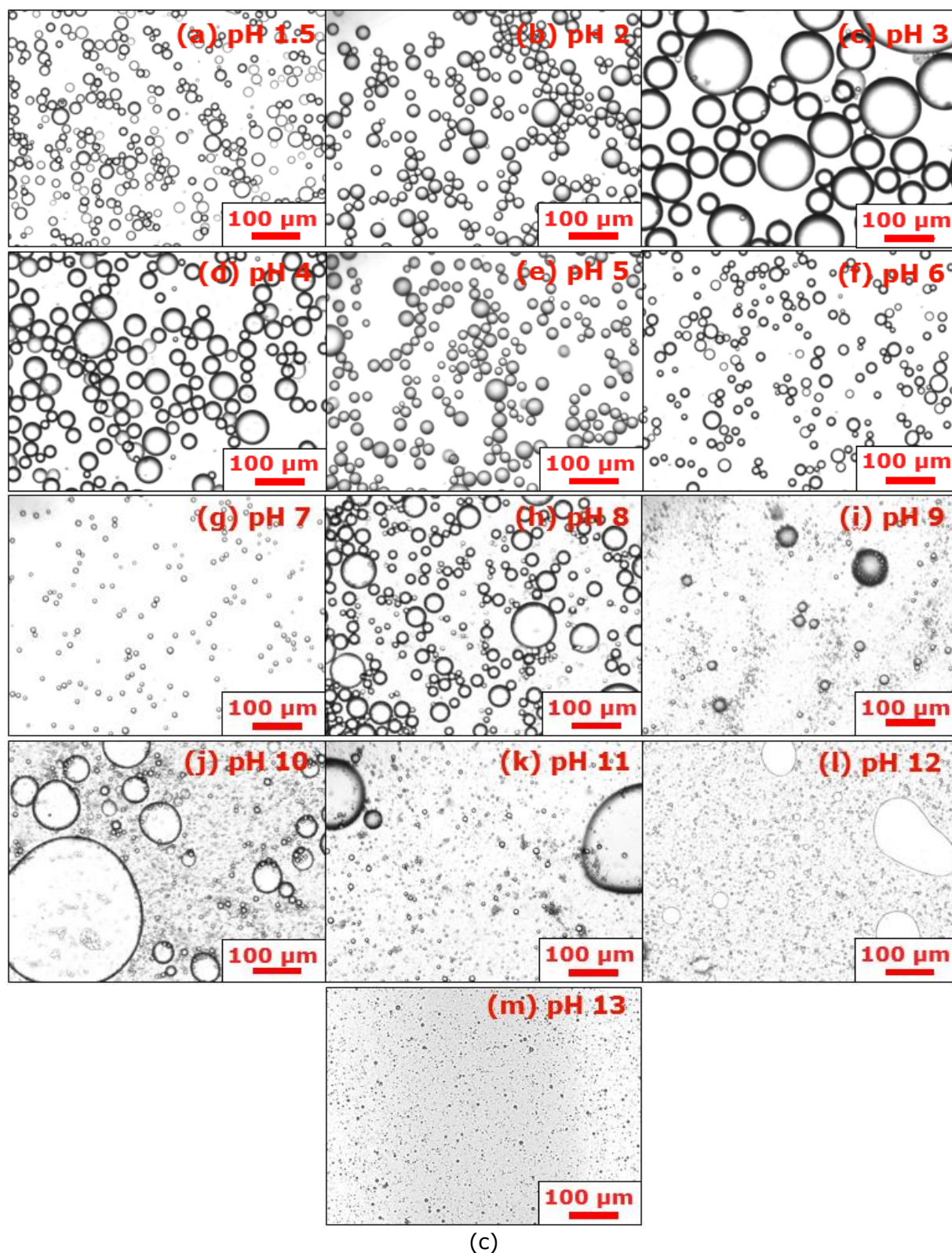


Figure 5.8. Microscopic images of O/W MCNC-PE at (a) pH 1.5, (b) pH 2, (c) pH 3, (d) pH 4, (e) pH 5, (f) pH 6, (g) pH 7, (h) pH 8, (i) pH 9, (j) pH 10, (k) pH 11, (l) pH 12, and (m) pH 13.

The emulsion diameter rise at alkali pH ranges (8 to 11) were most probably because MCNC can no longer stabilize Pickering emulsion due to their hydrophilic dominance at moderate alkali pH. However, due to the increase in zeta potential with increasing pH, smaller sized Pickering emulsions with temporal stability were produced. These Pickering emulsions, nevertheless, have no resistance to coalescence due to the high hydrophilicity of MCNC under pH 8 to 11. Thus, larger emulsions were observed as a result from the coalescence (see Figure 5.8h to k). The emulsion droplets diameter decreased substantially as pH was further adjusted to 13. This is likely that at pH 13, the surface wettability of MCNC reduced, thus results in increasing hydrophobicity as compared to MCNC nanocomposite at pH 8 to 11. Additionally the zeta potential also reduced to a ranges that favours stable Pickering emulsions at elevated pH, which thus resulting in the reduction of the overall mean emulsion droplets diameter (Figure 5.8m).

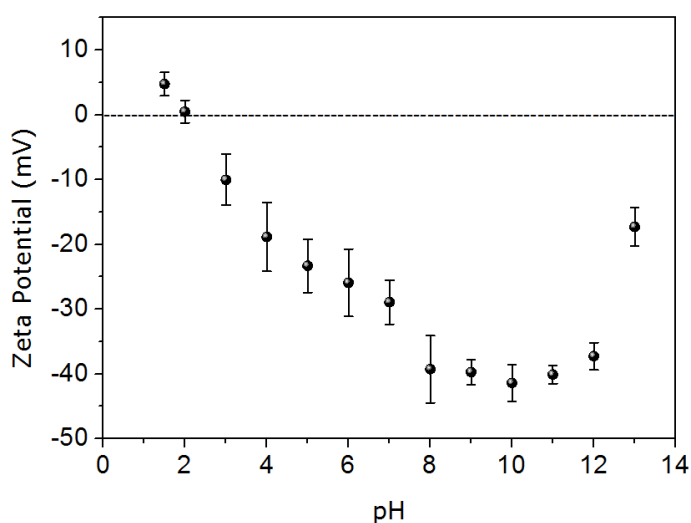


Figure 5.9. Zeta potential of MCNC particles as function of pH.

The storage stability of MCNC stabilized Pickering emulsion were analysed using the Pickering emulsion prepared at pH 6 and pH 8, as representative for stable and non-stable emulsions respectively. The photograph of Pickering emulsions at both pH during day 0, day 7, and day 14 of formulation was shown in Figure 5.10. The stable emulsion fraction was, therefore, measured and analysed.

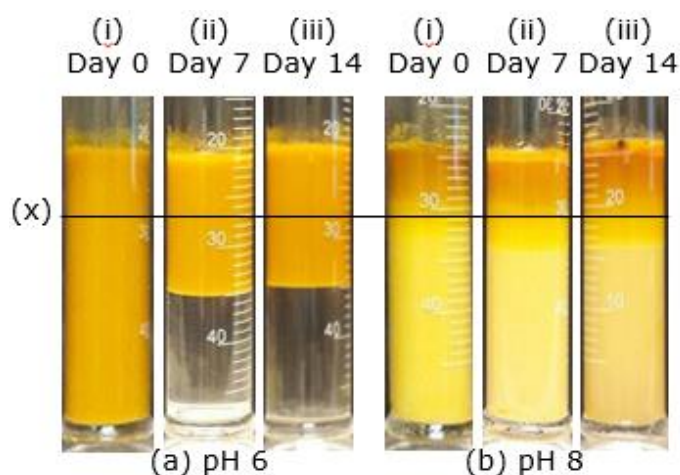


Figure 5.10. Storage stability for MCNC-PE with 0.05 wt% MCNC, produced under (a) pH 6, and (b) pH 8. Image captured in (i) day 0, (ii) day 7, and (iii) day 14 of formulation. Line (x) indicating the point where emulsion samples were extracted for mastersizer analysis.

From Figure 5.11a, the creaming index of Pickering emulsion at pH 6 was higher than those at pH 8. This is merely because the emulsions at pH 6 are micro-sized, where the effects of gravity were still noticeable. Thus the oil droplets that are lighter will tend to float. In fact, literature findings have proven that emulsions at nanoscale have good stability towards gravitational separation (Komaiko and McClements, 2016; Ostertag, Weiss, and McClements, 2012). On the other hand, Pickering emulsion prepared at pH 8 did not show clear water separation. This is due to the presence of nano-sized emulsions with temporal stability in the medium. However, creaming was noticed at the top sections of the pH 8 emulsion. The volume of creaming increased slowly from day 0 to day 14, indicating that there were emulsions coalescence. This is in agreement with our mastersizer analysis (Figure 5.7a) where bimodal distribution was observed in size distribution curve for Pickering emulsion prepared at pH 8.

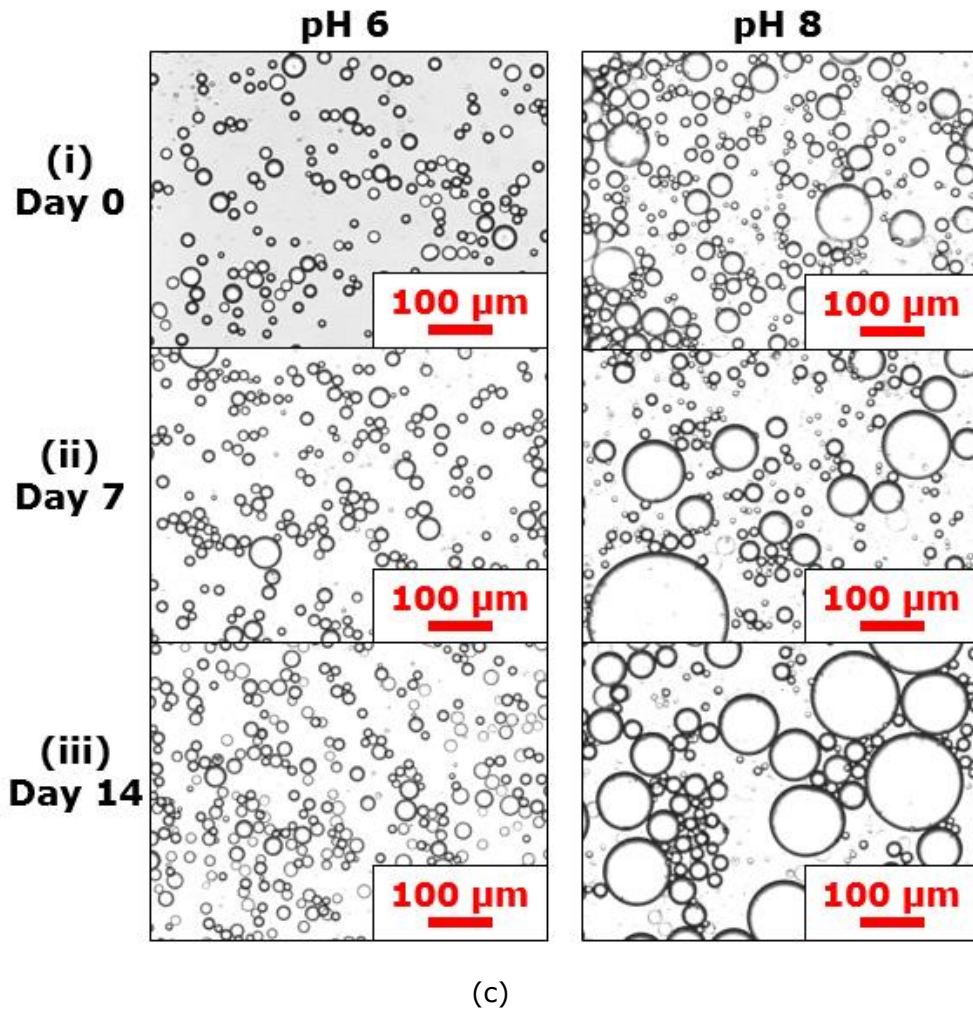
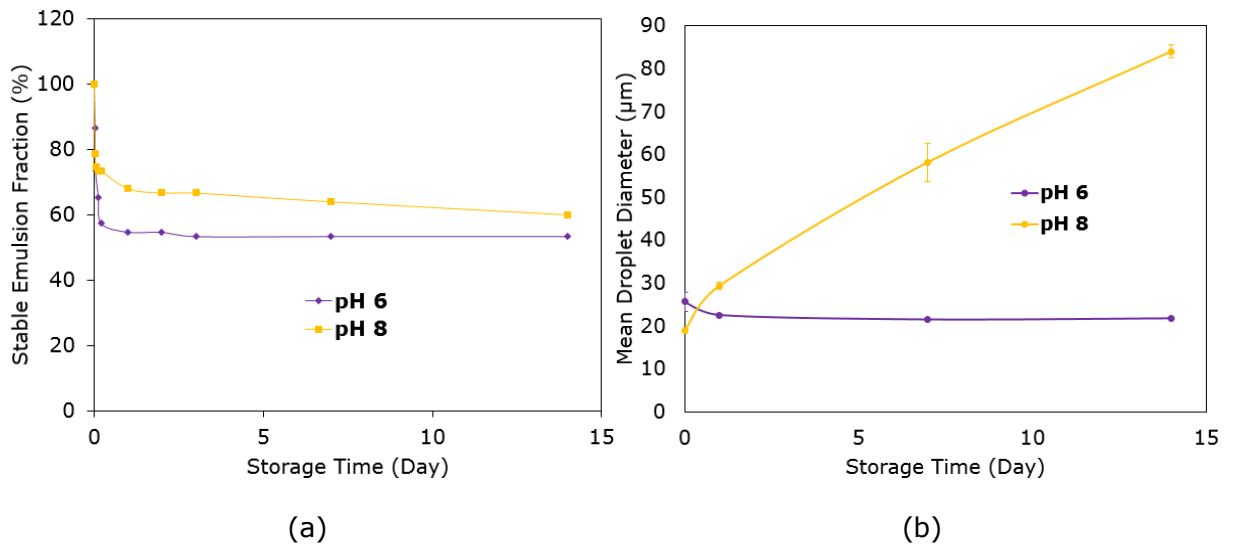


Figure 5.11. (a) Change in the volume fraction of the stable emulsion vs storage time for MCNC-PE at pH 6 and 8. (b) Change in emulsion droplets diameter of MCNC-PE at pH 6 and 8 up to 14 days of storage. (c) Microscopic images of MCNC-PE at pH 6 (Left), and pH 8 (Right), for (i) day 0, (ii) day 7, and (iii) day 14.

The mean droplets diameter of Pickering emulsion at pH 8 increases significantly after 1, 7, and 14 days of production, as shown in Figure 5.11b. It was clear that the emulsion droplets diameter at pH 8 were 18.80 μm in day 0, it increased to 58.16 μm in day 7 of production, and ultimately growth to 84.00 μm at day 14. In contrast, the droplets diameter at pH 6 remained unchanged throughout 14 days of storage. This have proven that emulsions prepared at pH 6 were stable up to 14 days of production. Emulsion droplets at pH 8, however, started coalescence even at first day of production, indicating that the emulsions are not stable. To support this, microscopic images of the Pickering emulsions at both pH were captured for day 0, day 7, and day 14 (see Figure 5.11c). The microscopic analysis strongly strengthen the statement on the stability of emulsion droplets at pH 6 and pH 8.

5.3.2.2 Effect of Solid Concentration

The sonochemically-induced MCNC nanocomposites were used to form Pickering emulsion with fixed oil phase volume fraction, $\varphi_{oil} = 0.3$. The oil loading content was determined to prevent the possible particle bridging effects as resulted from the high MCNC particle concentration. The details information is included in the next subsection in the investigation of the effect of oil loading. Results from fluorescent microscopy showed that calcofluor white-stained MCNCs (blue fluorescent) were absorbed on the surface of oil droplets as illustrated in Figure 5.12c(iii). Based on Figure 5.12a, all Pickering emulsion samples displayed monomodal size distribution regardless of MCNC particle concentration used. This laser diffraction particle size measurement was in good agreement with our optical microscope results where emulsion droplets formed by MCNCs were of uniform spherical shape and size, particularly in the presence of higher particle concentration of 0.100 to 0.300 wt% (Figure 5.12c). It has been observed that the mean droplet diameter of emulsion gradually decreased from 17.34 to 3.58 μm as MCNC particle concentration increased from 0.025 to 0.300 wt% (Figure 5.12b). This may be attributed to the increased coverage of particles network around the emulsion droplets as a result of an increase in

MCNC particle concentration. In the present study, the surface coverage of the emulsion droplets by MCNC particles was calculated using Equation (5.4) (Kalashnikova *et al.*, 2011).

$$S_{mcnc} = \frac{m_p D_{3,2}}{6h\rho V_{oil}} \quad \text{[Equation 5.4]}$$

where S_{mcnc} is the coverage by MCNC, m_p is the mass of MCNC, h is the thickness of MCNC, ρ is the density of MCNC, and V_{oil} is the volume of oil in the emulsion. The calculated surface coverage of Pickering emulsions prepared at different MCNC particle concentrations were presented in Table 5.1. As the particle concentration rise from 0.025 to 0.300 wt%, one could observe that the surface coverage of emulsions by MCNCs increased markedly from 8.496 to 21.025 %. This suggests that higher MCNC particle loading would lead to more surface coverage of the oil globules, leading to the formation of smaller emulsion droplet size with enhanced stability against coalescence.

Table 5.1. Surface coverage of MCNC-PE prepared under different MCNC concentration, C_{mcnc} .

MCNC Concentration, C_{mcnc} (wt%)	Surface Coverage, S_{mcnc} (%)
0.025	8.496
0.050	11.896
0.100	15.028
0.200	19.410
0.300	21.025

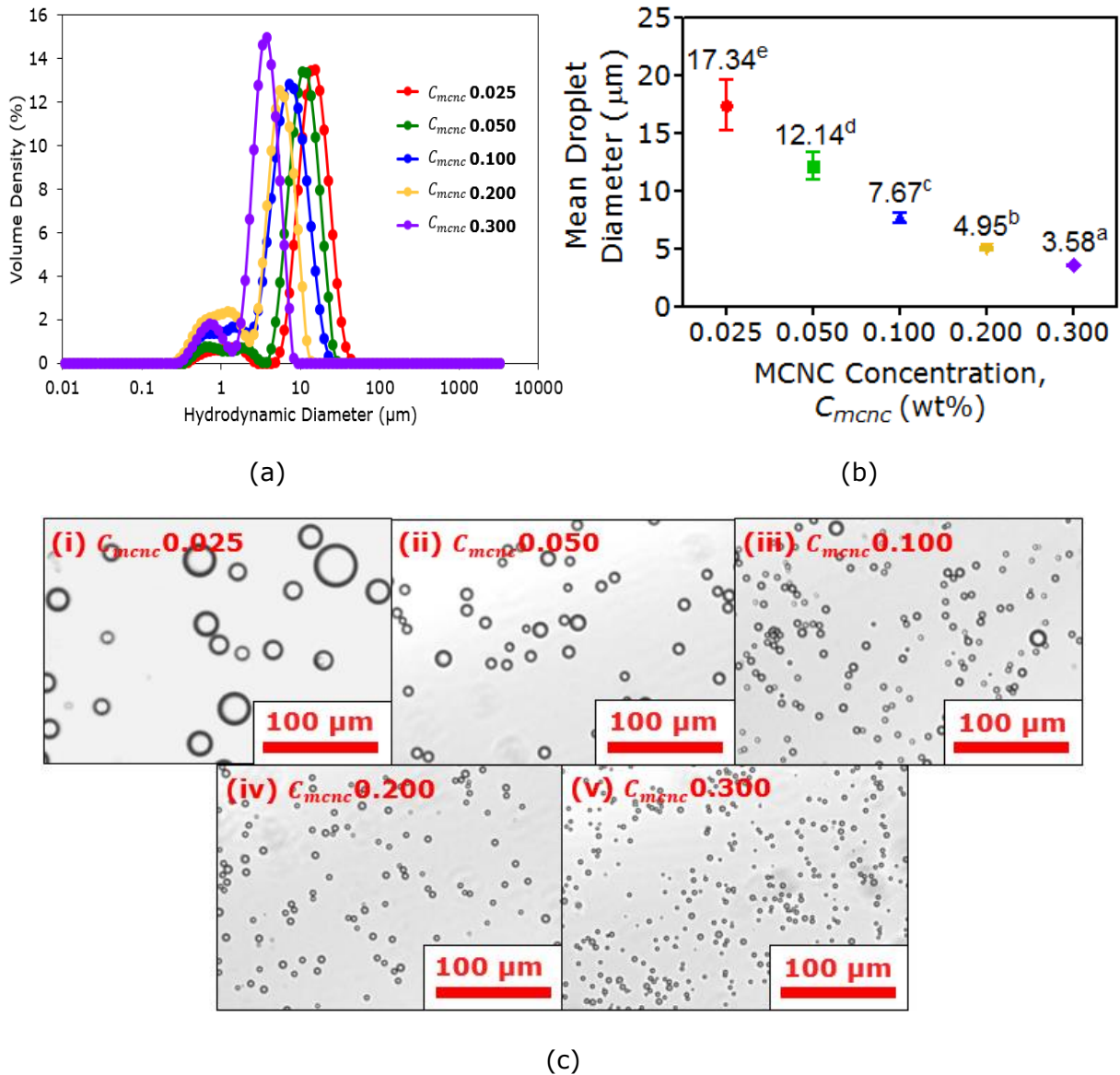


Figure 5.12. (a) Raw droplet size distribution data and (b) Mean droplet diameters of MCNC-PE as a function of MCNC concentration (wt%). All formulations contain fixed ϕ_{oil} of 0.3. Standard error of mean of triplicate readings were represented by the error bars in each graph, different alphabetic letters was significantly different at $P \leq 0.05$ by Bonferroni's Multiple Comparison Test. (c) Microscopic images of Pickering emulsion prepared at the MCNC particle concentration, C_{mcnc} of (i) 0.025, (ii) 0.050, (iii) 0.100, (iv) 0.200, and (v) 0.300 wt%.

The droplet size stability of the MCNC-stabilized Pickering emulsions was studied upon a storage duration of 14 days. As shown in Figure 5.13, it was noted that all the

emulsions showed no significant changes in the mean droplet diameter throughout the storage period at room temperature. At day 1, a slight increment in droplet size diameter (17 to 20 μm) had been observed in the emulsion prepared using 0.025 wt% MCNC. This could probably be due to low MCNC particle loading that is insufficient to provide a complete surface coverage at oil-water interface, leading to the occurrence of droplet coalescence. It had been reported that coalescence of the dispersed droplets could reduce the effective interfacial area between the oil and water phase, thus increase the free energy of the emulsion, rendering a lower colloidal stability (Caenn, Darley and Gray, 2011; Kokal and Wingrove, 2000). The results of this study showed that the stability of emulsion against coalescence was achieved when the MCNC particle concentration ≥ 0.05 wt%.

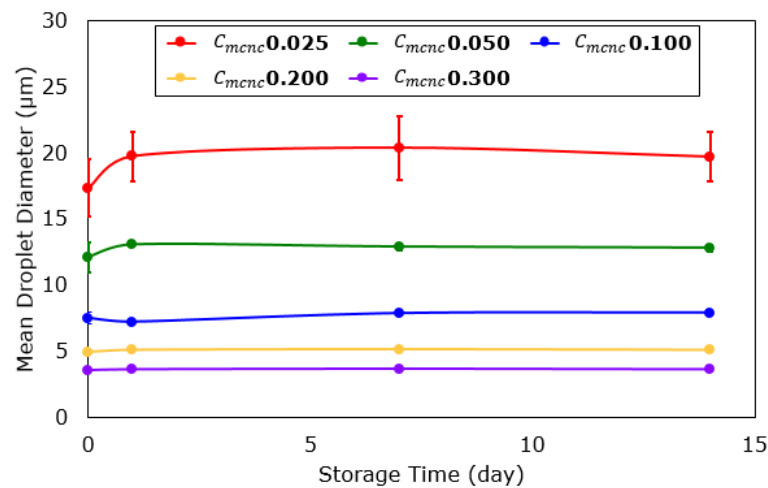


Figure 5.13. Changes in emulsion droplets diameter for MCNC-PE stabilized by MCNC nanocomposites at 0.025 to 0.300 wt% up to 14 days of storage.

Figure 5.14a and b showed the photographs of stability of MCNC-stabilized Pickering emulsions prepared using different MCNC particle concentrations over a storage period of 14 days. The extent of creaming of oil droplets was measured by the change in height of the bottom serum phase with storage time. The creaming index (CI) was determined according to Equation (5.5).

$$CI = \frac{h_{total} - h_{emul}}{h_{total}} \times 100\% \quad [\text{Equation 5.5}]$$

where h_{emul} is the height of emulsion, and h_{total} is the total height of all solution. The creaming rate of Pickering emulsions was also computed using Stoke's equation (Equation 5.6) (Yamaguchi, 2008).

$$v = \frac{gd^2(\rho_{cont} - \rho_{disp})}{18\eta_{cont}} \quad \text{[Equation 5.6]}$$

where v is the gravitational separation rate, g is the gravitational acceleration, d is the emulsion droplet diameter, ρ_{cont} and ρ_{disp} are density of continuous (water) and dispersed (oil) phases, and η_{cont} is the viscosity of the continuous phase. Based on Figure 5.14b and c, one could observe that the extent of emulsion creaming gradually decreased with increasing MCNC particle concentrations. The rate of creaming decreased progressively from 0.66 to 0.03 cm/hr as MCNC concentration increased from 0.025 to 0.300 wt% (Figure 5.14d). It is well-known that creaming occurs as a result of density difference between the dispersed oil and continuous phases. The larger sizes of emulsion droplets simply led to bigger effect of density difference between the continuous medium (water) and the droplets (oil), which thus caused the emulsions to have greater tendency to float (Mwangi *et al.*, 2016) as prescribed in Equation 4. Hence enhanced creaming and storage stability of emulsion samples was obtained when the emulsions sizes reduced as ascribed to increasing MCNC concentration.

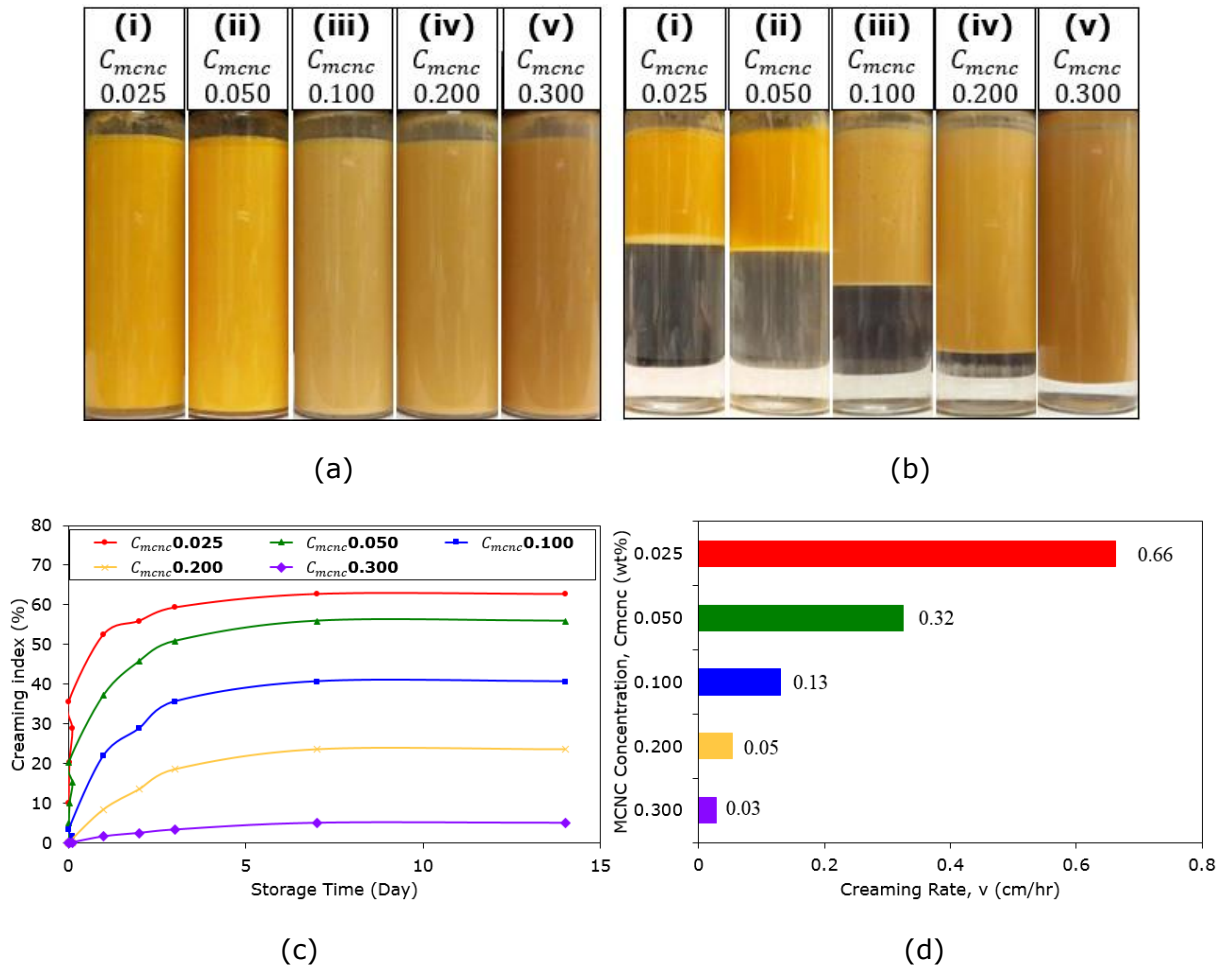


Figure 5.14. (a) Day 0 and (b) day 14 of photograph of O/W Pickering emulsion stabilized by MCNC at (i) 0.025, (ii) 0.050, (iii) 0.100, (iv) 0.200, and (v) 0.300 wt%. (c) creaming index, and (d) creaming rate of the respective Pickering emulsion.

5.3.2.3 Effect of Oil Loading

The influence of oil content on the surface properties and stability of MCNC-stabilized Pickering emulsion was also investigated. As shown in Table 5.2, at fixed MCNC particle concentration of 0.100 wt%, increasing the oil loading, ϕ_{oil} from 0.1 to 0.3 decreases the surface coverage of interfacial area by MCNC particles. The effective surface coverage values initially dropped from 16.556 to 12.070 % with increasing oil content, ϕ_{oil} from 0.1 to 0.2, and then rose from 12.070 to 19.872 % when the volume fraction of oil phase was further increased to 0.5. To further examine the relationship between the emulsion surface properties and oil loading, surface coverage were expressed in terms of $\frac{D}{V_{oil}}$ (the ratio of

droplets surface area mean diameter over the oil loading content in brief) (Equation 5.7) and the derived terms were calculated for different φ_{oil} and presented in Table 5.3. As expected, the calculated values showed similar trend with the surface coverage data, suggesting that increasing oil content level significantly affected the surface characteristics and emulsion droplet sizes given the constant amount of MCNC particles used.

$$C_{mcnc} = f\left(\frac{D}{V_{oil}}\right) \quad \text{[Equation 5.7]}$$

Table 5.2. Surface coverage of MCNC-PE prepared under different oil volume fraction φ_{oil} .

Oil volume fraction, φ_{oil}	Surface Coverage, S_{mcnc} (%)
0.1	16.556
0.2	12.070
0.3	13.088
0.4	15.698
0.5	19.872

Table 5.3. $\frac{D}{V_{oil}}$ of MCNC-PE prepared under different oil volume fraction φ_{oil} .

Oil volume fraction, φ_{oil}	$\frac{D_{3,2}}{V_{oil}}$ ($\mu\text{m/ml}$)
0.1	0.704
0.2	0.513
0.3	0.557
0.4	0.668
0.5	0.845

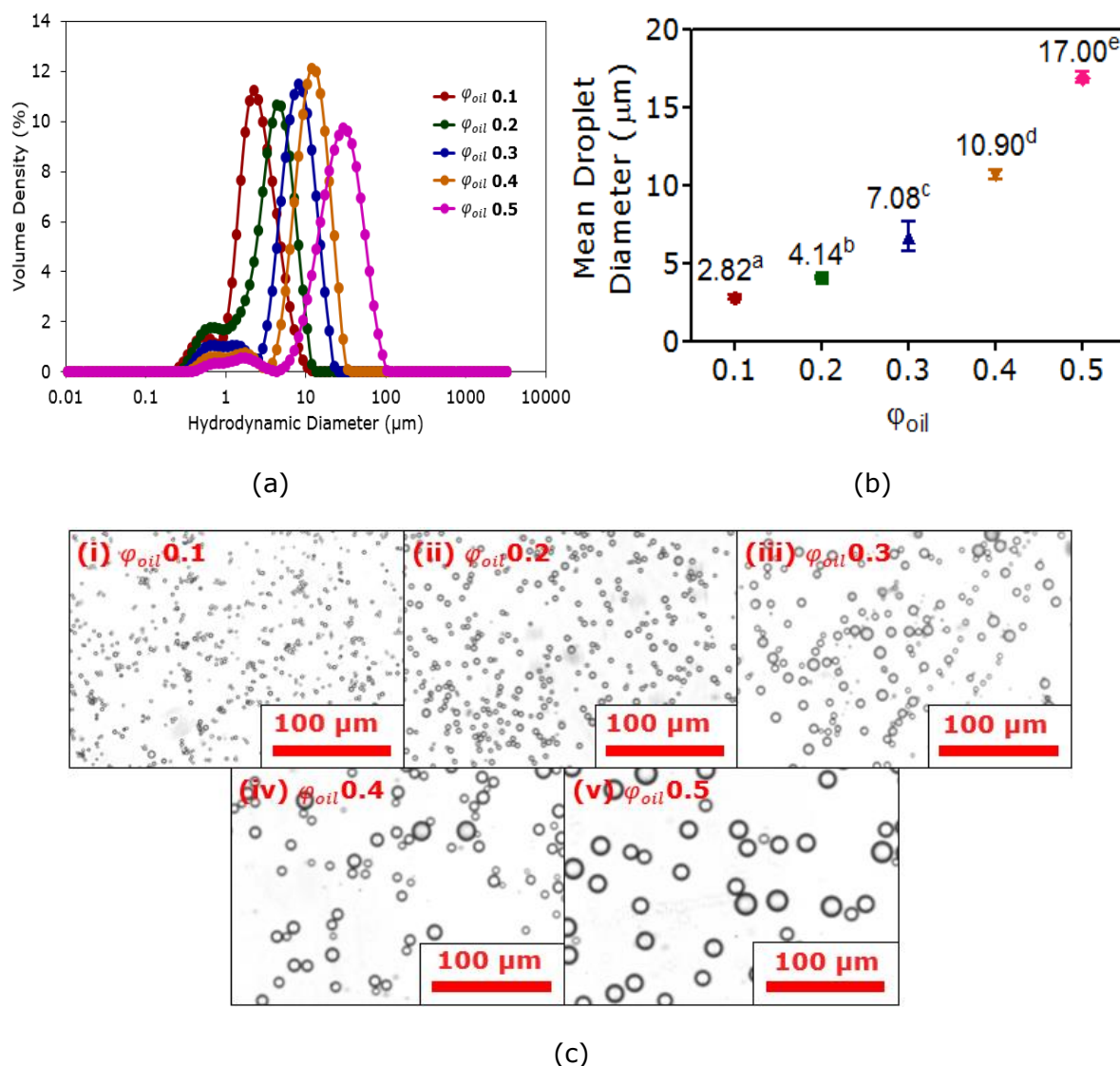
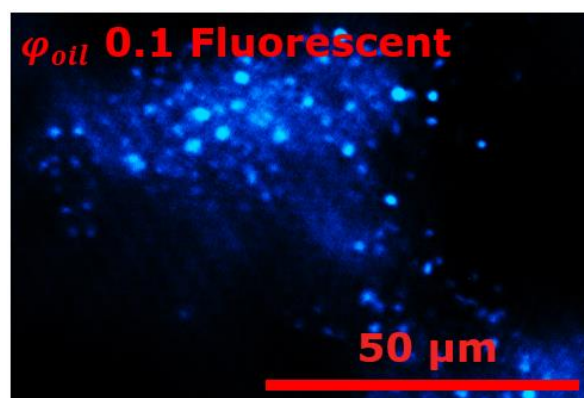
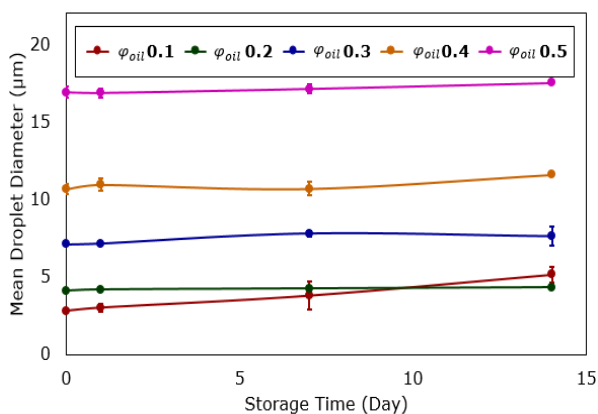


Figure 5.15. (a) Raw droplet size distribution data and (b) Mean droplet diameters of MCNC-PE prepared at different ϕ_{oil} of 0.1 to 0.5. All formulations contain fixed $C_{mcnc} = 0.100$ wt%. Standard error of mean of triplicate readings were represented by the error bars in each graph, different alphabetic letters was significantly different at $P \leq 0.05$ by Bonferroni's Multiple Comparison Test. (c) Microscopic images of MCNC-PE prepared at oil volume fraction, ϕ_{oil} of (i) 0.1, (ii) 0.2, (iii) 0.3, (iv) 0.4, and (v) 0.5.

Based on Figure 5.15b, the mean droplet diameter of emulsion was found to increase progressively with increasing ϕ_{oil} . This may be attributed to the limiting amount of MCNC particles available for Pickering stabilization as oil loading increased. At increasing ϕ_{oil} , the oil globule size reached is limited by the MCNC particle concentration used. In this study, minimum droplet size of 2.82 μm with narrowest monomodal distribution was attained at

the φ_{oil} of 0.1, indicating that concentration of MCNC particles used was sufficient enough to stabilize the emulsion against coalescence at low level of oil loading. The optical microscopic images showed the MCNC-stabilized emulsion droplets were of spherical shape and uniformly dispersed in continuous phase regardless of φ_{oil} concentrations used (Figure 5.15c). This observation was in consistent with our particle size measurement (Figure 5.15a).

Figure 5.16a presented the change of emulsion size as a function of storage time. It was noted that all the emulsions prepared at varying φ_{oil} from 0.2 to 0.5 exhibited no significant change in droplet diameter after 14 days of storage, as shown in Figure 5.15a. The mild increment in droplet size observed at $\varphi_{oil} = 0.1$ was most likely due to the particles bridging effects as a result of excessive amount of MCNC particles that renders a saturated covering of the oil-water interface. In this regard, fluorescent microscopy was carried out to visualize the particle size and morphology of emulsion droplets prepared at $\varphi_{oil} = 0.1$. As shown in Figure 5.16b, droplet aggregation was observed as a result of the formation of highly entangled network by MCNC particles in the continuous phase, rendering a larger emulsion sizes.



(a)

(b)

Figure 5.16. (a) Changes of MCNC-PE droplet diameter as a function of φ_{oil} throughout 14 days of storage. (b) Fluorescent microscopic image of MCNC-PE prepared at $\varphi_{oil} = 0.1$ (40x magnification). All formulations contain fixed $C_{mcnc} = 0.100$ wt%.

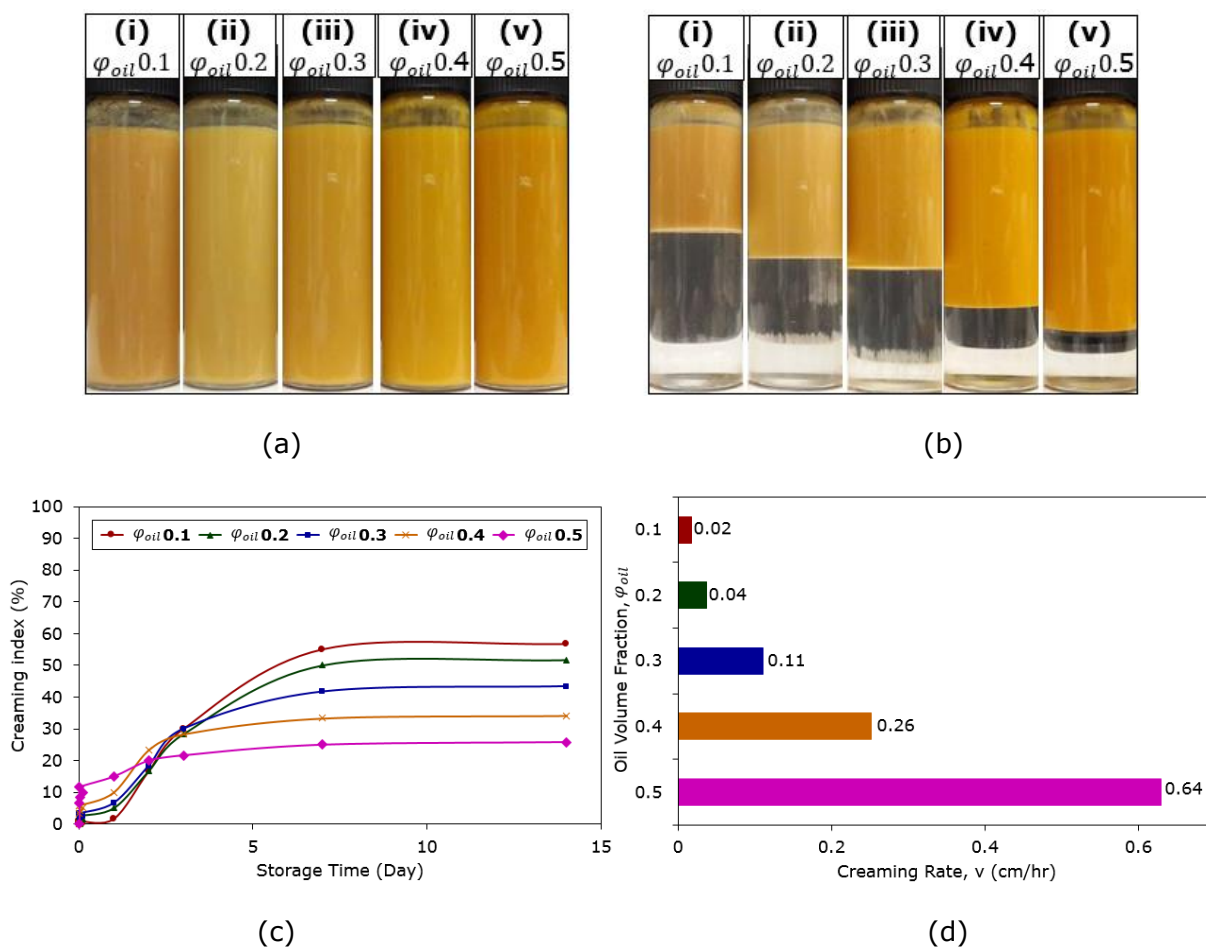


Figure 5.17. Photographs of MCNC-PE at (a) day 0, and (b) day 14, (c) creaming profile and, (d) creaming rate of the MCNC-PE prepared using different ϕ_{oil} . All formulations contain fixed $C_{mcnc} = 0.100$ wt%.

Figure 5.17a-c showed the storage stability of MCNC-stabilized Pickering emulsions produced at different ϕ_{oil} . It was observed that all the emulsion samples showed gradual creaming up to 14 days of storage with a well-defined separation line between the emulsion and water phase, and the creaming index decreased as ϕ_{oil} was increased from 0.2 to 0.5. The creaming rate of emulsions was calculated and presented in Figure 5.17d. The rate of creaming was found to increase sharply from 0.02 to 0.64 cm/hr when the oil volume fraction was increased from 0.1 to 0.5 (Figure 5.17d). It was apparent that Pickering emulsion prepared at ϕ_{oil} of 0.5 displayed the lowest degree and rate of creaming among all the emulsion samples. This could be explained by the fact that volume of emulsion creaming is directly related to the initial oil phase volume when preparing emulsion. Since

creaming occurred in all samples, and as φ_{oil} 0.1 emulsions have the lowest oil loading, despite that sample at $\varphi_{oil} = 0.1$ has the lowest creaming rate, the volume of creaming will eventually reached to a point as corresponded to its oil loading volume. A similar trend had been reported by He *et al.* (2013) in the investigation of stability of emulsion systems stabilized by graphene oxide.

5.3.2.4 Effect of Ultrasonic Power and Sonication Time

The sonochemically prepared MCNC nanocomposites were utilized as Pickering stabilizer for preparing Pickering emulsions with fixed MCNC particles concentration (0.1 wt%) and oil loading ($\varphi_{oil} = 0.3$ or 30 vol%). Figure 5.18 shows the effects of three different US power at various sonication times on the mean droplet diameter of the MCNC-stabilized Pickering emulsion. Results from mastersizer analysis (Figure 5.18a) showed that the mean droplets diameter of all Pickering emulsions substantially decreased from around 65 to 6.5 μm when sonication time increased from 0 (non-sonicated) to 3 min, and then remained relatively constant at around 6.5 μm under prolonged sonication time. This was highly similar to the generally observed trend in the literature where increasing sonication time led to higher shear applied to droplets, hence resulting in the production of finer emulsion droplets (Kentish *et al.*, 2008; Salvia-Trujillo *et al.*, 2014). The phenomena that happened with sonication time longer than 3 min, on the other hand, was most likely due to the limited amount of MCNC particles in the medium for emulsion stabilization. Since the MCNC particles concentration was fixed for all formulations, even with the formation of smaller emulsion droplets as resulted from long US cavitation, there were insufficient amount of MCNC particles to effectively adsorb onto the interfaces of newly formed droplets, hence the freshly formed emulsion droplets collided with each other (limited coalescence), leading to the constant trend in oil globule diameter as noticed. Besides that, it was clearly seen that increasing the US power allowed a shorter time requirement to prepare a Pickering emulsion with smallest achievable mean droplets diameter of around 6.5 μm . The obtained time requirement for US power of 40, 60 and 80 W are 3, 2 and 1 min respectively. The Pickering emulsion samples were found to demonstrate a narrower size distribution with

increasing US power (Figure 5.18b to d). This was in good agreement with their respective optical microscopic images (Figure 5.19), where the emulsion droplets formed were in uniform spherical shape and size, except for the samples prepared at low power and sonication time (i.e. 40 W, 0.5 min). This could be due to the fact that 0.5 min of US cavitation under 40 W was insufficient to effectively break down all the pre-mixed Pickering emulsion droplets into smaller sizes. To support that, Mason, Chemat and Ashokkumar (2014) have showed that a minimum US power is always necessary to emulsify an emulsion system completely.

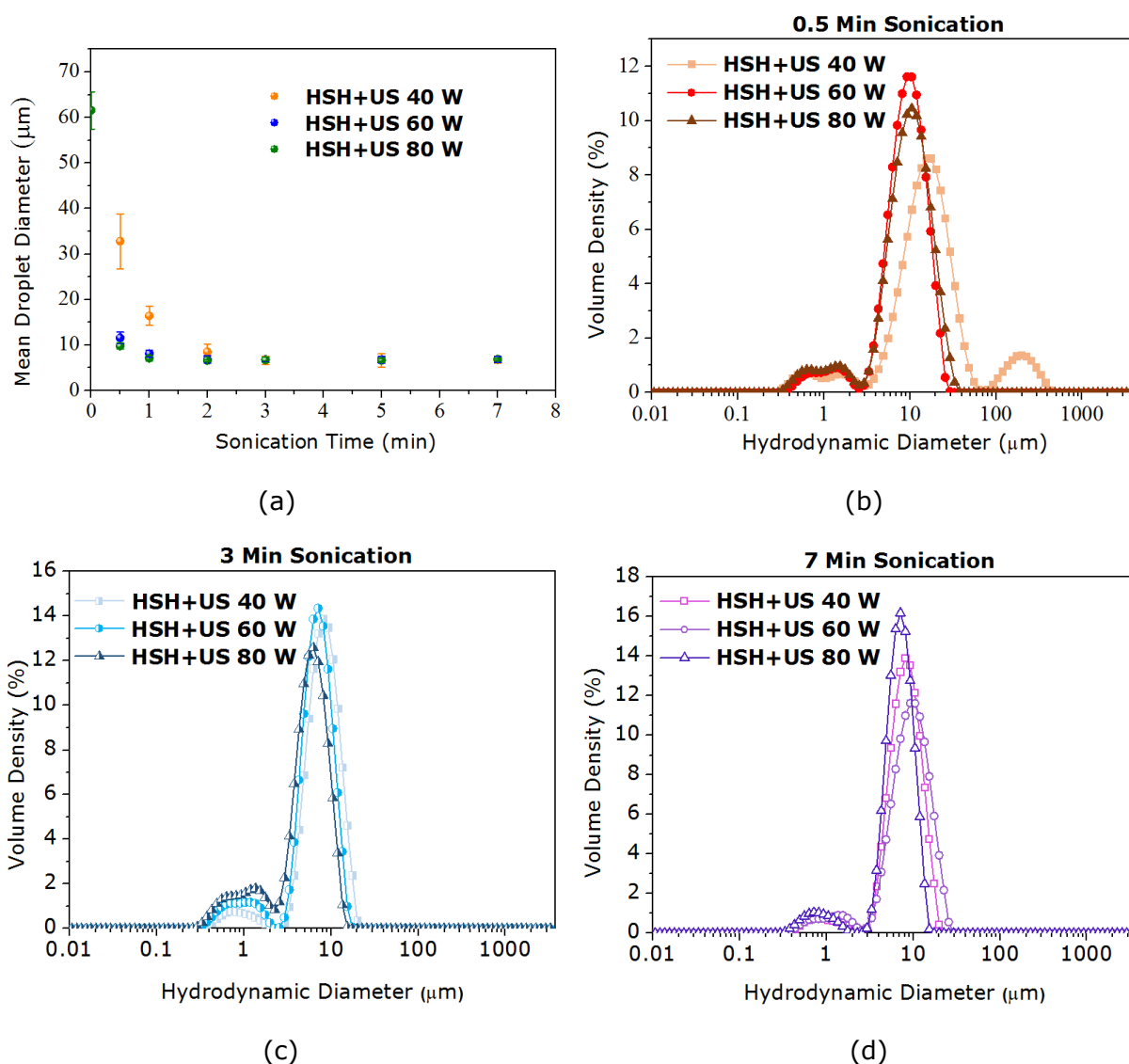
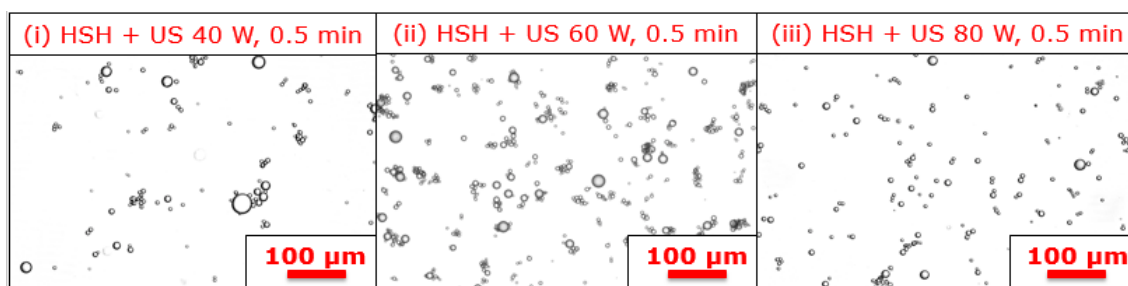
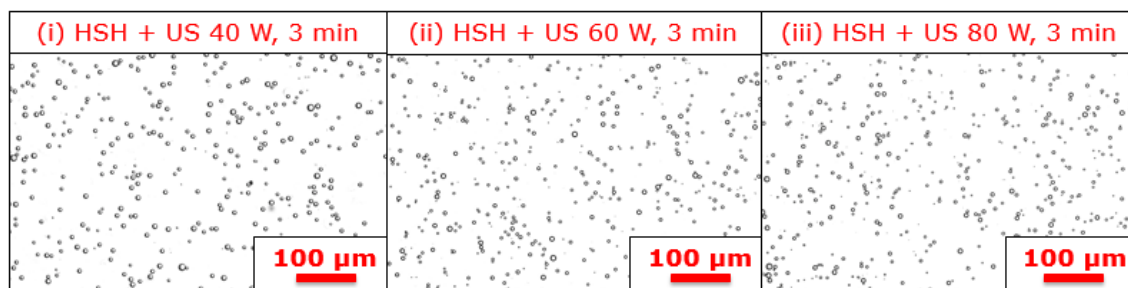


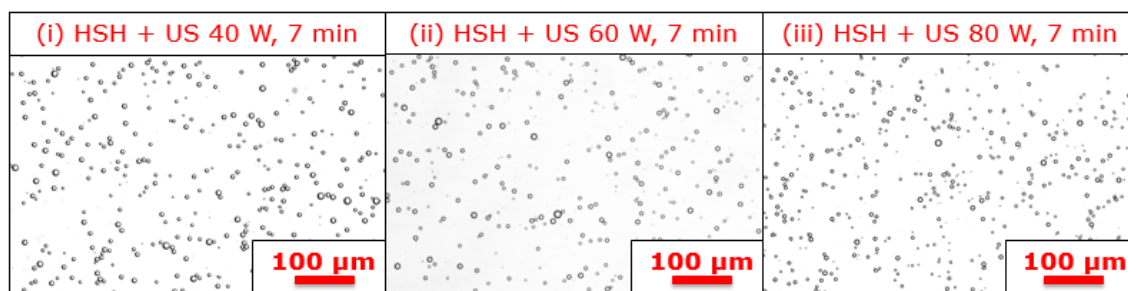
Figure 5.18. (a) Mean droplet diameters of MCNC-PE as a function of US power and time. Error bars represented the standard error in measurement. Raw droplet size distribution data of MCNC-PE under different US power at (b) 0.5, (c) 3 and (d) 7 min sonication time.



(a)



(b)



(c)

Figure 5.19. Optical microscopic images of MCNC-PE prepared using different US power at (a) 0.5, (b) 3 and (c) 7 min.

The storage stability of MCNC-stabilized Pickering emulsion prepared using different US power and sonication time was examined over a storage period of 30 days. The extent of creaming of droplets was measured by the change in the height of the bottom serum phase with storage time. The CI and gravitational separation rate was determined as shown in Figure 5.20. It can be observe that the extent of emulsion creaming gradually decreased with increasing US power. The rate of creaming decreased progressively from 2.4 to 0.1 cm/hr as the power increased from 40 to 80 W (Figure 5.20). A similar trend was observed when calculating the creaming indices as a function of sonication time. The emulsions

showed high creaming at the beginning of US cavitation, the creaming then slowly decreased as sonication time increased, and eventually reached a plateau after the produced Pickering emulsion achieved the minimum sizes. Creaming was a common characteristic of Pickering emulsions that occurs as a result of density difference between the dispersed oil and continuous phases due to the relatively large emulsion droplets diameter. From equation (5.7), one can envision that larger emulsion droplets give rise to higher creaming rate. Hence creaming of emulsion samples were reduced when the emulsions sizes reduced as ascribed to increasing US power and sonication time. Interestingly, although creaming was observed from all emulsion samples, results from Figure 5.21a to c demonstrated that the mean droplets diameter of all Pickering emulsion remained similar throughout 30 days of storage. The observed phenomenon further indicated that creaming is purely due to gravitational separation and not droplets coalescence. Hence, the as-prepared MCNC-stabilized Pickering emulsion was considered physically stable even at low sonication time of 30 s. This is likely to be due to the excellent partial wettability of MCNC that allows rapid and effective interfacial adsorption even when the sonication time was extremely short.

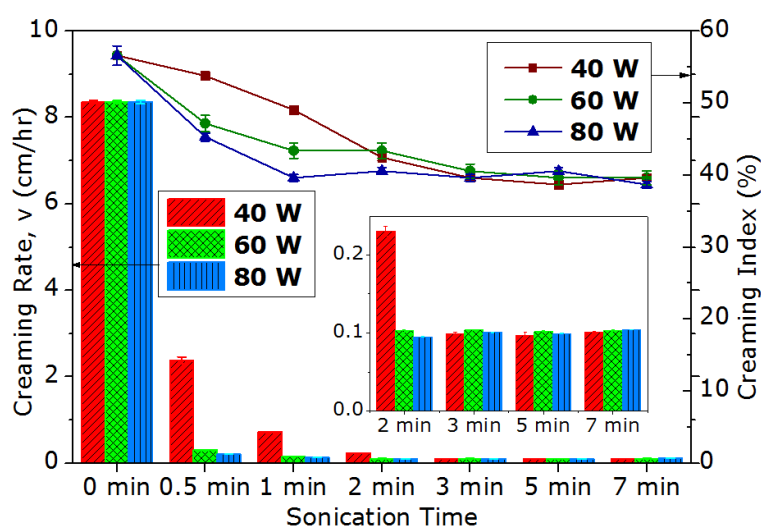


Figure 5.20. The creaming index and creaming rate of MCNC-PE prepared under different US power and sonication time. The inset shows a clearer view of the creaming rate of samples with sonication time of 2 min or longer.

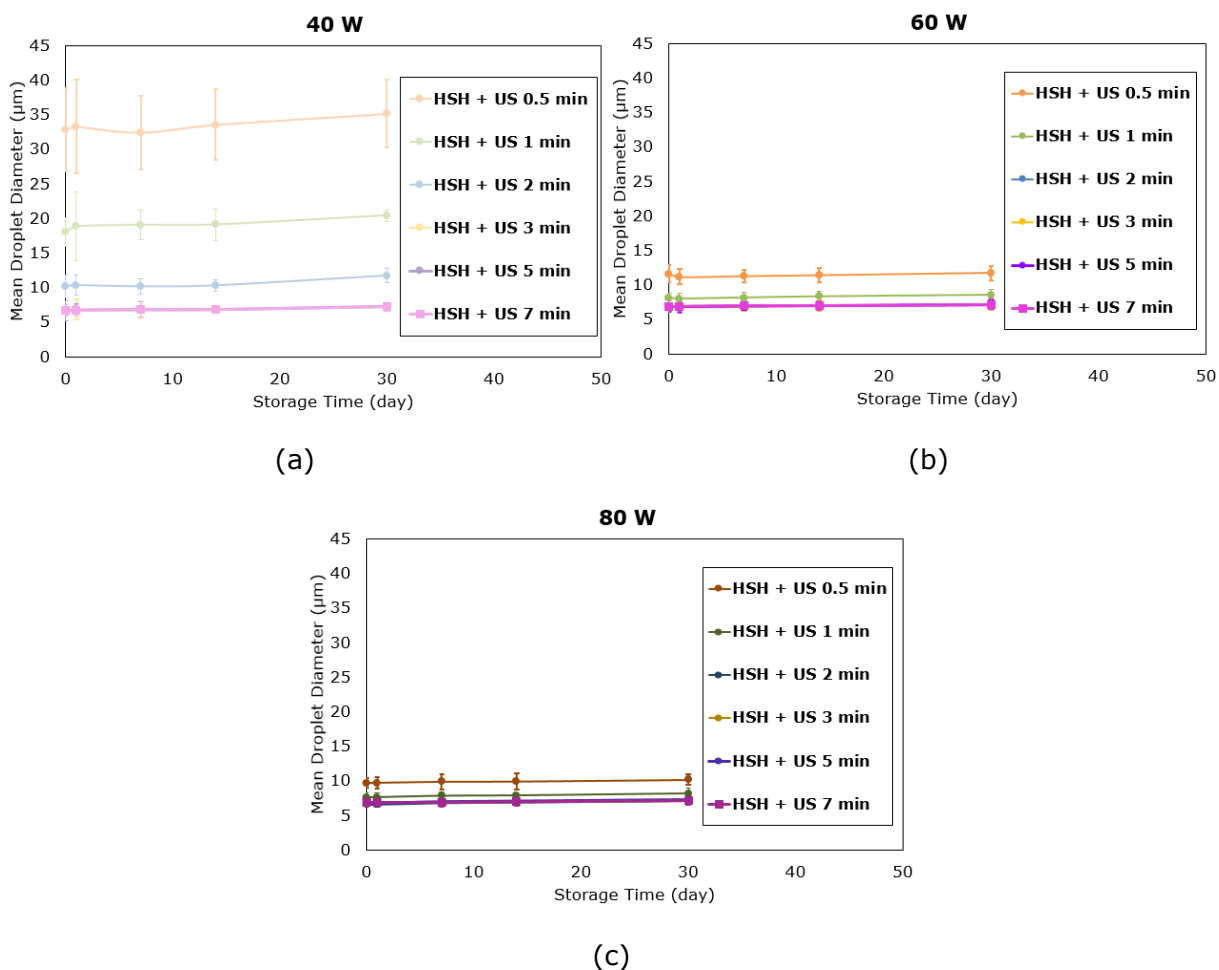


Figure 5.21. Changes in emulsion droplets diameter of MCNC-PE prepared under (a) 40, (b) 60 and (c) 80 W throughout a storage period of 30 days.

5.3.2.5 Effect of Ionic Strength

The effect of ionic strength on the emulsion stability was also investigated by varying the NaCl Concentration from 0 to 500 mM. All emulsion samples were stored under room conditions for 14 days prior to characterisation. Figure 5.22a to c revealed that all emulsion samples shows no marked change in the means droplet diameter under the influence of different salt concentrations, with measured droplet size ranging from 7 to 8 μm with extremely narrow size distribution as NaCl concentration increased. On the other hand, a mild increment in emulsion creaming ($< 10\%$ of CI) had been noticed with increasing the salt content. Based on the microscopic images (Figure 5.22c), aggregated bound droplets had been detected at all NaCl concentrations. The observed aggregation behaviour could

be ascribed to the electrostatic screening effects of the droplet surface charge induced by the increase in the ionic strength of the continuous phase (Tang *et al.*, 2014). Intriguingly, the optical micrographs (Figure 5.22c) demonstrated that the MCNC-stabilized Pickering emulsions were highly stable against coalescence for 2 weeks despite a pronounced aggregation had been detected upon the addition of NaCl. The stability of the emulsion to coalescence was further supported by the particle size analysis. One possible explanation to this phenomenon is that under conditions of high particle charge and weak screening, the coalescence of vast majority of particles is severely retarded by the presence of fixed amount of MCNC particles.

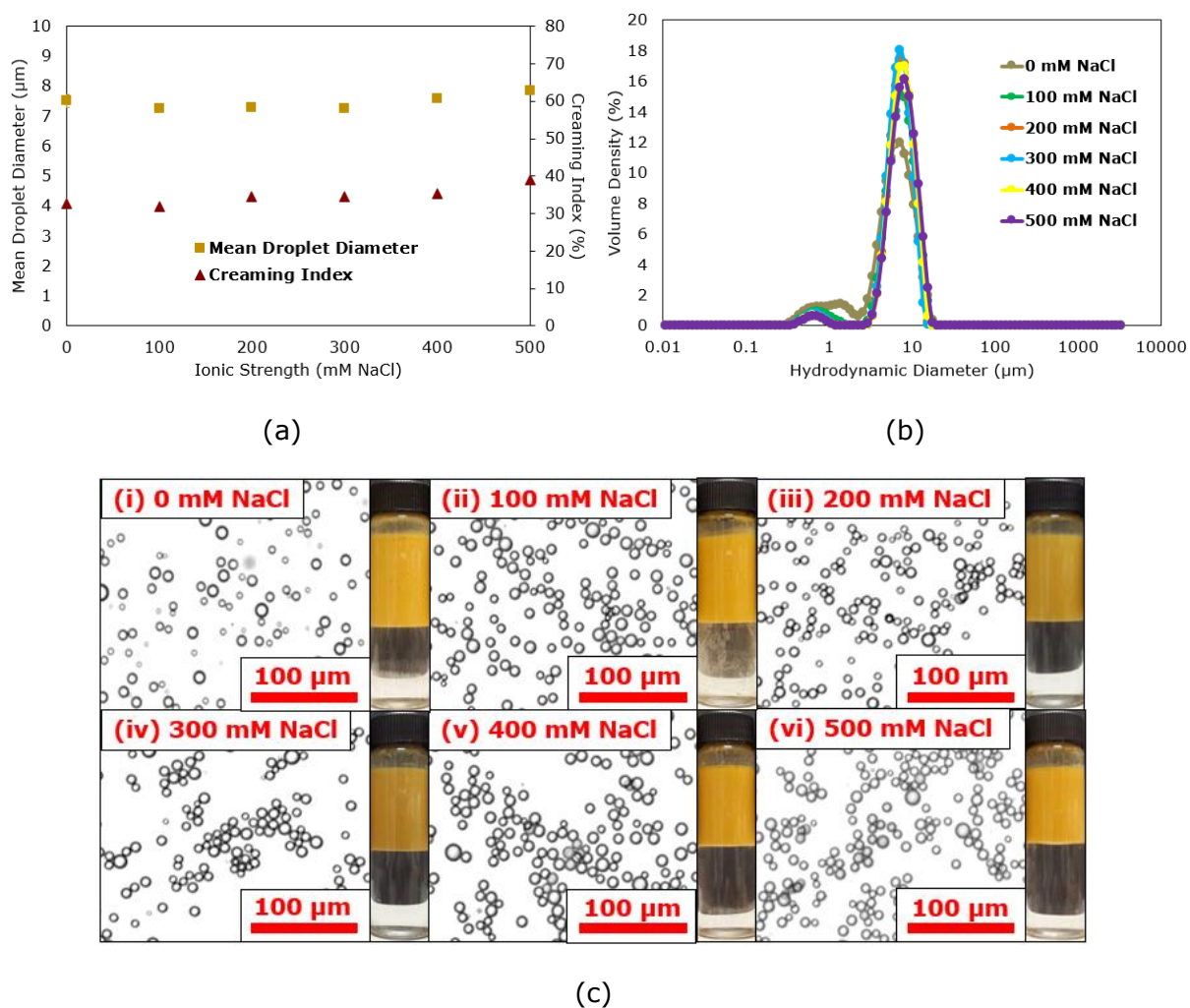


Figure 5.22. (a) Mean droplet diameter and creaming profiles as well as (b) Raw droplet size distribution data of MCNC-PE as a function of ionic strength (mM NaCl). All formulations contain fixed ϕ_{oil} of 0.3 and C_{mcnc} of 0.100 wt%. (c) Microscopic images of MCNC-PE prepared NaCl concentration of (i) 0, (ii) 100, (iii) 200, (iv) 300, (v) 400, and (vi) 500 mM.

To test this notion further, we have prepared two diluted dispersion containing 0.100 wt% MCNC particles at the salt concentration of 0 and 500 mM NaCl (Figure 5.23). The addition of NaCl into the dispersion triggered the partial sedimentation with the MCNC particles accumulated near the bottom phase of the container. These experiments, thus confirmed the hypothesis on the correlation between the charge effects and emulsion aggregation. The results of current study suggests that the stability of MCNC-stabilized Pickering emulsions against creaming and coalescence was unaffected by ionic strength (NaCl) from 100 to 500 mM, but was influenced by MCNC particle concentrations and oil loading.

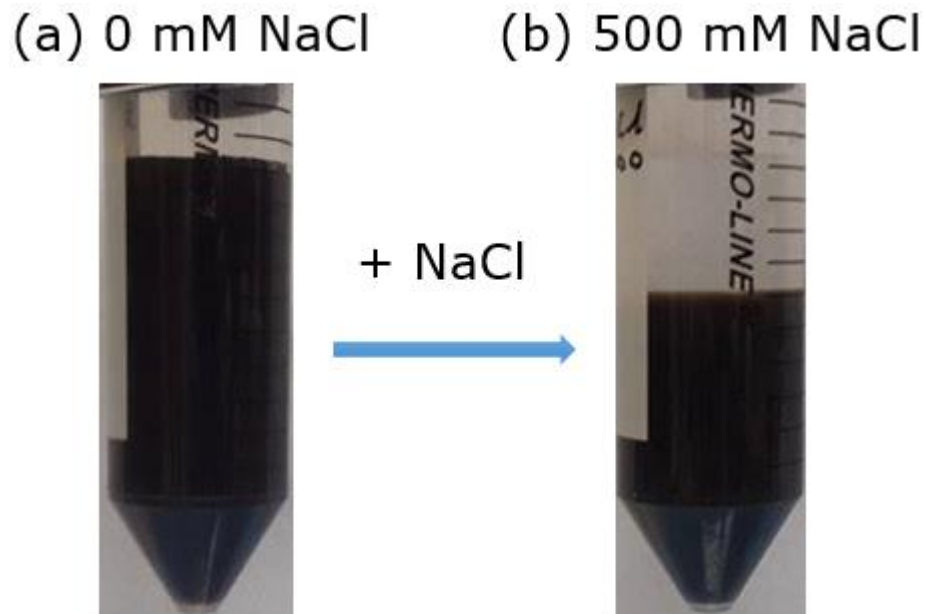


Figure 5.23. MCNC dispersions (a) without NaCl, and (b) with 500 mM NaCl.

5.4 Conclusions

Novel palm olein-in-water Pickering emulsions using MCNC nanocomposites as Pickering stabilizer were successfully developed. MCNC-stabilized Pickering emulsion (MCNC-PE) was prepared by first obtaining MCNC dispersion under neutral pH and then mixing with red palm olein under ultrasonic cavitation. MCNC played a dominant role in stabilizing the emulsion as compared to the two control samples since only MCNC was able to produce a stable emulsion system. The coverage of MCNC on the surface of the emulsion droplet was illustrated via fluorescent microscopy. The magnetic responsiveness of MCNC-PE was confirmed through evaluating the magnetic attractability with a magnet. The stability of the resultant Pickering emulsion has been observed to be strongly affected by pH, where very stable MCNC-PE were achievable in pH ranging from 1.5 to 7, and at 13. While phase separation was observed when pH was tuned to 8 to 11. The storage stability test demonstrated that gravitational separation does not affect the colloidal stability. The morphology and average emulsion sizes at pH 6 remained the same throughout 14 days of production despite the occurrence of creaming. The mean droplet diameter at pH 8, however, has increased greatly from 18.80 to 84.00 μm after 14 days. Increasing the MCNC concentration, C_{mcnc} led to a gradual decrease in mean droplet diameter of emulsions with improved creaming stability. The surface coverage of MCNC-PE was found to increase when MCNC particle content rose. As expected, an increase in the oil volume fraction, φ_{oil} resulted in an increase in MCNC-PE's size. Results showed that the surface coverage initially decreased and then increased progressively when φ_{oil} increased from 0.3 to 0.5. Increasing the US power and irradiation time first caused a gradual reduction in the mean droplets diameter, and then reached a plateau when the sonication time is higher than 2 min for all investigated US power. Varying the salt concentration showed no significant effects on the oil globule size and creaming stability as well as the magnetic properties of the particle-stabilized Pickering emulsions. The results of current study open up new opportunities for the future research and development of magnetic-responsive palm-olein based Pickering emulsions with the goal of utilizing them as controlled drug delivery carriers.

CHAPTER SIX

STIMULI-RESPONSIVENESS OF MCNC-PE

Overview

The pH-responsive characteristic of $\text{Fe}_3\text{O}_4@\text{CNC}$ (MCNC)-stabilized Pickering emulsions (MCNC-PEs) under the influence of an external magnetic field (EMF) were investigated. The outcomes demonstrated that the MCNC-PEs exhibited reversible pH-dependent stability that was affected by the presence of magnetic fields. The MCNC-PE droplets were observed to be stable in acidic solution (pH 1.5–5.0) but broken down in alkaline medium (pH ≥ 7.5). This phenomenon could be owing to an abrupt change of MCNC wetting properties as resulted by the combined effects of superparamagnetic hysteresis and high solubility of MCNCs in alkaline environment. Besides that, our findings showed that the formulated emulsion can be cycled between stable and unstable 3 times upon a simple pH variation. This unique pH-dependent stability was, however, diminished in the emulsion systems prepared with higher content of MCNCs (i.e. 0.5 wt%), which thus suggesting that MCNC-PE with higher degree of surface coverage by MCNC particles were highly stable against both pH changes and magnetic field. In overall, the work in this chapter revealed the reversible inter-droplet stability of MCNC-PEs upon changes in pH with the presence of magnetic field.

6.1 Introduction

Pickering emulsion is particle stabilized emulsion developed by Ramsden, (1903) and Pickering, (1907) in early 19th century. The Pickering stabilization phenomenon happened through the adsorption of colloidal particles at the interface of the two immiscible liquids, which in turn reduces the free energy on the interfaces and promotes shielding effects to prevent the emulsion droplet from coalescence. However, Pickering emulsion did not attract much attention until recent decades due to the limited choices of available particles to be employed (Wu and Ma, 2016). With the rapid development of material science that leads to numerous attractive organic/hybrid particles that are biodegradable, biocompatible and low in toxicity, significant interests are drawn towards researches on preparing a generation of emulsions that possess low toxicity and superior stability against coalescence as compared to the conventional emulsion stabilized by surfactant (Binks, 2002; Frelichowska *et al.*, 2009; Wu and Ma, 2016). These benefits have prompted the use of Pickering emulsions as replacement material for the conventional emulsions in the food (Jia *et al.*, 2015; Song *et al.*, 2015; Timgren, Rayner, Sjöo and Dejmek, 2011), biomedical (Chevalier and Bolzinger, 2013; Kim *et al.*, 2016; Tang, Quinlan and Lam, 2015; Wu and Ma, 2016), and pharmaceutical region (Frelichowska *et al.*, 2009a & 2009b; Marku *et al.*, 2012).

Among the particles developed as resulted from the rapid development of material technology, cellulose nanocrystals (CNC) is considered as one of the most promising candidates for Pickering stabilization due to its excellent surface partial wettability, biocompatibility, biodegradability, non-toxicity, and sustainability (Capron and Cathala, 2013; Cunha, *et al.*, 2014; Kalashnikova, Bizot, Cathala and Capron, 2011; Zoppe, Venditti and Rojas, 2012). In addition, due to the rich availability of reactive hydroxyl groups on the CNC surfaces, CNC can be incorporated with several stimuli-responsive materials to form smart CNC-based hybrid nanocomposites that are able to respond to certain external stimuli. This endorsed CNC-based Pickering emulsion to further outstretched its employment in applications that require temporal emulsion stabilization with remote-controllable de-stabilizing ability, including oil recovery (Sharma *et al.*, 2015; Tang, Quinlan and Lam, 2015), emulsion polymerization (Chen *et al.*, 2008; Tang, Quinlan and Lam,

2015) and drug delivery (Frelichowska *et al.*, 2009a & 2009b; Marku *et al.*, 2012; Tang, Quinlan and Lam, 2015). In literature, various stimuli-responsive cellulosic nanomaterials, such as thermoresponsive (Tang *et al.*, 2014; Wu *et al.*, 2015), pH sensitive (Tang *et al.*, 2014; Sarker, Tomczak and Lim, 2017) and magnetically attractable materials (Low *et al.*, 2016), have been successfully attempted for Pickering emulsion formation. For instance, Tang *et al.* (2014) successfully demonstrated the preparation of dual-responsive Pickering emulsions that exhibited both pH and temperature-dependent stability. Besides that, Fe₃O₄@CNC (MCNC) nanocomposites, prepared by dispersing the superparamagnetic Fe₃O₄ nanoparticles (MNPs) onto the CNC fibres, has been holding great potential to favour a green magnetic Pickering emulsion since both materials employed are biocompatible and non-toxic (Lattuada and Hatton, 2007; Low *et al.*, 2016; Szpak *et al.*, 2013).

MNP is an attractive superparamagnetic material that has been widely used in medical fields for magnetic resonance imaging (Kim *et al.*, 2001) and hyperthermia (Silva *et al.*, 2011) due to its low cost, good biocompatibility and negligible toxicity (Lattuada and Hatton, 2007; Szpak *et al.*, 2013). More importantly, the unique superparamagnetic properties of MNP that can be specifically magnetized by an applied magnetic field also outstand other stimuli-responsive behaviours that are passively dependent on the surrounding conditions. Furthermore, a recent work by Vepsäläinen and Saario (2010) reported an increase in dissolution of MNP in water with increasing pH. This strongly suggested the potential of MNP as a material that responds to magnetic and pH stimulus. Although prior studies exist on magnetic Pickering emulsion stabilized by MCNC (Low *et al.*, 2016; Low *et al.*, 2017), these works concerned on determining the desired formula for stable Pickering emulsions formation using the MCNC as stabilizer. Contrarily, the present study investigated the impact of a magnetic field on the pH-responsive behaviour of the MCNC-PE and showed a differed stimulation behaviour. Thus the finding from the current study will be of paramount importance and significance in the development of magnetic guidable MCNC-PE as a smart carrier for applications such as drug delivery and oil recovery that relates stimulus-driven event.

6.2 Materials and Methodology

6.2.1 Materials

Iron (II) chloride tetrahydrate ($\text{FeCl}_2 \cdot 4\text{H}_2\text{O}$, $\geq 99\%$), iron (III) chloride hexahydrate ($\text{FeCl}_3 \cdot 6\text{H}_2\text{O}$, 99%), ammonium hydroxide (28% NH_3 in H_2O), calcofluor white (for microbiology), Nile red (for microscopy) and potassium hydroxide were purchased from Sigma-Aldrich Chemicals Company (Malaysia). Cellulose nanocrystals (CNCs) (Freeze dried, 0.96 wt% sulphur content) was procured from the University of Maine. Red palm superolein (275 ppm β -carotene, melting point 19 °C) was acquired from Sime Darby Jomalina Sdn Bhd (Malaysia). Ultrapure water ($18.2 \text{ M}\Omega \text{ cm}^{-1}$) was used throughout the course of experiment in this paper and was generated using a Milli-Q® Plus apparatus (Millipore, Billerica, USA). Ethanol (AR standard), 1M hydrochloric acid (HCl), and sodium hydroxide (NaOH) obtained from R & M Chemical (Syarikat Saintifik Jaya, Malaysia). All chemicals used in this study are of reagent grade. All experiment involving ultrasound (US) treatment was carried out using an ultrasound probe sonicator (20 kHz, Lab750, Sinaptec) under pulse mode (15 s pulse on, 10 s pulse off).

6.2.2 Synthesis and Characterisation of MCNC Nanocomposites

MCNC nanocomposites were prepared through the US-assisted in-situ co-precipitation methods. First, 0.04 g of CNC was dispersed in 80 g of water under ultrasonic waves for 2 minutes to prepare 0.05 wt% CNC dispersion. Next, iron (III) chloride hexahydrate and iron (II) chloride tetrahydrate (1.5/1 $\text{Fe}^{3+}/\text{Fe}^{2+}$ mol ratio) were added into the CNC dispersion, and subsequently stirred and heated to 45 °C. Then, the mixtures were sonicated in the presence of ammonium hydroxide (to adjust the pH of the mixture to 11) for 5 minutes. After that, the resultant MCNCs were precipitated, magnetically separated and washed 3 times with ethanol to remove all residual ammonium hydroxide. The collected MCNCs were centrifuged at 4500 rpm for 20 minutes, and dried in an oven overnight. The harvested MCNCs were stored for characterisation according Chapter 3.

6.2.3 Formation and Characterisation of MCNC-PE

Pickering emulsions were prepared by using the as-synthesized MCNC nanocomposites as solid particle stabilizers and β -carotene rich red palm olein as the oil phase. The Pickering emulsions with fixed oil content (30 vol%) and varies MCNC particle concentrations (0.1, 0.2, 0.3, 0.4, 0.5 wt%) at pH 6.5 were prepared with US cavitation at 60 W for 3 min. The resultant emulsion was transferred to glass vials and stored at room temperature for further characterisation according to chapter 5.

6.2.4 Effects of External Magnetic Field (EMF), pH and MCNC Particles Concentration on MCNC-PE Stability

1 ml of freshly prepared MCNC-PEs with designated particle concentration of either 0.3, 0.4 or 0.5 wt% was dispersed in 9 ml of water. The pH values of the diluted emulsions were then adjusted to 1.5, 3.0, 5.0, 7.5 and 8.5 using either HCL or NaOH. To generate the oscillating EMF, the emulsion was stirred using a N52 neodymium magnet (magnetic strength: 7343 Oe) at 200 rpm for 6 days, and consequently left to stand for 1 day at room temperature. Then, the resultant emulsions photograph were captured and analysed by mastersizer and optical microscopy to track any changes of the MCNC-PE. The control samples without magnetic field are stirred mechanically using an overhead stirrer (RW20, IKA, USA).

6.2.5 Temperature Variation Test

In order to determine if heat was generated during the magnetic application, 10 ml of MCNC-PEs stabilized by 0.3 wt% particles was poured into a vials. The emulsion was then stirred under magnetic application at 3000 rpm for 6 min. Next, the EMF was switched off for 4 min, and the temperature test was repeated for another magnetic on-off cycle. The temperature of the emulsion medium was measured using a thermometer during the experiment.

6.2.6 Reversibility Potential of MCNC-PE Upon pH Changes

2 ml of freshly prepared MCNC-PEs stabilized with 0.3 wt% of MCNC particles was dispersed in 8 ml of ultrapure water. The pH values of the diluted emulsions were then adjusted to 1.5 and then stirred slowly as per previously mentioned (mechanically/magnetically) at 100 rpm for 1 day. The droplet size and morphology was measured using mastersizer and optical microscope as per previously mentioned. Subsequently, the pH of the emulsions was adjusted to 8.5 and gently stirred for another day prior to the size and morphological analysis. The analysis was then continued by switching the pH of the sample between 1.5 and 8.5 in every consecutive day until a clear change is observed in emulsion droplet diameter.

6.2.7 Statistical Analysis

Analysis of variance (ANOVA) was conducted using Prism software and $p < 0.05$ was considered as statistically significant. ImageJ was used to examine the particle size of MNPs on CNC.

6.3 Results and Discussion

6.3.1 Physical Stability of MCNC-PE

The MCNC nanocomposites were re-dispersed in water and used to form Pickering emulsion with fixed oil phase volume (30 vol%). Based on Figure 6.1a, all Pickering emulsion samples exhibited monomodal size distribution. This was in good agreement with our optical microscopic images where MCNC-stabilized emulsion droplets were of uniform spherical shape and micron size (Figure 6.1c). It has been noticed that the mean droplet diameter of emulsion gradually decreased from about 7 to 4 μm as MCNC particle concentration increased from 0.1 to 0.3 wt%. Further increasing the particles concentration to 0.5 wt% showed no significant changes in the mean droplet diameter (Figure 6.1b). This implies that saturated monolayer particle adsorption takes place at the oil–water interface at 0.3 wt% MCNC particles concentration. The observed size reduction could be attributed to

the high degree of droplet surface coverage as a result of increased MCNC content. To support our hypothesis, the surface coverage (S_{mcnc}) of MCNC particles covered on emulsion droplet was estimated using Equation (6.1) (Kalashnikova, Bizot, Cathala and Capron, 2011).

$$S_{mcnc} = \frac{m_p D_{3,2}}{6h\rho V_{oil}} \quad \text{[Equation 6.1]}$$

where m_p , h and ρ are the mass, thickness and density for MCNC respectively; while V_{oil} is the volume of oil in the emulsion. The calculated surface coverage of Pickering emulsions prepared at different MCNC particles concentration were presented in Table 6.1. Taking the estimated MCNC thickness of approximately 8.525 nm (From STEM image), the surface coverage of emulsions by MCNCs increased markedly from 13.503 to 36.912 % as the particles concentration rose from 0.1 to 0.5 wt%. No significant changes were observed in the mean droplet diameter throughout the storage period at room temperature (Figure 6.2), indicating that all emulsions were remarkably stable against coalescence.

Table 6.1 Droplet surface coverage by MCNCs at different particle concentrations.

MCNC particles concentration (wt%)	S_{mcnc} (%)
0.1	13.503
0.2	20.127
0.3	22.218
0.4	29.561
0.5	36.912

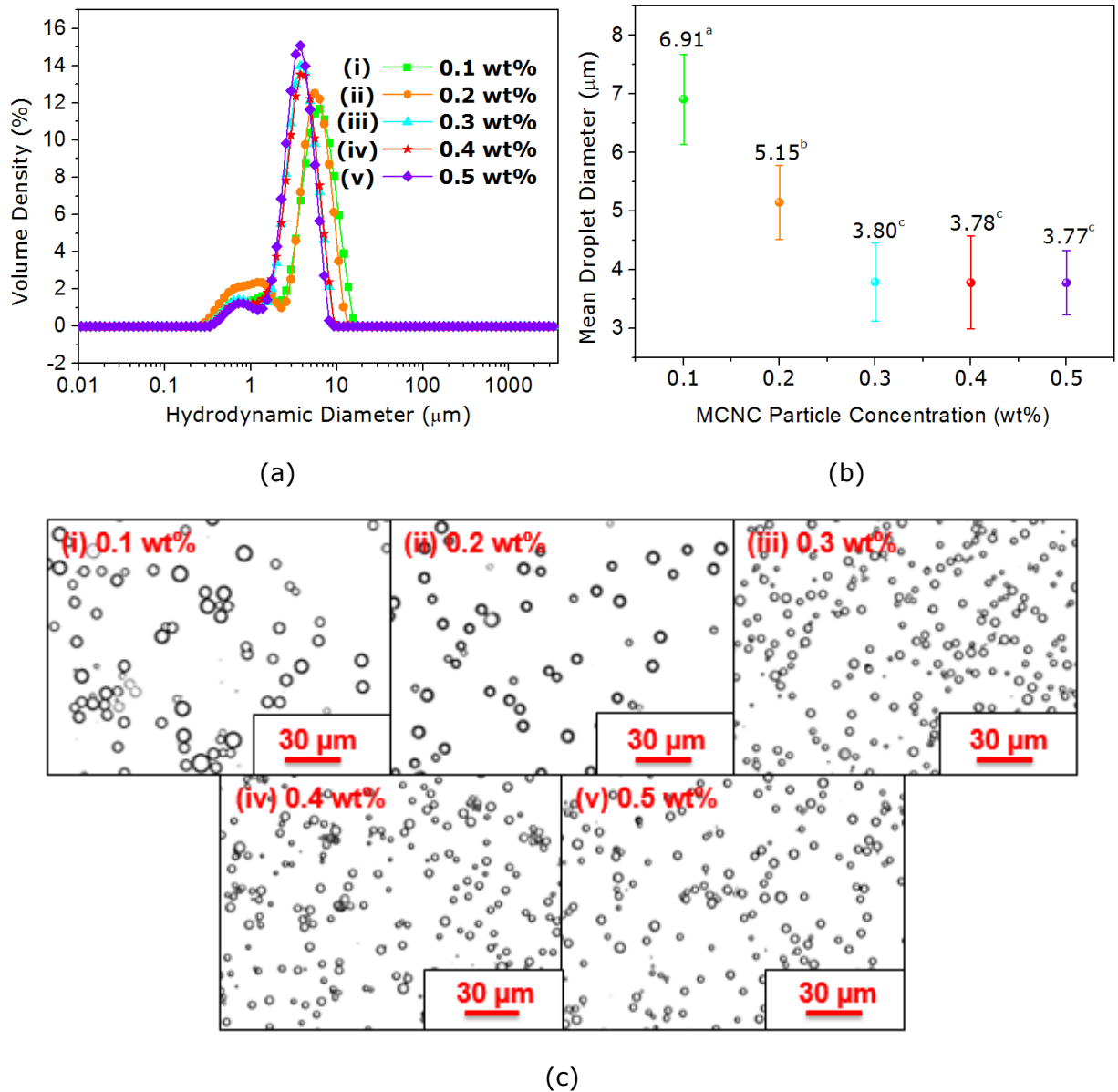


Figure 6.1. (a) Raw droplet size distribution data, (b) Mean droplet diameter, and (c) Optical micrograph of the MCNC-PE prepared at (i) 0.1, (ii) 0.2, (iii) 0.3, (iv) 0.4 and (v) 0.5 wt%. Error bar represents standard error in measurement. Different alphabetic letters were significantly different at $P \leq 0.05$ by Bonferroni's Multiple Comparison Test.

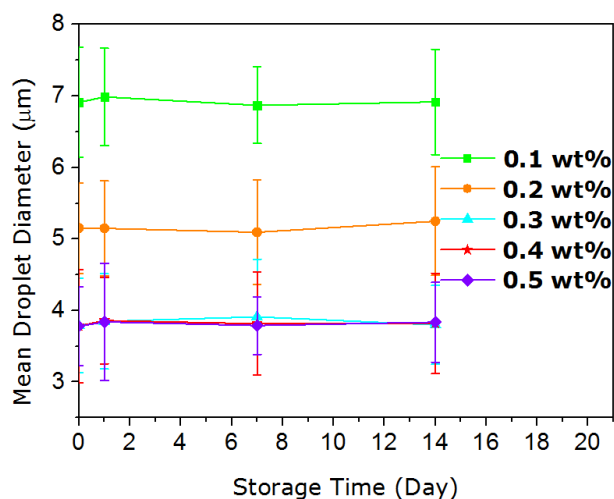


Figure 6.2. Changes in the mean droplet diameter of MCNC-PE upon storage up to 14 days. Error bar represents standard error in measurement.

Double staining with both calcofluor white and Nile red have been performed to detect the oil globules and the MCNC particle surface coverage around droplets. The fluorescent microscopy revealed that the emulsion droplets (red) were densely covered with MCNC particles (blue), indicating that these nanocomposite particles are irreversibly adsorbed at the oil-water interface (Figure 6.3a & b). Fig. 6.3c showed the fluorescent image of MCNC-PE based on the combination of two fluorochromes.

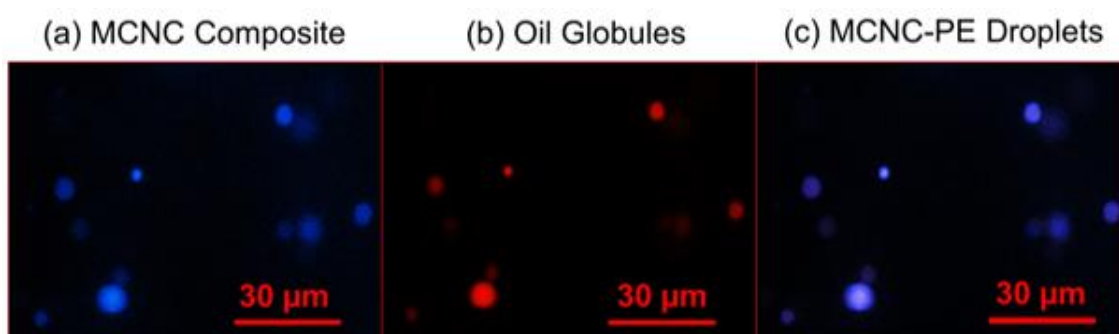


Figure 6.3. Fluorescent microscopic images of Pickering emulsion stabilized with 0.5 wt% MCNC nanocomposite, showing the location of (a) MCNC nanocomposite, (b) oil globule and (c) MCNC-PE droplets.

6.3.2 pH and Magneto-responsiveness of MCNC-PE

The effect of magnetic field on the pH-responsive properties of the Pickering emulsion was investigated with MCNC-PE prepared using various particles concentrations (0.3, 0.4 and 0.5 wt%). Freshly prepared emulsions were subjected to environmental changes by pH variation and with/without EMFs. The droplet size and morphological changes of the Pickering emulsion were then examined and analysed. The results unveiled that the emulsion remained stable regardless of pH changes and MCNC particle concentration used when magnetic field was absent (Figure 6.4a to d and Figure 6.5). Under the influence of magnetic field, the noticeable changes observed in mean droplet diameter of MCNC-PE was surprisingly found to be pH-dependent. A slight increment in mean droplet diameter was observed when the emulsion pH was altered to 1.5 and 3.0 (see Figure 6.6a to d, Figure 6.7a to c, (i)-(ii)) owing to the increased hydrophobicity of the MCNC nanocomposites as pH dropped (Low *et al.*, 2017; Vepsäläinen and Saario, 2010). As $\text{pH} \geq 7.5$, the emulsions become unstable due to the limited availability of particle stabilizer in the emulsion system as more MCNC particles get partitioned in alkali pH medium (Vepsäläinen and Saario, 2010) (Figure 6.7a to c, (iv)-(v)).

Two possible mechanisms have been proposed to explain the magnetic hyperthermia-induced MCNC-PE destabilization: (i) When exposing to EMFs, the adsorbed MCNC particles at oil-water interface become magnetized and subjected to an attractive force along the field direction (Blanco *et al.*, 2013). The particles will then be attracted and concentrated at the areas of strong magnetic flux fields, thus inducing a dilatational deformation of the fluid interface associated with the possible leakage of MCNC particles into the surrounding aqueous phase (Lam *et al.*, 2011). (ii) It is also hypothesized that when subjected to an alternating magnetic field, the superparamagnetic MCNC particles undergo dynamic hysteresis losses induced by Neel and Brownian relaxation processes and induce a local heating effect at the level of the colloidal particle layer near oil-water interface, causing a thermos-capillary instability of the interfacial film (Guibert, Dupuis, Peyre and Fresnais, 2015; Liu *et al.*, 2009; Oliveira *et al.*, 2013; Pradhan *et al.*, 2010). The combined effects of both magnetic field-induced phenomena could not only impart

catastrophic conformation changes on adsorbed layer composed of MCNC particles but also lead to the gradual leakage and solubilisation of MNP particles in the aqueous phase and eventually led to a keen disturbance on the physical stability of the MCNC-PE. The proposed stabilization-destabilization mechanism of MCNC-stabilized emulsion via magnetic hyperthermia is illustrated in Scheme 6.1. A temperature rise has been observed in the emulsion system (Figure 6.8). Intriguingly, the unique pH-responsive characteristic of MCNC-PE was, in the presence of magnetic field, not observed with emulsion system prepared respectively using MCNC particle concentration of 0.5 wt%, as evidenced in Figure 6.6 and Figure 6.7c. One possible reason is that the presence of high MCNC particle content in emulsion system give rise to a superior Pickering droplet stabilizing effect against the environmental changes with the formation of densely packed particle adsorption monolayer at the liquid-liquid interface. This study demonstrated that the application of EMF plays an important synergistic role in the system of a pH-sensitive MCNC-stabilized emulsion with reversible wetting tuning behaviour.

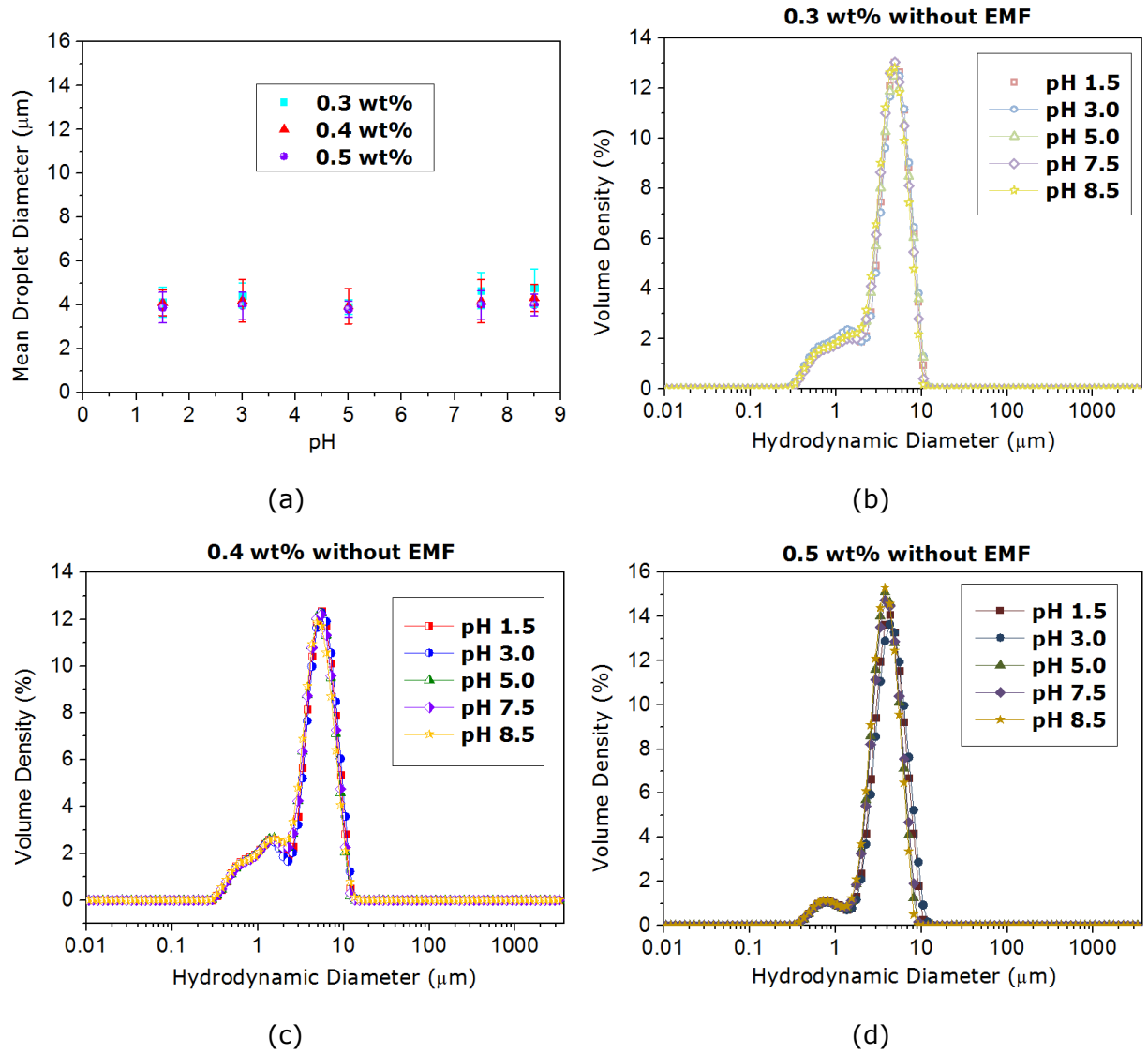
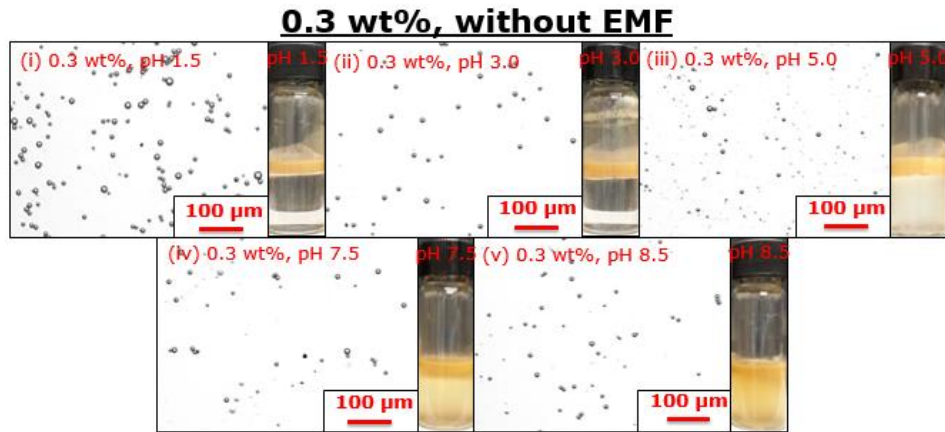
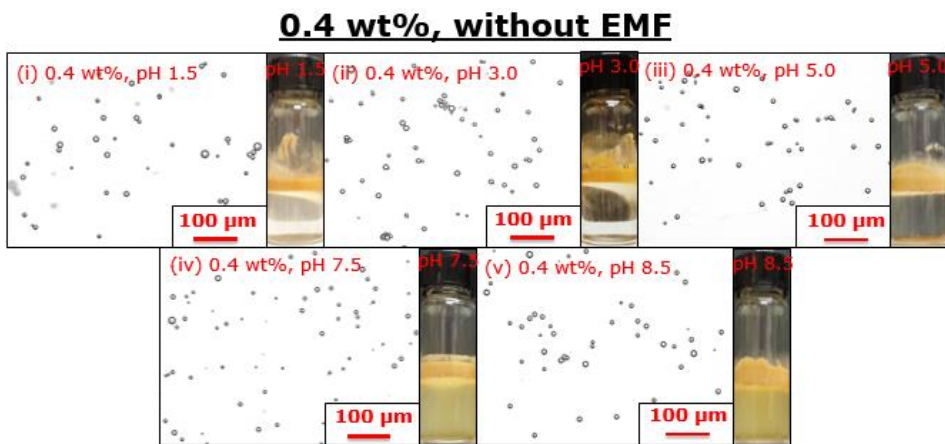


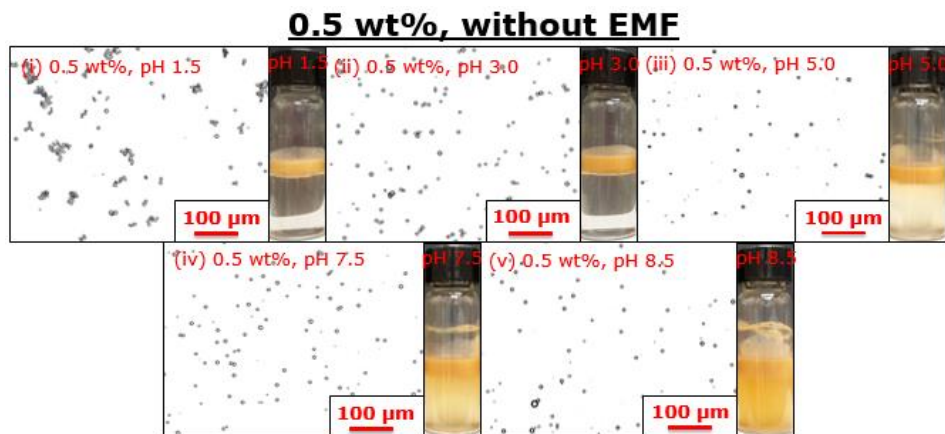
Figure 6.4. (a) Mean droplet diameter of MCNC-PE prepared under different MCNC particle concentration as a function of pH without EMFs, and the respective droplet size distribution data at (b) 0.3, (c) 0.4 and (d) 0.5 wt% MCNC content. Error bar represents standard error in measurement.



(a)



(b)



(c)

Figure 6.5. Optical microscopy and photograph of MCNC-PE stabilized using particles concentration of (a) 0.3 wt%, (b) 0.4 wt% and (c) 0.5 wt% at (i) pH 1.5, (ii) pH 3.0, (iii) pH 5.0, (iv) pH 7.5 and (v) pH 8.5 without EMF. The photograph of each emulsion is shown beside the optical microscope image.

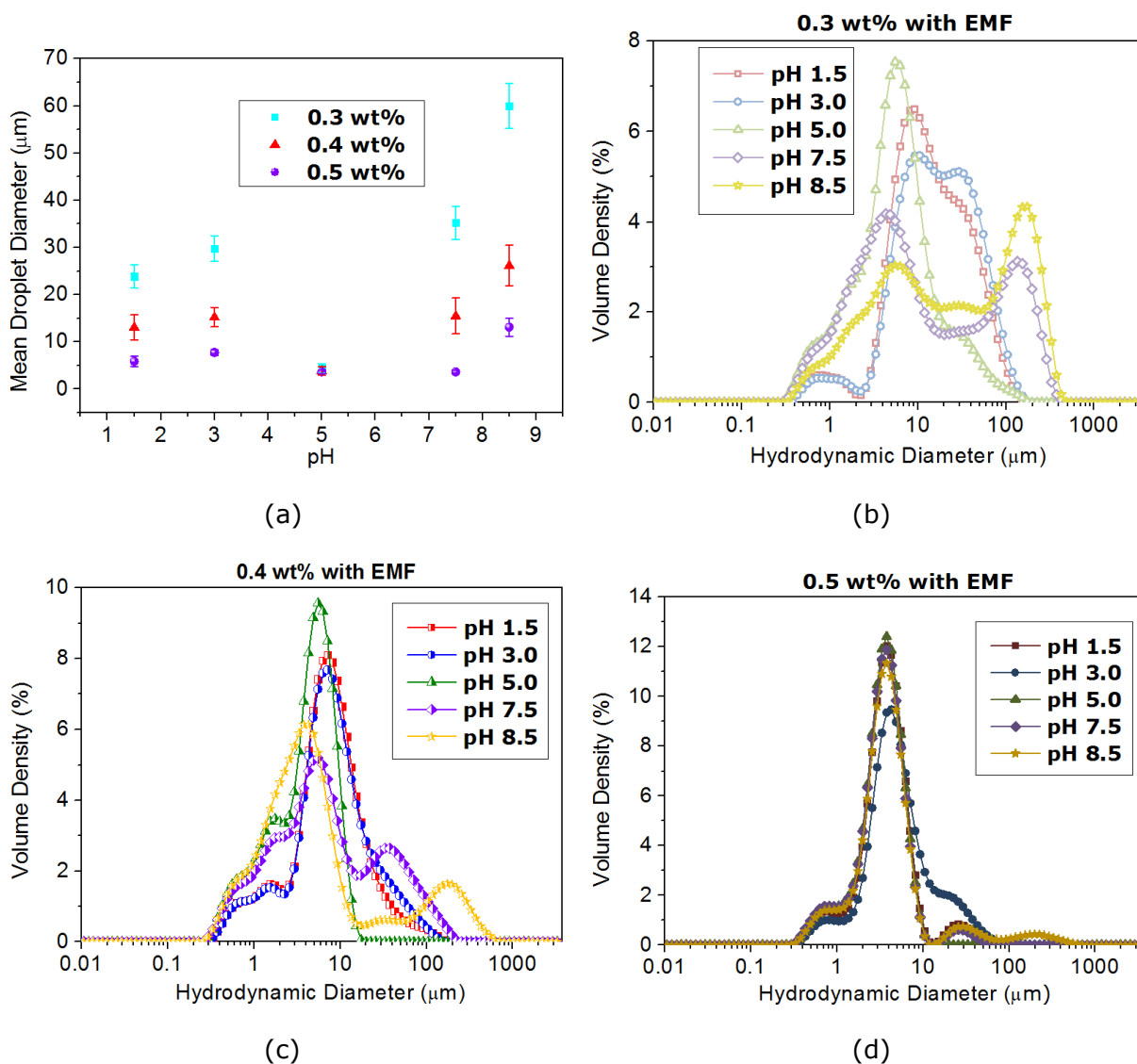
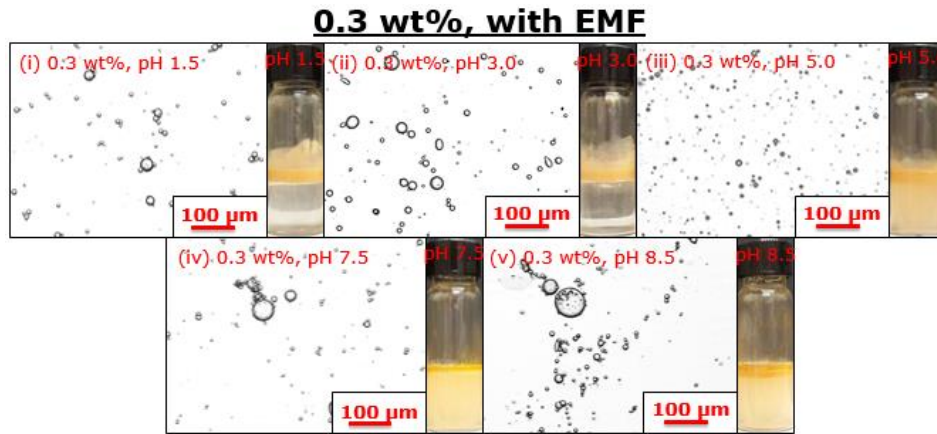
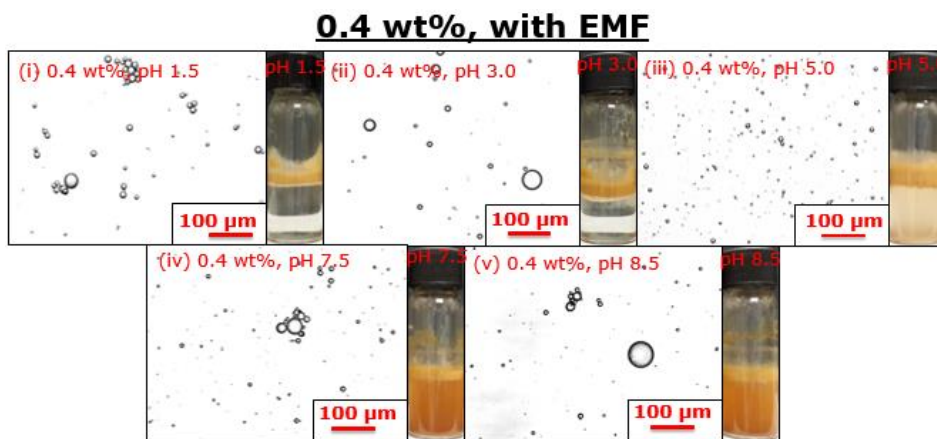


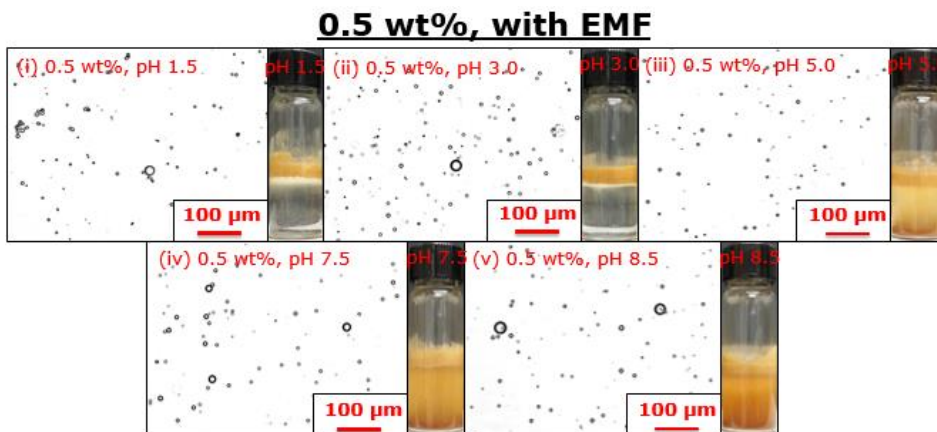
Figure 6.6. (a) Mean droplet diameter of MCNC-PE prepared under different MCNC particle concentration as a function of pH with EMFs, and the respective droplet size distribution data at (b) 0.3, (c) 0.4 and (d) 0.5 wt% MCNC content. Error bar represents standard error in measurement.



(a)



(b)



(c)

Figure 6.7. Optical microscopy and photograph of MCNC-PE stabilized using particles concentration of (a) 0.3 wt%, (b) 0.4 wt% and (c) 0.5 wt% at (i) pH 1.5, (ii) pH 3.0, (iii) pH 5.0, (iv) pH 7.5 and (v) pH 8.5 with EMF. The photograph of each emulsion is shown beside the optical microscope image.

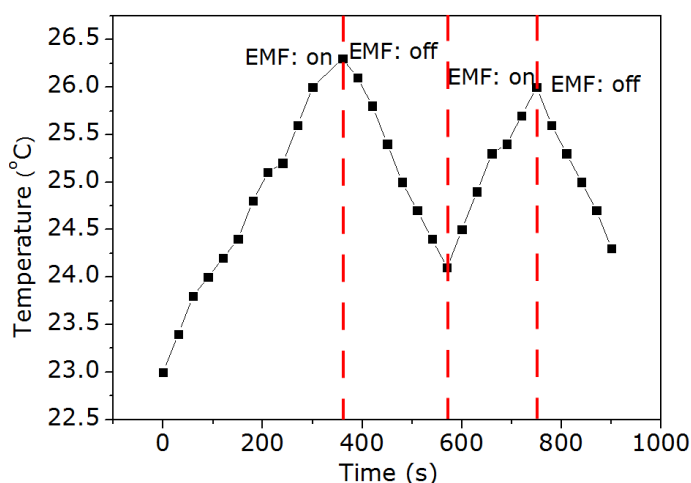
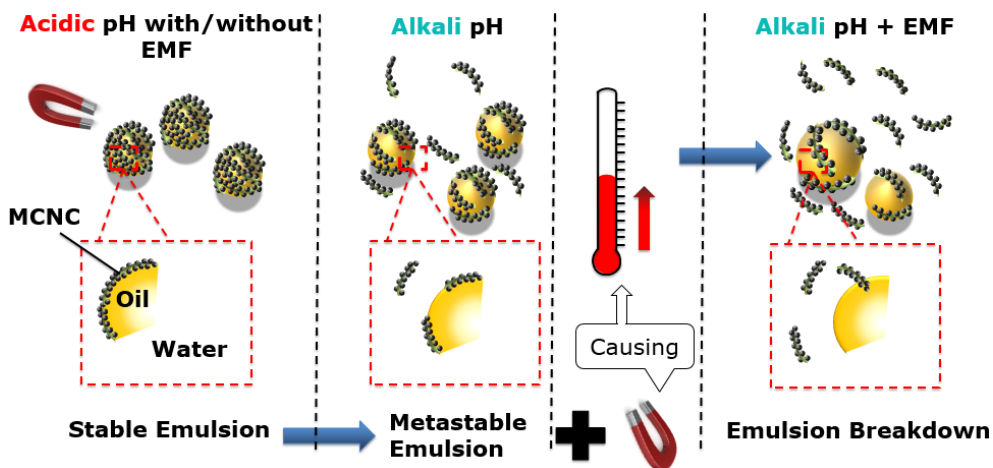


Figure 6.8. Temperature variation of MCNC-PE with and without its exposure to EMF.



Scheme 6.1. Schematic illustration of the MCNC-PE stabilization-destabilization mechanism.

In a separate experiment, the MCNC nanocomposite particles (using 0.3 wt% particle concentration) were used to form Pickering emulsion and subjected to alternating pH changes between 1.5 and 8.5 with/without the influence of magnetic field. The study showed that the formed MCNC-PE can be cycled between stable and unstable 3 times upon alternating the pH of the emulsion, with no apparent changes in the mean droplet diameter under the presence of the magnetic field. Presence of tiny amount of oil was detected on top of the emulsion at alkali condition (pH 8.5) (Figure 6.9 Insets). Lowering the pH to 1.5 restored the emulsion stability to original state with the

disappearance of the floating oil layer (Figure 6.9 Insets). Similar observations have been reported by Sarker *et al.* (2017) and Tang *et al.* (2014) in their Pickering emulsions preparations using protein nanocage and poly[2-(dimethylamino) ethyl methacrylate] grafted CNC, respectively. The observed emulsion breakdown could be attributed to increased solubility of MCNC particles at alkaline pH and occurrence of magnetic hysteresis that weaken the interfacial interactions between solid particles held in oil-water interface and consequently affecting the degree of bridging in a Pickering emulsion.

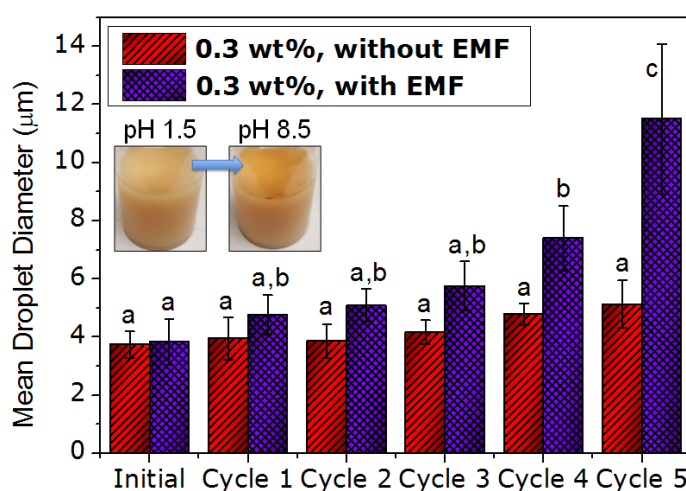


Figure 6.9. Mean droplet diameter of MCNC-PE after various destabilization and stabilization cycles with/without the presence of an EMF. The error bar represents the standard error in measurement. Different alphabetic letters were significantly different at $P \leq 0.05$ by Bonferroni's Multiple Comparison Test.

6.4 Conclusions

In the present work, a reversible Pickering emulsion system was developed based on the dual stimulus-responsive wetting behaviours of MCNC nanocomposites. The MCNC-based Pickering emulsions (MCNC-PEs) were ultrasonically prepared with 0.3 wt% particles and then subjected to droplet size stability and morphology characterisations. The study showed that the environmental conditions (pH and magnetic field) play a major role and influences the emulsion droplet stability. The pH-tunability of MCNC-PE was intensively investigated with regard to the pH region under the impact of permanent magnetic field, in which the emulsion systems become unstable. When a magnetic field is externally applied, good droplet stability was observed for the emulsions in the acidic medium (pH 1.5 – 5.0), whereas emulsions become physically unstable under alkaline conditions (pH \geq 7.5). Weak interfacial interactions between solid particles held in oil-water interface due to both the magnetic hysteresis effects and high aqueous solubility of MCNCs in alkaline pH may be responsible for the observed emulsion destabilization. Subsequent preparation of Pickering emulsions with 0.5 wt% particle contents, showed no changes in colloidal stability with pH variation and magnetic field application and thus demonstrated such exclusive pH-driven stabilization and destabilization to be MCNC particle concentration-dependent. We anticipate that these newly developed multifunctional MCNC-PEs may serve as a useful controlled delivery candidate for therapeutic drug cargo.

CHAPTER SEVEN

BIOACTIVE MICROENCAPSULATION AND TRIGGERED RELEASE

BEHAVIOUR OF MCNC-PE

Overview

Stimuli-responsive drug release and controlled delivery play crucial roles in enhancing the therapeutic efficacy and lowering over-dosage induced side effects. In this chapter, using curcumin as model drug, we investigated the drug loading, magnetically-triggered drug release and the *in-vitro* anti-colon cancer efficacy of palm olein-based MCNC-stabilized (MCNC-PE). The loading efficiency of curcumin in MCNC-PE template was found to be 99.35%. From the drug release test, it was observed that the release rates of curcumin from the MCNC-PE can be remarkably enhanced upon the application of external magnetic field (EMF). The exposure to EMF (0.7 T) stimulated the release of bioactive from particle-stabilized emulsion achieving 53.30 ± 5.08 % of the initial loading over a 4-day period. The MTT assay demonstrated that the curcumin-loaded MCNC-PE is effective in reducing human colon cancer cells growth down to 60% in the absence of EMF. A significant further reduction of $\sim 42\%$ in the cell viability was recorded when the magnetic field was applied externally. The results of our study opens a new avenue in the design and development of smart colloidal drug delivery systems for stimuli-triggered release of bioactive and therapeutics.

7.1 Introduction

In recent years much efforts have been devoted to the development of drug delivery carrier for more efficient cancer therapies, with the aim of reducing side effects while ensuring a superior outcomes. Part of the development has been focused on emulsion system that are presented as promising drug delivery systems owing to their unique characteristics such as colloidal stability, compartmentalization and ease to encapsulate different compound (Frelichowska *et al.*, 2009; Li *et al.*, 2014; Shah *et al.*, 2016; Wu and Ma, 2016). Furthermore, the encapsulation of drugs within the emulsion can also aid in preserving and protecting drugs from enzymatic degradation and gastrointestinal hydrolysis (Marti-Mestres and Nielloud, 2002). In fact, extensive work has been carried out on their preparation and characterisation, channeling a big leap into the development of such carrier. Emulsion is a system composing of two immiscible liquids where one of the liquid is dispersed in the other in the form of drops. A colloiddally stable emulsion generally required the uses of stabilizer to prevent them from deformation (Sivakumar, Tang and Tan, 2014; Tadros, 2013). Emulsion can either be stabilized by chemical surfactant or solid particles. In between the two, solid particles stabilized emulsion (commonly known as Pickering emulsion) is more preferred by researchers due to its less toxicity and enhanced resistance against droplet disruption (Binks, 2002; Frelichowska *et al.*, 2009; Wu and Ma, 2016).

By definition, the advanced resistances of Pickering emulsion to destabilization is recognized by the strong solid film barrier around the surfaces of the emulsion droplets as resulted from the irreversible adsorption of colloidal solid particles onto the interfaces of two immiscible liquids (Binks, 2002; Binks and Lumsdon, 2001; Cunha *et al.*, 2014; Tambe and Sharma, 1993; Wu and Ma, 2016). The superior shielding effects imparted by the solid particles, however, restricted the Pickering emulsion to be utilized in bio-applications that needed a temporal stability and subsequent remotely implied destabilization. The key characteristics of solid particles that affects their performance in stabilizing an emulsion is the surface wettability (Binks and Lumsdon, 2000). Thus, the abovementioned issue of Pickering emulsion can be overcome by utilizing stabilizing materials that undergo surface wettability transformation in respond to internal or external applied triggers. To date, many

stimulus have been attempted for the preparation of Pickering-based smart carrier. This includes pH (Lan *et al.*, 2007; Low *et al.*, 2018), temperature (Lee, Blumenthal and Ivkov, 2014), ultrasound (US) (Fabiilli *et al.*, 2010) and EMF (Low *et al.*, 2018; Sander *et al.*, 2012). Amongst, magneto-responsive Pickering emulsions have received growing attention due to its ability to precisely transport and disarming the Pickering-based carrier. Besides that, since drug delivery applications are often related to human body, the pH-responsive properties remained as another important stimulus to be noticed. In literature, Raju *et al.* (2013) has prepared pH-responsive magnetic Pickering Janus emulsion using chitosan and Fe_3O_4 (MNP) as the solid stabilizer. They, however mentioned that to form the Pickering emulsion, the MNP is needed to be incorporated into one of the oil phase while dispersing the MNPs solely in the aqueous phase led to failure in the fabrication of the Pickering emulsion (Raju *et al.*, 2018). In another study, Wang *et al.* (2013) incorporated MNP nanoparticles onto reduced graphene oxide and further utilizing it to prepare magnetic-responsive Pickering emulsion for magnetic resonance imaging (MRI) and drug delivery. The reported preliminary outcomes suggested an improved MRI performance as well as a pH-sensitive sustained drug releasing behavior (Wang *et al.*, 2013). Recently, Low *et al.* (2017) successfully prepared magnetic Pickering emulsions using Fe_3O_4 @Cellulose nanocrystal (MCNC) nanocomposite as the stabilizer. The incorporation of MNP onto the surfaces of cellulose nanocrystal (CNC) resulted in an increase in the surface hydrophobicity of the nanocomposite, improving its effectivity in stabilizing Pickering emulsion (Low *et al.*, 2016). Furthermore, the latter work demonstrated that the MCNC nanocomposite is an interesting particle that possessed both the magnetic- and pH-responsiveness (Low *et al.*, 2018). The MCNC-stabilized Pickering emulsion (MCNC-PE) was found to remain physically stable in acidic pH (1.5 – 6.5) while disrupted in mild alkali conditions (pH 7.5 – 8.5) in the presence of an oscillating EMF (Low *et al.*, 2018).

Considering the above positive outcomes and advantages in the earlier reports, we aimed, in this study, to investigate the drug release profile and kinetics as well as the *in-vitro* cytotoxicity of MCNC-PE against colorectal cancer cell line HCT116 using curcumin as a model drug since it has been claimed to be an organic bioactive that can inhibit the growth

of colon cancer cell line effectively without causing toxicity to normal cells (Shakibael et al., 2013; Vaiopoulos, Athanasoula and Papavassiliou, 2013). Here, we hypothesized that the MCNC-PE might be a promising yet biocompatible stimuli-responsive drug delivery platform which able to elicit a significant increase in cell toxicity associated with enhanced curcumin release kinetics under exposure of non-invasive oscillating magnetic field.

7.2 Materials and Methodology

7.2.1 Materials

Iron (II) chloride tetrahydrate ($\text{FeCl}_2 \cdot 4\text{H}_2\text{O}$, $\geq 99\%$), iron (III) chloride hexahydrate ($\text{FeCl}_3 \cdot 6\text{H}_2\text{O}$, 99%), ammonium hydroxide (28% NH_3 in H_2O), curcumin (from curcuma longa (turmeric), 65%), calcofluor white (for microbiology), Nile red (for microscopy), potassium hydroxide, Dimethyl sulfoxide (DMSO), 1M sodium dihydrogen phosphate (NaH_2PO_4 , 99%), 1M disodium monohydrogen phosphate (Na_2HPO_4 , 99%) were purchased from Sigma-Aldrich Chemicals Company (Malaysia). Cellulose nanocrystals (CNCs) (Freeze dried, 0.96 wt% sulphur content) was procured from University of Maine. Red palm superolein (275 ppm β -carotene, melting point 19 °C) was acquired from Sime Darby Jomalina Sdn Bhd (Malaysia). Ultrapure water ($18.2 \text{ M}\Omega \text{ cm}^{-1}$) was used in every experiment in this paper and was generated using a Milli-Q® Plus apparatus (Millipore, Billerica, USA). Methanol (AR standard), ethanol (AR standard), 1M hydrochloric acid (HCl), and sodium hydroxide (NaOH) obtained from R & M Chemical (Syarikat Saintifik Jaya, Malaysia). All chemicals used in this study were of analytical grade. All experiment involving US treatment was carried out using an ultrasound probe sonicator (20 kHz, Lab750, Sinaptec) under pulse mode (15 s pulse on, 10 s pulse off).

7.2.2 Synthesis and Characterisation of MCNC Nanocomposites

The synthesis of the Fe_3O_4 @CNC (MCNC) nanocomposites was done through an *in-situ* co-precipitation method with the help of US. Firstly, 0.05 wt% of CNC dispersion was prepared by dispersing 0.04 g of CNC into 80 g of water under ultrasonic waves for 2 minutes. Iron

(III) chloride along with iron (II) chloride was then added to the dispersion at a 1.5/1 ratio respectively and stirred. The dispersion was then heated to 45°C and sonicated for 5 minutes under the presence of 2.2 ml of ammonium hydroxide. Ethanol was then used to precipitate the resultant MCNC. To ensure MCNC is cleaned of residual Ammonium Hydroxide, the MCNC was washed and magnetically separated 3 times using ethanol. Lastly, the collected MCNC was centrifuged at 4500 rpm for 20 minutes and left dried overnight in an oven. The harvested MCNC nanocomposite was then stored for the characterisation as per mentioned in Chapter 3.

7.2.3 Preparation and Characterisation of MCNC-PE

Pickering emulsions were prepared by using the as-synthesized MCNC nanocomposites as solid particle stabilizers and β -carotene rich red palm olein as oil phase. The coarse Pickering emulsions with a fixed oil content (30 vol%) and a fixed MCNC particle concentration (0.1 wt%) at pH 6.5 were prepared using high-speed homogenizer (Model Ultra-Turrax T-25, IKA, Germany) at 5000 rpm for 5 min prior to US cavitation. Then, US was applied at 60 W for 3 min to prepare fine Pickering emulsions. To prepare the curcumin-encapsulated MCNC-stabilized Pickering emulsion (MCNC-PE), 1 mg/ml of curcumin was dissolved in red palm olein under heating at 40 °C and stirring for 12 hours prior to Pickering emulsion preparation to achieve a final curcumin concentration of 0.3 mg/ml emulsion. Subsequently, the curcumin-loaded MCNC-PE was formulated from procedure as prescribe earlier. The resultant emulsion was transferred to glass vials and stored at room temperature for further characterisation as per discussed in Chapter 5.

7.2.4 Curcumin Loading Efficiency in MCNC-PE

The curcumin-loaded Pickering emulsion was mildly centrifuged for 3 minutes at 1000 rpm to sediment all the undissolved or non-encapsulated curcumin. Subsequently, 1 ml of Pickering emulsion was extracted and added into 10 ml of methanol and stirred thoroughly using vortex shaker (IKA vortex 3 model, Germany) at maximum speed for 2 min. The mixture containing solvent and emulsion was then centrifuged again at 4500 rpm for 5 min

to separate them into two layers. The supernatant was then extracted and the curcumin content was measured at 425 nm using a UV-Vis spectrophotometer (Genesys 10s UV, Thermo Fisher Scientific, USA) against a blank prepared by substituting curcumin-loaded MCNC-PE to blank MCNC-PE. The percentage of encapsulation efficiency, %EE, of curcumin in the emulsion was calculated using the following equation:

$$\%EE_{cur} = \frac{\text{Amount of curcumin in the oil droplet}}{\text{Amount of curcumin in the formulation with respect to the same oil droplet volume}} \times 100\% \quad [\text{Equation 7.1}]$$

7.2.5 Retention of Curcumin in MCNC-PE

The Pickering emulsion sample was stored at room temperature in the dark for 9 days. Meanwhile, the concentration of curcumin was measured periodically every 24 hour using the method described above.

7.2.6 Stability of MCNC-PE with/without Exposure to EMFs

2 ml of freshly prepared curcumin-loaded MCNC-PEs was dispersed in 8 ml of buffer solution (pH 7.5). A N52 neodymium magnet is then used to generate the EMF via stirring the emulsion for 1 day, and consequently left to stand for 1 day at room temperature prior to photo capturing. The buffer solution is prepared as follow: 500 mL of 0.1 M buffer solution at pH 7.5 was prepared by mixing 5.965 g of disodium monohydrogen phosphate and 1.103 g of sodium dihydrogen phosphate in water.

7.2.7 In-vitro Curcumin Release Studies

The *in-vitro* release profile of curcumin from the MCNC-PE was examined in buffer solution (pH 7.5) with or without the presence of EMF according to the method described by Kondaveeti *et al.* (2018) with slight modification. 10 mL of emulsion was mixed with 1 mL of the buffer and the mixture was poured into a dialysis tube (MWCO: 3.5 kDa) and subsequently incubated in the buffer at room temperature for 96 hours using an incubator shaker operating at 120 rpm. Samples (1 mL) are the pipetted out and replaced with 1 mL of buffer to complete the initial volume at 24, 48, 72 and 96 hours to measure the

concentration of released curcumin. The absorbance of curcumin is measured as per described above using a spectrophotometer. To evaluate the effects of EMF, the emulsion mixture in dialysis tube is subjected to oscillating magnetic force using a N52 neodymium magnet (0.7 T), spinning at 120 rpm to replace the stirring by incubator shaker.

7.2.8 Determination of Anticancer Activity Using MTT Assay

The effect of curcumin-loaded MCNC-PE on cell viability of human cancer cell line HCT116 was determined using 3-(4,5-dimethylthiazol-2-yl)-2,5-diphenyltetrazolium bromide (MTT) assay according to the established method with minor modification (Tan *et al.*, 2015). HCT116 cells were seeded into a sterile flat bottom 96-well plate at a density of 5×10^3 cells/well and allowed to adhere overnight. Then, 20 μ L of the Pickering emulsion was added into each well with the final curcumin concentration of 30 μ g/mL. The concentration of DMSO used as the solvent was maintained at 0.5% (v/v) and also incorporated as negative control in all the experiments. The cells were further incubated with the Pickering emulsions before performing MTT assay. 20 μ L of 5 mg/mL of MTT was then added to each well and the plates were incubated at 37 °C in a humid atmosphere with 5 % CO₂, 95 % air for 4 h. The medium was then gently aspirated, and 100 μ L of DMSO was added to dissolve the formazan crystals. The absorbance of dissolved formazan product was determined spectrophotometrically at 570 nm (with 650 nm as the reference wavelength) using a microplate reader. The percentage of cell viability was calculated as follows:

$$\%cell\ viability = \frac{Absorbance\ of\ treated\ cells}{Absorbance\ of\ untreated\ cells\ (control)} \quad [Equation\ 7.2]$$

The effect of EMFs was evaluated using a method similar to Oliveira *et al.* (2013) with slight modification. Briefly, the incubated cells were exposed to oscillating magnetic force using a N52 neodymium magnet for 15 min, 3 times every 24 hours (with a 2 hour interval between exposures) up to 96 hours.

7.2.9 Apoptotic Hallmark Detection by Hoechst 33342 Nuclear Staining

Hoechst 33342 nuclear staining was used to detect the apoptotic cells by observing the apoptotic nuclear morphology using fluorescence microscopy. Briefly, HCT116 cells were plated in 6 well plate at 1×10^6 cells/well and allowed to adhere overnight. Cells were treated with or without Pickering emulsion with indicated concentration. After treatments, the cells were harvested in PBS and followed by exposure to 0.05 g/L Hoechst 33342 dye in PBS for 30 min at room temperature. The samples were observed and analysed under an inverted fluorescence microscope (Olympus IX81, Olympus Corporation, Japan).

7.2.10 Cellular Uptake of MCNC-PE

To measure the uptake of Pickering emulsions by cells, HCT116 cells were incubated with Nile red-stained Pickering emulsion samples as described by Tikekar, Pan and Nitin (2013) with slight modifications. The cells were plated in glass bottom 96 well plate. After incubation with MCNC-PE, the cells were rinsed with PBS 3 times to remove the emulsion. The cells were suspended in PBS and imaged using the Olympus IX81 fluorescence microscope at 40x magnification.

7.2.11 Statistical Analysis

Analysis of variance (ANOVA) were conducted using Prism software and $p < 0.05$ was considered as statistically significant.

7.3 Results and Discussion

7.3.1 Preparation and Characterisation of Curcumin-loaded MCNC-PE

The drug delivery carrier in this work is prepared by encapsulating curcumin as a model bioactive ingredient at 1 mg/ml oil in Pickering emulsion. The Pickering emulsion is formed with fixed oil content (30 vol%) using the MCNC nanocomposites as the stabilizer. Based on Fig 7.1, both the blank MCNC-PE and curcumin-loaded MCNC-PE displayed monomodal size distribution with an average sizes around 7.5 μm . This revealed the non-significant

influences of the curcumin encapsulation on the physical characteristics of the MCNC-PE. Besides that, it has been noticed that there was no significant changes in the mean droplet diameter throughout the storage period at room temperature, thus suggesting that the emulsions prepared in the present study were physically stable for at least 14 days.

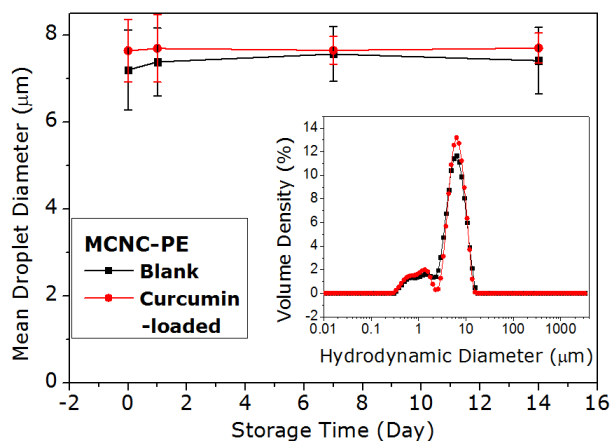


Figure 7.1. Mean droplet diameter of the curcumin-loaded MCNC-PE. Error bar represents standard error in measurement. Inset shows the raw droplet size distribution data.

Using Equation (7.1), a high encapsulation efficiency of curcumin in the Pickering emulsions ($\approx 99.35\%$) is obtained. This was reasonable since the curcumin was fully dissolved into the oil phase prior to emulsification. Additionally, without the presence of non-emulsified oil, hypothetically all dissolved curcumin should be present in the Pickering emulsion droplets. The percent retention of curcumin in the MCNC-PE was then investigated as a function of storage period in MCNC-PE. As shown in Figure 7.2, approximately 15% of curcumin was degraded in the first 24 hours in the present emulsion system. The half-life of the encapsulated curcumin has been determined to be around 5 storage days (≈ 120 hr). This showed a 40-fold improvement when compared to the stability of curcumin in aqueous buffer medium (Wang *et al.*, 1997). In comparison to other Pickering emulsion systems, the results of the present study were highly similar to those reported by Shah *et al.* (2016) in food grade Pickering emulsion stabilized by chitosan-tripolyphosphate nanoparticles. Their results showed that the half-life of curcumin in chitosan-tripolyphosphate nanoparticles-stabilized Pickering emulsion (droplet size $\geq 50\ \mu\text{m}$) was approximately 5 days. Accounting the as-prepared MCNC-PE (droplet size $\approx 7\ \mu\text{m}$) with larger oil/water effective interfacial

contact area, the curcumin encapsulated in MCNC-PE can be considered to have enhanced stability.

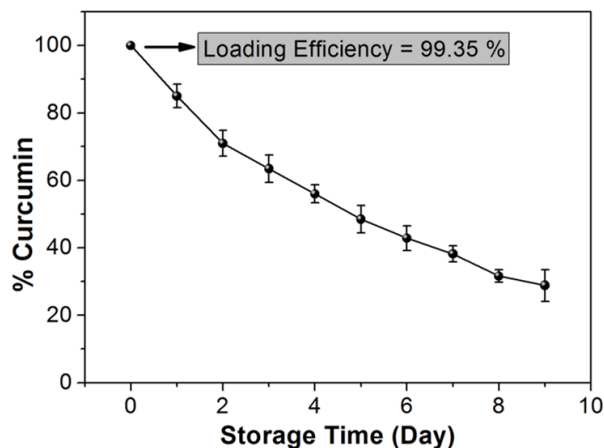


Figure 7.2. Percent retention of curcumin in Pickering emulsions stabilized with 0.1 wt% MCNC particles. Black arrow indicates the loading efficiency of curcumin in the respective sample. Error bar represents standard error in measurement.

7.3.2 In-vitro Release Profile of Curcumin from MCNC-PE

As a means to assess the influence of the exposure of curcumin-loaded MCNC-PE to EMFs, curcumin release study was performed in buffer solution (pH 7.5). From Figure 7.3a, the curcumin content released was observed to be 14.59 ± 3.66 and 53.30 ± 5.08 % for MCNC-PE without and with EMFs respectively. The findings revealed an increased CUR released rate of approximately 39% (or $4.03 \mu\text{g}/\text{ml}\cdot\text{min}$) under EMFs thus evidenced that the EMF triggered the release of CUR from the MCNC-PE. To understand the drug release mechanisms further, the curcumin release data were fitted using the Korsmeyer – Peppas model, a semi-empiric model that is often used to understand the release kinetics of drug from a carrier to the elapsed time, t :

$$\frac{M_t}{M_n} = kt^n \quad \text{[Equation 7.6]}$$

where M_t and M_n are the amount of drug released at time t and at equilibrium respectively (levelling off stage), k is a kinetic constant of the drug delivery system and n is the diffusion exponent that relates the drug transport mechanisms. The n values were calculated from the slope of the plot of $\log(M_t/M_n)$ against $\log t$ (Figure 7.3b) and tabulated in Table 7.1.

For the Korsmeyer–Peppas model, if $n < 0.45$, the drug is released via Fickian diffusion, $0.45 < n < 0.89$ indicates non-Fickian or anomalous diffusion while $n > 0.89$ refers to zero-order (case II) transport that is normally obtained when a burst release of drug is observed (Dash *et al.*, 2010; Luo *et al.*, 2017; Shi *et al.*, 2014; Tan *et al.*, 2016). Figure 7.3b reveals that the release behaviour of curcumin from MCNC-PE can be well fitted with the Korsmeyer–Peppas model. The n values calculated (see Table 7.1) indicated that the drug diffusion exponent, n increased from 0.19 to 0.78 when the MCNC-PE is exposed to the EMFs. This suggested that the presence of EMFs enhanced the release of curcumin. The magneto-controllable increases in drug released can be mainly ascribed to the disruption of MCNC-PE upon the introduction of EMFs. Under magnetic exposure, the adsorbed MCNC particles at oil-water interface turned magnetized and get attracted towards the field direction (Blanco *et al.*, 2013). As the particles get attracted and concentrated around the source of magnetic force, they induced a dilatational deformation of the fluid interface and thus releasing of the MCNC particles into the aqueous phase (Lam *et al.*, 2011). The escape of MCNC particles from the interfaces then de-stabilized the MCNC-PE and exposed the curcumin-loaded oil droplets to the buffer medium and thus resulted in higher release of curcumin. The disruption of MCNC-PEs under EMFs were observed in our emulsion photograph and optical microscopic images (Figure 7.4).

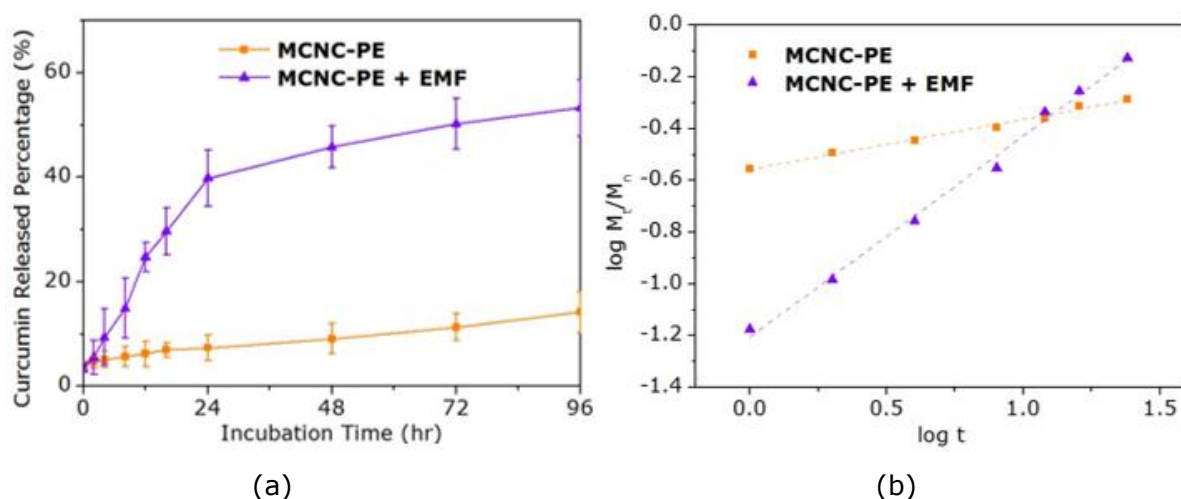


Figure 7.3. (a) Percent curcumin released from different emulsion samples under pH 7.5. (b) Plots of the release of curcumin from the both MCNC-PEs samples based on Korsmeyer–Peppas model.

Table 7.1 Release parameters of curcumin from different emulsion samples based on Korsmeyer – Peppas model. Different alphabetic letters was significantly different at $P \leq 0.05$ by Bonferroni's Multiple Comparison Test.

	n	R²
MCNC-PE	0.19 ^a	0.9904
MCNC-PE + EMF	0.78 ^b	0.9946

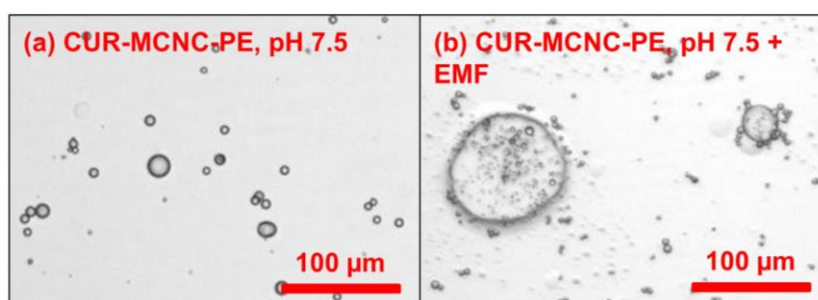


Figure 7.4. Optical microscopic image and photograph of MCNC-PE at pH 7.5 (a) without and (b) with exposure to oscillating EMF.

7.3.3 Anticolon Cancer Efficacy of Curcumin-loaded MCNC-PE

The potential use of curcumin-loaded MCNC-PE as the anti-colon cancer drug delivery system was examined by evaluating the cytotoxic effect of curcumin-loaded MCNC-PE against HCT116 colon cancer cell based on MTT assay. In brief, MTT assay is generally used to measure the mitochondrial activity in viable cells utilizing the activity of mitochondrial dehydrogenase enzyme, which convert the yellow tetrazolium MTT into purple formazan crystal. The amount of formazan crystal formed thus indicates the number of metabolically active viable cells (Twentyman and Luscombe, 1987). The cell viability of HCT116 cell line is monitored after 24, 48, 72 and 96 hours of treatment with a fixed concentration of the curcumin-loaded MCNC-PE with or without the presence of oscillating EMFs. For control study, the results suggested a negligible toxicity of bare MCNC-PE against the HCT116 colon cancer cell (Figure 7.5, orange bar). Besides that, another treatment using the blank MCNC-PE with EMFs revealed a 25 ± 2 % reduction in cell viability upon incubated for 96 hours

(green bar). This is most likely due to the magnetic hyperthermia effects implied by the MCNC particles that undergo dynamic hysteresis losses induced by Neel and Brownian relaxation processes, which thus induce a local heating effect that inhibited the growth of the colon cancer cells (Guibert *et al.*, 2015; Liu *et al.*, 2009; Oliveira *et al.*, 2013; Pradhan *et al.*, 2010). In fact, gradual cell viability reduction was observed when the HCT116 colon cancer cells were incubated with MCNC particles in the presence of the EMFs (Figure 7.6).

The MTT assay results obtained using the curcumin-loaded MCNC-PE showed that only 60 ± 1 % of the cells retained their viability upon 96 hours exposure to the drug loaded MCNC-PE (Figure 7.5, blue bar), suggesting a gradual release of curcumin across 4 days of incubation. As expected, the introduction of EMFs abruptly increases the termination of the living HCT116 cells, giving a total 82 ± 2 % cells death (purple bar) after 96 hours of treatment. These significant growth inhibitory activity not only indicates that the curcumin-loaded MCNC-PE exhibited certain extent of the cytotoxic effect on the colon cancer cell line HCT116, but also showed the significant improvement in cell growth inhibition from the synergistic effects between the triggered released of curcumin and the magnetic hyperthermia upon introduction of oscillating EMFs.

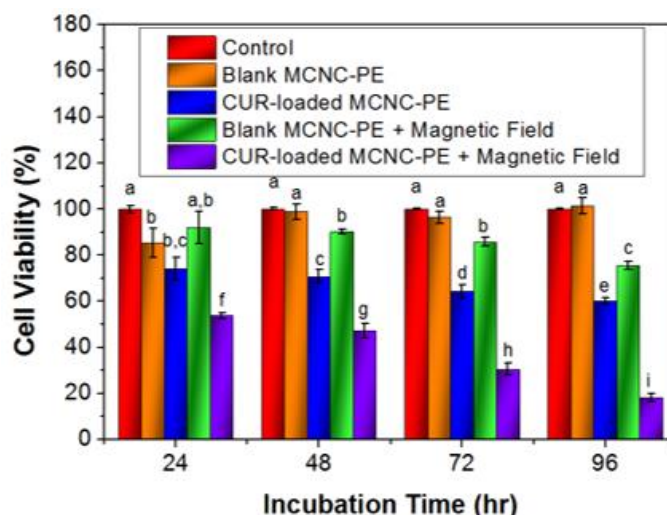


Figure 7.5. Cell viability test of curcumin-loaded MCNC-PE on HCT116 colon cancer cell line. The cell line analysis was performed using MCNC-PE stabilized by 0.1 wt% of MCNC nanocomposite, with curcumin content of $30 \mu\text{g/ml}$ of incubation serum (equivalent to 1 mg/ml oil basis). Error bar represents standard error in measurement. Different alphabetic letters was significantly different at $P \leq 0.05$ by Bonferroni's Multiple Comparison Test.

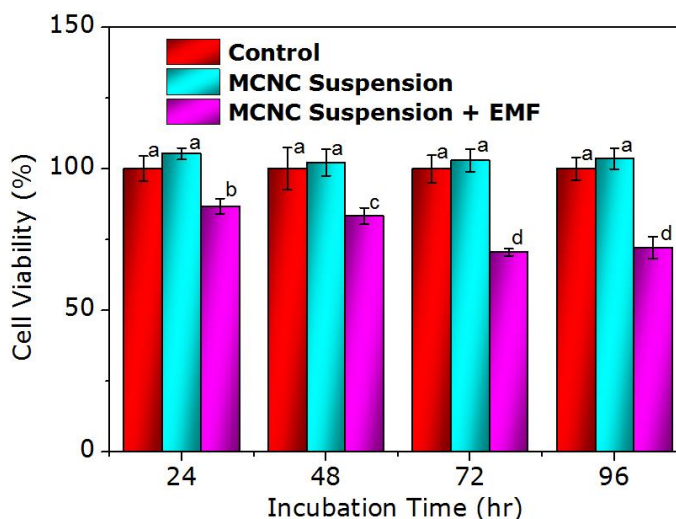


Figure 7.6. Cell viability test of MCNC suspensions with or without EMF on HCT116 colon cancer cell line. The cell line analysis was performed using 0.1 wt% of MCNC nanocomposite. Error bar represents standard error in measurement. Different alphabetic letters was significantly different at $P \leq 0.05$ by Bonferroni's Multiple Comparison Test.

Although significant cells toxicity results were obtained in the current investigation, it should be stressed that the MTT assay is not able to discern between cell growth inhibition and an increase in cell death. To proclaim the results from MTT assay, the optical image of the HCT116 cells after each incubation time point is captured. Firstly, obvious reduction in cell counts was observed 96 hours after incubating the HCT116 cells with the curcumin-loaded MCNC-PE (Figure 7.7). From the optical microscopy, most of the cells in control and blank MCNC-PE samples appeared as normal angular and spindle shapes (Figure 7.7a and b). In contrast, cell shrinkage with lesser cytoplasm mass was observed in cells treated with curcumin-loaded MCNC-PE as well as those with inclusion of EMFs (Figure 7.7c and d). The morphological results of HCT116 cells suggested that the cytotoxic effect of the curcumin-loaded carrier may be mediated through apoptotic cell death (Goh *et al.*, 2014).

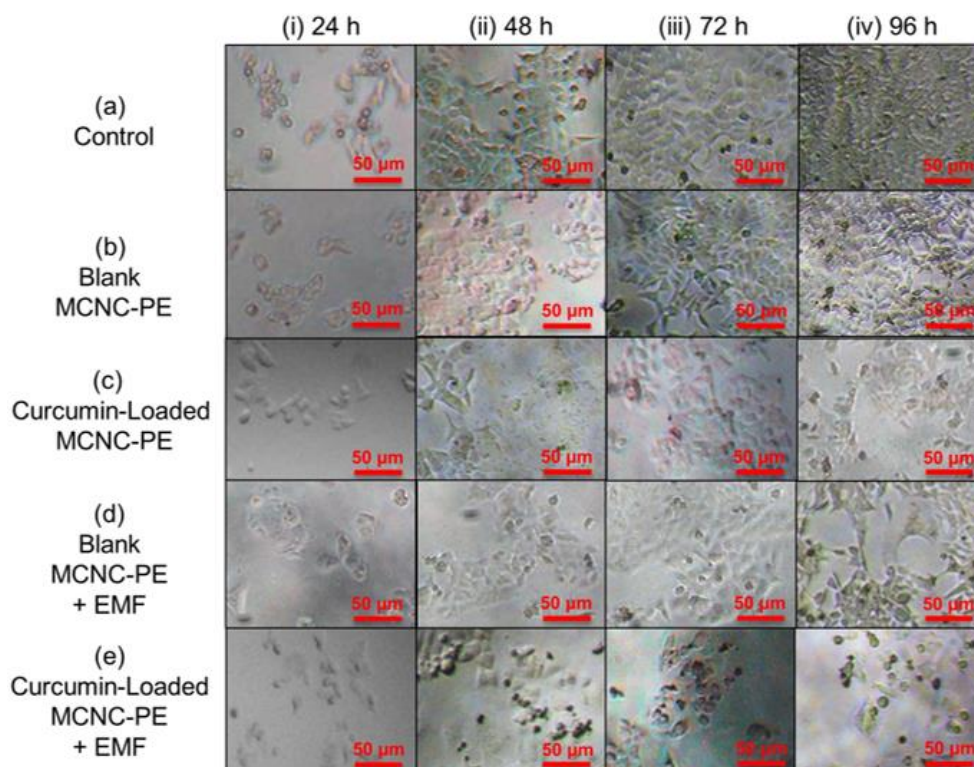


Figure 7.7. Morphological changes of HCT116 cells at different time point for (a) control, (b) pure curcumin, (c) blank MCNC-PE, (d) curcumin-loaded MCNC-PE and (e) curcumin-loaded MCNC-PE + EMF treated samples.

To further elucidate whether the HCT116 cell death induced by the carrier occurred through apoptosis induction, apoptosis detection was performed via Hoechst 33342 nuclear staining. As shown in Figure 7.8, the cells experienced notable nuclear morphological changes after treatment with curcumin-loaded MCNC-PE, suggesting cell death mediated by apoptosis. The non-treated cells were uniformly stained with faint blue fluorescence (Figure 7.8a). Contrarily, Figure 7.8b displayed an ascent in the intensity of blue fluorescence after treating the cells with the curcumin-loaded carrier. This specified the nuclear shrinkage or condensation, which is well known as one of the typical signs of apoptosis. Moreover, prolonged treatment of the cells resulted in marked increase in the intensity of blue fluorescence signals, showing the increased number of cells undergoing apoptosis. Overall the results from MTT assay, in conjunction with the optical micrograph and nuclear fluorescence images of the cells, have asserted the death of HCT116 cells upon

exposure to curcumin-loaded MCNC-PE. However, further studies under both *in-vitro* and *in-vivo* environment are still required to validate the effect of curcumin-loaded MCNC-PE on the viability of colon cancer cell. The Nile red stained MCNC-PE were also used to further evaluate the uptake interaction between the Pickering emulsion and cells. Figure 7.9 shows the distribution of the stained Pickering emulsions as well as the loaded CUR within HCT116 cells. The images evidently demonstrate a uniform distribution of Nile red and CUR within the cytoplasm of individual cells. This vastly suggests the effective uptake of MCNC-PE by the cells and further validated the toxicity of CUR-loaded MCNC-PE towards HCT116 cells.

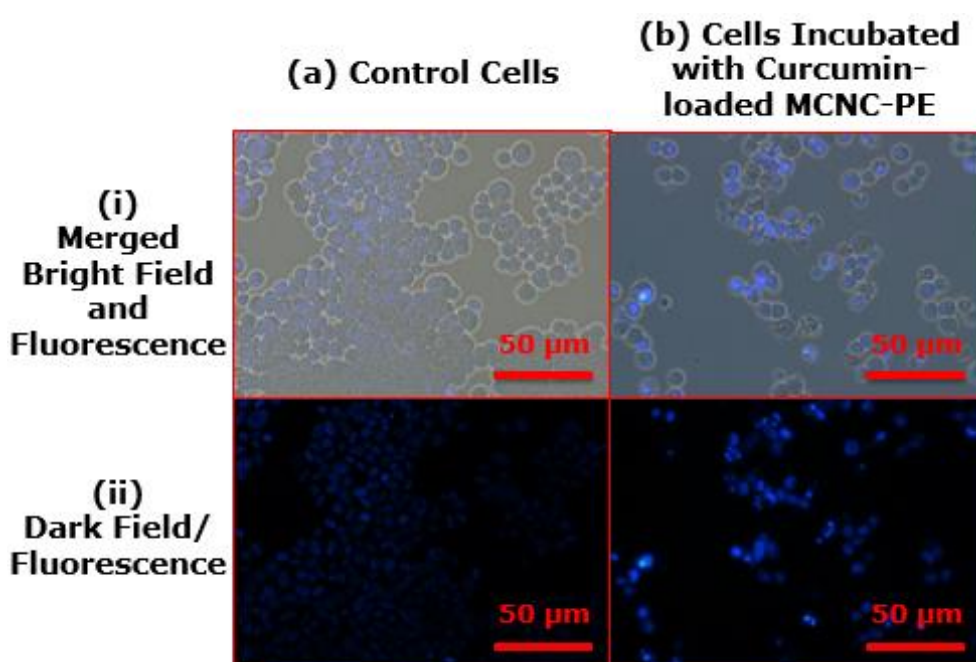


Figure 7.8. Nuclear morphology changes of HCT116 cells at 24 hour incubation for (a) control and (b) curcumin-loaded MCNC-PE treated samples.

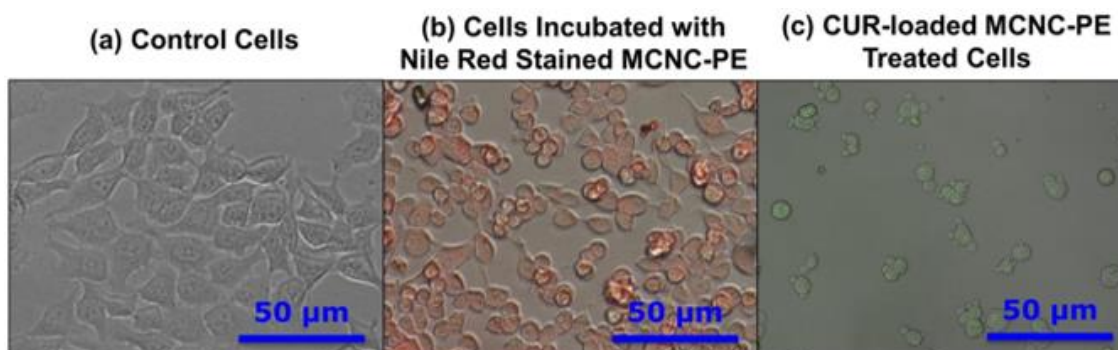


Figure 7.9. Bright field-fluorescence overlay images of HCT116 cells after 2 hours incubation (a) without treatment, (b) with Nile red stained MCNC-PE and (c) with CUR-loaded MCNC-PE.

7.4 Conclusions

In this work, the drug release profile and kinetics as well as the inhibition of colorectal cancer cell proliferation colorectal cancer cell proliferation *in-vitro* of palm-based MCNC-PEs were investigated and discussed. The results showed that a total of 39 % increase in the release of CUR from the MCNC-PE carrier was observed upon exposure to EMF. The *in-vitro* drug release study revealed that the bioactive diffusion process under magnetic field stimulus was much faster than that of without the influence of EMF. In order to assess the effect of EMF on intracellular release of CUR, colon cancer cells were exposed to MCNC-PE media and then subjected of EMF for consecutive 4 days. Results showed that the magnetic field was able to stimulate and cause more bioactive to be released from CUR-loaded MCNC-PE into intracellular compartment and induced a remarkable increase of about 82 % in cell toxicity compared to that of without EMF exposure (40 %). Conversely, negligibly low or no cytotoxic effect was observed in both blank MCNC-PE and control respectively. Both the optical microscopy and fluorescence images suggested that the CUR-induced cell death in colorectal cancer cells is inhabited by apoptosis process. It is believed that upon exposure to EMF, the magnetic field not only triggers and further increases the release rate of CUR from MCNC-PE but also generates a very local heating through dynamic hysteresis loss induced by Brownian and Néel relaxation process at the micron scale, causing synergistic CUR and magnetic hyperthermia-induced cell toxicity with enhanced anti-colon cancer efficacy. Overall, the results of our study provided a road map for rational design of magnetic Pickering emulsions as bioactive and therapeutic colloidal drug delivery system, which coupled with external magnetic stimulus, can improve inhibitory effect on the cell viability and differentiation.

FUTURE WORKS

Following several investigations as described above, three main research areas arising from this thesis that need to be explored for future work in conjunction with the design and development of MCNC-based palm olein Pickering emulsion as novel controlled drug delivery system:

I. Facile Sonochemical Preparation of Oil Palm Mesocarp Fiber (OPMF)-based MCNCs as Sustainable Pickering Stabilizer

A facile sonochemical co-precipitation method had been developed to produce well-dispersed MCNC nanocomposites. This simple yet rapid approach not only inhibited the oxidation of Fe_3O_4 to Fe_2O_3 but also gave rise to the formation of MCNCs with higher magnetic strength. However, the preparation of magnetic palm-derived CNCs using proposed sonochemical technique has not been tested and reported. In Malaysia, oil palm mesocarp fiber (OPMF) is the biomass residue or waste generated in the palm oil mill after oil extraction stage. Being rich in lignocellulose, there is potential for the production of MCNCs based on the nanocellulose isolated from OPMF as particle stabilizers for colloidal drug delivery purposes.

II. Investigation of Controlled On-demand Drug Release of MCNC-PE under Pulsed Electromagnetic Fields (PEMF)

The developed MCNC-PE containing curcumin as model drug was subjected to in-vitro release study under a static EMF. The results demonstrated that the exposure to EMF significantly enhanced the release of bioactive from the emulsion template. Static magnetic stimulus changed the drug release kinetics from Fickian diffusion to anomalous transport. However, the manipulation of drug release from MCNC-PE under pulsed magnetic fields has not yet been explored. Thus, a proper study and verification of on-demand triggered release mechanism under PEMF should be considered in the future work.

III. *in vivo* Evaluation and Cancer Targeting Potential of Bioactive-loaded MCNC-PE

In vitro findings demonstrated that the curcumin-loaded MCNC-PE was capable of inhibiting the growth of HCT116 colon cancer cells, particularly in presence of EMF. Nevertheless, extensive research in the establishment of *in vitro* biodistribution and toxicity studies is required in the future. *In vivo* testing is of paramount importance in translate scientific findings into practical clinical applications. Besides, the possibility of targeted cancer therapy can also be explored by functionalizing the MCNC-PE and coupling it to monoclonal antibodies (mAb), a targeting ligand for colorectal cancer cells (CRC). Targeting CRC tumours with ligand-functionalized MCN-PE represents a new promising active targeting approach and can be potentially used to treat advanced colorectal cancer.

REFERENCES

- Adar, F. (2014) Molecular Spectroscopy Workbench: Raman Spectra of Metal Oxides. [online] Available at: http://www.horiba.com/fileadmin/uploads/Scientific/Documents/Raman/Specy_WorkBench-FAdar-Raman_Spectra_of_Metal_Oxides-Oct_2014.pdf [Accessed 10th July, 2016].
- Agarwal, U. P., Sabo, R., Reiner, R. S., Clemons, C. M., and Rudie, A. W. (2012). Spatially Resolved Characterization of Cellulose Nanocrystal-Polypropylene Composite by Confocal Raman Microscopy. *Applied Spectroscopy*, 66(7), pp.750–756.
- Agotegaray, M., Palma, S., and Lassalle, V. (2014). 'Novel Chitosan Coated Magnetic Nanocarriers For The Targeted Diclofenac Delivery'. *j. nanosci. Nanotech*, 14(5), pp.3343–3347.
- Ahmed, S., Dong, J., Yui, M., Kato, T., Lee, J., and Park, E. Y. (2013). Quantum dots incorporated magnetic nanoparticles for imaging colon carcinoma cells. *Journal of Nanobiotechnology*, 11(1), pp.28–36.
- Akhlaghi, S., Berry, R., and Tam, K. (2013). Surface modification of cellulose nanocrystal with chitosan oligosaccharide for drug delivery applications. *Cellulose*, 20(4), pp.1747–1764.
- Anirudhan, T. S. and Rejeena, S. R. (2014). Aminated B -Cyclodextrin-Modified-Carboxylated Magnetic Cobalt/Nanocellulose Composite For Tumor-Targeted Gene Delivery. *Journal of Applied Chemistry*, 2014, pp.1–10.
- Anuchapreeda, S., Fukumori, Y., Okonogi, S., and Ichikawa, H. (2012). Preparation of Lipid Nanoemulsions Incorporating Curcumin for Cancer Therapy. *Journal of Nanotechnology*, 2012, pp.1–11.
- Apsel, S. E., Emmert, J. W., Deng, J., and Bloomfield, L. A. (1996). Surface-Enhanced Magnetism in Nickel Clusters. *Physical Review Letters*, 76(9), pp.1441–1444.
- Ashby, N. and Binks, B. P. (2000). Pickering emulsions stabilised by Laponite clay particles.

Physical Chemistry Chemical Physics, 2(24), pp.5640–5646.

Aveyard, R., Binks, B. P., and Clint, J. (2003) Emulsions Stabilised Solely By Colloidal Particles. *Advances in Colloid and Interface Science*, 100-102, pp.503–546.

Awwad, A. M. and Salem, N. M. (2012). A Green and Facile Approach for Synthesis of Magnetite Nanoparticles. *Nanoscience and Nanotechnology*, 2(6), pp.208–213.

Axe, J. (2015). 8 Colloidal Silver -Benefits & Uses-. Retrieved July 29, 2015, from <http://draxe.com/colloidal-silver-benefits/>

AzoNano.com. (2013). Dynamic Light Scattering - Understanding the Basics. Retrieved August 3, 2015, from <http://www.azonano.com/article.aspx?ArticleID=3662>

Bang, J. and Suslick, K. S. (2007). Sonochemical synthesis of nanosized hollow hematite. *Journal of the American Chemical Society*, 129(8), pp.2242–2243.

Bean, C. P. and Livingston, J. D. (1959). Superparamagnetism. *Journal of Applied Physics*, 30(4), p.S120

Binks, B. P. and Lumsdon, S. O. (2000a). Catastrophic Phase Inversion of Water-in-Oil Emulsions Stabilized by Hydrophobic Silica. *Langmuir*, 16(6), pp.2539–2547.

Binks, B. P. and Lumsdon, S. O. (2000b). Effects of oil type and aqueous phase composition on oil–water mixtures containing particles of intermediate hydrophobicity. *Physical Chemistry Chemical Physics*, 2(13), pp.2959–2967.

Binks, B. P. and Lumsdon, S. O. (2000c). Influence of Particle Wettability on the Type and Stability of Surfactant-Free Emulsions†. *Langmuir*, 16(23), pp.8622–8631.

Binks, B. P. and Lumsdon, S. O. (2001). Pickering emulsions stabilized by monodisperse latex particles: effects of particle size. *Langmuir*, 17(15), pp.4540–4547.

Binks, B. P. (2002). Particles as surfactants—similarities and differences. *Current Opinion in Colloid & Interface Science*, 7(1-2), pp.21–41.

- Blanco, E., Lam, S., Smoukov, S. K., Velikov, K. P., Khan, S. A., and Veley, O. D. (2013). Stability and Viscoelasticity of Magneto-Pickering Foams. *Langmuir*, 29(32), pp.10019–10027
- Boateng, J., Verghese, M., Chawan, C. B., Shackelford, L., Walker, L. T., Khatiwada, J., and Williams, D. S. (2006). Red palm oil suppresses the formation of azoxymethane (AOM) induced aberrant crypt foci (ACF) in Fisher 344 male rats. *Food and Chemical Toxicology*, 44(10), pp.1667–1673.
- Bogart, L. K., Pourroy, G., Murphy, C. J., Puentes, V., Pellegrino, T., Rosenblum, D., Peer, D., and Lévy, R. (2014). Nanoparticles for imaging, sensing, and therapeutic intervention. *ACS nano*, 8(4), pp.3107–3122.
- Bonferoni, M. C., Sandri, G., Delleria, E., Rossi, S., Ferrari, F., Mori, M., and Caramella, C. (2014). Ionic polymeric micelles based on chitosan and fatty acids and intended for wound healing. Comparison of linoleic and oleic acid. *European Journal of Pharmaceutics and Biopharmaceutics: Official Journal of Arbeitsgemeinschaft Für Pharmazeutische Verfahrenstechnik e.V.*, 87(1), pp.101–106.
- Bonnie, T. Y. P. and Choo, Y. M. (2000). Valuable minor constituents of commercial red palm olein: carotenoids, vitamin E, ubiquinones and sterols. *Journal of Oil Palm Research*, 12(1), oo. 14–24.
- Borase, H. P., Patil, C. D., Salunkhe, R. B., Suryawanshi, R. K., Salunke, B. K., and Patil, S. V. (2014). Catalytic and synergistic antibacterial potential of green synthesized silver nanoparticles: Their ecotoxicological evaluation on *Poecillia reticulata*. *Biotechnology and Applied Biochemistry*, 61(4), pp.385–394.
- Brailsford, F. (1966). *Physical Principles of Magnetism*. *van Nostrand*. London, England. Chapters 2 and 5 on §1.
- Caenn, R., Darley, H., and Gray, G. (2011). *Composition And Properties Of Drilling And Completion Fluids*; Gulf Professional Pub.: Waltham, MA, pp.537–596.

- Cai, Y., Shen, Y., Xie, A., Li, S., and Wang, X. (2010). Green synthesis of soya bean sprouts-mediated superparamagnetic Fe₃O₄ nanoparticles. *Journal of Magnetism and Magnetic Materials*, 322(19), pp.2938–2943.
- Capron, I. and Cathala, B. (2013). Surfactant-Free High Internal Phase Emulsions Stabilized by Cellulose Nanocrystals. *Biomacromolecules*, 14(2), pp.291–296.
- Carmen Bautista, M., Bomati-Miguel, O., del Puerto Morales, M., Serna, C., and Veintemillas-Verdaguer, S. (2005). Surface characterisation of dextran-coated iron oxide nanoparticles prepared by laser pyrolysis and coprecipitation. *Journal of Magnetism and Magnetic Materials*, 293(1), pp.20–27.
- Chin, S. F., Binti Romainor, A. N., and Pang, S. C. (2014). Fabrication of hydrophobic and magnetic cellulose aerogel with high oil absorption capacity. *Materials Letters*, 115, pp.241–243.
- Chen, C. -W. (1977a). Ferromagnetism AND Ferrimagnetism. In E. P. Wohlfarth, ed. *Magnetism and Metallurgy of Soft Magnetic Materials*. New York, USA: Elsevier North-Holland Inc., pp.15–60.
- Chen, C. -W. (1977b). INTRODUCTION. In E. P. Wohlfarth, ed. *Magnetism and Metallurgy of Soft Magnetic Materials*. New York, USA: Elsevier North-Holland Inc., pp.1–14.
- Chen, J. H., Cheng, C. -Y., Chiu, W. -Y., Lee, C. -F., and Liang, N. -Y. (2008). Synthesis of ZnO/polystyrene composites particles by Pickering emulsion polymerization. *European Polymer Journal*, 44(10), pp.3271–3279.
- Chen, H., Khemtong, C., Yang, X., Chang, X., and Gao, J. (2011). Nanonization strategies for poorly water-soluble drugs. *Drug Discovery Today*, 16(7-8), pp.354–360.
- Cherian, B. M., Leão, A. L., Souza, S. F. de, Olyveira, G. M. de, Costa, L. M. M., Brandão, C. V. S., and Narine, S. S. (2013). Bacterial Nanocellulose for Medical Implants. In S.

- Thomas, P. M. Visakh, & A. P. Mathew (Eds.), *Advances in Natural Polymers* (Vol. 18, pp. 337–359). Berlin, Heidelberg: Springer Berlin Heidelberg.
- Chevalier, Y. and Bolzinger, M. (2013). Emulsions stabilized with solid nanoparticles: Pickering emulsions. *Colloids and Surfaces A: Physicochemical and Engineering Aspects*, 439, pp.23–34.
- Choi S. J., Won J. W., Park K. M., and Chang P. -S. (2014). A new method for determining the emulsion stability index by backscattering light detection. *Journal of Food Process Engineering*, 37, pp.229–236.
- Criado, P., Frascini, C., Salmieri, S., Becher, D., Safrany, A., and Lacroix, M. (2016). Free radical grafting of gallic acid (GA) on cellulose nanocrystals (CNCS) and evaluation of antioxidant reinforced gellan gum films. *Radiation Physics and Chemistry*, 118, pp.61–69.
- Cunha, A. G., Mougel, J., Cathala, B., Berglund, L. A., and Capron, I. (2014). Preparation of Double Pickering Emulsions Stabilized by Chemically Tailored Nanocelluloses. *Langmuir*, 30(31), pp.9327–9335.
- Dang, F., Kamada, K., Enomoto, N., Hojo, J., and Enpuku, K. (2007). Sonochemical Synthesis Of The Magnetite Nanoparticles In Aqueous Solution. *Journal of the Ceramic Society of Japan*, 115(1348), pp.867–872.
- Dang, F., Enomoto, N., Hojo, J., and Enpuku, K. (2009). Sonochemical Synthesis Of Monodispersed Magnetite Nanoparticles By Using An Ethanol–Water Mixed Solvent. *Ultrasonics Sonochemistry*, 16(5), pp.649–654.
- Demetriades, K., Coupland, J. N., and McClements, D. J. (1997). Physical Properties of Whey Protein Stabilized Emulsions as Related to pH and NaCl. *Journal of Food Science*, 62(2), pp.342–347.

- Destribats, M., Rouvet, M., Gehin-Delval, C., Schmitt, C., and Binks, B. (2014). Emulsions Stabilised By Whey Protein Microgel Particles: Towards Food-Grade Pickering Emulsions. *Soft Matter*, 10(36), pp.6941–6954.
- Dhar, P., Kumar, A., and Katiyar, V. (2016). Magnetic Cellulose Nanocrystal Based Anisotropic Polylactic Acid Nanocomposite Films: Influence On Electrical, Magnetic, Thermal, And Mechanical Properties. *ACS Appl. Mater. Interfaces*, 8(28), pp.18393-18409.
- Dickinson, E. (1992). *An Introduction to Food Colloids*. Oxford Univ. Press, Oxford, United Kingdom.
- Dickinson, E. (2012). Use of nanoparticles and microparticles in the formation and stabilization of food emulsions. *Trends in Food Science & Technology*, 24(1), pp.4–12.
- Dixon, A., Dhanaliwala, A., Chen, J., and Hossack, J. (2013). Enhanced intracellular delivery of a model drug using microbubbles produced by a microfluidic device. *Ultrasound in medicine & biology*, 39(7), pp.1267–1276.
- Dolores, R., Raquel, S., and Adianez, G. (2015). Sonochemical Synthesis of Iron Oxide Nanoparticles Loaded with Folate and Cisplatin: Effect of Ultrasonic Frequency'. *Ultrasonics Sonochemistry*, 23, pp.391–398.
- Dong, X. M., Revol, J. F., and Gray, D. G. (1998). Effect of microcrystallite preparation conditions on the formation of colloid crystals of cellulose, *Cellulose*, 5(1), pp.19–32.
- Dorniani, D., Hussein, M., Kura, A., Fakurazi, S., Shaari, A., and Ahmad, Z. (2012). Preparation of Fe₃O₄ magnetic nanoparticles coated with gallic acid for drug delivery. *International journal of nanomedicine*, 7, pp.5745–5756.
- Dufresne, A. (2006). Comparing the Mechanical Properties of High Performances Polymer Nanocomposites from Biological Sources. *Journal of Nanoscience and Nanotechnology*, 6(2), pp.322–330.
- Dufresne, A. (2008). Polysaccharide nano crystal reinforced nanocomposites. *Canadian*

Journal of Chemistry, 86(6), pp.484–494.

Dyab, A. K. F., Al-Lohedan, H. A., Essawy, H. A., Abd El-Mageed, A. I. A., and Taha, F. (2014). Fabrication of core/shell hybrid organic–inorganic polymer microspheres via Pickering emulsion polymerization using laponite nanoparticles. *Journal of Saudi Chemical Society*, 18(5), pp.610–617.

El Azzouzi, S. (2006). Auto Organisation de whiskers de cellulose en suspension dans l'eau ou dans les solvants organiques apolaires, PhD thesis, Joseph Fourier University, Grenoble.

Fabiilli, M. L. (2010). *Ultrasound-Triggered Drug Delivery using Acoustic Droplet Vaporization*. The University of Michigan.

Fabiilli, M. L., Haworth, K. J., Sebastian, I. E., Kripfgans, O. D., Carson, P. L., and Fowlkes, J. B. (2010). Delivery of chlorambucil using an acoustically-triggered perfluoropentane emulsion. *Ultrasound in Medicine & Biology*, 36(8), pp.1364–1375.

Frelichowska, J., Bolzinger, M. -A., Pelletier, J., Valour, J. -P., and Chevalier, Y. (2009a). Topical delivery of lipophilic drugs from o/w Pickering emulsions. *International Journal of Pharmaceutics*, 371(1-2), pp.56–63.

Frelichowska, J., Bolzinger, M. -A., Valour, J. -P., Mouaziz, H., Pelletier, J., and Chevalier, Y. (2009b). Pickering w/o emulsions: drug release and topical delivery. *International Journal of Pharmaceutics*, 368(1-2), pp.7–15.

Fortin, J., Wilhelm, C., Servais, J., M'enager, C., Bacri, J. and Gazeau, F. (2007). Size-sorted anionic iron oxide nanomagnets as colloidal mediators for magnetic hyperthermia. *Journal of the American Chemical Society*, 129(9), pp.2628–2635.

Fujii, S., Okada, M., and Furuzono, T. (2007). Hydroxyapatite nanoparticles as stimulus-responsive particulate emulsifiers and building block for porous materials. *Journal of Colloid and Interface Science*, 315(1), pp.287–296.

- Gatenholm, P. and Klemm, D. (2010). Bacterial Nanocellulose as a Renewable Material for Biomedical Applications. *MRS Bulletin*, 35(3), pp.208–213.
- Gautier, F., Destribats, M., Perrier-Cornet, R., Dech'ezelles, J., Giermanska, J., H'eroguez, V., Ravaine, S., Leal-Calderon, F., and Schmitt, V. (2007). Pickering emulsions with stimuable particles: from highly-to weakly-covered interfaces. *Physical Chemistry Chemical Physics*, 9(48), pp.6455–6462.
- Gnanaprakash, G., Philip, J., Jayakumar, T., and Raj, B. (2007). Effect Of Digestion Time And Alkali Addition Rate On Physical Properties Of Magnetite Nanoparticles. *The Journal of Physical Chemistry B*, 111(28), pp.7978–7986.
- Goh, B. H., Chan, C. K., Kamarudin, M. N. A., and Kadir, H. A. (2014). Swietenia macrophylla King induces mitochondrial-mediated apoptosis through p53 upregulation in HCT116 colorectal carcinoma cells. *J. Ethnopharmacol*, 153(2), pp.375–385.
- Gong, X., Wang Y., and Chen, L. (2017). Enhanced emulsifying properties of wood-based cellulose nanocrystals as Pickering emulsion stabilizer. *Carbohydrate Polymers*, 169, pp.295–303.
- Gonzalez-Fernandez, M. A., Torres, T., Andrés-Vergés, M., Costo, R., Presa, P., Serna, C. J., Morales, M. P., Marquina, C., Ibarra, M. R., and Goya, G. F. (2009). Magnetic Nanoparticles for Power Absorption: optimizing size, shape and magnetic properties. *Journal of Solid State Chemistry*, 182(10), pp.1–15.
- Gu, J., Catchmark, J., Kaiser, E., and Archibald, D. (2013). Quantification of cellulose nanowhiskers sulfate esterification levels. *Carbohydrate Polymers*, 92(2), pp.1809–1816.
- Guibert, C., Dupuis, V., Peyre, V., and Fresnais, J. (2015) Hyperthermia of Magnetic Nanoparticles: Experimental Study of the Role of Aggregation, *J. Phys. Chem. C*, 119(50), pp.28148–28154.

- Guzey, D. and McClements, D. J. (2006). Formation, stability and properties of multilayer emulsions for application in the food industry. *Advances in Colloid and Interface Science*, 128-130, pp.227–248.
- Habibi, Y., Lucia, L. A., and Rojas, O. J. (2010). Cellulose Nanocrystals: Chemistry, Self-Assembly, and Applications. *Chem. Rev.*, 110(6), pp.3479–3500.
- Hamad, W. (2006). On the Development and Applications of Cellulosic Nanofibrillar and Nanocrystalline Materials. *Can. J. Chem. Eng.*, 84(5), pp.513–519.
- Hanesch, M. (2009). Raman Spectroscopy Of Iron Oxides And (Oxy)Hydroxides At Low Laser Power And Possible Applications In Environmental Magnetic Studies. *Geophysical Journal International*, 177(3), pp.941–948.
- He, Y., Wu, F., Sun, X., Li, R., Guo, Y., Li, C., Zhang, L., Xing, F., Wang, W., and Gao, J. (2013). Factors That Affect Pickering Emulsions Stabilized By Graphene Oxide. *ACS Appl. Mater. Interfaces*, 5(11), pp.4843–4855.
- Helbert, W., Chanzy, H., Husum, T. L., Schüle, M., and Ernst, S. (2003). Fluorescent cellulose microfibrils as substrate for the detection of cellulase activity. *Biomacromolecules*, 4(3), pp.481–487.
- Hitchhiker's Guide. (2015). Domain Theory. *Institute of Rock Magnetism, University of Minnesota*. [ONLINE] Available at: http://www.irm.umn.edu/hg2m/hg2m_d/hg2m_d.html. [Accessed 24th June 2015]
- Huang, Hailong Yu, and Qiaomei Ru. (2010). Bioavailability and Delivery of Nutraceuticals Using Nanotechnology. *Concise Reviews and Hypotheses in Food Science*, 75(1), pp.50–57.
- Israelachvili, J. N. (1992). *Intermolecular and surface forces*. London: Academic Press.
- Jadhav, N. V., Prasad, A. I., Kumar, A., Mishra, R., Dhara, S., Babu, K., Prajapat, C., Misra, N., Ningthoujam, R., Pandey, B., and Vatsa, R. (2013). Synthesis Of Oleic Acid

Functionalized Fe₃O₄ Magnetic Nanoparticles And Studying Their Interaction With Tumor Cells For Potential Hyperthermia Applications. *Colloids and Surfaces B: Biointerfaces*, 108, pp.158–168.

Jatin, K., Somnath, S., and Dash, A. K. (2010). Multiple Emulsion. In M. Fanun (Ed.), *Colloids in Drug Delivery* (1st ed., pp. 177–202). New York, USA: CRC Press. Retrieved from <https://books.google.com/books?id=JF1w6m6Kmd4C&pgis=1>

Jia, X., Xu, R., Shen, W., Xie, M., Abid, M., Jabbar, S., Wang, P., Zeng, X., and Wu, T. (2015). Stabilizing Oil-In-Water Emulsion With Amorphous Cellulose. *Food Hydrocolloids*, 43, pp.275–282.

Johnston, J. H., Moraes, J., and Borrmann, T. (2005). Conducting Polymers on Paper Fibres. *Synthetic Metals*, 153(1-3), pp.65–68.

Johnston, H., Kelly, F. M., Moraes, J., Borrmann, T., and Flynn, D. (2006). Conductive polymer composites with cellulose and protein fibres. *Curr. Appl. Phys.* 6(3), pp.587–590.

Ju, X., Bowden, M., Brown, E., and Zhang, X. (2015). An improved X-ray diffraction method for cellulose crystallinity measurement. *Carbohydrate Polymers*, 123, pp.476–481.

Kalashnikova, I., Bizot, H., Cathala, B., and Capron, I. (2011). New Pickering Emulsions Stabilized by Bacterial Cellulose Nanocrystals. *Langmuir*, 27(12), pp.7471–7479.

Kalashnikova, I., Bizot, H., Cathala, B., and Capron, I. (2012). Modulation of cellulose nanocrystals amphiphilic properties to stabilize oil/water interface. *Biomacromolecules*, 13(1), pp.267–275.

Kalska-Szostko, B., Wykowska, U., Satula, D., and Nordblad, P. (2015). Thermal treatment of magnetite nanoparticles. *Beilstein J. Nanotechnol.*, 6, pp.1385–1396.

Kamel, S. (2007). Nanotechnology and its applications in lignocellulosic composites, a mini review. *Express Polym. Lett.*, 1(9), pp.546–575.

- Kaptay, G. (2006). On the equation of the maximum capillary pressure induced by solid particles to stabilize emulsions and foams and on the emulsion stability diagrams. *Colloids and Surfaces A: Physicochemical and Engineering Aspects*, 282-283, pp.387–401.
- Katepalli, H. (2014). *Formation and Stability of Emulsions: Effect of Surfactant-Particle Interactions and Particle Shape*. University of Rhode Island.
- Kentish, S., Wooster, T. J., Ashokkumar, M., Balachandran, S., Mawson, R., and Simons, L. (2008). The use of ultrasonics for nanoemulsion preparation. *Innov. Food Sci. & Emerg. Technol.*, 9, pp.170–175
- Khan, M. K. and Sundararajan, P. (2011). Encapsulation of dye molecules and nanoparticles in hollow organogelfibers of a nonchiral polyurethane model compound. *Chem. Eur. J.*, 17(4), pp.1184–1192.
- Kim, D., Mikhaylova, M., Wang, F., Kehr, J., Bjelke, B., Zhang, Y., Tsakalagos, T., and Muhammed, M. (2003). Starch-Coated Superparamagnetic Nanoparticles as MR Contrast Agents. *Chemistry of Materials*, 15(23), pp.4343–4351.
- Kim, D. K., Zhang, Y., Kehr, J., Klason, T., Bjelke, B., and Muhammed, M. (2001). Characterization and MRI study of surfactant-coated superparamagnetic nanoparticles administered into the rat brain. *Journal of Magnetism and Magnetic Materials*, 225(1-2), pp.256–261.
- Kim, K., Kim, S., Ryu, J., Jeon, J., Jang, S. G., Kim, H., Gweon, D., Im, W. B., Han, Y., Kim, H., and Choi, S. Q. (2017). Processable high internal phase Pickering emulsions using depletion attraction. *Nature Communications*, 8, pp.1–8.
- Kim, Y. J., Liu, Y. D., Choi, H. J., and Park, S. -J. (2013). Facile fabrication of Pickering emulsion polymerized polystyrene/laponite composite nanoparticles and their electrorheology. *Journal of Colloid and Interface Science*, 394, pp.108–114.

- Kokal, S. and Wingrove, M. (2000). Emulsion Separation Index: From Laboratory To Field Case Studies. In *SPE Annual Technical Conference and Exhibition*; Society of Petroleum Engineers: Dallas.
- Komaiko, J. S. and McClements, D. J. (2016). Formation of Food-Grade Nanoemulsions Using Low-Energy Preparation Methods: A Review of Available Methods. *Comprehensive Reviews in Food Science and Food Safety*, 15(2), pp.331–352.
- Lam, S., Blanco, E., Smoukov, S. K., Velikov, K. P., Khan, S. A., and Veleev, O. D. (2011). Magnetic Responsive Pickering Foams, *J. Am. Chem. Soc.*, 133(35), pp.13856–13859.
- Lan, Q., Liu, C., Yang, F., Liu, S., Xu, J., and Sun, D. (2007). Synthesis of bilayer oleic acid-coated Fe₃O₄ nanoparticles and their application in pH-responsive Pickering emulsions. *Journal of Colloid and Interface Science*, 310(1), pp.260–269.
- Lattuada, M. and Hatton, T. A. (2007). Functionalization of monodisperse magnetic nanoparticles. *Langmuir: the ACS journal of surfaces and colloids*, 23(4), pp.2158–2168.
- Lee, G., Kang, H., Lee, S. C., Kweon, K., and Kim, H. J. (2010). Large-scale Facile Synthesis of Monodisperse Iron Oxide Nanoparticles in Alcohol. *Journal of Analytical Science & Technology*, 1(2), pp.130–133.
- Lee, J.-H., Blumenthal, R., and Ivkov, R. (2014). Magnetically Triggered Drug Release from Liposome Embedded Gel. *Journal of Nanomedicine & Biotherapeutic Discovery*, 4(3), 1000130, pp.1–6.
- Lee, Y., Du, Z., Lin, W., and Yang, Y. (2006). Monolayer behavior of silica particles at air/water interface: a comparison between chemical and physical modifications of surface. *Journal of colloid and interface science*, 296(1), pp.233–241.
- Li, C., Sun, P., and Yang, C. (2012). Emulsion stabilized by starch nanocrystals. *Starch - Stärke*, 64(6), pp.497–502.

- Li, J., Hughes, A. D., Kalantar, T. H., Drake, I. J., Tucker, C. J., and Moore, J. S. (2014). Pickering-Emulsion-Templated Encapsulation of a Hydrophilic Amine and Its Enhanced Stability Using Poly(allyl amine). *ACS Macro Lett.*, 3(10), pp.976–980.
- Li, P., Jiang, E. Y., and Bai, H. L. (2011). Fabrication of ultrathin epitaxial $\gamma\text{Fe}_2\text{O}_3$ films by reactive sputtering. *J. Phys. D: Appl. Phys.*, 44(7), pp.075003.
- Li, Y., Zhu, H., Gu, H., Dai, H., Fang, Z., Weadock, N. J., Guo, Z., and Hu, L. (2013). Strong Transparent Magnetic Nanopaper Prepared By Immobilization Of Fe_3O_4 Nanoparticles In A Nanofibrillated Cellulose Network. *Journal of Materials Chemistry A*, 1(48), pp.15278–15283.
- Li, Z., Xiao, M., Wang, J., and Ngai, T. (2013). Pure Protein Scaffolds from Pickering High Internal Phase Emulsion Template. *Macromol. Rapid Commun.*, 34(2), pp.169–174.
- Liao, M. and Chen, D. (2002). Preparation and characterization of a novel magnetic nano-adsorbent. *Journal of Materials Chemistry*, 12(12), pp.3654–3659.
- Lin, K.-Y. A., Yang, H., Petit, C., and Lee, W. (2015). Magnetically controllable Pickering emulsion prepared by a reduced graphene oxide-iron oxide composite. *Journal of Colloid and Interface Science*, 438, pp.296–305.
- Lin, N. and Dufresne, A. (2014). Surface chemistry, morphological analysis and properties of cellulose nanocrystals with gradiented sulfation degrees. *Nanoscale*, 6(10), pp.5384–5393.
- Lin, N., Huang, J., and Dufresne, A. (2012). Preparation, properties and applications of polysaccharide nanocrystals in advanced functional nanomaterials: a review. *Nanoscale*, 4(11), pp.3274–3294.
- Lin, N., Huang, J., Chang, P. R., Feng, L., and Yu, J. (2011). Effect of polysaccharide nanocrystals on structure, properties, and drug release kinetics of alginate-based microspheres. *Colloids and Surfaces B: Biointerfaces*, 85(2), pp.270–279.

- Linderoth, S., Hendriksen, P., Bødker, F., Wells, S., Davies, K., Charles, S., and Mørup, S. (1994). On Spin-Canting In Maghemite Particles. *J. Appl. Phys.*, 75(10), pp.6583–6585.
- Liu, F. and Tang, C. -H. (2013). Soy Protein Nanoparticle Aggregates as Pickering Stabilizers for Oil-in-Water Emulsions. *Journal of Agricultural and Food Chemistry*, 61(37), pp.8888–8898.
- Liu, H., Wang, C., Zou, S., Wei, Z., and Tong, Z. (2012). Simple reversible emulsion system switched by pH on the basis of chitosan without any hydrophobic modification. *Langmuir*, 28, pp.11017–11024.
- Liu, K., Nasrallah, J., Chen, L., Huang, L., and Ni, Y. (2015). Preparation of CNC-dispersed Fe₃O₄ nanoparticles and their application in conductive paper. *Carbohydrate Polymers*, 126, pp.175–178.
- Liu, S., Luo, X., and Zhou, J. (2013). Magnetic Responsive Cellulose Nanocomposites and Their Applications, Cellulose - Medical, Pharmaceutical and Electronic Applications, Dr. Theo G.M. Van De Ven (Ed.), InTech, pp.105–124. Available from: <http://www.intechopen.com/books/cellulose-medical-pharmaceutical-and-electronic-applications/magnetic-responsive-cellulose-nanocomposites-and-their-applications>.
- Liu, T., Liu, K., Liu, D., Chen, S., and Chen, I. (2009). Temperature-Sensitive Nanocapsules for Controlled Drug Release Caused by Magnetically Triggered Structural Disruption. *Adv. Funct. Mater.*, 19(4), pp.616–623.
- Loganathan, R., Subramaniam, K. M., Radhakrishnan, A. K., Choo, Y., and Teng, K. (2017). Health-promoting effects of red palm oil: evidence from animal and human studies. *Nutrition Review*, 75(2), pp.98–113.
- Low, L. E., Tey, B. T., Ong, B. H., Chan, E. S., and Tang, S. Y. (2016). Dispersion Stability, Magnetivity, and Wettability of Cellulose Nanocrystal (CNC)-dispersed

- Superparamagnetic Fe₃O₄ nanoparticles: impact of CNC Concentration†. *RSC Advances*, 6(114), pp.113132–113138.
- Low, L. E., Tey, B. T., Ong, B. H., Chan, E. S., and Tang, S. Y. (2017). Palm Olein-In-Water Pickering Emulsion Stabilized By Fe₃O₄-Cellulose Nanocrystal Nanocomposites And Their Responses To Ph. *Carbohydrate Polymers*, 155, pp.391–399.
- Low, L. E., Tey, B. T., Ong, B. H., and Tang, S. Y. (2018). Unravelling pH-responsive Behaviour of Fe₃O₄@CNCs-stabilized Pickering Emulsions under the Influence of Magnetic Field. *Polymer*, 141, pp.93–101.
- Low, L. E., Tey, B. T., Ong, B. H., and Tang, S. Y. (2018). A Facile and Rapid Sonochemical Synthesis of Monodispersed Fe₃O₄@Cellulose Nanocrystal Nanocomposites without Inert Gas Protection. *Asia-Pac. J. Chem. Eng.*, e2209, pp.1–13.
- Luo, H., Ao, H., Li, G., Li, W., Xiong, G., Zhu, Y., and Wan, Y. (2017). Bacterial cellulose/graphene oxide nanocomposite as a novel drug delivery system. *Current Applied Physics*, 17(2), pp.249–254.
- Luo, Z., Murray, B. S., Yusoff, A., Morgan, M. R. A., Povey, M. J. W., and Day, A. J. (2011). Particle-Stabilizing Effects of Flavonoids at the Oil–Water Interface. *Journal of Agricultural and Food Chemistry*, 59(6), pp.2636–2645.
- Lopez, J. A., González, F., Bonilla, F. A., Zambrano, G., and Gómez, M. E. (2010). Synthesis and characterization of Fe₃O₄ magnetic nanofluid. *Revista Latinoamericana de Metalurgia y Materiales*, 30(1), pp.60–66.
- Lu, A., Salabas, E., and Schuth, F. (2007). Magnetic nanoparticles: synthesis, protection, functionalization, and application. *Angewandte Chemie International Edition*, 46(8), pp.1222–1244.

- Mahdavi, M., Ahmad, M., Haron, M., Namvar, F., Nadi, B., Rahman, M., and Amin, J. (2013). Synthesis, Surface Modification And Characterisation Of Biocompatible Magnetic Iron Oxide Nanoparticles For Biomedical Applications. *Molecules*, 18(7), pp.7533–7548.
- Mahmoud, K. A., Lam, E., Hrapovic, S., and Luong, J. H. T. (2013). Preparation of Well-Dispersed Gold/Magnetite Nanoparticles Embedded on Cellulose Nanocrystals for Efficient Immobilization of Papain Enzyme. *ACS Applied Materials & Interfaces*, 5(11), pp.4978–4985.
- Marefati, A., Sjöo, M., Timgren, A., Dejmek, P., and Rayner, M. (2015). Fabrication of encapsulated oil powders from starch granule stabilized W/O/W Pickering emulsions by freeze-drying. *Food Hydrocolloids*, 51, pp.261–271.
- Marku, D., Wahlgren, M., Rayner, M., Sjöo, M., and Timgren, A. (2012). Characterization of starch Pickering emulsions for potential applications in topical formulations. *International Journal of Pharmaceutics*, 428(1-2), pp.1–7.
- Marrucci, G. (1969). A theory of coalescence. *Chemical Engineering Science*, 24(6), pp.975–985.
- Marti-Mestres, G. and Nielloud, F. (2002). Emulsions in Health Care Applications – An Overview. *Journal of Dispersion Science and Technology*, 23(1-3), pp.419–439.
- Mason, T. J. and Peters, D. (2003). *Practical Sonochemistry: Power Ultrasound Uses and Applications*. 2nd ed. Chichester: Hoorwood Publishing. pp.2333–2334.
- Mason, T. J., Chemat, F., and Ashokkumar, M. (2014). Power Ultrasonics for food processing. In Gallego-Juarez, J. A., Graff, K. F. (Eds.), *Power Ultrasonics: Applications of High-intensity Ultrasound*. (pp. 815–839). Cambridge, UK: Elsevier Ltd.

- Mascolo, M. C., Pei, Y., and Ring, T. A. (2013). Room Temperature Co-Precipitation Synthesis Of Magnetite Nanoparticles In A Large Ph Window With Different Bases. *Materials*, 6(12), pp.5549–5567.
- Melle, S., Lask, M., and Fuller, G. (2005). Pickering emulsions with controllable stability. *Langmuir*, 21(6), pp.2158–2162.
- Moon, R., Martini, A., Nairn, J., Simonsen, J., and Youngblood, J. (2011). Cellulose nanomaterials review: structure, properties and nanocomposites. *Chemical Society Reviews*, 40(7), pp.3941–3994.
- Moulder, J. F., Stickle, N. F., Sobol, P. E., and Bomben, K. D. (1995). Handbook of X-ray photoelectron spectroscopy. Minnesota, USA: PHI Perkin Elmer Corp, pp.251.
- Mwangi, W. W., Ho, K. W., Tey, B. T., and Chan, E. S. (2016). Effects Of Environmental Factors On The Physical Stability Of Pickering-Emulsions Stabilized By Chitosan Particles. *Food Hydrocolloids*, 60, pp.543–550.
- Nan, F., Wu, J., Qi, F., Fan, Q., Ma, G., and Ngai, T. (2014). Preparation of uniform-sized colloidosomes based on chitosan-coated alginate particles and its application for oral insulin delivery. *Journal Materials Chemistry B*, 2, pp.7403–7409.
- Nanocomposix. (2016). *ZETA POTENTIAL ANALYSIS OF NANOPARTICLES*. [online] Available at: <http://50.87.149.212/sites/default/files/nanoComposix%20Guidelines%20for%20Zeta%20Potential%20Analysis%20of%20Nanoparticles.pdf> [Accessed 3rd May, 2016].
- Navarro, J. R. G., Conzatti, G., Yu, Y., Fall, A. B., Mathew, R., Edén, M., and Bergström, L. (2015). Multicolor fluorescent labeling of cellulose nanofibrils by click chemistry. *Biomacromolecules*, 16(4), pp.1293–1300.

- Nazrul Islam, M., Van Phong, L., Jeong, J., and Kim, C. (2011). A Facile Route To Sonochemical Synthesis Of Magnetic Iron Oxide (Fe₃O₄) Nanoparticles. *Thin Solid Films*, 519(23), pp.8277–8279.
- Nypelö, T., Rodriguez-abreu, C., Rivas, J., Dickey, M. D., and Rojas, O. J. (2014). Magneto-Responsive Hybrid Materials Based On Cellulose Nanocrystals. *Cellulose*, 21(4), pp.2557–2566.
- Oliveira, H., Pérez-Andrés, E., Thevenot, J., Sandre, O., Berra, E., and Lecommandoux, S. (2013). Magnetic field triggered drug release from polymersomes for cancer therapeutics. *Journal of Controlled Release*, 169(3), pp.165–170.
- Olsson, R. T., Azizi Samir, M. A. S., Salazar Alvarez, G., BelovaL, StromV, Berglund, L. A., Ikkala, O., Nogués, J., and Gedde, U. W. (2010). Making flexible magnetic aerogels and stiff magnetic nanopaper using cellulose nanofibrils as templates. *Nat. Nano*, 5(8), pp.584–588.
- Ostertag, F., Weiss, J., and McClements, D. J. (2012). Low-energy formation of edible nanoemulsions: factors influencing droplet size produced by emulsion phase inversion. *Journal of Colloid and Interface Science*, 388(1), pp.95–102.
- Peng, J., Liu, Q., Xu, Z., and Masliyah, J. (2012). Synthesis of Interfacially Active and Magnetically Responsive Nanoparticles for Multiphase Separation Applications. *Adv. Funct. Mater.*, 22(8), pp.1732–1740.
- Petersson, L., Kvien, I., and Oksman, K. (2007). Structure and thermal properties of poly(lactic acid)/cellulose whiskers nanocomposite materials. *Composites Science and Technology*, 67(11-12), pp.2535–2544.
- Pichot, R. (2010). *Stability and Characterisation of Emulsions in the presence of Colloidal Particles and Surfactants*. University of Birmingham.
- Pickering, S. U. (1907). Emulsions. *Journal of the Chemical Society*, 91,2001-2021.

- Plank, C., Schillinger, U., Scherer, F., Bergemann, C., R'emy, J., Krotz, F., Anton, M., Lausier, J., and Rosenecker, J. (2003). The magnetofection method: using magnetic force to enhance gene delivery. *Biological chemistry*, 384(5), pp.737–747.
- Pradhan, P., Giri, J., Rieken, F., Koch, C., Mykhaylyk, O., Döblinger, M., Banerjee, R., Bahadur, D., and Plank, C. (2010). Targeted temperature sensitive magnetic liposomes for thermo-chemotherapy. *J. Control. Release*, 142(1), pp.108–121.
- Qiao, X., Zhou, J., Binks, B. P., Gong, X., and Sun, K. (2012). Magnetorheological behavior of Pickering emulsions stabilized by surface-modified Fe₃O₄ nanoparticles. *Colloids and Surfaces A: Physicochemical and Engineering Aspects*, 412(1), pp.20–28.
- Qu, J., Liu, G., Wang, Y., and Hong, R. (2010). Preparation of Fe₃O₄-chitosan nanoparticles used for hyperthermia. *Advanced Powder Technology*, 21(4), pp.461–467.
- Quy, D. V., Hieu, N. M., Tra, P. T., Nam, N. H., Hai, N. H., Son, N. T., Nghia, P. T., Anh, N. T. V., Hong, T. T., and Luong, N. H. (2013). Synthesis of Silica-Coated Magnetic Nanoparticles and Application in the Detection of Pathogenic Viruses. *Journal of Nanomaterials*, 2013(603940), pp.1–6.
- Ramsden, W. (1903). Separation of Solids in the Surface-Layers of Solutions and 'Suspensions' (Observations on Surface-Membranes, Bubbles, Emulsions, and Mechanical Coagulation). -- Preliminary Account. *Proceedings of the Royal Society of London*, 72(477-486), pp.156–164.
- Reddy, L. H., Arias, J. L., Nicolas, J., and Couvreur, P. (2012). Magnetic nanoparticles: Design and characterization, toxicity and biocompatibility, pharmaceutical and biomedical applications. *Chemical Reviews*, 112(11), pp.5818–5878.
- Rescignano, N., Fortunati, E., Montesano, S., Emiliani, C., Kenny, J. M., Martino, S., and Armentano, I. (2014). PVA bio-nanocomposites: A new take-off using cellulose nanocrystals and PLGA nanoparticles. *Carbohydrate Polymers*, 99, pp.47–58.

- Roca, A. G., Morales, M. P., O'Grady, K., and Serna, C. J. (2006). Structural and magnetic properties of uniform magnetite nanoparticles prepared by high temperature decomposition of organic precursors. *Nanotechnology*, 17(11), pp.2783–2788.
- Roonasi, P. and Holmgren, A. (2009). A Study On The Mechanism Of Magnetite Formation Based On Iron Isotope Fractionation. In *EPD Congress*; TMS: San Francisco; pp.829–836.
- Thomas, S. (2008). A review of the physical, biological and clinical properties of a bacterial cellulose wound. *Journal of Wound Care*, 17(8), pp.349–352.
- Saifuddin, N. and Dinara, S. (2012). Immobilization of *Saccharomyces cerevisiae* onto cross-linked chitosan coated with magnetic nanoparticles for adsorption of uranium (VI) ions. *Adv. Nat. Appl. Sci.*, 6(2), pp.249–267.
- Salvia-Trujillo, L., Alejandra Rojas-Graü, M., Soliva-Fortuny, R., and Martín-Belloso, O. (2014). Impact of micro fluidization or ultrasound processing on the antimicrobial activity against *Escherichia coli* of lemongrass oil-loaded nanoemulsions. *Food Control*, 37(1), pp.292–297.
- Sander, J. S., Erb, R. M., Denier, C., and Studart, A. R. (2012). Magnetic transport, mixing and release of cargo with tailored nanoliter droplets. *Advanced Materials (Deerfield Beach, Fla.)*, 24(19), pp.2582–2587, 2510.
- Schenzel, K. and Fischer, S. (2001). NIR FT Raman spectroscopy – a rapid analytical tool for detecting the transformation of cellulose polymorphs. *Cellulose*, 8(49), pp.49–57.
- Schubert, H. and Engel, R. (2004). Product And Formulation Engineering Of Emulsions. *Chemical Engineering Research and Design*. 82(A9), pp.1137–1143.
- Shah, B. R., Li, Y., Jin, W., An, Y., He, L., Li, Z., Xu, W., and Li, B. (2016). Preparation and optimization of Pickering emulsion stabilized by chitosan-tripolyphosphate nanoparticles for curcumin encapsulation, *Food Hydrocolloids*, 52, pp.369–377.

- Shakibaei, M., Mobasheri, A., Lueders, C., Busch, F., Shayan, P., and Goel, A. (2013). Curcumin Enhances the Effect of Chemotherapy against Colorectal Cancer Cells by Inhibition of NF- κ B and Src Protein Kinase Signaling Pathways. *PLoS One* 8, e57218.
- Sharma, T., Kumar, G. S., and Sangwai, J. S. (2015). Comparative effectiveness of production performance of Pickering emulsion stabilized by nanoparticle–surfactant–polymer over surfactant–polymer (SP) flooding for enhanced oil recovery for Brownfield reservoir. *Journal of Petroleum Science and Engineering*, 129, pp.221–232.
- Sharma, T., Velmurugan, N., Patel, P., Chon, B. H., and Sangwai, J. S. (2015). Use of oil-in-water pickering emulsion stabilized by nanoparticles in combination with polymer flood for enhanced oil recovery. *Petroleum Science and Technology*, 33(17–18), pp.1959–1604.
- Shi, X., Zheng, Y., Wang, G., Lin, Q., and Fan, J. (2014). pH- and electro-response characteristics of bacterial cellulose nanofiber/sodium alginate hybrid hydrogels for dual controlled drug delivery. *RSC Advances*, 4(87), pp.47056–47065.
- Silva, A. C., Oliveira, T. R., Mamani, J. B., Malheiros, S. M., Malavolta, L., Pavon, L. F., Sibov, T. T., Amaro Jr, E., Tannus, A., Vidoto, E. L., Martins, M. H., Santos, R. S., and Gamarra, L. F. (2011). Application of hyperthermia induced by superparamagnetic iron oxide nanoparticles in glioma treatment. *Int. J. Nanomedicine*, 6(3), pp.591–603.
- Sivakumar, M., Tang, S. Y., and Tan, K. W. (2014). Cavitation technology – A greener processing technique for the generation of pharmaceutical nanoemulsions. *Ultrason. Sonochem.*, 21(6), pp.2069–2083.
- Skaff, H., Ilker, M., Coughlin, E., and Emrick, T. (2002). Preparation of cadmium selenide-polyolefin composites from functional phosphine oxides and ruthenium-based metathesis. *Journal of the American Chemical Society*, 124(20), pp.5729–5733.

- Sorensen, C. M. (2002). Magnetism. In K. J. Klabunde, (Eds.), *Nanoscale Materials in Chemistry*. New York, USA: John Wiley & Sons, Inc., pp.169–221.
- Song, X., Pei, Y., Qiao, M., Ma, F., Ren, H., and Zhao, Q. (2015). Preparation And Characterizations Of Pickering Emulsions Stabilized By Hydrophobic Starch Particles. *Food Hydrocolloids*, 45, pp.256–263.
- Suganuma, S., Nakajima, K., Kitano, M., Yamaguchi, D., Kato, H., and Hayashi, S. (2008). Hydrolysis of Cellulose by Amorphous Carbon Bearing SO₃H, COOH, and OH Groups. *J. Am. Chem. Soc.*, 130(38), pp.12787–12793.
- Sun, S. and Zeng, H. (2002). Size-controlled synthesis of magnetite nanoparticles. *Journal of the American Chemical Society*, 124(28), pp.8204–8205.
- Sun, Y., Duan, L., Guo, Z., DuanMu, Y., Ma, M., Xu, L., Zhang, Y., and Gu, N. (2005). An improved way to prepare superparamagnetic magnetite-silica core-shell nanoparticles for possible biological application. *Journal of Magnetism and Magnetic Materials*, 285(1), pp.65–70.
- Supramaniam, J., Adnan, R., Kaus, N. H. M., and Bushra, R. (2018). Magnetic nanocellulose alginate hydrogel beads as potential drug delivery system. *International Journal of Biological Macromolecules*, 118(A), pp.640–648
- Suslick, K. S. and Price, G. J. (1999) *Applications of ultrasound to materials chemistry*. [online] Available at: <http://www.annualreviews.org/doi/pdf/10.1146/annurev.matsci.29.1.295>. [Accessed 15th August, 2014].
- Szpak, A., Kania, G., Skórka, T., Tokarz, W., Zapotoczny, S., and Nowakowska, M. (2012). Stable aqueous dispersion of superparamagnetic iron oxide nanoparticles protected by charged chitosan derivatives. *Journal of Nanoparticle Research*, 15(1), pp.1372–1379.

- Tadros, T. (2013). *Emulsion Formation, Stability, And Rheology, In Emulsion Formation And Stability*; Wiley-VCH Verlag GmbH & Co. KGaA: Weinheim, Germany, pp.1–8.
- Tam, J. (2012). Nanocrystalline Cellulose: A Novel, Renewable Antioxidant. [online] Available at: <http://wwsef.uwaterloo.ca/archives/2012/12TamReport.pdf> [Accessed 8th July, 2016].
- Tambe, D. E. and Sharma, M. M. (1993). Factors Controlling the Stability of Colloid-Stabilized Emulsions. *Journal of Colloid and Interface Science*, 157(1), pp.244–253.
- Tan, K. W., Tang, S. Y., Thomas, R., Vasanthakumari, N., and Manickam, S. (2016). Curcumin-loaded sterically stabilized nanodispersion based on non-ionic colloidal system induced by ultrasound and solvent diffusion-evaporation. *Pure Appl. Chem.*, 88(1-2), pp.43–60.
- Tan, L. T. -H., Ser, H. -L., Yin, W. -F., Chan, K. -G., Lee, L. -H., and Goh, B. -H. (2015). Investigation of Antioxidative and Anticancer Potentials of *Streptomyces* sp. MUM236 Isolated from Malaysia Mangrove Soil, *Front. Microbiol.*, 6(1316), pp.1–12.
- Tan, Y., Xu, K., Liu, C., Li, Y., Lu, C., and Wang, P. (2012). Fabrication of starch-based nanospheres to stabilize pickering emulsion. *Carbohydrate Polymers*, 88(4), pp.1358–1363.
- Tang, J., Lee, M. F. X., Zhang, W., Zhao, B., Berry, R. M., and Tam, K. C. (2014). Dual Responsive Pickering Emulsion Stabilized by Poly[2-(dimethylamino)ethyl methacrylate] Grafted Cellulose Nanocrystals. *Biomacromolecules*, 15(8), pp.3052–3060.
- Tang, J., Quinlan, P. J., and Tam, K. C. (2015). Stimuli-responsive Pickering emulsions: recent advances and potential applications. *Soft Matter*, 11(18), pp.3512–3529.
- Tcholakova, S., Denkov, N. D., and Lips, A. (2008). Comparison of solid particles, globular proteins and surfactants as emulsifiers. *Physical Chemistry Chemical Physics*, 10(12), pp.1608–1627.

- Teo, B. M., Suh, S. K., Hatton, T. A., Ashokkumar, M., and Grieser, F. (2011). Sonochemical Synthesis Of Magnetic Janus Nanoparticles. *Langmuir*, (27)1, pp.30–33.
- Timgren, A., Rayner, M., Sjöö, M., and Dejmek, P. (2011). Starch Particles For Food Based Pickering Emulsions. *Procedia Food Science*, 1, pp.95–103.
- Tikekar, R. V., Pan, Y., and Nitin, N. (2013). Fate of curcumin encapsulated in silica nanoparticle stabilized Pickering emulsion during storage and simulated digestion. *Food Research International*, 51(1), pp.370–377.
- Tremaine, P. R. and Leblanc, J. C. (1980). The solubility of Magnetite and the Hydrolysis and Oxidation of Fe²⁺ in water to 300 °C. *Journal of Solution Chemistry*, 9(6), pp.95–103.
- Tsabet, E. and Fradette, L. (2015). Effect of the properties of oil, particles, and water on the production of Pickering emulsions. *Chemical Engineering Research and Design*, 97, pp.9–17.
- Twentyman, P. R. and Luscombe, M. (1987). A study of some variables in a tetrazolium dye (MTT) based assay for cell growth and chemosensitivity. *Br. J. Cancer*, 56(3), pp.279–285.
- Urquidi-Macdonald, M. and Macdonald, D. D. (1998). Prediction of Radiation Fields in Pressurized Water Nuclear Reactors, In P. M. Natishan (Eds.), *Proceedings of the Symposium on passivity and its breakdown*. (pp. 91–99). Pennington, New Jersey: The Electrochemical Society.
- Valentini, L., Bittolo Bon, S., Cardinali, M., Fortunati, E., and Kenny, J. M. (2014). Cellulose nanocrystals thin films as gate dielectric for flexible organic field-effect transistors. *Materials Letters*, 126, pp.55–58.
- Vaiopoulos A. G., Athanasoula, K. C., and Papavassiliou A. G. (2013). NF-κB in colorectal cancer. *Journal of Molecular Medicine*, 91(9), pp.1029–1037.

- Vepsäläinen, M. and Saario, T. (2010). *Magnetite dissolution and deposition in NPP secondary circuit*. Finland. Retrieved from <http://www.vtt.fi/inf/julkaisut/muut/2010/VTT-R-09735-10.pdf>
- Vidal-Vidal, J., Rivas, J., and L'opez-Quintela, M. (2006). Synthesis of monodisperse maghemite nanoparticles by the microemulsion method. *Colloids and Surfaces A: Physicochemical and Engineering Aspects*, 288(1), pp.44–51.
- Vijayakumar, R., Koltypin, Y., Felner, I., and Gedanken, A. (2000). Sonochemical synthesis and characterization of pure nanometer-sized Fe₃O₄ particles. *Materials Science and Engineering: A*, 286(1), pp.101–105.
- Wahlgren, M., Engblom, J., Sjöo, M., and Rayner, M. (2013). The Use of Micro- and Nanoparticles in the Stabilisation of Pickering-Type Emulsions for Topical Delivery. *Current Pharmaceutical Biotechnology*, 14(15), pp.1222–1234.
- Walstra, P. (1996). Dispersed systems: Basic considerations. in *Food Chemistry*, O.R. Fennema (Ed.). Marcel Dekker, New York. pp.95–155.
- Wang, H., Shao, Z., Bacher, M., Liebner, F., and Rosenau, T. (2013). Fluorescent cellulose aerogels containing covalently immobilized (ZnS)_x(CuInS₂)_{1-x}/ZnS (core/shell) quantum dots. *Cellulose*, 20(6), pp.3007–3024.
- Wang, J., Sun, J., Sun, Q., and Chen, Q. (2003). One-step hydrothermal process to prepare highly crystalline Fe₃O₄ nanoparticles with improved magnetic properties. *Materials Research Bulletin*, 38(7), pp.1113–1118.
- Wang, X., Jiang Y., Wang Y., Huang, M., Ho, C., and Huang, Q. (2008). Enhancing anti-inflammation activity of curcumin through O/W nanoemulsions. *Food Chemistry*, 108(2), pp.419–424.
- Wang, Y. J., Pan, M. H., Cheng, A. L., Lin, L. I., Ho, Y. S., Hsieh, C. Y., and Lin, J. K. (1997). Stability of curcumin in buffer solutions and characterization of its degradation

- products. *J. Pharm. Biomed. Anal.*, 15(12), pp.1867–1876.
- Webster, T. J. (2007). Nanotechnology: better materials for all implants. *Mater. Sci. Forum*, 539, pp.511–516.
- Wei, Z., Wang, C., Zou, S., Liu, H., and Tong, Z. (2012). Chitosan nanoparticles as particular emulsifier for preparation of novel pH-responsive Pickering emulsions and PLGA microcapsules. *Polymer*, 53, pp.1229–1235.
- Welss, T., Basketter, D. A., and Schröder, K. R. (2004). In vitro skin irritation: facts and future. State of the art review of mechanisms and models. *Toxicology in Vitro: An International Journal Published in Association with BIBRA*, 18(3), pp.231–243.
- Wu, H., Gao, G., Zhou, X., Zhang, Y., and Guo, S. (2012). Control on the formation of Fe₃O₄ nanoparticles on chemically reduced graphene oxide surfaces†. *CrstEngComm.*, 14(2), pp.499–504.
- Wu, W., He, Q., and Jiang, C. (2009). Magnetic iron oxide nanoparticles: synthesis and surface functionalization strategies. *Nanoscale Res. Lett.*, 3(11), pp.397–415.
- Wu, W., Huang, F., Pan, S., Mu, W., Meng, X., Yang, H., Xu, Z., Ragauskas, A. J., and Deng, Y. (2015). Thermo-responsive and fluorescent cellulose nanocrystals grafted with polymer brushes. *J. Mater. Chem. A*, 3(5), pp.1995–2005.
- Wu, W., Jing, Y., Gong, M., Zhou, X., and Dai, H. (2011). Preparation And Properties Of Magnetic Cellulose Fiber Composites. *BioResources*, 6(3), pp.3396–3409.
- Wu, J. and Ma, G. (2016) Recent Studies Of Pickering Emulsions: Particles Make The Difference. *Small*, 12(34), pp.4633–4648.
- Xiong, J., Jiao, C., Li, C., Zhang, D., Lin, H., and Chen, Y. (2014). A versatile amphiprotic cotton fiber for the removal of dyes and metal ions. *Cellulose*, 21(4), pp.3073–3087.
- Xiong, R., Lu, C., Wang, Y., Zhou, Z., and Zhang, X. (2013). 'Nanofibrillated Cellulose As The Support And Reductant For The Facile Synthesis Of Fe₃O₄/Ag Nanocomposites

- With Catalytic And Antibacterial Activity'. *Journal of Materials Chemistry A*, 1(47), pp.14910–14918.
- Yallapu, M. M., Dobberpuhl, M. R., Maher, D. M., Jaggi, M., and Chauhan, S. C. (2012). Design of Curcumin loaded Cellulose Nanoparticles for Prostate Cancer. *Current Drug Metabolism*, 13(1), pp.120–128.
- Yamaguchi, H. (2008). Newtonian Flow. In *Engineering Fluid Mechanics* (pp. 279–397). Dordrecht: Springer Netherlands.
- Zhang, J. and Misra, R. (2007). Magnetic drug-targeting carrier encapsulated with thermosensitive smart polymer: core-shell nanoparticle carrier and drug release response. *Acta Biomaterialia*, 3(6), pp.838–850.
- Zhang, K., Feldner, A., and Fischer, S. (2011). FT Raman spectroscopic investigation of cellulose acetate. *Cellulose*, 18(4), pp.995–1003.
- Zhang, K., Wu, W., Meng, H., Guo, K., and Chen, J. -F. (2009). Pickering emulsion polymerization: Preparation of polystyrene/nano-SiO₂ composite microspheres with core-shell structure? *Powder Technology*, 190(3), pp.393–400.
- Zhang, L., He, R., and Gu, H. (2006). Oleic Acid Coating On The Monodisperse Magnetite Nanoparticles. *Applied Surface Science*, 253(5), pp.2611–2617.
- Zhang, Q. (2007). Synthesis and Characterization of Novel Magnetite Nanoparticle Block Copolymer Complexes. Retrieved from <http://scholar.lib.vt.edu/theses/available/etd-04262007-003618/>.
- Zhang, S., Zhang, Y., Liu, J., Xu, Q., Xiao, H., Wang, X., Xu, H., and Zhou, J. (2013). Thiol modified Fe₃O₄@SiO₂ as a robust, high effective, and recycling magnetic sorbent for mercury removal. *Chem. Eng. J.*, 226, pp.30–38
- Zhang, Y. P., Chodavarapu, V. P., Kirk, A. G., and Andrews, M. P. (2012). Nanocrystalline cellulose for covert optical encryption. *Journal of Nanophotonics*, 6(1), pp.063516.

- Zhen, H. (2015). *TAILORING CELLULOSE NANOCRYSTAL, POLYMER AND SURFACTANT INTERACTIONS FOR GELS, EMULSIONS, AND FOAMS*. McMaster University.
- Zheng, Y., Cheng, Y., Bao, F., and Wang, Y. (2006). Synthesis and magnetic properties of Fe₃O₄ nanoparticles. *Materials Research Bulletin*, 41(3), pp.525–529.
- Zhou, J., Qiao, X., Binks, B. P., Sun, K., Bai, M., Li, Y., and Liu, Y. (2011). Magnetic Pickering Emulsions Stabilized By Fe₃O₄ Nanoparticles. *Langmuir*, 27(7), pp.3308–3316.
- Zhou, J., Wang, L., Qiao, X., Binks, B. P., and Sun, K. (2012). Pickering emulsions stabilized by surface-modified Fe₃O₄ nanoparticles. *Journal of Colloid and Interface Science*, 367(1), pp.213–224.
- Zhu, A., Yuan, L., and Liao, T. (2008). Suspension of Fe₃O₄ nanoparticles stabilized by chitosan and o-carboxymethylchitosan. *International Journal of Pharmaceutics*, 350(1-2), pp.361–368.
- Zimmermann, T., Bordeanu, N., and Strub, E. (2010). Properties of nanofibrillated cellulose from different raw materials and its reinforcement potential. *Carbohydrate Polymers*, 79(4), pp.1086–1093.
- Zubarev, A. and Iskakova, L. (2004). To the theory of rheological properties of ferrofluids: influence of drop-like aggregates. *Physica A: Statistical Mechanics and its Applications*, 343(C), pp.65–80.
- Zoppe, J. O., Habibi, Y., Rojas, O. J., Venditti, R. A., Johansson, L. -S., Efimenko, K., Osterberg, M., and Laine, J. (2010). Poly(N-isopropylacrylamide) Brushes Grafted from Cellulose Nanocrystals via Surface-Initiated Single-Electron Transfer Living Radical Polymerization. *Biomacromolecules*, 11(10), pp.2683–2691
- Zoppe, J. O., Venditti, R. A., and Rojas, O. J. (2012). Pickering emulsions stabilized by cellulose nanocrystals grafted with thermo-responsive polymer brushes. *Journal of Colloid and Interface Science*, 369(1), pp.202–209.